Identifying Changes of Functional Brain Networks using Graph Theory

Dissertation

zur Erlangung des akademischen Grades

Dr. rer. med.

an der Medizinischen Fakultät

der Universität Leipzig

eingereicht von:

Diplom Informatiker Alexander Schäfer
geboren am 19.07.1983 in Meiningen/Deutschland

angefertigt am:

Max-Planck-Institut für Kognitions- und Neurowissenschaften

Betreuer:

Prof. Dr. Arno Villringer
Dr. Daniel Margulies

Gutachter:

Prof. Dr. Karl-Titus Hoffmann, Abteilung für Neuroradiologie, Leipzig
Prof. Dr. Felix Blankenburg, AB Neurocomputation und Neuroimaging, FU Berlin

Einreichungsdatum: 25.04.2014
Verteidigungsdatum: 26.03.2015
Beschluss über die Verleihung des Doktorgrades vom: 21.04.2015

“Change is the only constant in life.”
— Heraclitus

Content

Bibliographic description

Schäfer, Alexander
Identifying Changes of Functional Brain Networks using Graph Theory
Universität Leipzig, Dissertation
109 pages, 76 references, 3 figures

Articles included in this thesis:

- Margulies D., Böttger J., Long X., Lv Y., Kelly C., **Schäfer A.**, Goldhahn D., Abbushi A., Milham M., Lohmann G. and Villringer A., Resting developments: a review of fMRI post-processing methodologies for spontaneous brain activity, Magnetic Resonance Materials in Physics, Biology and Medicine, 23(5–6), 289–307, 2010
- **Schaefer A.**, Quinque E., Kipping J., Arélin K., Frisch S., Roggenhofer E., Villringer A., Mueller K., and Schroeter M., Early small vessel disease affects fronto-parietal and cerebellar hubs in close correlation with clinical symptoms – A resting-state fMRI study, Journal of Cerebral Blood Flow and Metabolism, 34(7), 1091–1095, 2014
- Sehm B.*, **Schäfer A.***, Kipping J., Margulies D., Conde V., Villringer A., and Ragert P., Dynamic modulation of intrinsic functional connectivity by transcranial direct current stimulation, Journal of Neurophysiology, 108(12), 3253–3263, 2012
  (*) equally contributing authors
- Böttger J., **Schäfer A.**, Lohmann G., Villringer A., and Margulies D., Three-dimensional mean-shift edge bundling for the visualization of functional connectivity in the brain, IEEE Transactions of Visualization and Computer Graphics, 20(3), 471–480, 2014
- **Schaefer A.**, Margulies D., Lohmann G., Gorgolewski K., Smallwood J., Kiebel S., and Villringer A., Dynamic network participation of functional connectivity hubs assessed by resting-state fMRI, Frontiers in Human Neuroscience, 8(15), 2014

Referat:

Brain disorders are seen as one of the main health challenges of the 21st century due to high prevalence and their high burden on the patients and their social environment (Wittchen et al., 2011). In the past 30 years, structural brain imaging such as cranial Computed Tomography (CT) and Magnetic Resonance Imaging (MRI) have become diagnostic cornerstones of clinical neurology and psychiatry. However, lesions detected with these structural methods are usually already irreversible and therefore great hopes are put into techniques which may detect brain diseases already at an early level with only “functional” and thus reversible changes. Functional Magnetic Resonance Imaging (fMRI) is such a method, however, due to a number of shortcomings (dependence on patients’ cooperation and on specific tasks), its clinical utility is very limited. However, a recently developed variant, resting-state fMRI (rs-fMRI), seems to overcome these limitations providing promising results in health and disease (Reijneveld et al., 2007; Fox and Greicius, 2010) based on a single examination of only few minutes duration. In this thesis, I contribute some further methodological advances to rs-fMRI to estimate in-vivo changes of functional brain networks in health and disease.
These functional brain networks can be analyzed using various methods. An overview over such methods is given in Study 1 (Margulies et al., 2010).

Functional brain networks are characterized by the synchronization of gray matter regions. These gray matter regions are connected and communicate through white matter fibers. In Study 2 (Schaefer et al., 2014b) we investigated the impact of small lesions in the white matter onto the communication between functional gray matter regions. We found a severe reduction of cerebral gray matter connectivity (synchronized signal) in subjects with white matter lesions using network centrality analysis. This effect was also reflected in the severity of the lesions. Behaviorally we found a psycho-motor slowing in the patients with white matter lesions.

The excitability of neurons in the gray matter can be influenced by electrical stimulation. The method of transcranial Direct Current Stimulation (tDCS) is a non-invasive electrical brain stimulation technique which has been shown to influence cortical excitability and alter behavior and learning. In Study 3 (Sehm et al., 2012) we analyzed the effects of tDCS to whole brain functional connectivity before, during and after stimulation of the primary motor cortex using network centrality analysis. Besides effects to the functional connectivity of motor and pre-motor areas we also found widespread effects during stimulation as compared to the sham condition.

One drawback of centrality approaches is their inherent reduction of spatial information. This reduction is often done for statistical reasons but also for reasons of visualization. The richness of the data makes it difficult to give a good display of all connections in the original anatomical space as they strongly overlap. A clear display in the anatomical space may be especially relevant in a neurosurgical context. In Study 4 (Böttger et al., 2014a) we addressed this limitation by bundling connections which connect similar areas in the brain. This approach is able to compress redundant information which reduces unnecessary clutter. As a consequence, this method might enhance the information gained for a human viewer of whole brain functional connectivity.

While the previous studies addressed alterations of functional brain networks between scans, in Study 5 (Schaefer et al., 2014a) we investigated the ongoing changes during the scan. While these ongoing networks dynamics could be of interest for clinical applications, their non-artifactual origin needs to be validated using external measures (Hutchison et al., 2013a). In our analysis we show a relationship between the dynamics of connectivity networks and self-generated-thoughts, as well as age. These results provide support for a non-artifactual origin of functional networks dynamics.

Functional brain networks estimated by resting-state fMRI offer a tool to measure and investigate changes due to brain diseases and therapy. This thesis shows how to estimate these changes and relate them to the severity of the disease. Further, it comprises new methods to investigate changes on even short time scales. The amount of change on these short time scales might offer a new window to characterize and investigate brain diseases.

List of Symbols

BOLD Blood Oxygenation Level Dependent

CT Computed Tomography

EEG Electro EncephaloGraphy

EPI Echo Planar Imaging

M1 primary motor cortex

MRI Magnetic Resonance Imaging

fMRI functional Magnetic Resonance Imaging

rs-fMRI resting-state functional Magnetic Resonance Imaging

SM1 primary sensorimotor cortex

tDCS transcranial Direct Current Stimulation

1 Introduction

1.1 General Introduction

Brain disorders, comprising mental and neurologic disorders, are described as one of the core health challenges for the 21st century (Wittchen et al., 2011; Collins et al., 2011). While functional Magnetic Resonance Imaging (fMRI) was expected to be a crucial method for the detection and prognosis of brain disorders (Thulborn et al., 1996), it has seen only few successful translations to the clinical realm (Matthews et al., 2006; Bullmore, 2012). fMRI was used for a long time in the framework of specifically designed experiments in which certain brain areas were expected to show atypical activations. This task-based fMRI stands in stark contrast to the significantly more successful structural neuroimaging (e.g. cranial CT, MRI) which provides whole brain images without any patient compliance. However, functional neuroimaging can be crucial for an early detection of pathological brain changes. This thesis will use fMRI and network theory to investigate clinically relevant functional changes of the human brain without regional constraints or the need of a specific task.

1.2 Functional Magnetic Resonance Imaging

While in-vitro studies have enhanced our general knowledge of the brain, a better understanding and detection of brain diseases in humans can only be achieved by in-vivo measurements. The in-vivo study of the human brain has been enabled by recent methodological advances. One very promising method for in-vivo neuroimaging, besides the well-established cranial Computed Tomography (CT) and Magnetic Resonance Imaging (MRI), is functional MRI (fMRI).

Functional Magnetic Resonance Imaging is a widely applied form of non-invasive in-vivo imaging. It is an MRI procedure which aims to provide large-scale images of neuronal population activity. In this thesis it will be used to investigate the human brain and its alterations. The main form of fMRI uses the blood oxygen level dependent (BOLD) contrast developed by Ogawa et al. (2000). fMRI BOLD is an indirect measure of neural activity which is based on the relationship between cerebral blood flow, energy demand and neural activity (Logothetis, 2002). fMRI BOLD uses strong magnetic fields to measure alterations of deoxyhemoglobin concentrations. The deoxyhemoglobin alterations are seen as a reflection of the blood oxygen level and indirectly energy consumption. However, blood oxygenation depends on the dynamics of oxygen consumption, cerebral blood flow and cerebral blood volume (Logothetis, 2002). Despite its indirectness, fMRI has been repeatedly shown to correlate with neuronal activity (Logothetis et al., 2001; Mukamel et al., 2005; Shmuel et al., 2006).

1.3 Resting-state fMRI

Despite its success as a research tool, task-based fMRI has seen little translation into the clinic (Fox and Greicius, 2010). In general, fMRI abnormalities seen in clinical research populations have not translated into the ability to provide practically useful diagnostic or prognostic information in individual patients (Matthews et al., 2006). Vast promise for improving the clinical applicability of fMRI evolves from focusing on intrinsic spontaneous modulations in the BOLD signal that occur during the “resting-state” (Fox and Greicius, 2010).

Intrinsic spontaneous slow oscillations, commonly captured during the resting-state in the BOLD signal, show correlated signal in functionally coupled networks (Biswal, 1995). These networks resemble task-based co-activation maps (Smith et al., 2009) and persist across various states, such as task performance, wakeful rest, sleep and loss of consciousness (Fox and Raichle, 2007). This property makes resting-state fMRI (rs-fMRI) a power tool to map multiple large-scale functional networks simultaneously. In this context rs-fMRI can serve multiple purposes, as the same dataset enables the investigation of various research questions. Compared to task-based-fMRI, rs-fMRI offers several advantages such as a short acquisition time, a simple acquisition process, a good signal-to-noise ratio, a high reliability (Shehzad et al., 2009) and easier standardization. In recent years, neuroimaging researchers have begun to build up large publicly available data collections to enable exploration and validation of brain networks (Van Essen et al., 2012; Nooner et al., 2012).

Besides identifying the functional architecture of the brain, rs-fMRI has recently also been applied in the research of brain diseases (Fox and Greicius, 2010). The most prominent strategy to identify abnormalities is the comparison of two groups, patients with a neurological pathology and healthy individuals. The relation of an altered synchronization in intrinsic fluctuations with respect to relevant clinical variables provides evidence for the clinical relevance and confidence of the found abnormalities. We follow this idea in Study 2 (Schaefer et al., 2014b). rs-fMRI also enables the clinically crucial identification of acute pathology on a single-subject level (Lv et al., 2013).

1.4 Brain Networks and Graph Theory

As rs-fMRI enables to map out the human brain in a single experiment it has also strengthened the view of the brain as a complex network. The organization of brain networks can and should be understood in the context of other complex systems as many of the open challenges for science in all disciplines – whether meteorology, sociology or molecular biology – involve understanding and forecasting complex systems. In general, the complexity of these systems does not arise directly from their units or agents (entities which are able to act) but from the dynamic interaction of those agents. While each interaction between a pair of agents might be simple, it opens up a sheer infinite amount of configurations for the system. In the context of fMRI the agents can be brain regions and the interactions can be seen as functional synchronization between these regions.
Graph theory opens up a unified framework to model and investigate complex systems. The interactions between the agents can be described as a graph or network, in which the interactions are formalized as edges and the agents as vertices. The structure of such a network can then inform about the behavior of the complex system.

The functional structure of this large-scale network can be mapped using rs-fMRI (Yeo et al., 2011; Power et al., 2011; Bellec et al., 2010). This network, as any network, can be analyzed with methods developed in the field of graph theory (Diestel, 2005). In graph theory, a graph is defined as a tuple G=(V,E) where V is a set of vertices and E is a set of edges. I will use the terms edges and connections interchangeably throughout the thesis. In the following section, I will explain the different possibilities of defining vertices and edges in graphs derived from fMRI data. The process of graph construction is illustrated in Figure 1.

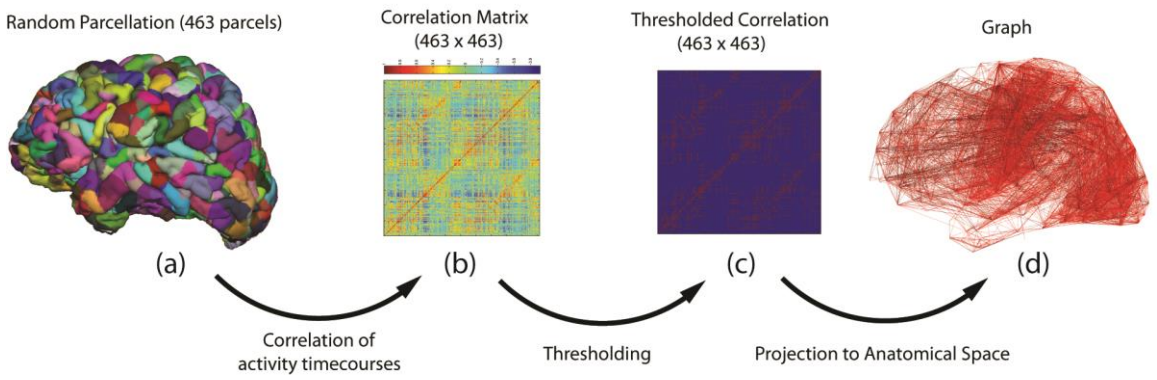

Figure 1 Overview of graph construction. (a) Random parcellation of a human brain in 463 cortical and subcortical areas (section 1.4.1). (b) Correlation of average signal from the areas results in a matrix. (c) Thresholded matrix where connections with low correlation values are eliminated. (d) Visualization of resulting network in anatomical space. Figure adopted from Study 4 (Böttger et al., 2014a), © 2014 IEEE.

1.4.1 Vertices of an fMRI connectivity graph

The definition of vertices is the first crucial step in a network analysis. In the following section, the four most common approaches of vertex definition in macro-scale neuroimaging will be discussed.

The most straightforward definition of vertices is a voxel-based parcellation. Here every voxel of an fMRI scan becomes a vertex (examples in Lohmann et al., 2010; Zuo et al., 2012). This allows for the highest possible resolution and provides good reliability, given a good registration between the individual images and a common template space. However, its validity as in the question of why the resolution of the MR scanner should be the most informative brain unit remains unclear.

Furthermore, the high resolution of the vertex space makes the analysis computationally very intensive and only very efficient algorithms can be applied. The voxel-based parcellation was used in Studies 2 and 3 (Schaefer et al., 2014b; Sehm et al., 2012).

A more coarse definition of vertices is an anatomical parcellation of the brain. Here every anatomical region of the brain becomes a vertex (Tzourio-Mazoyer et al., 2002). These parcellations are highly reliable and fast to compute given an anatomical atlas. Given the lower number of vertices also more computationally expensive algorithms can be applied. However, the lower resolution can also be regarded as a limitation as it reduces sensitivity. The validity is unclear as the functional brain organization might not be limited by its underlying structure (Koch et al., 2002; Deco et al., 2011). Furthermore, the strong variation in the volumetric size of the vertices might be confounding.

Random parcellations split a brain into coherent regions of uniform size (Cammoun et al., 2012). By iteratively splitting these regions they offer multiple resolutions of the same brain. While random parcellations reduce the vertex size variations their validity and reliability are

unclear. A random parcellation was used in Study 4 (Böttger et al., 2014a) and is illustrated in Figure 1a.

Functional parcellations aim to define functional units as vertices. The parcellation is based on prior functional information and can either be derived from a meta-analysis (Dosenbach et al., 2010) or from functional homogeneity analyses (Smith et al., 2009; Varoquaux et al., 2011; Craddock et al., 2012). Functional parcellations offer good reliability and validity. However, they may miss some regions and are difficult to apply to structural data. A functional parcellation (Craddock et al., 2012) was used in Study 5 (Schaefer et al., 2014a).

1.4.2 Edges of an fMRI connectivity graph

To construct a graph the definition of the edges remains to be carried out. Currently the relationship between regions is often characterized by the synchrony of their temporal signals. However, the best way to define connectivity is still debated in the field (Smith et al., 2011). In the following three different measures of connectivity will be discussed.

The most common approach to define edges is the Pearson's correlation coefficient r, which is defined as:

$$r = \frac{\sum_{i=1}^{n}(X_i - \overline{X})(Y_i - \overline{Y})}{\sum_{i=1}^{n}(X_i - \overline{X})^2 \sum_{i=1}^{n}(Y_i - \bar{Y})^2}$$

where X_i is the i-th timepoint in the timeseries of vertex x and $\bar{X}$ is the mean of timeseries X. This holds for Y respectively. All edges in a network are estimated by computing the Pearson's correlation coefficients between the time series of every pair of regions (Figure 1b). Often only the highest correlation values are used as edges to construct a graph (Figure 1c). The reasoning is that lower correlation values are noise as they show an overall lower test-retest reliability (Schwarz and McGonigle, 2011; Patriat et al., 2013). We followed this idea in Study 4 and 5 (Böttger et al., 2014a; Schaefer et al., 2014a). While Pearson`s correlation is simple to compute it performs surprisingly well (Smith et al., 2011). However, its major problem is to induce indirect edges, so called trianglular edges. For example, if A is connected with B and B is connected with C then there is a high likelihood that A and C will be connected. The edge between A and C can arise from the variance that is unique for B and is considered as a false positive.

An approach to overcome this limitation is to exclude the unwanted variance using partial correlation: Before estimating the correlation between A and C, the variance from B will be subtracted out to remove indirect connections. However, regressing out a variable removes a degree of freedom and becomes problematic when the number of data points (degrees of freedom) in the rs-fMRI signal is smaller than the number of edges. The degrees of freedom in the resting state signal are limited as the majority of the power is between 0.01–0.05 Hz (Schölvinck et al., 2010) and the relatively short scanning time of 15 minutes or less. Therefore, partial correlation is often not applicable to networks with more than 50 vertices.

The problem of high dimensional data with a low number of data-points is not unique to neuroscience. One approach to address this problem is the assumption of a sparse network. In other words, only a few connections are necessary to explain the data. As it is difficult to find this sparse representation approximation algorithms are often employed (Friedman et al., 2008). In the neuroimaging community sparse approaches are beginning to be used but are far from being common (Varoquaux and Craddock, 2013).

For the analysis and comparison of the resulting fMRI networks we refer to the graph analysis section in Study 1 (Margulies et al., 2010) and to other more recent reviews (Varoquaux and Craddock, 2013; Fornito et al., 2013).

1.5 White-Matter Lesions and Small Vessel Disease

Functional brain networks are gray matter areas which communicate through white matter axons. Both white and gray matter can be damaged by vascular infarcts or lesions. MRI white matter abnormalities reflect lesions of subcortical and periventricular white matter as lacunes reflect cerebrospinal fluid (CSF)-filled cavities (Selnes and Vinters, 2006). White matter lesions may provide a good model to study the relationship between white matter connections and gray matter functional connectivity. In Study 2 (Schaefer et al., 2014b) we addressed the impact of white matter lesions on gray matter functional connectivity. Subsequently, we assessed the relevance of the connectivity changes to altered task performances in order to demonstrate the behavioral significance of our results.

Vascular white and gray matter lesions are also highly relevant in the clinical context. White matter hyper-intensities and lacunar infarcts are considered as evidence for small vessel disease. It is known that white matter lesions can lead to cognitive impairment which worsens with increasing lesion load (Longstreth et al., 2005). Accordingly, the presence of white matter lesions doubles the risk of a later dementia (Vermeer et al., 2003). Until recently the effect of white matter lesions onto brain function has been mainly assessed using task-based activation studies (Venkatraman et al., 2010; Aizenstein and Andreescu, 2011).

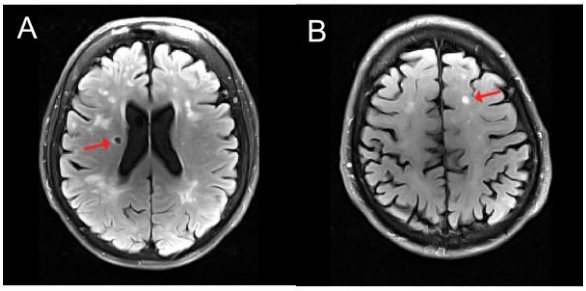

Figure 2 Example for markers of structural changes in small vessel disease in T2-weighted images. Characteristic abnormality related to lacune (A) and white matter lession (B). Figure from Publication 2 (Schaefer et al., 2014b).

1.6 Transcranial Direct Current Stimulation

Changes in functional brain networks cannot only occur as a result of vascular lesions; they can also be induced by external stimulation. tDCS is a non-invasive brain stimulation technique which uses low currents delivered directly to a brain area via surface electrodes. The effect of tDCS onto brain function depends on depolarization or hyperpolarization in the neuronal membrane potential (Creutzfeldt et al., 1962; Nitsche et al., 2003a). Unilateral tDCS can be used to facilitate motor learning (Nitsche et al., 2003b). Recently, bilateral or bihemispheric tDCS over M1 has been suggested (Vines et al., 2008) and employed as an additional therapeutic tool for neurorehabilitation in stroke patients with motor deficits (Lindenberg et al., 2010; Bolognini et al., 2011). Bilateral tDCS of M1 might not only facilitate neural activity in the damaged hemisphere but additionally help to rebalance maladaptive interhemispheric interactions by inhibition of the contralesional motor cortex.

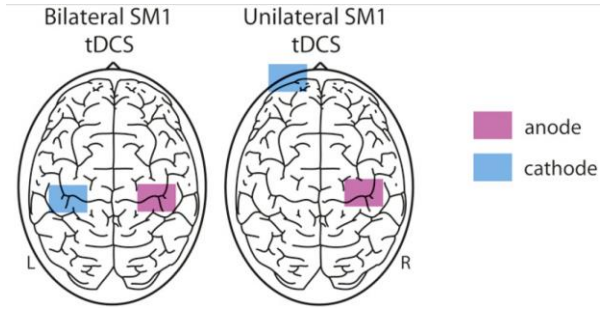

Figure 3 Bilateral tDCS over primary sensorimotor cortex (SM1), the anode was mounted over the right SM1 while the cathode was mounted over the homologous left SM1. For unilateral SM1 tDCS, the anode was again placed over the right SM1, while the cathode electrode was mounted over the contralateral supraorbital region. Figure from Study 3 (Sehm et al., 2012).

Besides these clinical aspects, tDCS can also be used as a tool to investigate brain function in healthy humans. In this context prefrontal tDCS has been shown to modulate the connectivity between large scale functional brain networks (Keeser et al., 2011). In Study 3 (Sehm et al., 2012) we investigated the effects of such stimulation on the supplementary motor cortex (Figure 3). We have used a data-driven whole brain graph-theoretical approach to analyze the impact of bilateral and unilateral tDCS (Figure 3) applied to the motor cortex during resting-state fMRI scans.

1.7 Dynamic Functional Connectivity

Until recently it was implicitly assumed that the functional connectivity during a task-free fMRI scan is constant. However, recent studies challenged this view by showing variations in the fMRI synchronization over the scan (Chang and Glover, 2010). These variations of connectivity were shown to be related to the electro encephalography (EEG) signal (Britz et al., 2010; Musso et al., 2010; Tagliazucchi et al., 2012) and are present in the absence of any head motion (Hutchison et al., 2013b). While dynamic connectivity could be a valuable tool for clinical applications its non artifactual origin needs to be validated by external measures (Hutchison et al., 2013a). Possible strategies are relating dynamic functional connectivity to ongoing electrophysiological measures (Tagliazucchi et al., 2012; Chang et al., 2013) or behavior (Thompson et al., 2013). In our analysis in Study 5 (Schaefer et al., 2014a) we show a relationship between the dynamic functional connectivity and ongoing self-generated-thoughts, as well as age.

In this thesis I want to show the applicability of the graph theoretic methods described in Publication 1 (Margulies et al., 2010) to investigate clinically relevant changes of functional brain networks. Further, we developed these methods further to enhance the relevance to the clinical realm and address changes of brain networks on even shorter time scales.

2 Publications

2.1 Resting developments: a review of fMRI post-processing methodologies for spontaneous brain activity

Margulies D., Böttger J., Long X., Lv Y., Kelly C., Schäfer A., Goldhahn D., Abbushi A., Milham M., Lohmann G. and Villringer A., Resting developments: a review of fMRI post-processing methodologies for spontaneous brain activity, Magnetic Resonance Materials in Physics, Biology and Medicine, 23(5–6), 289–307, 2010. The final publication is available at http://link.springer.com/article/10.1007%2Fs10334-010-0228-5.

Magn Reson Mater Phy manuscript No.
(will be inserted by the editor)

Resting Developments

A review of fMRI post-processing methodologies for spontaneous brain activity

Daniel S Margulies* · **Joachim Böttger*** · **Xiangyu Long** · **Yating Lv** · **Clare Kelly** · **Alexander Schäfer** · **Dirk Goldhahn** · **Alexander Abbushi** · **Michael P Milham** · **Gabriele Lohmann** · **Arno Villringer**

Received: date / Accepted: date

Abstract Analytic tools for addressing spontaneous brain activity, as acquired with fMRI during the "resting-state," have grown dramatically over the past decade. Along with each new technique, novel hypotheses about the functional organization of the brain are also available to researchers. We review six prominent categories of resting-state fMRI data analysis: seed-based functional connectivity, independent component analysis, clustering, pattern classification, graph theory, and two "local" methods. In surveying these methods, we address their underlying assumptions, methodologies, and novel applications.

Keywords resting state · functional connectivity · brain networks

Introduction

Entering a cocktail party with three friends, each of us might intermingle—meet new people, loiter by the hors d'œuvres—but throughout the evening we would no doubt exchange glances, watch for indications that all is well, or subtly communicate that it may be time to leave.

Upon exiting, the traditional mapping of new social connections might be discussed as we recount the people we met and the new connections that were formed. However, a much less tangible aspect of the social dynamic is the intermittent communication that maintained the link throughout the party.

These two facets of social connectedness find correlates in models of brain connectivity, which have been roughly categorized as either anatomical or functional. While anatomical connectivity may be understood as the concrete pathways of potential information exchange (such as collected phone numbers and email addresses in the social realm), functional connectivity may be better defined as the intermittent interactions maintaining those lines of communication.

But how would we summarize and describe these dynamic connections? One early definition established functional connectivity as "the temporal correlation of a neurophysiological index measured in different brain areas" [1]; however, over the past two decades, the shift in focus beyond mere correlation has led to the development of increasingly complex frameworks to describe functional relationships between brain regions

In the case of our party, how would we describe the dynamic interactions throughout the evening? Would we chose an individual, perhaps a central figure such as the host, and describe her interactions with each of the guests (*seed-based functional connectivity*)? Would we map out the predominant lines of conversation (*independent component analysis*) or the cliques that formed and disassembled throughout the evening(*clustering*)? Would it be more appropriate to map and abstract the lines of communication (*graph theory*) or search for de-

* Authors contributed equally.
D.S. Margulies · X. Long · Y. Lv · A. Schäfer · D. Goldhahn · G. Lohmann · A. Villringer
Max Planck Institute for Human Cognitive and Brain Sciences
Stephanstrasse 1a
04103 Leipzig, Germany
Tel.: +49 341 9940-2256
Fax: +49 341 9940-2221
E-mail: margulies@cbs.mpg.de
URL: http://www.cbs.mpg.de

J. Böttger · A. Abbushi
Department of Neurosurgery
Charité – Universitätsmedizin Berlin

C. Kelly · M.P. Milham
P. Green and R. Cōwen Institute for Pediatric Neuroscience
New York University School of Medicine

lineating patterns of activity (*pattern classification*)? Or would we disregard the question of connectivity and simply describe the behavior of the guests individually (*"local" approaches*)? Each of these approaches requires a unique methodology, each is based in specific assumptions about the structure of social interactions, and each implies an optimal description. Before beginning an analysis, it would be advantageous to consider these aspects—likewise, with respect to the brain.

Over the past decade, researchers examining functional connectivity using **"resting-state" functional magnetic resonance imaging (fMRI) data** have witnessed a dramatic increase in the analytic options for describing and summarizing the functional organization of the brain. Although, by convention, we will often use the term "resting-state" to denote the data for which these analyses have been largely developed, we also recognize the controversies surrounding this designation [2,3]. While other terms have been adopted to supplant "resting-state" (e.g., "intrinsic" and "spontaneous" [4]), and, when contextually appropriate, have become practically interchangeable, we will maintain the convention of "resting-state" due to its referential role within the field's literature. Nevertheless, it is crucial to recognize that the methods described here are not limited to data acquired during a "resting" condition, and can equally be used as a **model-free** analysis for any **steady-state** fMRI data set (e.g., [5]).

Numerous studies and reviews have explored the implications of various pre-processing steps (e.g., [6–11]); however, only a few to date have broadly addressed post-processing techniques (for a recent review of functional connectivity methodologies with emphasis on the computational aspects, see: [12,13,**?**]; or for emphasis on clinical applications, see: [14,15]). In the following review, we will address the diverse array of post-procesing techniques available, with a focus on the theoretical presuppositions of each for exploring brain organization and function (see Fig. 1).

We will identify six analytic categories as they are applied to resting-state fMRI data:

1. seed-based functional connectivity
2. independent component analysis
3. clustering
4. pattern classification
5. graph theory
6. "local" methods[1]

We will discuss their different underlying theoretical assumptions and provide a basic methodological review for their implementation. Such a framework may also help to highlight analytic techniques that could be further explored and developed. Given the wide scope of this review, we will only attempt a general intuition for the different measures. Thus, the aim of the current review will be to offer an introduction to analytic methodologies of resting-state fMRI data.

[1] We use the term "local" to denote methods that do not address long-distance functional connectivity, but rather assess local voxelwise activity.

1 Seed-Based Functional Connectivity

Seed-based functional connectivity analysis is the correlation between activity in an *a priori* region-of-interest (ROI), or "**seed region**", and activity in all other voxels in the brain. Another widely used approach is to correlate the activity of several distributed ROIs.

The technique was initially applied to resting-state fMRI data by Bharat Biswal and colleagues in 1995 [16]. Using a seed region in the motor cortex, resting-state functional connectivity was shown to replicate patterns of motor task activation.

The straightforward statistics and comprehensible results have made seed-based functional connectivity a popular technique. But despite the statistical transparency, the technique suffers from the primary drawback of requiring *a priori* selection of seed regions or reduction to a limited number of ROIs. Among the predominant techniques for determining functional connectivity, seed-based procedures are the most explicitly model-based [12].

1.1 Techniques

Seed-based analysis comprises two basic steps:

1. extraction of a model time-series from a specified area; and,
2. quantifying the similarity between the model time-series with the time-series from other voxels or ROIs.

In its simplest form, the correlation of an averaged ROI time-series with all other voxels is clear-cut and easily implemented. Long-facilitated by general fMRI data processing **software** such as AFNI[2] and SPM[3], other software packages have recently emerged focusing specifically on streamlined processing of resting-state functional connectivity using MATLAB in conjunction with SPM: "REST"[4] and "MATLAB Toolbox for Functional Connectivity"[5] [17]).

[2] `http://afni.nimh.nih.gov/afni/`
[3] `http://www.fil.ion.ucl.ac.uk/spm/`
[4] `http://sourceforge.net/projects/resting-fMRI/`
[5] `http://groups.google.com/group/fc-toolbox`

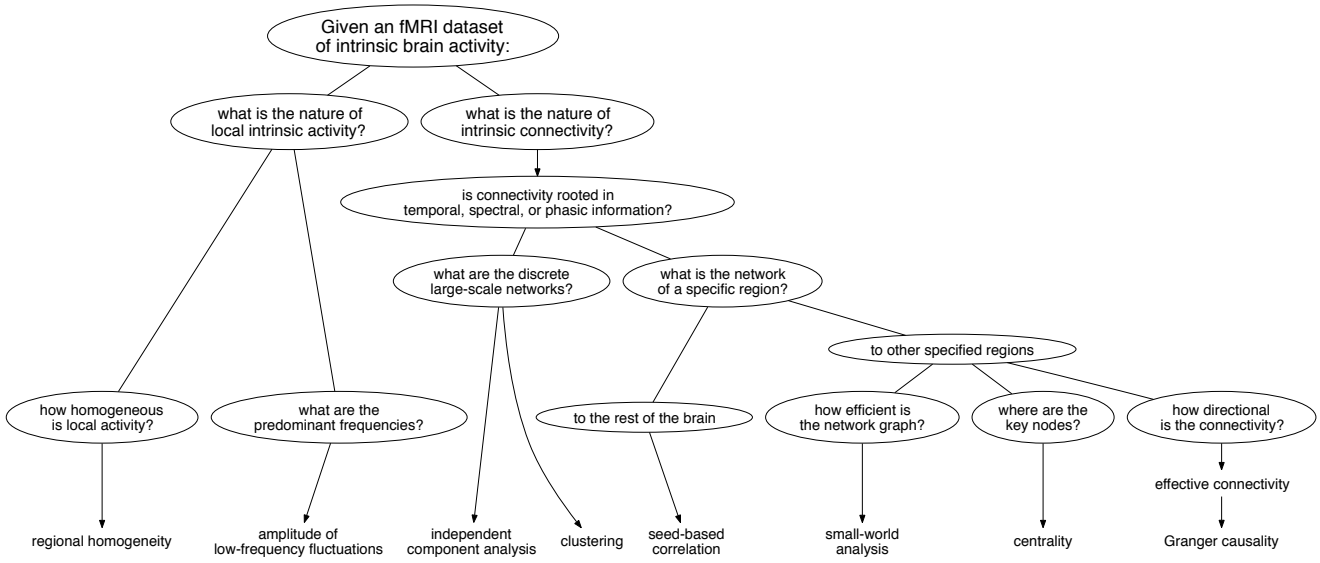

Fig. 1 A flowchart of possible questions that could be addressed with current methodologies given a resting-state fMRI data set.

Over the past decade, assessing functional connectivity with seed-based approaches has expanded to include assorted signal processing and statistical techniques aimed at extracting more refined and considered relationships between regions. The following overview will address several of the innovations developed for both steps of the seed-based analysis.

Time-series extraction for a seed region raises issues regarding the most viable method to purify signal from a set of contiguous voxels. The conceptually basal method is averaging the value at each time point, thus cancelling out extraneous noise. A novel **interactive** implementation has recently been made available with the aforementioned analysis package AFNI. *InstaCorr* allows the selection of a seed region to be virtually simultaneous with the mapping of the correlation map. It is possible to modify the radius of the seed region and the degree of spatial smoothing (traditionally implemented by defining the size of a Gaussian filter that assigns a value to each voxel based on the weighted average of surrounding voxels), thus facilitating the exploration of these decisions on resultant correlation maps. The significance of seed size and spatial smoothing decisions becomes relevant when considering the signal-to-noise ratio of the data, assumptions about hemodynamic response throughout the brain, and the desired anatomical specificity of the resultant functional connectivity maps.

More computationally advanced alternatives, such as **principal component analysis (PCA)** have also been implemented for time-series extraction. Essentially, PCA transforms the seed region time-series into a set of "components" that successively account for the greatest amount of variance in the data. Zhong and colleagues recently demonstrated that using PCA to extract the signal from an ROI for regression-based functional connectivity analysis could improve the accuracy and true positive rate for detecting the default-mode[6] and motor networks, when compared to averaging over the seed region [21]. Their method has the advantage of combining data-driven optimization of the model time-series with statistically straightforward model-driven regression, thus capitalizing on the strengths of both techniques.

After a model time-series has been extracted, myriad statistical techniques are available for **quantifying the relationship** between the seed region and other voxels or ROIs. As each addresses different aspects of the signal, each also implies specific hypotheses about the mode of communication assessed with functional connectivity. The **blood oxygen-level dependent (BOLD) signal** reflects the response of **deoxyhemoglobin (deoxy-Hb)** concentration to changes in local neuronal activity and is determined by vascular (blood velocity, blood volume: "neurovascular coupling") and metabolic (oxygen consumption: "neurometabolic coupling") factors. The analytic tool employed inherently makes certain assumptions about the temporal dynamics of the deoxy-Hb response across the entire brain.

[6] The "default-mode network" consists of medial prefrontal, posteromedial, and inferior lateral parietal cortex, and received its name due to greater activity during the baseline "resting" condition [18,19]. For a recent review, see: [20].

For instance, **temporal correlation** (or **covariance**) can describe synchronous fluctuations, whereas **cross-correlation** can accommodate lags in communication between areas. These approaches would be appropriate if neurovascular coupling were globally consistent; however, if we cannot make that assumption, then a statistical method which is insensitive to the temporal domain might be more suitable.

While cross-correlation quantifies the relation between two signals in the time-domain, **coherence** operates equivalently in the frequency-domain. Coherence thus provides a means for assessing functional connectivity that is insensitive to inter-regional differences in neurovascular coupling dynamics [22,23]. Shifts in the frequency spectrum do not alter the degree of coherence (just as lags in the time-domain do not alter cross-correlation coefficients), considering the low-frequency spectral band in which functional connectivity is detected [16,24,25], low-pass filtering at 0.1 Hz, or even lower, is an essential preprocessing step for this method. Higher frequencies due to cardiac or respiratory artifacts would otherwise interfere in coherence analyses. Furthermore, different networks have been shown to correlate at distinct low-frequency bands at rest [26,27], and are modulated in the low-frequency domain during motor task-involved [28] and cognitive effort [29].

Another approach, rather than looking at the magnitude of the spectral information, is to explore the **phase-spectrum delay** between regions. Sun and colleagues developed a novel method of addressing latency between regions in conjunction with connectivity through the combined analysis of phase-delay and coherence [30].

When more than one seed region is analyzed, the *specificity* of functional connectivity to only one of the regions is a critical issue. **Partial correlation** (or **multiple regression**) reveals the functional connectivity between a pair of regions, removing influences from others [31]. For example, partial correlation has been used to parcellate the thalamus with respect to cortical regions, by eliminating the influence of all other cortical regions [32]. The influential role of the posteromedial component of the default-mode network in the networks functioning has also been demonstrated using such methods [33].

The definition of functional connectivity is often described within the neuroimaging literature in contrast to **effective connectivity**, which addresses the *directionality* of influence between regions. While numerous techniques have been developed to address causal interactions in fMRI data, one popular approach in resting-state analysis is **Granger causality** [34]. The analysis assumes that better *prediction* is an indication of *influence*, and tests whether past values of time-series A better *predict* future values of time-series B than past values of time-series B alone. It has been used to address control of the default-mode network [35, 36] and the changing influences between networks with respect to age [37]. Nonetheless, due in part to temporal blurring induced by the hemodynamic response, the potential utility of effective connectivity to resting-state fMRI data, without experimental manipulation, remains a source of debate (see the section *Correlation and Causality* in [13]) and methodological innovation (e.g., [38]). The rest of the current review, however, will focus on methods for the analysis of functional connectivity.

1.2 Applications

Early studies of resting-state functional connectivity focused on describing well-charted neural systems from the cognitive neuroscience literature, such as the motor cortical network [39,40], visual network [41–43], a language network, including Broca's and Wernicke's areas [44], a cerebellar-prefrontal network [45], and networks based in the amydgala and hippocampus [40]. Of interest to the emergence of the"resting-state" fMRI research field, Greicius and colleagues were the first to use seed-based functional connectivity to map the default-mode network in 2003 [46], thus effectively linking the resting-state functional connectivity literature (whose lineage is traced to Bharat Biswal et al., 1995 [16]) with the "resting-state" of cognitive neuroscience (which emerged from Shulman et al., 1997 [18] and several publications in 2001 by Marcus Raichle, Deborah Gusnard, and colleagues [47,48]).

While a significant concern of these initial studies was to establish the validity of studying functional connectivity in the absence of an attributable cognitive or behavioral state, more recent research into resting-state functional connectivity has taken advantage of its strengths in order to address topics that are beyond the practical scope of task-based fMRI. For instance, the detection of functional subdivisions within complex regions usually requires large-scale meta-analysis (e.g., striatum [49], anterior cingulate [50], and cerebellum [51]); however, systematic placement of seed regions throughout such regions has revealed similar subdivisions in striatum [52,53], anterior cingulate [54], and cerebellum [55,56], as well as amygdala [57,58], medial temporal cortex [59], cross-modal auditory-visual connectivity during rest [60], and the red nucleus [61]. Other studies have observed the presence of novel subdivisions with the precuneus [62] and the default-mode

network [36], somatotopic organization within the motor cortex [63], differentiation of the dorsal and ventral attention streams [64], a hippocampal-parietal memory network [65], and a fronto-parietal control network [66]. The efficiency of these approaches for exploring functional neuroanatomy with data sets comprising merely dozens of participants, rather than a meta-analysis of an equal number of studies, is evident.

Furthermore, these approaches have been fruitful in cross-species animal research. The default-mode network is found in the anesthetized macaque monkey [67], as well as the posterior parahippocampal network [68], and posteromedial subdivisions reflecting the anatomical tracing literature [62]. In the rat, the sensorimotor and visual networks have been mapped [69,70]. The general flexibility of resting-state scanning has enabled rapid innovation for addressing cross-species questions using parallel non-invasive techniques.

Amidst these advances, the issue of how to best optimize ROI-selection persists as the most evident weakness of seed-based approaches. Meta-analyses have provided an effective strategy for probing specific distributed systems. For instance, in order to examine the test-retest reliability of resting-state data, Shehzad and colleagues [71] specified 3 sets of regions of interest (ROIs), derived from four different and representative studies [72–75]. However, the further development of computationally-oriented, *a priori*-free selection criteria is still much needed.

1.3 Discussion

In summary, seed-based approaches constitute one of the primary analytic strategies for resting-state data, and offer an unambiguous means of quantifying functional connectivity. The limitations of *a priori* seed region selection, size, and shape, are a substantial drawback, as these choices can alter findings, and may bias the results. Furthermore, proper delineation of subdivisions becomes a methodological question in itself.

Potential solutions to these issues take the form of several other prominent methodologies (ICA, cluster analyses), which will be discussed in the following sections.

2 Independent Component Analysis

Assuming the brain is organized into a number of functionally discrete networks, an optimal analytic technique would determine the signals unique to each network from the data alone. **Blind source separation** (or **decomposition**) techniques address the problem of determining distinct components within a set of signals with minimal *a priori* assumptions. Rather than requiring the specification of seed regions to derive networks, **independent component analysis (ICA)** has gained prominence in resting-state fMRI data analysis as a method to determine the spatial distribution of distinct functional connectivity networks [76–79]. In comparison with the aforementioned seed-based approaches, ICA offers several advantages:

- It does not require assumptions about locations of networks.
- Networks can be distributed, without a focal seed region.
- It can be conducted with minimal preprocessing, as noise is extracted as components during the analysis.

Nonetheless, ICA is not the perfect answer to functional connectivity analysis, as will become clear from a closer inspection of the methods.

2.1 Technique

The aim of ICA is to delineate maximally independent spatial or temporal components. As fMRI data generally consists of more spatial than temporal data points, spatial ICA is more widely applied. Thus, ICA assumes that an fMRI data set consists of a mix of independent signals from a number of spatially distributed sources, and decomposes the data into several such independent components.

Many software tools are available to implement ICA. For example, probablistic ICA with MELODIC[7] is available with FSL; GIFT and FIT[8] can be applied using SPM; cortex-based ICA can be conducted in BrainVoyager 2000[9]; and ICASSO offers ICA reliability analysis[10] [80].

Although ICA claims to require no initial assumptions, the approach does require specification of the number of components. While toolboxes such as MELODIC can automatically estimate this number through prior PCA-based estimation, in practice, the dimensions are often estimated by the user.

In deriving independent components, ICA extracts components due to "artifactual" signal such as scanner noise, head movement, and physiological "artifacts" (e.g., cardiac and respiratory signal) alongside functionally meaningful networks. While the extraction of these

[7] www.fMRIb.ox.ac.uk/fsl/melodic/index.html
[8] http://icatb.sourceforge.net/
[9] http://www.brainvoyager.com/BrainVoyager.htm
[10] http://www.cis.hut.fi/projects/ica/icasso/

"noise" components is advantageous—such artifact extraction has even been proposed as a preprocessing step for seed-based correlation analysis [81]—it requires that the user exercises judgment in separating meaningful networks from noise components [82–85], or develop classification techniques [86], [84]. Thus, while minimal *a priori* assumptions are required, ICA does require substantial *a posteriori* selection of valid components, whether though visual inspection or automated methods.

Group-level ICA analysis is a substantially more complicated issue due to the difficulty of selecting corresponding components across individuals [87,88]. The order of ICA components is unconstrained, and cannot be used for selection. One approach for classifying a network consistently across individuals is **template matching** [89,90]. Individual-level independent components are first discarded based on temporal criteria (e.g., valid components must consist of characteristic low-frequencies). Then, all remaining individual-level components are compared to a set of researcher-defined spatial templates for "goodness of fit". Although template matching is an effective means for consistent selection of analogous networks across individuals, it relies on assuming appropriate templates.

Group-level ICA would seem like the obvious choice for their derivation; however, it too presents significant complications. One proposed solution is to conduct **group-level ICA** on co-registered and concatenated individual datasets. The group-level results of **temporal concatenation ICA (TC-ICA)** can then be used as templates in order to derive individual-level maps. Such approaches have been fruitful in discerning distinct cortico-cerebellar networks [91].

Dual-regression ICA has recently been developed as a method to derive more accurate group-level comparisons based on TC-ICA templates. After creating the templates, spatial regression is conducted on the individual level to extract a temporal model for a second temporal regression. The resultant statistical maps are then used for group-level analysis [92,25,93].

An alternative, proposed by Calhoun and colleagues [94], addresses the problem of combining components across individuals. Rather than use a template-matching scheme, the individual data sets are entered into a single ICA analysis, and then **back-reconstructed**. This procedure ensures that the components are consistently ordered across individuals.

Other automated group-level approaches aim to cluster components across subjects based on spatial configurations (e.g., **partner-matching** [95]).

2.2 Applications

ICA has been responsible for a significant shift in understanding large-scale network structure in the brain. Owing to its exploratory, data-driven procedure, several networks were consistently classified across studies and subject groups [78,79,96,97]. ICA-derived networks are consistent across participants [79] and scan sessions [98,99], with the default-mode network demonstrating particularly robust reproducibility and cross-research selection reliability [100,101]. ICA has been applied to infants as young as 24 weeks [102] and has also been widely used to study clinical populations (e.g., Alzheimer's disease [89,103], mild cognitive impairment [104], depression [105], schizophrenia [106], Huntington's disease [107], lateral sclerosis [108], temporal lobe epilepsy [109], and non-communicative brain damaged patients [110]).

The impact of data-driven approaches such as ICA was demonstrated in a recent paper by Stephen Smith and colleagues [111]: 20 ICA components were extracted from resting-state data from 36 individuals, as well as 7,342 peak coordinates from the collection of functional studies contained in the BrainMap database. The sets of components were highly consistent, demonstrating the structural persistence of these functional networks at rest, and suggesting that these networks may provide a foundation for discerning the modular building-blocks of cognitive functions.

2.3 Discussion

Blind-source analysis methods are data driven, and do not require specification of seed-regions. However, they are nonetheless hypothesis driven, because the "true" number of components present in the data is not known, and has to be more or less empirically chosen (techniques for the automatic calculation of the number of components exist, and have demonstated high test-retest reliability, but there is poor concordance across the various estimation algorithms [99]). The reproducibility of ICA is another significant challenge. The ICA algorithm begins with a random assumption with each iteration, thus producing results that are variable across analyses.

Secondly, following component identification, the selection of meaningful components remains a problem. Manual selection through visual inspection is prone to human error. While automated methods are promising, they either rely on preexisting templates (i.e., template-matching) or are computationally intensive (i.e., back-reconstruction). Novel methods for automated ICA dimensionality and group-level analysis is an area of ongoing development. Nevertheless, the automaticity and

model-independence of ICA makes it a convenient tool for whole-brain functional connectivity analysis.

One fundamentally dubious assumption of ICA is the independence of network signals in the brain. Considering the extraordinary degree of interconnectivity between the entire brain, striving to derive independent networks would not seem to be an effective method at generating a physiological plausible model of functional organization. Daubechies and colleagues have recently suggested that the ICA algorithms used in fMRI data analysis are tuned to detect sparsity, rather than independence [112], a more likely model.

3 Clustering

Although model-free approaches to resting-state functional connectivity, such as ICA, overcome one of the greatest problems associated with model-based (i.e., seed-based) approaches, namely, the dependence of findings on the initial selection of seed ROIs, these model-free approaches still entail a degree of subjectivity and human judgment both in dimensionality estimation and in the selection of "meaningful" components or networks. One approach that is gaining popularity in the attempt to overcome these issues is the application of clustering techniques to resting-state data.

Clustering is essentially a family of mathematical techniques that searches for patterns in data. More specifically, clustering is the unsupervised partitioning (classification) of data into subsets (clusters) so that observations assigned to the same cluster are more similar to one another than they are to observations assigned to another cluster.

In the context of resting-state functional connectivity analysis, clustering algorithms have been used to partition the brain into groups (clusters) of voxels or regions that are functionally connected with one another [113], or that exhibit similar patterns of functional connectivity with the rest of the brain [115]. The former represents a method akin to ICA, aimed at detecting distinct large-scale resting state networks, while the latter is an emerging approach aimed at breaking the brain down into its smallest detectable distinct functional units. The main results of these studies are briefly reviewed below, but it is worth noting that neuroimaging applications of clustering approaches are not restricted to resting-state studies, as clustering has been applied to structural connectivity (e.g., diffusion tensor imaging), task activation and neurotransmitter receptor data with equally impressive results (e.g., [124–129]).

3.1 Technique

As we have noted, clustering is a family of techniques, and researchers face a plethora of options with regard to the specific clustering approach to apply to their data. In RSFC applications, those most commonly employed include:

- **hierarchical clustering approaches**, which start by treating each data point as a singleton cluster, then, as K decreases, successively merge previously established clusters (visualized as a dendrogram or tree) (e.g., [115,130,131,114]);
- **partitional clustering (such as *k*-means)**, which determine all K clusters at once, typically by attempting to minimize intra-cluster variance (e.g., [130, 132];
- **spectral clustering approaches**, which perform an eigendecomposition of (the graph Laplacian of) the similarity matrix as an initial data reduction step, then use one of the more standard clustering algorithms (e.g., k-means) to perform the final partition of the data on the basis of the resultant matrix of eigenvectors (the data's spectrum) (e.g., [113]).

There are, of course, many other clustering techniques (e.g., non-metric clustering [133]), and the development and improvement of clustering methods is a topic of intense research in fields such as **machine learning** (e.g., [116]), which will be addressed in the following section on **pattern classification**.

3.2 Applications

In the first application of clustering techniques to resting-state functional connectivity data, Cordes and colleagues [131] applied **hierarchical clustering** using single linkage to frequency-specific inter-voxel correlations. Due to the computational complexity involved, the analysis was limited to four slices covering auditory, motor and visual cortex (1300-2400 voxels). They detected several, mostly bilateral clusters that were readily identifiable as functionally distinct areas, including sensorimotor cortex, auditory cortex, fusiform gyrus and primary visual cortex, as well as a number of "nuisance" clusters corresponding to CSF or other artifacts. Furthermore, they demonstrated that, for the majority of clusters detected, cardiac, respiratory and motion-related contributions to functional connectivity between the voxels were minimal.

Salvador and colleagues [114] used hierarchical clustering and **multidimensional scaling** to identify six networks. However, their methods formed clusters that grouped regions according to anatomical location (e.g.,

Table 1 A digest of some representative "resting-state" research articles for each section.

Section	References	Desription
Seed-based Functional Connectivity	Biswal et al. 1995 [16] Margulies et al. 2007 [54] Sun et al. 2005 [30]	Makes use of temporal correlation from a selected region-of-interest, or "seed" region. Now termed "seed-based" functional connectivity, the technique relies (and expands) on the basic premise, which defines it as "the temporal correlation of a neurophysiological index measured in different brain areas."
Independent Component Analysis	De Luca et al. 2006 [96] Damoiseaux et al. 2006 [79] Beckmann et al. 2005 [78]	Assumes that resting-state data is composed as a mixture of unknown, but uncorrelated signals. Decomposes rs-fMRI data into spatially or temporally independent components (networks).
Clustering	van den Heuvel et al. 2008 [113] Salvador et al. 2005 [114] Cohen et al. 2008 [115]	A family of statistical techniques that searches for patterns in data. Unsupervised partitioning (classification) of data into subsets (clusters).
Pattern Recognition	Craddock et al. 2009 [116] Zhu et al. 2008 [117] Shen et al. 2009 [118]	Involves the application of multivariate pattern classification algorithms. These algorithms use the characteristics of objects to identify classes to which they belong. In fMRI data, these characteristics are generally brain activation or connectivity patterns, and the classes are usually brain or cognitive states.
Graph Theory	Bassett & Bullmore 2007 [119] Achard & Bullmore 2007 [120] He et al. 2009 [121]	A mathematical tool whose aim is to characterize aspects of a network structure using a variety of measurements. One such approach characterizes the brain as a *small-world network* .
Local Methods	Zang et al. 2004 [122] Zou et al. 2008 [123] Zuo et al. 2010 [25]	Two measures which quantify the function of the brain locally can be implemented in resting-state fMRI studies: *regional homogeneity* (ReHo) and *amplitude of low frequency fluctuations* (ALFF).

frontal, temporal, subcortical), and thus the resultant networks differ from the resting-state networks with which we are now more familiar. In contrast, Thirion and colleaguees [134] clustered coherence measures of resting-state data using **Gaussian Mixture Models**, and observed several plausible networks, including medial and lateral visual networks, and a bilateral fronto-parietal network, although consistency across the small subject sample was low.

Of course, many of these early clustering studies were limited by the computational capabilities available at the time. As a result, researchers were required to reduce the volume of data entered into their analyses, either by acquiring data from only a limited number of slices, rather than the whole brain [131], or by resampling the brain according to a parcellation scheme (e.g., [114,134]).

More recently however, vast improvements in computational resources have made it possible to perform clustering analyses at the voxel level, permitting the performance of analyses at a finer scale that remains close to that of the original data. Consequently, there is increasing sophistication in the methods employed and, most important, increasing convergence with the results of other resting-state analysis methods (e.g., ICA).

Two exemplars of this increased sophistication and convergence are provided by Van den Heuvel and colleagues [113] and Bellec and colleagues [130]. The first of these studies, by Van den Heuvel and colleagues, used spectral clustering, specifically, the **Ncut** method devised by Shi and Malik [135], to partition whole-brain grey matter on the basis of voxelwise functional connectivity (expressed as temporal correlation) in 26 participants. One notable methodological advance detailed in their paper was the computation of a consistency matrix, which quantifies the frequency with which voxels were assigned to the same cluster across participants. In order to determine group-level clustering solutions, spectral clustering was performed on this consistency matrix, the result being a set of cluster solutions (networks) exhibiting the most consistent (stable) functional connectivity across subjects. Their analysis produced seven networks, strikingly similar to those identified using both seed-based analyses and ICA, including the default mode network, right and left fronto-parietal networks, and a sensorimotor/visual network.

In their paper, Bellec and colleagues [130] also made use of consistency matrices, in the context of a bootstrap approach to k-means clustering of resting state time series, which sought to identify the most stable large-scale networks (clusters) detectable at both the single-subject and group levels. Interestingly, this approach, named "**bootstrap analysis of stable clusters (BASC)**," also identified seven networks that were remarkably similar to those identified in other studies, including the default mode, sensorimotor, visual and fronto-parietal networks. In addition, the authors drew attention to the fact that good stability was observable at finer spatial scales (i.e., larger numbers of clusters), and the likelihood of good agreement between solutions at these finer scales and the results of high dimensional ICA analyses, such as that those of Smith and colleagues [111] and Kiviniemi and colleagues [97].

Several other papers have directly focused on clustering at finer spatial scales. These studies have demonstrated the ability of clustering methods to identify the organization of the brain at the local level, in terms of its division into functionally distinct regions, rather than at the global level of large-scale networks.

For example, Mezer and colleagues [132] applied the k-means clustering algorithm to time-dependent measures of functional connectivity to identify clusters in grey matter, white matter and thalamus that closely matched known anatomical distinctions in terms of cytoarchitecture/microstructure (e.g., Brodmann's areas) and morphology. Interestingly, Mezer and colleagues concluded that their results were primarily driven by non-functional contributions to the BOLD signal, such as head motion, a suggestion that seems overly-pessimistic in the context of their consistency with the resting-state literature.

A more optimistic tone is struck in work by Cohen and colleagues [115], who performed voxelwise hierarchical clustering on the basis of the eta^2 index, which quantifies the pairwise similarity between voxels' functional connectivity profiles. Cohen and colleagues showed that, in a single participant, hierarchical clustering was highly successful at partitioning regions exhibiting different functional connectivity profiles, thus likely constituting functionally distinct areas.

3.3 Discussion

In summary, clustering approaches applied to resting state data have proved highly successful at detecting known functional, anatomical and architectonic subdivisions in the brain. They are not without their flaws however, with the most significant stumbling block being that almost all available techniques require the user to define a number of clusters (K) into which to partition the data. Because the true number of clusters is often unknown (referred to as the **"cluster validity" problem**), researchers typically compute multiple solutions, then use some metric of "goodness" to determine the "optimal" cluster solution from those produced. Unfortunately, however, there is no single or best measure of solution optimality, and different studies have employed different methods or sets of methods (e.g., silhouette distance; linkage threshold; between-group similarity of clustering solutions; minimized Ncut cost; information criteria). Ultimately, it is unlikely that clustering will escape the involvement of human judgment, as users have to assess the suitability of the clustering results against known or hypothesized networks or functional subdivisions. However, the advantage of clustering approaches (as well as ICA approaches), is that this human judgment is incorporated at a high perceptional cluster- or network-level, rather than during the early-stage ROI selection, as is required in seed-based approaches.

4 Pattern Classification

In recent years **multivariate pattern analysis (MVPA)** (also referred to as **multi-voxel pattern analysis**) has gained increasing importance in fMRI data analysis (for reviews, see [136,137]). Like other multivariate approaches (e.g., ICA, clustering) MVPA takes into account multi-voxel patterns of brain activity or connectivity. Information contained in these patterns can then be decoded by applying powerful pattern-classification algorithms. This method thus incorporates spatially distributed patterns of activity into the analysis, unlike univariate methods which treat every brain voxel independently.

MVPA has become a valuable fMRI data analysis method for classifying cognitive states and drawing relationships between neural activity (or connectivity) and these states. MVPA was mainly initiated in the domain of visual perception [138–140], but was extended to other types of mental states as well [141]. MVPA has also been applied to the study of neural coding [137, 142], and utilized in the field of memory research [143].

4.1 Technique

In MVPA, **pattern classification** algorithms assign objects to **classes** using specific **features**. In the analysis of fMRI data, these characteristics are generally patterns of brain activation or connectivity and the

classes are brain states or cognitive states. Introductory guides are available [144,145], as well as easy to use software [146].

In brief, application of the technique entails the following basic steps:

1. Choosing the **features** that are descriptive of the objects and a way to represent them.
2. **Selecting** a subset of these **features** to be used for classification.
3. Selecting the **pattern classification algorithm**.
4. Dividing of the data in two parts: a **"training set"** and a **"testing set"**.
5. Utilizing the training set to train the **classifier** with the features and the prespecified classes of objects. The classifier thus "learns" a functional relationship between the features and the classes.
6. **Testing** of the classification algorithm for its generalization capabilities with the testing set, and measuring the percentage of correct classifications.

Effective feature selection is necessary to prevent the classifier from overfitting the data or reducing complexity. This can be done automatically by using mathematical methods that select relevant discriminative features [147]. Another possibility is **manual feature selection** (e.g., the limitation to certain ROIs). This manual method is of course application specific.

When choosing the proper classifier, certain issues should be considered. In MVPA, a supervised machine learning algorithm is usually used for pattern classification. Examples of such algorithms are support vector machines (SVM), neural networks, or linear discriminant analysis (LDA). They can be used to learn a functional relationship between the features and the classes. Rarely unsupervised machine learners (e.g., clustering) are utilized. Unsupervised algorithms find structure on data without prior knowledge about classes, but one cannot be sure whether it is the desired structure that is found, so supervised learners are normally applied. It is important to state that there is no single algorithm that works best on all problems. There are some classifiers like SVMs that achieve good results for a wide range of problems, but caution is required when relying on this. One thing that can be incorporated when choosing a classifier is knowledge about the functional relationship between the features and the classes. If this relation is assumed to be linear a linear classifier should be used (e,g., LDA, linear SVM). In the non-linear case a technique that can account for non-linearity (e.g., non-linear SVM, neural networks) is advised, although this does not always lead to better results [139]. Finally there are different ways to divide the data into "training set" and "testing set" for testing the generalization capabilities of the classifier. One often-used possibility is cross-validation (see [144] for advantages of this technique).

4.2 Applications

Multivariate pattern classification as applied to resting-state fMRI data is still a young field of research. Similar to its application in task-based studies, it has primarily been used for **disease-state prediction** to discriminate between patients and healthy control groups on the basis of resting-state functional networks.

In a study of attention-deficit / hyperactivity disorder (ADHD), Zhu and colleagues used **principal component analysis-based Fisher discriminative analysis (FDA)** [117] and **pseudo-FDA** [148] for classification. On the basis of **regional homogeneity** as features, they were able to discriminate between patients with ADHD and healthy subjects. The results were also used to identify discriminative regions. They also achieved a high generalization rate when comparing results to **linear support vector machines** and **batch perceptrons**.

Wang and colleagues examined patients with an early stage of Alzheimer's disease using a linear classifier based on ICA and FDA [149]. They put particular emphasis on the choice of features for classification. Correlation coefficients of two intrinsically anti-correlated networks were utilized as features to distinguish patients with Alzheimer's disease from healthy controls. When comparing their classification results to features based on whole-brain functional connectivity, their approach outperformed the latter. They thus concluded that the two anti-correlated networks play an important role in early stages of Alzheimer's disease.

Schizophrenia was investigated by Jafri and colleagues, who used a **three-layer feed-forward neural network** approach to analyze ICA components [150]. Shen et al. utilized a **nonlinear unsupervised-learning classifier** for discrimination and to map statistically relevant regions [118]. They used a **nonlinear learning technique (locally linear embedding)** to reduce dimensionality of the resting-state data. Then **C-means clustering** was applied to discriminate between schizophrenia patients and healthy controls. Classification error rate was very low and it performed better than linear classifiers it was evaluated against.

Major depressive disorder was also the subject of investigation. Craddock and colleagues used a **support vector machine classifier** to distinguish healthy persons from depressed ones [116]. Their focus was on testing different feature selection methods. They incorporated **filter** and **wrapper feature selection** and

also reliability information. This reliability measure improved the results of classification significantly.

These approaches demonstrate that disease-related differences in resting-state functional connectivity are feasible for disease state prediction and for the identification of discriminative regions of the brain.

4.3 Discussion

In summary, the application of MVPA has been successfully expanded to the field of resting-state fMRI. While MVPA has been primarily used in the small domain of disease state prediction, it also has potential for a wider applications in addressing differential functional connectivity across general brain states. MVPA have also prove promising in pharmacological studies where medications and placebos are contrasted.

The small number of studies involving MVPA and resting-state fMRI give rise to many open questions. For instance there are a lack of comparative studies. While a portion of the aforementioned studies do compare different features, feature selection methods or classifiers in a very narrow context, this is far from sufficient to assess various strengths and weaknesses for different applications. For example, it would be valuable to investigate if or how involved features and methods could be applied to diseases other than those included in each respective study.

Another important issue that has not yet been investigated is the influence of spatial resolution. While spatial resolution is a crucial factor for all fMRI approaches, it is of particular interest for pattern classification which aims to detect subtle patterns in the data. Many analyses described here, particularly those involving networks and pattern classification, are conducted at a relatively low-resolution scale (50-100 units). Significant efforts and methodological advances are needed to understand how such findings may generalize to higher resolutions.

5 Graph Theory

The mathematical field of graph theory has developed over centuries to characterize various aspects of network structure. Building on the functional connectivity approaches previously discussed, graph theory can be applied to the brain by positing that regions-of-interest (or single voxels) constitute **vertices**, and the connections between them, **edges**. This insight makes it possible to exploit the already existing graph theory knowledge to analyze functional brain networks. As the techniques thus far presented have predominantly focused on mapping the spatial extent of networks, graph theory, in contrast, provides tools to describe and characterize various intrinsic properties of network configuration (e.g., efficiency and modularity).

5.1 Technique

Given a selected set of regions from a resting-state fMRI data set, **each ROI corresponds to a vertex**, the **edges are defined by the functional connectivity between vertices** (see Figure 2). An edge can be assigned between two vertices if the correlation coefficient exceeds a certain threshold, or each correlation coefficient itself can be used to **weight** each edge. A **path** in a graph is a sequence of vertices in which all succeeding vertices are connected by edges, and the length of a path is the number of edges traversed. The **distance** between two vertices of a graph is the minimum length among all paths connecting them. The **degree** of a vertex is the number of edges connecting to it. The (open) neighborhood of a vertex is all vertices that are connected to it by an edge.

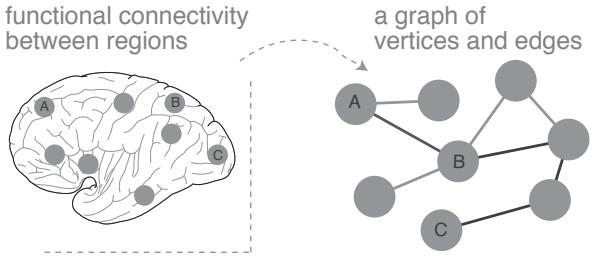

Fig. 2 A schematic illustration depicting the transformation from ROIs to graph representation. The **distance** between vertices A and C is 4, as marked with the darkened line. The **degree** of vertex B is 4, A is 2, and C is 1, as measured by the number of edges connecting to each. Vertex A is part of vertex B's neighborhood, but C is not, because it is not directly connected to B by an edge.

Diestel offers a general introduction to graph theory [151]. For an overview with respect to applications to brain connectivity, see the recent review by Bullmore and Sporns [152]. For implementation, a MATLAB-based "Brain Connectivity Toolbox" is also freely available[11].

5.2 Applications

Numerous measurements have been developed for the characterization of graphs. We will describe **local** mea-

[11] `http://www.brain-connectivity-toolbox.net/`

sures (assigning values to each vertex individually) and **global** measures (characterizing the graph as a whole).

One simple concept to measure the *global structure* of a graph is the **degree distribution** $P(k)$. This function gives the likelihood that a randomly chosen vertex from a graph has degree k. fMRI data have been found to have various degree distributions: power law [153], exponential [154] and exponentially truncated power law [155,156]. These three different findings could be related to the different spatial scales employed by the studies (ROIs *vs.* voxels).

Degree distribution offers information about the number of vertices which have a very high degree, termed: "**hubs**". Such hubs have been the topic of a recent study by Buckner and colleagues [157], who found that regions of high "hub-ness," or **centrality**, were most prone to deterioration in individuals with Alzheimer's disease. **Eigenvector centrality** has also recently been applied to the analysis of fMRI data using both linear correlation and spectral coherence as distance measures [158]. The computational advantage of eigenvector centrality allows for the inclusion of all voxels in the brain.

Degree distribution can also be used to explore the vulnerability of a graph with **random error** and **target attacks** [159]. In "random error", a random vertex is repeatedly deleted from the graph, while "target attack" repeatedly deletes the vertex with the actual highest degree. After each step, the vulnerability of the graph to the attack is then measured using a variety of tools, among them: *clustering coefficient*, *average path length*, *small-world properties*, and *local* and *global efficiency*, which will be further discussed below.

These concepts can be applied to probing the *resilience* or *vulnerability* of the brain's functional organization. For instance, Achard et al. [155] showed that networks observed in wavelet transformed resting-state fMRI data are more resilient to target attacks than a random scale-free network but equally resilient to random error.

One concept used to measure the *local structure* of a graph is the **local clustering coefficient**, which checks whether the triangle between a vertex and two connected vertices is closed by an existing edge. The measurement counts all existing triangles in the neighborhood and divides them by the number of theoretically possible triangles. The clustering coefficient has been interpreted as a measure of resilience to random error [160], since if a vertex is deleted, its neighbors stay connected. The local clustering coefficient can also be used as a global local measurement by averaging over all vertices of a graph.

Another measurement for the global topology is the **average path length** of a graph, which is the mean of all distances between any pair of vertices. The average path length can be understood as a measurement of how well integrated a graph is.

Measures of **modularity** describe how well a network is divisible into separate components ("*modules*") with high internal connectivity, but sparse inter-module connections. He and colleagues found that recognizable sensory and cognitive systems a highly interconnected modules with sparser intermodule connections [121]. Shen and colleagues [161] analyzed the **modularity function** by Newmann [162]—which finds dense substructures in a graph by taking the ratio of the number of *existing* to *theoretically-possible* edges within a community— and two similar approaches called **cut** and **Ncut** on resting-state fMRI data. They concluded that whole-brain parcellation is feasible with the three approaches, and that the **Ncut** algorithm is the appropriate way to do so.

Ferrarini and colleagues [163] described a different approach. Their technique is based on a **non-degree biased cluster coefficient** [164], and the subsequent application of a hierarchical clustering algorithm [165]. Using this approach they showed modularity between frontal, subcortical, parietal and temporal regions of the brain.

Combining these measurements one can characterize a network as being a **small-world network**. This term was first introduced by Watts and Strogatz in 1998 [166], who demonstrated that certain real-world networks have a significantly higher clustering coefficient than their random counterpart, without a significantly higher average path length. They proposed that this could also be the case for many other real-world networks—a hypothesis that was later confirmed by findings ranging from road maps [167], food webs [168], airplane passenger traffic [169], metabolite processing networks [170], mobile call graphs [171], ownership links among German companies [172], and, of course, brain networks [173].

There are certain empirical and theoretical reasons for understanding the brain as a small-world network [119]: the brain supports both modular and distributed processing of information. Considering that network architecture underlies cognitive processing, a network with a small topology is most efficiently configured for various scales of information exchange: high clustering supports modular processing, while short distances support distributed processing. Small-world networks thus maximize efficient parallel processing, minimize wiring costs, and are fault tolerant—all optimal properties of a central nervous system.

Many studies have examined the small-world characteristics of brain networks, and they will not all be

reviewed in detail here. For a comprehensive review of this particular topic, please see the superlative article by Bassett and Bullmore [119]. Small-world analyses seem to have particular relevance for the study of disease states. For example, Supekar et al. [174] performed a study on wavelet transformed resting-state fMRI data acquired from patients with Alzheimer's disease. They observed a significantly reduced clustering coefficient in patients with Alzheimer's disease. Furthermore, the clustering coefficient distinguishes participants with Alzheimer's from controls with high sensitivity and specificity, suggesting the decreased small-world property may be a viable diagnostic marker.

Nakamura et al. [154] used resting-state fMRI data acquired at different time-points during recovery from traumatic brain injury. They showed an increasing "small-worldness" during the recovery process. Hayasaka and Laurienti [175] made a comparison of small-world characteristics between region-based and voxel-based brain networks. They showed that voxel-based networks have a higher clustering coefficient ratio than region-based networks, suggesting that voxel-based networks are more "small-world–like".

In addition to the "classical" small-world parameters, **local** and **global efficiency** can be used to measure the network's ability for information transmission [176]. Although these measurements are very similar, they have the conceptual advantage that they can deal with disconnected graphs. Achard and Bullmore [177] showed lower efficiency in frontal and temporal cortical and subcortical regions in an elderly group of participants. From a more methodological perspective, Wang et al. [178] found different network efficiencies depending on which atlas was used to determine ROIs.

5.3 Discussion

Graph theory offers a host of tools for characterizing brain organization that extend beyond the network itself. While graph theory is effective at analyzing topology, such as small-world or modularity and even changing topology (by deleting hubs), it is not appropriate for the analysis of real-time dynamics. In a sense one also has to pay for the generality of the various graph theory metrics with a loss of specialization. Due to the computational complexity of many of the described approaches, their application to the whole-brain set of voxels is not feasible, and they are in practice applied to groups of voxels of a set of ROIs. Since these regions of interest have to be defined *a priori*, the same problems of ROI selection outlined earlier apply. Undeniably, graph approaches require assumption in order to reduce the complexity of the network. Analytic approaches are computationally difficult, and one must often work with heuristics.

6 "Local" Methods

Although the majority of analytic techniques for resting-state fMRI data address functional connectivity, approaches that address local activity are also possible.

Two such "local" measures are: the **amplitude of low frequency fluctuations (ALFF)**, which calculates the voxelwise magnitude of specific frequency bands in the frequency domain, and **regional homogeneity (ReHo)**, which is computed only from the direct neighborhood of single voxels. The measures are conceptually and practically straightforward, and are complementary to the other resting-state post-processing tools.[12]

6.1 Amplitude of Low Frequency Fluctuations

ALFF is defined as the total power within a defined low-frequency range (for example: 0.01–0.1 Hz) [179, 25]. Fractional ALFF (fALFF), a measure with reduced sensitivity to physiological noise, can be obtained by taking the ratio of the low-frequency power to the sum across the whole frequency range [123].

It should be noted that several physiological and neural factors can impact low frequency fluctuations; for example, Biswal and colleagues observed that low frequency fluctuations were suppressed by hypercapnea [180], and that ALFF was higher in gray matter than in white matter [16]. Some studies showed that ALFF measures are susceptible to possible artifactual findings in the vicinity of blood vessels and cerebral ventricles [123, 25]. Special care has to be taken when reporting results of ALFF calculation near these brain areas.

Areas within the default mode network have been observed to exhibit higher ALFF during resting-state than other areas [181, 179, 123, 25]. ALFF of visual cortices in eyes-open condition was reported to be significantly higher than in eyes-closed condition [181]. Zuo and colleagues revealed significant and highly reliable ranking orders of ALFF among anatomical parcellation units [25]. The method has also been applied in studies which compared clinical populations to healthy controls. Children with ADHD showed decreased ALFF in inferior frontal cortex and increased ALFF in anterior cingulate and left sensorimotor cortex [182]. Patients

[12] Both techniques can be implemented using the MATLAB toolbox REST: `http://groups.google.com/group/fc-toolbox`

with schizophrenia showed reduced ALFF in lingual gyrus, cuneus and precuneus and increased ALFF in left parahippocampal gyrus [183].

6.2 Regional Homogeneity

Zang and colleagues [122] initially proposed ReHo to measure the functional coherence of a given voxel with its nearest neighbors based on the hypothesis that abutting voxels within a functional brain area synchronize their metabolic activity under certain conditions. Homogeneity is measured using **Kendall's coefficient of concordance (KCC)**, a calculation of similarity which uses ranking—a more stable measure—rather than a linear statistical measure.

ReHo analysis is highly affected by the magnitude of spatial smoothing and the size of the "neighborhood" (7, 19, or 27 voxels, respectively) included in the analysis [122]. The pattern of resting-state brain activities obtained using ReHo has been shown to be consistent with the default mode network [122,184]. In a study of cerebellar seed-based functional connectivity, He and colleagues integrated ReHo into the seed-selection process by using the areas of high ReHo to derive coordinates for masks regions [185].

ReHo analysis has been widely applied to the study of brain diseases. For instance, in a group of patients with schizophrenia ReHo values are decreased in bilateral frontal, temporal, occipital, cerebellar posterior, right parietal and left limbic lobes. [186]. Boys with attention deficit hyperactivity disorder showed decreased ReHo in frontal-striatal-cerebellar circuits and increased ReHo in occipital cortex [187]. A study also found significant decreases of ReHo in the posteromedial cortex of patients with Alzheimer's disease [188]. Decreased ReHo in frontal, temporal, parietal lobes and increased ReHo in putamen, frontal, parietal lobes were found in remitted geriatric depression patients [189]. Parkinson's disease (PD) patients showed decreased ReHo in putamen, thalamus and supplementary motor areas and increased ReHo in cerebellum, primary sensorimotor cortex and premotor areas [190]. Paakki and colleagues have demonstrated decreased ReHo in right temporal, frontal and bilateral cerebellar crus 1 areas and increased ReHo in right thalamus, left frontal areas in patients with autism spectrum disorders [191].

Another variation on the ReHo approach was implemented by Uddin and colleagues to measure the **network homogeneity (NetHo)**, which is the KCC for each voxel within a pre-defined network mask [192].

6.3 Discussion

In summary, ReHo and ALFF methods are both easily implemented, straightforward techniques which can be used to characterize spontaneous local brain activity. While initial innovations have made use of such voxel-wise techniques for subsequent functional connectivity analysis, much room remains for exploration.

Conclusions

We hope that the above review has provided a flavor of each of the many options for interrogating brain organization with resting-state fMRI data, the assumptions and advantages of each, and the kinds of questions and hypotheses that they can be employed to evaluate. The release of the *1000 Functional Connectomes* resting-state data consortium[13] leaves little want for analytic fodder [193]. Thus, the challenge in study design may rather shift to cross-polinating methodologies. An exciting area of research has recently blossomed which explores the effects of task and mental state on spontaneous "resting" brain activity [29,194–197] .

Looking forward, the most promising resting-state approaches will successfully integrate multiple sources of information concerning the connectivity of the brain, for example: task-based functional localization providing information about co-activation, diffusion measures of structural connectivity and known anatomical connectivity, as well as data obtained with EEG or MEG, and the simultaneous combination of EEG or optical imaging with fMRI. Several studies have already made considerable strides in these directions (e.g., [62,111, 198–204]), suggesting that researchers will soon witness further exciting methodological advancements that will elevate the field of resting-state functional connectivity to the next level of excellence.

Acknowledgements

The authors wish to thank Jonathan Adelstein and Shereen Chaudhry for helpful suggestions with the manuscript and The Neuro Bureau for continued creative support. Financial support for M.P.M. was provided by grants from the Stavros S. Niarchos Foundation, the Leon Levy Foundation, and Autism Speaks.

References

1. Friston KJ, Frith CD, Liddle PF, Frackowiak RS (1993) Functional connectivity: the principal-component analysis

[13] http://www.nitrc.org/projects/fcon_1000/

of large (PET) data sets. J Cereb Blood Flow Metab, 13, 5–14.
2. Buckner RL, Vincent JL (2007) Unrest at rest: default activity and spontaneous network correlations. Neuroimage, 37, 1091–6; discussion 1097–9.
3. Morcom AM, Fletcher PC (2007) Does the brain have a baseline? why we should be resisting a rest. Neuroimage, 37, 1073–82.
4. Fox MD, Raichle ME (2007) Spontaneous fluctuations in brain activity observed with functional magnetic resonance imaging. Nat Rev Neurosci, 8, 700–711.
5. Lohmann G, Hoehl S, Brauer J, Danielmeier C, Bornkessel-Schlesewsky I, Bahlmann J, Turner R, Friederici A (2010) Setting the frame: the human brain activates a basic low-frequency network for language processing. Cereb Cortex, 20, 1286–1292.
6. Dijk KRAV, Hedden T, Venkataraman A, Evans KC, Lazar SW, Buckner RL (2010) Intrinsic functional connectivity as a tool for human connectomics: theory, properties, and optimization. J Neurophysiol, 103, 297–321.
7. Weissenbacher A, Kasess C, Gerstl F, Lanzenberger R, Moser E, Windischberger C (2009) Correlations and anticorrelations in resting-state functional connectivity MRI: a quantitative comparison of preprocessing strategies. Neuroimage, 47, 1408–1416.
8. Gavrilescu M, Stuart GW, Rossell S, Henshall K, McKay C, Sergejew AA, Copolov D, Egan GF (2008) Functional connectivity estimation in fMRI data: Influence of preprocessing and time course selection. Hum Brain Mapp, 29, 1040–52.
9. Chang C, Glover GH (2009) Effects of model-based physiological noise correction on default mode network anticorrelations and correlations. Neuroimage, 47, 1448–1459.
10. Fox MD, Zhang D, Snyder AZ, Raichle ME (2009) The global signal and observed anticorrelated resting state brain networks. J Neurophysiol, 101, 3270–83.
11. Auer DP (2008) Spontaneous low-frequency blood oxygenation level-dependent fluctuations and functional connectivity analysis of the 'resting' brain. Magn Reson Imaging, 26, 1055–64.
12. Li K, Guo L, Nie J, Li G, Liu T (2009) Review of methods for functional brain connectivity detection using fMRI. Comput Med Imaging Graph, 33, 131–139.
13. Cole DM, Smith SM, Beckmann CF (2010) Advances and pitfalls in the analysis and interpretation of resting-state fmri data. Front Syst Neurosci, 4, 8.
14. Liu Y, Wang K, Yu C, He Y, Zhou Y, Liang M, Wang L, Jiang T (2008) Regional homogeneity, functional connectivity and imaging markers of alzheimer's disease: a review of resting-state fmri studies. Neuropsychologia, 46, 1648–1656.
15. Fornito A, Bullmore ET (2010) What can spontaneous fluctuations of the blood oxygenation-level-dependent signal tell us about psychiatric disorders? Curr Opin Psychiatry.
16. Biswal B, Zerrin Yetkin F, Haughton VM, Hyde JS (1995) Functional connectivity in the motor cortex of resting human brain using echo-planar MRI. Magnetic Resonance in Medicine, 34, 537–541.
17. Zhou D, Thompson WK, Siegle G (2009) MATLAB toolbox for functional connectivity. Neuroimage, 47, 1590–1607.
18. Shulman GL, Fiez JA, Corbetta M, Buckner RL, Miezin FM, Raiche ME, Petersen SE (1997) Common blood flow changes across visual tasks: II. decreases in cerebral cortex. Journal of Cognive Neuroscience, 9, 648–663.
19. Gusnard DA, Raichle ME (2001) Searching for a baseline: functional imaging and the resting human brain. Nat Rev Neurosci, 2, 685–94.
20. Buckner RL, Andrews-Hanna JR, Schacter DL (2008) The brain's default network: anatomy, function, and relevance to disease. Ann N Y Acad Sci, 1124, 1–38.
21. Zhong Y, Wang H, Lu G, Zhang Z, Jiao Q, Liu Y (2009) Detecting functional connectivity in fMRI using PCA and regression analysis. Brain Topogr, 22, 134–44.
22. Mller K, Mildner T, Lohmann G, von Cramon DY (2003) Investigating the stimulus-dependent temporal dynamics of the bold signal using spectral methods. J Magn Reson Imaging, 17, 375–382.
23. Sun FT, Miller LM, D'Esposito M (2004) Measuring interregional functional connectivity using coherence and partial coherence analyses of fMRI data. Neuroimage, 21, 647–58.
24. Cordes D, Haughton VM, Arfanakis K, Carew JD, Turski PA, Moritz CH, Quigley MA, Meyerand ME (2001) Frequencies contributing to functional connectivity in the cerebral cortex in "resting-state" data. AJNR Am J Neuroradiol, 22, 1326–33.
25. Zuo XN, Martino AD, Kelly C, Shehzad ZE, Gee DG, Klein DF, Castellanos FX, Biswal BB, Milham MP (2010) The oscillating brain: complex and reliable. Neuroimage, 49, 1432–1445.
26. Wu CW, Gu H, Lu H, Stein EA, Chen JHH, Yang Y (2008) Frequency specificity of functional connectivity in brain networks. Neuroimage, 42, 1047–55.
27. Salvador R, Martinez A, Pomarol-Clotet E, Gomar J, Vila F, Sarro S, Capdevila A, Bullmore E (2008) A simple view of the brain through a frequency-specific functional connectivity measure. Neuroimage, 39, 279–89.
28. Duff EP, Johnston LA, Xiong J, Fox PT, Mareels I, Egan GF (2008) The power of spectral density analysis for mapping endogenous bold signal fluctuations. Hum Brain Mapp, 29, 778–90.
29. Barnes A, Bullmore ET, Suckling J (2009) Endogenous human brain dynamics recover slowly following cognitive effort. PLoS One, 4, e6626.
30. Sun FT, Miller LM, D'Esposito M (2005) Measuring temporal dynamics of functional networks using phase spectrum of fMRI data. Neuroimage, 28, 227–37.
31. Fisher RA (1924) The distribution of the partial correlation coefficient. Metron, 3, 329–332.
32. Zhang ZQQ, Lu GMM, Zhong Y, Tan QFF, Zhu JGG, Jiang L, Chen ZLL, Wang ZQQ, Shi JXX, Zang YFF, Liu YJJ (2008) Application of amplitude of low-frequency fluctuation to the temporal lobe epilepsy with bilateral hippocampal sclerosis: an fMRI study. Zhonghua Yi Xue Za Zhi, 88, 1594–8.
33. Fransson P, Marrelec G (2008) The precuneus/posterior cingulate cortex plays a pivotal role in the default mode network: Evidence from a partial correlation network analysis. Neuroimage, 42, 1178–84.
34. Granger CWJ (1969) Investigating causal relations by econometric models and cross-spectral methods. Econometrica, 37, 424–438.
35. Sridharan D, Levitin DJ, Menon V (2008) A critical role for the right fronto-insular cortex in switching between central-executive and default-mode networks. Proc Natl Acad Sci U S A, 105, 12569–74.
36. Uddin LQ, Kelly AMC, Biswal BB, Castellanos FX, Milham MP (2009) Functional connectivity of default mode network components: correlation, anticorrelation, and causality. Hum Brain Mapp, 30, 625–37.
37. Stevens MC, Pearlson GD, Calhoun VD (2009) Changes in the interaction of resting-state neural networks from adolescence to adulthood. Hum Brain Mapp, 30, 2356–66.
38. Hemmelmann D, Ungureanu M, Hesse W, Wstenberg T, Reichenbach JR, Witte OW, Witte H, Leistritz L (2009)

Modelling and analysis of time-variant directed interrelations between brain regions based on bold-signals. Neuroimage, 45, 722–737.
39. Xiong J, Parsons LM, Gao JH, Fox PT (1999) Interregional connectivity to primary motor cortex revealed using MRI resting state images. Hum Brain Mapp, 8, 151–6.
40. Lowe MJ, Mock BJ, Sorenson JA (1998) Functional connectivity in single and multislice echoplanar imaging using resting-state fluctuations. Neuroimage, 7, 119–32.
41. Cordes D, Haughton VM, Arfanakis K, Wendt GJ, Turski PA, Moritz CH, Quigley MA, Meyerand ME (2000) Mapping functionally related regions of brain with functional connectivity MR imaging. AJNR Am J Neuroradiol, 21, 1636–44.
42. Hampson M, Olson IR, Leung HCC, Skudlarski P, Gore JC (2004) Changes in functional connectivity of human MT/V5 with visual motion input. Neuroreport, 15, 1315–9.
43. Lowe MJ, Dzemidzic M, Lurito JT, Mathews VP, Phillips MD (2000) Correlations in low-frequency bold fluctuations reflect cortico-cortical connections. Neuroimage, 12, 582–587.
44. Hampson M, Peterson BS, Skudlarski P, Gatenby JC, Gore JC (2002) Detection of functional connectivity using temporal correlations in MR images. Hum Brain Mapp, 15, 247–62.
45. Allen G, McColl R, Barnard H, Ringe WK, Fleckenstein J, Cullum CM (2005) Magnetic resonance imaging of cerebellar-prefrontal and cerebellar-parietal functional connectivity. Neuroimage, 28, 39–48.
46. Greicius MD, Krasnow B, Reiss AL, Menon V (2003) Functional connectivity in the resting brain: a network analysis of the default mode hypothesis. Proc Natl Acad Sci U S A, 100, 253–8.
47. Gusnard DA, Akbudak E, Shulman GL, Raichle ME (2001) Medial prefrontal cortex and self-referential mental activity: relation to a default mode of brain function. Proc Natl Acad Sci U S A, 98, 4259–64.
48. Raichle ME, MacLeod AM, Snyder AZ, Powers WJ, Gusnard DA, Shulman GL (2001) A default mode of brain function. Proc Natl Acad Sci U S A, 98, 676–82.
49. Postuma RB, Dagher A (2006) Basal ganglia functional connectivity based on a meta-analysis of 126 positron emission tomography and functional magnetic resonance imaging publications. Cereb Cortex, 16, 1508–1521.
50. Bush, Luu, Posner (2000) Cognitive and emotional influences in anterior cingulate cortex. Trends Cogn Sci, 4, 215–222.
51. Stoodley CJ, Schmahmann JD (2009) Functional topography in the human cerebellum: a meta-analysis of neuroimaging studies. Neuroimage, 44, 489–501.
52. Martino AD, Scheres A, Margulies DS, Kelly AMC, Uddin LQ, Shehzad Z, Biswal B, Walters JR, Castellanos FX, Milham MP (2008) Functional connectivity of human striatum: a resting state fMRI study. Cereb Cortex, 18, 2735–2747.
53. Robinson S, Basso G, Soldati N, Sailer U, Jovicich J, Bruzzone L, Kryspin-Exner I, Bauer H, Moser E (2009) A resting state network in the motor control circuit of the basal ganglia. BMC Neurosci, 10, 137.
54. Margulies DS, Kelly AMC, Uddin LQ, Biswal BB, Castellanos FX, Milham MP (2007) Mapping the functional connectivity of anterior cingulate cortex. Neuroimage, 37, 579–88.
55. Krienen FM, Buckner RL (2009) Segregated frontocerebellar circuits revealed by intrinsic functional connectivity. Cereb Cortex, 19, 2485–97.
56. O'Reilly JX, Beckmann CF, Tomassini V, Ramnani N, Johansen-Berg H (2010) Distinct and overlapping functional zones in the cerebellum defined by resting state functional connectivity. Cereb Cortex, 20, 953–965.
57. Roy AK, Shehzad Z, Margulies DS, Kelly AMC, Uddin LQ, Gotimer K, Biswal BB, Castellanos FX, Milham MP (2009) Functional connectivity of the human amygdala using resting state fMRI. Neuroimage, 45, 614–626.
58. Etkin A, Prater KE, Schatzberg AF, Menon V, Greicius MD (2009) Disrupted amygdalar subregion functional connectivity and evidence of a compensatory network in generalized anxiety disorder. Arch Gen Psychiatry, 66, 1361–72.
59. Kahn I, Andrews-Hanna JR, Vincent JL, Snyder AZ, Buckner RL (2008) Distinct cortical anatomy linked to subregions of the medial temporal lobe revealed by intrinsic functional connectivity. J Neurophysiol, 100, 129–139.
60. Eckert MA, Kamdar NV, Chang CE, Beckmann CF, Greicius MD, Menon V (2008) A cross-modal system linking primary auditory and visual cortices: evidence from intrinsic fMRI connectivity analysis. Hum Brain Mapp, 29, 848–57.
61. Nioche C, Cabanis EA, Habas C (2009) Functional connectivity of the human red nucleus in the brain resting state at 3T. AJNR Am J Neuroradiol, 30, 396–403.
62. Margulies DS, Vincent JL, Kelly C, Lohmann G, Uddin LQ, Biswal BB, Villringer A, Castellanos FX, Milham MP, Petrides M (2009) Precuneus shares intrinsic functional architecture in humans and monkeys. Proc Natl Acad Sci U S A, 106, 20069–74.
63. van den Heuvel MP, Pol HEH (2010) Specific somatotopic organization of functional connections of the primary motor network during resting state. Hum Brain Mapp, 31, 631–644.
64. Fox MD, Corbetta M, Snyder AZ, Vincent JL, Raichle ME (2006) Spontaneous neuronal activity distinguishes human dorsal and ventral attention systems. Proc Natl Acad Sci U S A, 103, 10046–10051.
65. Vincent JL, Snyder AZ, Fox MD, Shannon BJ, Andrews JR, Raichle ME, Buckner RL (2006) Coherent spontaneous activity identifies a hippocampal-parietal memory network. J Neurophysiol, 96, 3517–31.
66. Vincent JL, Kahn I, Snyder AZ, Raichle ME, Buckner RL (2008) Evidence for a frontoparietal control system revealed by intrinsic functional connectivity. J Neurophysiol, 100, 3328–42.
67. Vincent JL, Patel GH, Fox MD, Snyder AZ, Baker JT, Van Essen DC, Zempel JM, Snyder LH, Corbetta M, Raichle ME (2007) Intrinsic functional architecture in the anaesthetized monkey brain. Nature, 447, 83–6.
68. Vincent JL, Kahn I, Essen DCV, Buckner RL (2010) Functional connectivity of the macaque posterior parahippocampal cortex. J Neurophysiol, 103, 793–800.
69. Pawela CP, Biswal BB, Cho YR, Kao DS, Li R, Jones SR, Schulte ML, Matloub HS, Hudetz AG, Hyde JS (2008) Resting-state functional connectivity of the rat brain. Magn Reson Med, 59, 1021–9.
70. Kannurpatti SS, Biswal BB, Kim YR, Rosen BR (2008) Spatio-temporal characteristics of low-frequency bold signal fluctuations in isoflurane-anesthetized rat brain. Neuroimage, 40, 1738–47.
71. Shehzad Z, Kelly AMC, Reiss PT, Gee DG, Gotimer K, Uddin LQ, Lee SH, Margulies DS, Roy AK, Biswal BB, Petkova E, Castellanos FX, Milham MP (2009) The resting brain: Unconstrained yet reliable. Cereb Cortex, 19, 2209–29.
72. Dosenbach NUF, Fair DA, Miezin FM, Cohen AL, Wenger KK, Dosenbach RAT, Fox MD, Snyder AZ, Vincent JL, Raichle ME, Schlaggar BL, Petersen SE (2007) Distinct brain networks for adaptive and stable task control in humans. Proc Natl Acad Sci U S A, 104, 11073–8.

73. Kennedy DN, Lange N, Makris N, Bates J, Meyer J, Caviness VS (1998) Gyri of the human neocortex: an MRI-based analysis of volume and variance. Cereb Cortex, 8, 372–384.
74. Makris N, Meyer JW, Bates JF, Yeterian EH, Kennedy DN, Caviness VS (1999) MRI-based topographic parcellation of human cerebral white matter and nuclei II. rationale and applications with systematics of cerebral connectivity. Neuroimage, 9, 18–45.
75. Toro R, Fox PT, Paus T (2008) Functional coactivation map of the human brain. Cereb Cortex, 18, 2553–2559.
76. Kiviniemi V, Kantola JH, Jauhiainen J, Hyvrinen A, Tervonen O (2003) Independent component analysis of nondeterministic fMRI signal sources. Neuroimage, 19, 253–260.
77. van de Ven VG, Formisano E, Prvulovic D, Roeder CH, Linden DE (2004) Functional connectivity as revealed by spatial independent component analysis of fMRI measurements during rest. Hum Brain Mapp, 22, 165–78.
78. Beckmann CF, DeLuca M, Devlin JT, Smith SM (2005) Investigations into resting-state connectivity using independent component analysis. Philos Trans R Soc Lond B Biol Sci, 360, 1001–13.
79. Damoiseaux JS, Rombouts SA, Barkhof F, Scheltens P, Stam CJ, Smith SM, Beckmann CF (2006) Consistent resting-state networks across healthy subjects. Proc Natl Acad Sci U S A, 103, 13848–53.
80. Himberg J, Hyvrinen A, Esposito F (2004) Validating the independent components of neuroimaging time series via clustering and visualization. Neuroimage, 22, 1214–1222.
81. Arfanakis K, Cordes D, Haughton VM, Moritz CH, Quigley MA, Meyerand ME (2000) Combining independent component analysis and correlation analysis to probe interregional connectivity in fMRI task activation datasets. Magn Reson Imaging, 18, 921–30.
82. Thomas CG, Harshman RA, Menon RS (2002) Noise reduction in bold-based fMRI using component analysis. Neuroimage, 17, 1521–1537.
83. Perlbarg V, Bellec P, Anton JL, Plgrini-Issac M, Doyon J, Benali H (2007) Corsica: correction of structured noise in fMRI by automatic identification of ICA components. Magn Reson Imaging, 25, 35–46.
84. Tohka J, Foerde K, Aron AR, Tom SM, Toga AW, Poldrack RA (2008) Automatic independent component labeling for artifact removal in fMRI. Neuroimage, 39, 1227–1245.
85. Starck T, Remes J, Nikkinen J, Tervonen O, Kiviniemi V (2010) Correction of low-frequency physiological noise from the resting state BOLD fMRI-effect on ICA default mode analysis at 1.5T. J Neurosci Methods, 186, 179–185.
86. Martino FD, Gentile F, Esposito F, Balsi M, Salle FD, Goebel R, Formisano E (2007) Classification of fMRI independent components using IC-fingerprints and support vector machine classifiers. Neuroimage, 34, 177–194.
87. Guo Y, Pagnoni G (2008) A unified framework for group independent component analysis for multi-subject fMRI data. Neuroimage, 42, 1078–1093.
88. Calhoun VD, Liu J, Adali T (2009) A review of group ICA for fMRI data and ICA for joint inference of imaging, genetic, and ERP data. Neuroimage, 45, S163–S172.
89. Greicius MD, Srivastava G, Reiss AL, Menon V (2004) Default-mode network activity distinguishes Alzheimer's disease from healthy aging: evidence from functional MRI. Proc Natl Acad Sci U S A, 101, 4637–42.
90. Seeley WW, Crawford RK, Zhou J, Miller BL, Greicius MD (2009) Neurodegenerative diseases target large-scale human brain networks. Neuron, 62, 42–52.
91. Habas C, Kamdar N, Nguyen D, Prater K, Beckmann CF, Menon V, Greicius MD (2009) Distinct cerebellar contributions to intrinsic connectivity networks. J Neurosci, 29, 8586–94.
92. Filippini N, MacIntosh BJ, Hough MG, Goodwin GM, Frisoni GB, Smith SM, Matthews PM, Beckmann CF, Mackay CE (2009) Distinct patterns of brain activity in young carriers of the APOe-epsilon4 allele. Proc Natl Acad Sci U S A, 106, 7209–7214.
93. Beckmann CF, Mackay CE, Filippini N, Smith SM (2009) Group comparison of resting-state fMRI data using multi-subject ICA and dual regression. NeuroImage, 47, S39–S41.
94. Calhoun VD, Adali T, McGinty VB, Pekar JJ, Watson TD, Pearlson GD (2001) fMRI activation in a visual-perception task: network of areas detected using the general linear model and independent components analysis. Neuroimage, 14, 1080–8.
95. Wang Z, Peterson BS (2008) Partner-matching for the automated identification of reproducible ICA components from fMRI datasets: algorithm and validation. Hum Brain Mapp, 29, 875–893.
96. De Luca M, Beckmann CF, De Stefano N, Matthews PM, Smith SM (2006) fMRI resting state networks define distinct modes of long-distance interactions in the human brain. Neuroimage, 29, 1359–67.
97. Kiviniemi V, Starck T, Remes J, Long X, Nikkinen J, Haapea M, Veijola J, Moilanen I, Isohanni M, Zang YF, Tervonen O (2009) Functional segmentation of the brain cortex using high model order group PICA. Hum Brain Mapp, 30, 3865–3886.
98. Chen S, Ross TJ, Zhan W, Myers CS, Chuang KS, Heishman SJ, Stein EA, Yang Y (2008) Group independent component analysis reveals consistent resting-state networks across multiple sessions. Brain Res, 1239, 141–151.
99. Zuo XN, Kelly C, Adelstein JS, Klein DF, Castellanos FX, Milham MP (2010) Reliable intrinsic connectivity networks: Test-retest evaluation using ICA and dual regression approach. Neuroimage, 49, 2163–2177.
100. Meindl T, Teipel S, Elmouden R, Mueller S, Koch W, Dietrich O, Coates U, Reiser M, Glaser C (2010) Test-retest reproducibility of the default-mode network in healthy individuals. Hum Brain Mapp, 31, 237–246.
101. Franco AR, Pritchard A, Calhoun VD, Mayer AR (2009) Interrater and intermethod reliability of default mode network selection. Hum Brain Mapp, 30, 2293–303.
102. Fransson P, Skiőld B, Horsch S, Nordell A, Blennow M, Lagercrantz H, Aden U (2007) Resting-state networks in the infant brain. Proc Natl Acad Sci U S A, 104, 15531–6.
103. Sorg C, Riedl V, Muhlau M, Calhoun VD, Eichele T, Laer L, Drzezga A, Forstl H, Kurz A, Zimmer C, Wohlschlager AM (2007) Selective changes of resting-state networks in individuals at risk for Alzheimer's disease. Proc Natl Acad Sci U S A, 104, 18760–5.
104. Qi Z, Wu X, Wang Z, Zhang N, Dong H, Yao L, Li K (2010) Impairment and compensation coexist in amnestic MCI default mode network. Neuroimage, 50, 48–55.
105. Greicius MD, Flores BH, Menon V, Glover GH, Solvason HB, Kenna H, Reiss AL, Schatzberg AF (2007) Resting-state functional connectivity in major depression: abnormally increased contributions from subgenual cingulate cortex and thalamus. Biol Psychiatry, 62, 429–37.
106. Jafri MJ, Pearlson GD, Stevens M, Calhoun VD (2008) A method for functional network connectivity among spatially independent resting-state components in schizophrenia. Neuroimage, 39, 1666–81.
107. Wolf RC, Sambataro F, Vasic N, Schnfeldt-Lecuona C, Ecker D, Landwehrmeyer B (2008) Aberrant connectivity of lateral prefrontal networks in presymptomatic huntington's disease. Exp Neurol, 213, 137–144.
108. Mohammadi B, Kollewe K, Samii A, Krampfl K, Dengler R, Münte TF (2009) Changes of resting state brain networks in amyotrophic lateral sclerosis. Exp Neurol, 217, 147–53.

109. Zhang Z, Lu G, Zhong Y, Tan Q, Yang Z, Liao W, Chen Z, Shi J, Liu Y (2009) Impaired attention network in temporal lobe epilepsy: A resting fMRI study. Neurosci Lett, 458, 97–101.
110. Vanhaudenhuyse A, Noirhomme Q, Tshibanda LJF, Bruno MAA, Boveroux P, Schnakers C, Soddu A, Perlbarg V, Ledoux D, Brichant JFF, Moonen G, Maquet P, Greicius MD, Laureys S, Boly M (2010) Default network connectivity reflects the level of consciousness in non-communicative brain-damaged patients. Brain, 133, 161–71.
111. Smith SM, Fox PT, Miller KL, Glahn DC, Fox PM, Mackay CE, Filippini N, Watkins KE, Toro R, Laird AR, Beckmann CF (2009) Correspondence of the brain's functional architecture during activation and rest. Proc Natl Acad Sci U S A, 106, 13040–5.
112. Daubechies I, Roussos E, Takerkart S, Benharrosh M, Golden C, D'Ardenne K, Richter W, Cohen JD, Haxby J (2009) Independent component analysis for brain fMRI does not select for independence. Proc Natl Acad Sci U S A, 106, 10415–10422.
113. van den Heuvel M, Mandl R, Hulshoff Pol H (2008) Normalized cut group clustering of resting-state fMRI data. PLoS One, 3, e2001.
114. Salvador R, Suckling J, Coleman MR, Pickard JD, Menon D, Bullmore E (2005) Neurophysiological architecture of functional magnetic resonance images of human brain. Cereb Cortex, 15, 1332–42.
115. Cohen AL, Fair DA, Dosenbach NU, Miezin FM, Dierker D, Van Essen DC, Schlaggar BL, Petersen SE (2008) Defining functional areas in individual human brains using resting functional connectivity MRI. Neuroimage, 41, 45–57.
116. Craddock RC, Holtzheimer rP.E., Hu XP, Mayberg HS (2009) Disease state prediction from resting state functional connectivity. Magn Reson Med, 62, 1619–28.
117. Zhu CZ, Zang YF, Cao QJ, Yan CG, He Y, Jiang TZ, Sui MQ, Wang YF (2008) Fisher discriminative analysis of resting-state brain function for attention-deficit/hyperactivity disorder. Neuroimage, 40, 110–20.
118. Shen H, Wang L, Liu Y, Hu D (2010) Discriminative analysis of resting-state functional connectivity patterns of schizophrenia using low dimensional embedding of fMRI. Neuroimage, 49, 3110–21.
119. Bassett DS, Bullmore E (2006) Small-world brain networks. Neuroscientist, 12, 512–523.
120. Achard S, Bullmore E (2007) Efficiency and cost of economical brain functional networks. PLoS Comput Biol, 3, e17.
121. He Y, Wang J, Wang L, Chen ZJ, Yan C, Yang H, Tang H, Zhu C, Gong Q, Zang Y, Evans AC (2009) Uncovering intrinsic modular organization of spontaneous brain activity in humans. PLoS ONE, 4, e5226.
122. Zang Y, Jiang T, Lu Y, He Y, Tian L (2004) Regional homogeneity approach to fMRI data analysis. Neuroimage, 22, 394–400.
123. Zou QHH, Zhu CZZ, Yang Y, Zuo XNN, Long XYY, Cao QJJ, Wang YFF, Zang YFF (2008) An improved approach to detection of amplitude of low-frequency fluctuation (ALFF) for resting-state fMRI: fractional ALFF. J Neurosci Methods, 172, 137–41.
124. Beckmann M, Johansen-Berg H, Rushworth MF (2009) Connectivity-based parcellation of human cingulate cortex and its relation to functional specialization. J Neurosci, 29, 1175–90.
125. Klein JC, Behrens TE, Robson MD, Mackay CE, Higham DJ, Johansen-Berg H (2007) Connectivity-based parcellation of human cortex using diffusion MRI: Establishing reproducibility, validity and observer independence in BA 44/45 and SMA/pre-SMA. Neuroimage, 34, 204–11.
126. Palomero-Gallagher N, Vogt BA, Schleicher A, Mayberg HS, Zilles K (2009) Receptor architecture of human cingulate cortex: evaluation of the four-region neurobiological model. Hum Brain Mapp, 30, 2336–55.
127. Fischer H, Hennig J (1999) Neural network-based analysis of mr time series. Magn Reson Med, 41, 124–131.
128. Goutte C, Toft P, Rostrup E, Nielsen F, Hansen LK (1999) On clustering fmri time series. Neuroimage, 9, 298–310.
129. Wismüller A, Lange O, Dersch DR, Leinsinger GL, Hahn K, Pütz B, Auer D (2004) Cluster analysis of biomedical image time-series. International Journal of Computer Vision, 46, 103–28.
130. Bellec P, Rosa-Neto P, Lyttelton OC, Benali H, Evans AC (2010) Multi-level bootstrap analysis of stable clusters in resting-state fmri. Neuroimage, 51, 1126–1139.
131. Cordes D, Haughton V, Carew JD, Arfanakis K, Maravilla K (2002) Hierarchical clustering to measure connectivity in fMRI resting-state data. Magn Reson Imaging, 20, 305–17.
132. Mezer A, Yovel Y, Pasternak O, Gorfine T, Assaf Y (2009) Cluster analysis of resting-state fMRI time series. Neuroimage, 45, 1117–25.
133. Wismüller A, Lange O, Auer D, Leinsinger G (2010) Model-free functional mri analysis for detecting low-frequency functional connectivity in the human brain. Society of Photo-Optical Instrumentation Engineers (SPIE) Conference Series, mar, vol. 7624 of Presented at the Society of Photo-Optical Instrumentation Engineers (SPIE) Conference.
134. Thirion B, Dodel S, Poline JB (2006) Detection of signal synchronizations in resting-state fMRI datasets. Neuroimage, 29, 321–7.
135. Shi J, Malik J (2000) Normalized cuts and image segmentation. IEEE transactions on pattern analysis and machine intelligence, 22, 888–905.
136. Norman KA, Polyn SM, Detre GJ, Haxby JV (2006) Beyond mind-reading: multi-voxel pattern analysis of fMRI data. Trends Cogn Sci, 10, 424–430.
137. Haynes JD, Rees G (2006) Decoding mental states from brain activity in humans. Nat Rev Neurosci, 7, 523–534.
138. Haxby JV, Gobbini MI, Furey ML, Ishai A, Schouten JL, Pietrini P (2001) Distributed and overlapping representations of faces and objects in ventral temporal cortex. Science, 293, 2425–2430.
139. Cox DD, Savoy RL (2003) Functional magnetic resonance imaging (fMRI) "brain reading": detecting and classifying distributed patterns of fMRI activity in human visual cortex. Neuroimage, 19, 261–270.
140. Haynes JD, Rees G (2005) Predicting the orientation of invisible stimuli from activity in human primary visual cortex. Nat Neurosci, 8, 686–691.
141. Haynes JD, Sakai K, Rees G, Gilbert S, Frith C, Passingham RE (2007) Reading hidden intentions in the human brain. Curr Biol, 17, 323–328.
142. Kriegeskorte N, Goebel R, Bandettini P (2006) Information-based functional brain mapping. Proc Natl Acad Sci U S A, 103, 3863–3868.
143. Polyn SM, Natu VS, Cohen JD, Norman KA (2005) Category-specific cortical activity precedes retrieval during memory search. Science, 310, 1963–1966.
144. Pereira F, Mitchell T, Botvinick M (2009) Machine learning classifiers and fMRI: a tutorial overview. Neuroimage, 45, S199–S209.
145. Mur M, Bandettini PA, Kriegeskorte N (2009) Revealing representational content with pattern-information fMRI–an introductory guide. Soc Cogn Affect Neurosci, 4, 101–109.

146. Hanke M, Halchenko YO, Sederberg PB, Hanson SJ, Haxby JV, Pollmann S (2009) PyMVPA: A python toolbox for multivariate pattern analysis of fMRI data. Neuroinformatics, 7, 37–53.
147. Guyon I, Elisseeff A (2003) An introduction to variable and feature selection. J. Mach. Learn. Res., 3, 1157–1182.
148. Zhu CZ, Zang YF, Liang M, Tian LX, He Y, Li XB, Sui MQ, Wang YF, Jiang TZ (2005) Discriminative analysis of brain function at resting-state for attention-deficit/hyperactivity disorder. Med Image Comput Comput Assist Interv, 8, 468–75.
149. Wang K, Jiang T, Liang M, Wang L, Tian L, Zhang X, Li K, Liu Z (2006) Discriminative analysis of early Alzheimer's disease based on two intrinsically anti-correlated networks with resting-state fMRI. Med Image Comput Comput Assist Interv, 9, 340–7.
150. Jafri MJ, Calhoun VD (2006) Functional classification of schizophrenia using feed forward neural networks. Conf Proc IEEE Eng Med Biol Soc, Suppl, 6631–4.
151. Diestel R (2005) Graph Theory, vol. 173 of Graduate Texts in Mathematics. Springer, 3rd edn.
152. Bullmore E, Sporns O (2009) Complex brain networks: graph theoretical analysis of structural and functional systems. Nat Rev Neurosci, 10, 186–198.
153. Eguluz VM, Chialvo DR, Cecchi GA, Baliki M, Apkarian AV (2005) Scale-free brain functional networks. Phys Rev Lett, 94, 018102.
154. Nakamura T, Hillary FG, Biswal BB (2009) Resting network plasticity following brain injury. PLoS ONE, 4, e8220.
155. Achard S, Salvador R, Whitcher B, Suckling J, Bullmore E (2006) A resilient, low-frequency, small-world human brain functional network with highly connected association cortical hubs. J. Neurosci., 26, 63–72.
156. Wang L, Zhu C, He Y, Zang Y, Cao Q, Zhang H, Zhong Q, Wang Y (2009) Altered small-world brain functional networks in children with attention-deficit/hyperactivity disorder. Hum Brain Mapp, 30, 638–49.
157. Buckner RL, Sepulcre J, Talukdar T, Krienen FM, Liu H, Hedden T, Andrews-Hanna JR, Sperling RA, Johnson KA (2009) Cortical hubs revealed by intrinsic functional connectivity: mapping, assessment of stability, and relation to Alzheimer's disease. J Neurosci, 29, 1860–1873.
158. Lohmann G, Margulies DS, Horstmann A, Pleger B, Lepsien J, Goldhahn D, Schloegl H, Stumvoll M, Villringer A, Turner R (2010) Eigenvector centrality mapping for analyzing connectivity patterns in fmri data of the human brain. PLoS One, 5, e10232.
159. Reka A, Barabási (2002) Statistical mechanics of complex networks. Rev. Mod. Phys., 74, 47–97.
160. Stam CJ, Reijneveld JC (2007) Graph theoretical analysis of complex networks in the brain. Nonlinear Biomed Phys, 1, 3.
161. Shen X, Papademetris X, Constable RT (2010) Graph-theory based parcellation of functional subunits in the brain from resting-state fMRI data. Neuroimage, 50, 1027–35.
162. Newman MEJ (2006) Modularity and community structure in networks. Proceedings of the National Academy of Sciences, 103, 8577–8582.
163. Ferrarini L, Veer IM, Baerends E, van Tol MJJ, Renken RJ, van der Wee NJ, Veltman DJ, Aleman A, Zitman FG, Penninx BW, van Buchem MA, Reiber JH, Rombouts SA, Milles J (2009) Hierarchical functional modularity in the resting-state human brain. Human brain mapping, 30, 2220–2231.
164. Soffer SN, Vázquez A (2005) Network clustering coefficient without degree-correlation biases. Phys. Rev. E, 71, 057101.
165. Sokal RR, Michener CD (1958) A statistical method for evaluating systematic relationships. University of Kansas Scientific Bulletin, 28, 1409–1438.
166. Watts DJ, Strogatz SH (1998) Collective dynamics of "small-world" networks. Nature, 393, 440–442.
167. Jiang B, Claramunt C (2004) Topological analysis of urban street networks. Environment and Planning B: Planning and Design, 31, 151–162.
168. MONTOYA JM, SOL RV (2002) Small world patterns in food webs. Journal of Theoretical Biology, 214, 405–412.
169. Amaral LAN, Scala A, Barth M, Stanley HE (2000) Classes of small-world networks. Proceedings of the National Academy of Sciences of the United States of America, 97, 11149–11152.
170. Fell DA, Wagner A (2000) The small world of metabolism. Nature Biotechnology, 18, 1121–1122.
171. Nanavati AA, Gurumurthy S, Das G, Chakraborty D, Dasgupta K, Mukherjea S, Joshi A (2006) On the structural properties of massive telecom call graphs: findings and implications. CIKM '06: Proceedings of the 15th ACM International Conference on Information and Knowledge management, pp. 435–444, ACM.
172. Kogut B, Walker G (2001) The small world of germany and the durability of national networks. American Sociological Review, 66, 317–335.
173. Sporns O, Zwi JD (2004) The small world of the cerebral cortex. Neuroinformatics, 2, 145–162.
174. Supekar K, Menon V, Rubin D, Musen M, Greicius MD (2008) Network analysis of intrinsic functional brain connectivity in Alzheimer's disease. PLoS Comput Biol, 4, e1000100.
175. Hayasaka S, Laurienti PJ (2010) Comparison of characteristics between region-and voxel-based network analyses in resting-state fMRI data. NeuroImage, 50, 499–508.
176. Latora V, Marchiori M (2001) Efficient behavior of small-world networks. Physical Review Letters, 87, 198701+.
177. Achard S, Bullmore E (2007) Efficiency and cost of economical brain functional networks. PLoS Comput Biol, 3, e17.
178. Wang J, Wang L, Zang Y, Yang H, Tang H, Gong Q, Chen Z, Zhu C, He Y (2009) Parcellation-dependent small-world brain functional networks: A resting-state fMRI study. Hum Brain Mapp, 30, 1511–23.
179. Zang YFF, He Y, Zhu CZZ, Cao QJJ, Sui MQQ, Liang M, Tian LXX, Jiang TZZ, Wang YFF (2007) Altered baseline brain activity in children with ADHD revealed by resting-state functional MRI. Brain Dev, 29, 83–91.
180. Biswal B, Hudetz AG, Yetkin FZ, Haughton VM, Hyde JS (1997) Hypercapnia reversibly suppresses low-frequency fluctuations in the human motor cortex during rest using echo-planar MRI. J Cereb Blood Flow Metab, 17, 301–308.
181. Yang H, Long XYY, Yang Y, Yan H, Zhu CZZ, Zhou XPP, Zang YFF, Gong QYY (2007) Amplitude of low frequency fluctuation within visual areas revealed by resting-state functional MRI. Neuroimage, 36, 144–52.
182. Cao QJ, Zang YF, Wang YF (2007) [brain functions in attention deficit hyperactivity disorder combined and inattentive subtypes: A resting-state functional magnetic resonance imaging study]. Beijing Da Xue Xue Bao, 39, 261–5.
183. Hoptman MJ, Zuo XNN, Butler PD, Javitt DC, D'Angelo D, Mauro CJ, Milham MP (2010) Amplitude of low-frequency oscillations in schizophrenia: A resting state fMRI study. Schizophr Res, 117, 13–20.
184. Long XYY, Zuo XNN, Kiviniemi V, Yang Y, Zou QHH, Zhu CZZ, Jiang TZZ, Yang H, Gong QYY, Wang L, Li KCC, Xie S, Zang YFF (2008) Default mode network as revealed with multiple methods for resting-state functional MRI analysis. J Neurosci Methods, 171, 349–55.

185. He Y, Zang Y, Jiang T, Liang M, Gong G (2004) Medical image computing and computer-assisted intervention MICCAI 2004 Barillot C, Haynor DR, Hellier P (eds.), Detecting functional connectivity of the cerebellum using low frequency fluctuations (LFFs), pp. 907–915, Springer.
186. Liu H, Liu Z, Liang M, Hao Y, Tan L, Kuang F, Yi Y, Xu L, Jiang T (2006) Decreased regional homogeneity in schizophrenia: a resting state functional magnetic resonance imaging study. Neuroreport, 17, 19–22.
187. Cao Q, Zang Y, Sun L, Sui M, Long X, Zou Q, Wang Y (2006) Abnormal neural activity in children with attention deficit hyperactivity disorder: a resting-state functional magnetic resonance imaging study. Neuroreport, 17, 1033–6.
188. He Y, Wang L, Zang Y, Tian L, Zhang X, Li K, Jiang T (2007) Regional coherence changes in the early stages of Alzheimer's disease: a combined structural and resting-state functional MRI study. Neuroimage, 35, 488–500.
189. Yuan Y, Zhang Z, Bai F, Yu H, Shi Y, Qian Y, Liu W, You J, Zhang X, Liu Z (2008) Abnormal neural activity in the patients with remitted geriatric depression: A resting-state functional magnetic resonance imaging study. J Affect Disord, 111, 145–52.
190. Wu T, Long X, Zang Y, Wang L, Hallett M, Li K, Chan P (2009) Regional homogeneity changes in patients with parkinson's disease. Hum Brain Mapp, 30, 1502–10.
191. Paakki JJ, Rahko J, Long XY, Moilanen I, Tervonen O, Nikkinen J, Starck T, Remes J, Tuula H, Haapsamo H, Jussila K, Kuusikko-Gauffin S, Mattila ML, Zang YF, Kiviniemi V (2010) Alterations in regional homogeneity of resting-state brain activity in autism spectrum disorders. Brain Res, 1321, 169–79.
192. Uddin LQ, Kelly AM, Biswal BB, Margulies DS, Shehzad Z, Shaw D, Ghaffari M, Rotrosen J, Adler LA, Castellanos FX, Milham MP (2008) Network homogeneity reveals decreased integrity of default-mode network in ADHD. J Neurosci Methods, 169, 249–54.
193. Biswal BB, Mennes M, Zuo XN, Gohel S, Kelly C, Smith SM, Beckmann CF, Adelstein JS, Buckner RL, Colcombe S, Dogonowski AM, Ernst M, Fair D, Hampson M, Hoptman MJ, Hyde JS, Kiviniemi VJ, Ktter R, Li SJ, Lin CP, Lowe MJ, Mackay C, Madden DJ, Madsen KH, Margulies DS, Mayberg HS, McMahon K, Monk CS, Mostofsky SH, Nagel BJ, Pekar JJ, Peltier SJ, Petersen SE, Riedl V, Rombouts SARB, Rypma B, Schlaggar BL, Schmidt S, Seidler RD, Siegle GJ, Sorg C, Teng GJ, Veijola J, Villringer A, Walter M, Wang L, Weng XC, Whitfield-Gabrieli S, Williamson P, Windischberger C, Zang YF, Zhang HY, Castellanos FX, Milham MP (2010) Toward discovery science of human brain function. Proc Natl Acad Sci U S A, 107, 4734–4739.
194. Jiang T, He Y, Zang Y, Weng X (2004) Modulation of functional connectivity during the resting state and the motor task. Hum Brain Mapp, 22, 63–71.
195. Xiong J, Ma L, Wang B, Narayana S, Duff EP, Egan GF, Fox PT (2009) Long-term motor training induced changes in regional cerebral blood flow in both task and resting states. Neuroimage, 45, 75–82.
196. Harrison BJ, Pujol J, Ortiz H, Fornito A, Pantelis C, Yucel M (2008) Modulation of brain resting-state networks by sad mood induction. PLoS ONE, 3, e1794.
197. Albert NB, Robertson EM, Miall RC (2009) The resting human brain and motor learning. Curr Biol, 19, 1023–7.
198. Mantini D, Perrucci MG, Del Gratta C, Romani GL, Corbetta M (2007) Electrophysiological signatures of resting state networks in the human brain. Proc Natl Acad Sci U S A, 104, 13170–5.
199. van den Heuvel MP, Mandl RC, Kahn RS, Hulshoff Pol HE (2009) Functionally linked resting-state networks reflect the underlying structural connectivity architecture of the human brain. Hum Brain Mapp, 30, 3127–41.
200. Hagmann P, Cammoun L, Gigandet X, Meuli R, Honey CJ, Wedeen VJ, Sporns O (2008) Mapping the structural core of human cerebral cortex. PLoS Biol, 6, e159.
201. Honey CJ, Sporns O, Cammoun L, Gigandet X, Thiran JP, Meuli R, Hagmann P (2009) Predicting human resting-state functional connectivity from structural connectivity. Proc Natl Acad Sci U S A, 106, 2035–40.
202. Skudlarski P, Jagannathan K, Calhoun VD, Hampson M, Skudlarska BA, Pearlson G (2008) Measuring brain connectivity: Diffusion tensor imaging validates resting state temporal correlations. Neuroimage, 43, 554–61.
203. Teipel SJ, Bokde ALW, Meindl T, Amaro E, Soldner J, Reiser MF, Herpertz SC, Mőller HJJ, Hampel H (2010) White matter microstructure underlying default mode network connectivity in the human brain. Neuroimage, 49, 2021–32.
204. Greicius MD, Supekar K, Menon V, Dougherty RF (2009) Resting-state functional connectivity reflects structural connectivity in the default mode network. Cereb Cortex, 19, 72–8.

2.2 Early small vessel disease affects fronto-parietal and cerebellar hubs in close correlation with clinical symptoms – A resting-state fMRI study

Schaefer, A., Quinque, E. M., Kipping, J. A, Arélin, K., Roggenhofer, E., Frisch, S., Villringer, A., Mueller, K., and Schroeter, M. L. Journal of Cerebral Blood Flow and Metabolism, 34(7), 1091–1095, 2014

Early small vessel disease affects fronto-parietal and cerebellar hubs in close correlation with clinical symptoms – A resting-state fMRI study

Alexander Schaefer[a*] Dipl. Inf., Eva M Quinque[a] MPhil, Judy A Kipping[a] MSc, Katrin Arélin[a,b,c] MD, Elisabeth Roggenhofer[a,c,d] MD, Stefan Frisch[a,e] PhD, Arno Villringer[a,b,c,f,g] MD, PhD, Karsten Mueller[a] PhD, Matthias L Schroeter[a,b,c,h] MD, PhD

a Max Planck Institute for Human Cognitive and Brain Sciences, Leipzig, Germany;

b Leipzig Research Center for Civilization Diseases, University Leipzig, Germany;

c Clinic of Cognitive Neurology, University Leipzig, Leipzig, Germany;

d Integrated Research and Treatment Center Adiposity Diseases, University Leipzig, Germany;

e Department of Neurology, J. W. Goethe University, Frankfurt/Main, Germany;

f Berlin School of Mind and Brain, Mind and Brain Institute, Berlin, Germany;

g Center for Stroke Research, Charité – Universitätsmedizin, Berlin, Germany;

h German Consortium for Frontotemporal Lobar Degeneration, Germany

[*] **corresponding author**: Alexander Schäfer, MPI for Human Cognitive and Brain Sciences, Stephanstrasse 1a, 04103 Leipzig, Germany, Phone: +49 341 9940 2433, Fax: +49 341 9940 2221, email: aschaefer@cbs.mpg.de

Abstract

Cerebral small vessel disease, mainly characterized by white matter lesions and lacunes, has a high clinical impact as it leads to vascular dementia. Recent studies have shown that this disease impairs fronto-parietal networks. Here, we apply resting-state magnetic resonance imaging and data-driven whole brain imaging analysis methods (eigenvector centrality) to investigate changes of the functional connectome in early small vessel disease. We show reduced connectivity in fronto-parietal networks, whereas connectivity increases in the cerebellum. These functional changes are closely related to white matter lesions and typical neuropsychological deficits associated with small vessel disease.

Keywords: small vessel disease, microangiopathy, centrality, functional connectivity

Introduction

Cerebral small vessel disease (SVD) or cerebral microangiopathy describes a state of impaired blood circulation in the arterioles of the brain and is an important cause of cognitive impairment and vascular dementia[1,2]. Magnetic resonance imaging (MRI) is successfully employed to identify lacunar infarcts, white matter lesions (WML, example in Supplementary Figure S1) and alterations in white matter diffusivity in this disease[3]. These indirect markers can be related to cognitive impairment[1,3]. It has been shown that white matter integrity affects functional connectivity[4]. However, the effects of small WML on functional connectivity remain widely unknown.

Although patients in early SVD, a pre-stage of vascular dementia[3], show behavioral differences, the underlying alterations of large-scale functional connectivity might provide us with a more objective measure of the effects of WML. Objective and early clinical diagnostics might aid and complement therapeutical interventions.

In this study we aim to identify alterations in the functional connectome due to SVD using resting-state functional MRI (rs-fMRI). Alterations in connectivity have been reported for the posterior cingulate cortex[5,6] and in the default mode network[7]. As recent investigations have demonstrated a cerebellar role in cognitive processes[8] we also included the cerebellum in our analysis. Subsequently, we assess the behavioral relevance of the functional changes.

For analyzing the human connectome network centrality analysis has become an important tool which captures the importance of each brain region by its connectedness[9]. We use this data-driven approach to investigate the relationship between whole-brain alterations, physiological scores and behavioral performance in patients suffering from early SVD. As our patients were mainly affected by WML in frontal and parietal areas we hypothesized reductions of particularly fronto-parietal connectivity in correlation with WML. White matter hyperintensities are consistently associated with neuropsychological impairments, namely psychomotor slowing[1,2]. We hypothesized a reduction of connectivity in areas particularly involved in attention processes such as the inferior frontal junction, and complex motoric actions such as premotor and supplementary motor area.

Material & Methods

rs-fMRI, T1- and T2-weighted anatomical data were acquired from all patients and controls. rs-fMRI data were acquired using echo-planar image pulse sequences (300 volumes, TR of 2.3 s, voxel resolution of 3*3*4 mm^3). T1 anatomical scans were obtained using a MPRAGE sequence (voxel resolution of 1 mm^3).

Twelve patients with early SVD were recruited among former patients of the Clinic for Cognitive Neurology of the University Hospital Leipzig. Twenty-five healthy individuals matched for age, intelligence, education, and gender (Supplementary Table S1) were included from the volunteer database of the MPI CBS, Leipzig. Four control individuals were excluded due to microangiopathic alterations (age-related white-matter changes[10] (ARWMC) score >2) and one patient due to an cerebellar infarct. Patients had been diagnosed with SVD after thorough clinical examination and all had an ARWMC score >2. Further exclusion criteria for all subjects were a history of psychiatric or neurological disorders including stroke, craniocerebral injury or neurodegenerative disease or dementia. The research protocol was approved by the ethics committee of the University of Leipzig and was in accordance with the latest version of the Declaration of Helsinki. All participants gave informed written consent.

T2-weighted and FLAIR images were rated independently by two experienced clinicians blind to the clinical data according to the ARWMC scale[10]. WML were defined as hyperintensities on both T2-weighted and FLAIR images of >5 mm in diameter. Lacunes were defined as

hypointense signal alterations on both T2-weighted and FLAIR images >2 mm in diameter and rated within the same regions. Alterations >15 mm in diameter were rated as infarcts and respective subjects excluded. Interrater agreement measured with intraclass correlation coefficient κ was high (WML score κ=0.98; lacunes score κ=0.89). The two ratings were averaged for further analyses. Neuropsychological testing was performed using the Consortium to Establish a Registry for Alzheimer's disease (CERAD) test battery including tests of global functioning (Mini-Mental State Examination), executive function and speed[3] (Trail-Making-Test part A and B, phonemic and semantic fluency). Additionally, executive functions were assessed by a Stroop task[2]. Further subtests of the CERAD were included to control for memory abilities (word list immediate and delayed recall, recognition and figure recall), visuoconstructive abilities (figure copying) and word-finding (Boston Naming Test). A vocabulary test was administered to match groups for premorbid verbal intelligence (Supplementary Table S1). The testing was performed by two experienced psychology master students balanced across groups within 90 minutes.

rs-fMRI data were preprocessed using FSL, AFNI and SPM. The steps comprised: discarding the first four volumes, slice-time correction, B0-fieldmap and motion correction, 6 mm FWHM spatial smoothing, 4D mean-based intensity normalization, removing linear and quadratic trends, regressing out eight nuisance signals (white matter, cerebrospinal fluid and six motion parameters), band-pass temporal filtering (0.01-0.1 Hz). Spatial linear normalization to MNI space was performed using individual skull-stripped T1 as a prior. Supplementary Material contains a more detailed description.

Eigenvector centrality (EC) is a network centrality analysis[9] which reflects local connectivity and weights each connection by its importance. Connections to regions which are themselves highly connected receive a higher weight and vice versa. EC is computationally efficient which enables centrality mapping on the voxel level and does not require any initial thresholding of connections. We used the EC implementation in LIPSIA.

For statistical testing we used AFNI with age, gender and micro-movements as covariates. Micro-movements were measured in average frame displacement which is the average of rotation and translation differences across time-points in mm. We performed a two-sample t-test for our group effect and whole-brain correlation analysis between the centrality of every voxel and the physiological and behavioral scores across all individuals (patients and controls). Changes in connectivity with respect to clinical symptoms were only evaluated in those behavioral tasks where patients showed significantly poorer performance in comparison with healthy controls (Supplementary Table S2). All centrality group results were thresholded with $p<0.01$ on a voxel and $p<0.05$ at a cluster level (39 voxels) using AlphaSim (AFNI). Visualization of the cerebrum was performed using SUMA, flat maps of the cerebellum were created with CARET and SUIT.

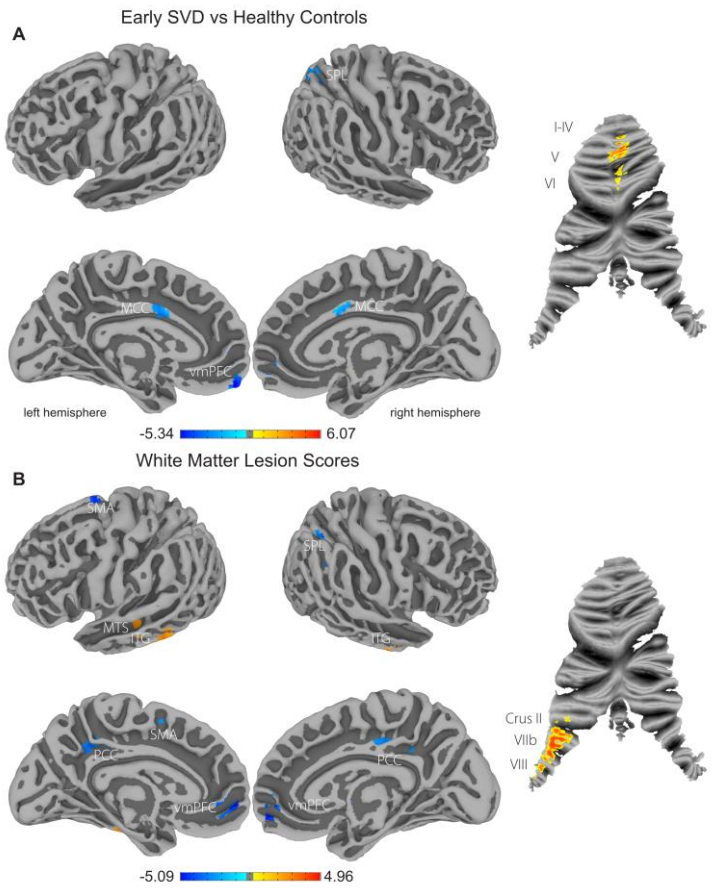

Figure 1 Functional connectivity changes are displayed on cerebral surface maps and cerebellar flat maps. Increases are marked in hot colors and decreases are marked in cold colors (p<0.05, cluster corrected). **A** Significant differences in eigenvector centrality between the group of small vessel disease patients and healthy controls. Increases are found in cerebellar regions I-VI, while decreases are found in ventromedial prefrontal cortex (vmPFC), midcingulate cortex (MCC) and superior parietal lobe (SPL). **B** Regions with a significant correlation to the white matter lesion score. Positive correlations are found in the middle temporal sulcus (MTS) inferior temporal gyrus (ITG), lobules Crus II, VIIb and VIII, negative correlations are found in vmPFC, supplementary motor area (SMA), posterior cingulate cortex (PCC) and SPL.

Results

The group comparison of functional connectivity yielded significant centrality changes in SVD (Figure 1A). Patients showed decreased connectivity in left ventromedial prefrontal cortex (vmPFC, d=0.95, r=0.43), bilateral midcingulate cortex (MCC, d=1.16, r=0.50) and right superior parietal lobe (SPL, d=1.27, r=0.54) as well as increased centrality in bilateral cerebellar regions I-VI (d=1.28, r=0.54). Correlation between WML scores and centrality maps (Figure 1B) over the whole sample revealed decreased centrality in bilateral vmPFC (r=-0.59), posterior cingulate cortex (PCC, r=-0.66), left supplementary motor area (SMA, r=-0.64) and right SPL (r=-0.63) and increased centrality in bilateral inferior temporal gyrus (ITG, r=0.52) and left middle temporal sulcus (MTS, r=0.68). In the cerebellum, connectivity was increased in left lobules VIIb/VIII

and Crus II in the patient group (r=0.67). Correlation of lacunar scores with centrality did not reveal significant results.

Relevance of changes in connectivity to clinical symptoms is represented as significant correlations between task performance measures and the centrality measure (Figure 2). Patients showed a slower processing speed in the Trail-Making-Test part A (TMT-A), neutral and incongruent conditions of the Stroop task, and semantic and phonemic fluency measures (Supplementary Table 2). We found positive correlations between performance on the phonemic fluency task and centrality in bilateral SPL (r=0.63), SMA (r=0.64), premotor cortex (PM, r=0.66), MCC and posterior superior frontal sulcus (SFS, r=0.60; Figure 2A). For reaction time in the neutral condition of the Stroop task we found negative correlations to centrality in bilateral PM (r=-0.62), SFS (r=-0.71), left inferior frontal sulcus (IFS, r=-0.71), left SMA (r=-0.71), left MTS (r=-0.73) and right MCC (r=-0.68) and positive correlations with

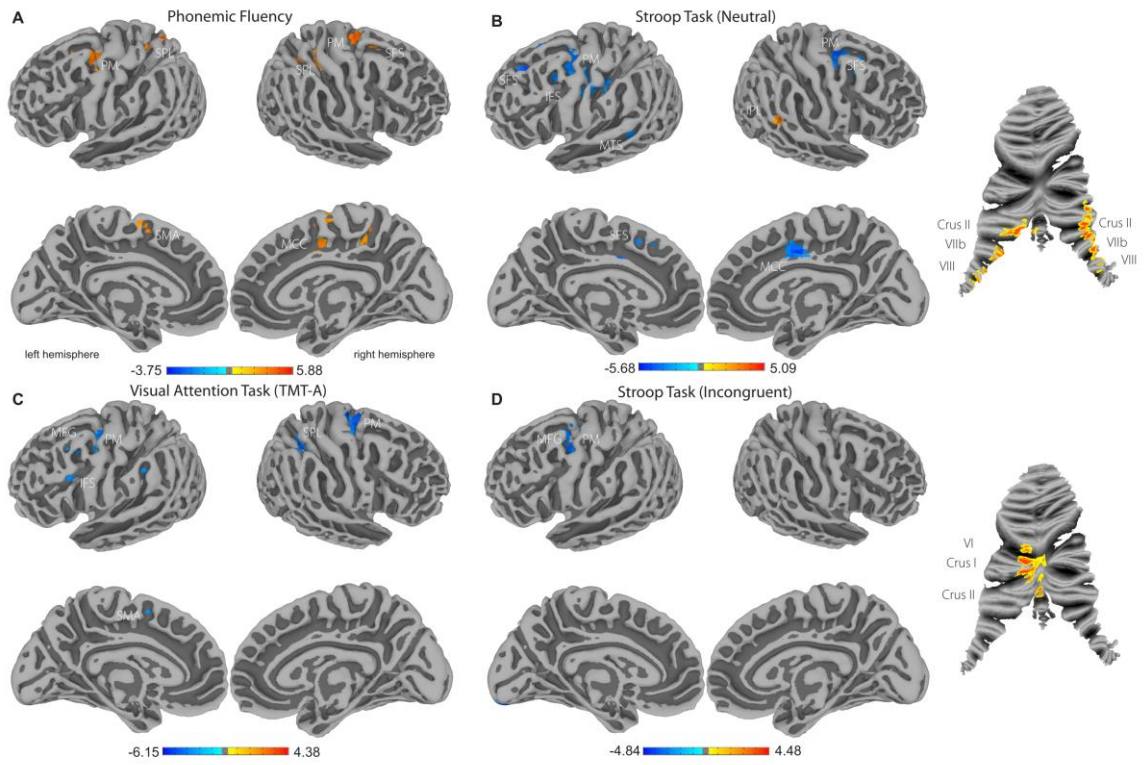

Figure 2 Cerebral surface maps and cerebellar flat maps show significant correlations between task performance and centrality for tasks with significant group differences. Positive correlations are displayed in hot and negative correlations in cold colors ($p<0.05$, cluster corrected). **A** Correlation between centrality and number of words produced in a phonemic fluency task. Positive correlations are found in premotor (PM), posterior superior frontal sulcus (SFS), midcingulate cortex (MCC), supplementary motor area (SMA), and superior parietal lobe (SPL). **B** Correlation between centrality and reaction time in the neutral condition of the Stroop task. Negative correlations were found in PM, SFS, inferior frontal sulcus (IFS), middle temporal sulcus (MTS) and MCC. Positive correlations were found in Crus II, VIIb and VIII of the cerebellum and the inferior parietal lobe (IPL). **C** Correlation between centrality and time needed to complete a visual attention task (TMT A – Trail-Making-Test part A). Negative correlations were found in PM, middle frontal gyrus (MFG), supplementary motor area (SMA), SPL, and inferior frontal IFS. **D** Correlation between centrality and reaction time in the incongruent condition of the Stroop task. Negative correlations were found in PM/posterior MFG. Positive correlations were found in VI, Crus I and II of the cerebellum.

inferior parietal lobe (r=0.65) and cerebellar lobules Crus II, VIIb and VIII (left r=0.69, right r=0.75, Figure 2B). For reaction time in the TMT-A we found negative correlation to centrality in bilateral PM (right r=-0.69, left r=-0.65), left posterior middle frontal gyrus (MFG, r=-0.65), left IFS (r=-0.69), right SPL (r=-0.56), and left SMA (r=-0.65) (Figure 2C). For reaction time in the incongruent condition of the Stroop task we found negative correlations to centrality in left PM/posterior MFG (r=-0.73) and positive correlations with cerebellar regions VI, Crus I and Crus II (r=0.58, Figure 2D). We found performance in the TMT-A and the phonemic fluency task to be linearly dependent (r=-0.47, p=0.007), the incongruent condition of the Stroop task was correlated with the TMT-A (r=0.59, p=0.0004) and the phonemic fluency task (r=-0.53, p=0.002). None of the other presented task parameters showed collinearity. For semantic fluency no significant association with centrality was observed. Supplementary Figures S2-S7 present scatter plots of the corresponding results in Figures 1 and 2. Supplementary Figures S8-S9 represent the correlation between centrality and time needed in TMT-A and Stroop neutral condition without the respective slowest subject, who might be regarded as an outlier and suspected to have driven the results. Removing this subject did not change the analysis' results substantially.

Discussion

In this study we investigated alterations of the functional connectome due to early SVD and evaluated their relevance to clinical symptoms. For the group difference we have shown a breakdown of fronto-parietal hubs in patients with early SVD, closely related to WML scores. Effects can be explained by the disruption of fronto-parietal white matter pathways due to WML which in our sample were mainly located in frontal and parietal areas (Supplementary Table S1) and gives further evidence for the hypothesis that fronto-parietal networks are primarily disrupted in SVD[2,11]. The reduction of centrality in the vmPFC and SPL are in line with results by Yi et al.[7]. We found fewer widespread group differences, which might be explained by the earlier disease-state of our patient cohort (MMSE of 27.6+-1.5 compared to MMSE of 25.7+-2.7) or the different centrality method (degree centrality) used. Reduced connectivity to the medial frontal cortex due to white matter hyperintensities was also found by Wu et al.[6].

While our cohort was not dement (Supplementary Table S1, S2) the subjects with more severe disease state showed reduced centrality in the PCC, an area which has been shown to have reduced metabolism and perfusion in Alzheimer's disease and its prodromal syndrome mild cognitive impairment[12]. This finding is particularly interesting as Alzheimer's disease is often associated with SVD.

The relevance of our brain findings for clinical symptoms revealed that the lower the centrality in sensorimotor areas, the slower the reaction times in the TMT-A and the two conditions of the Stroop task. Together with positive correlations between centrality in secondary sensorimotor areas and phonemic fluency these findings reflect upon the concept that WML express itself in mild psychomotor slowing rather than a severe degree of specific cognitive impairments[1,2]. Although correlations between neuropsychological test scores and centrality measures identified additionally prefrontal areas, known to be related specifically to executive dysfunction[2], the group and correlation analysis with WML scores did not confirm effects in these brain regions.

Task-fMRI studies report increased and decreased activation in association with WML. Venkatraman et al.[13] report a reduced activation in motor and premotor areas during psychomotor performance in individuals with more WML. However, Aizenstein et al.[14] found

that patients with late life depression show a positive correlation between activation in prefrontal and limbic areas and WML using an affective reactivity task. Although we also found premotor and higher order regions to be affected by WML, the relationship between functional connectivity and activation is complex[15] and difficult to interpret.

The consistent inverse pattern of increased centrality in the cerebellum and decreased centrality in the cerebrum has to our knowledge not been reported in SVD yet. We found connectivity changes in cerebellar regions which are connected to fronto-parietal cognitive networks (lobules Crus II, VIIb) as well as sensorimotor regions (lobules I-V, VIII)[8]. As WML occur mainly in fronto-parietal regions one might hypothesize that fronto-parietal hypoconnectivity might be compensated by cerebellar hyperconnectivity.

Although SVD is a heterogeneous disease which makes group analysis and region-specific hypothesis testing difficult, the application of data-driven centrality analysis enabled us to identify affected network hubs.

This cross-sectional human imaging study only provides correlational but no causal associations which might be approached by longitudinal study designs. Micro-movements represent another limitation of the current study. Although we could not find a significant group difference (Supplementary Table S1), we accounted for this potential bias by using average frame displacement as a covariate in our analyses.

In conclusion, our study provides a link between the disruption of white matter pathways, behavioral impairment and functional interaction between gray matter regions in early small vessel disease.

Acknowledgments: KA, AV & MLS are supported by LIFE – Leipzig Research Center for Civilization Diseases at the University of Leipzig – funded by European Union, European Regional Development Fund and by Free State of Saxony within the framework of the excellence initiative. MLS is additionally supported by the German Consortium for Frontotemporal Lobar Degeneration, funded by the German Federal Ministry of Education and Research, by MaxNet Aging, and, together with KM, by the Parkinson's Disease Foundation (Grant No. PDF-IRG-1307). ER and AV are supported by IFB - Integrated Research and Treatment Center Adiposity Diseases at the University of Leipzig, funded by German Federal Ministry of Education and Research.

Disclosure: The authors declare no conflict of interest.

References

1 Selnes OA, Vinters H V. Vascular cognitive impairment. *Nat Clin Pr Neuro* 2006; **2**: 538–47.

2 Schroeter ML, Cutini S, Wahl MM, Scheid R, von Cramon DY. Neurovascular coupling is impaired in cerebral microangiopathy—An event-related Stroop study. *Neuroimage* 2007; **34**: 26–34.

3 Quinque EM, Arelin K, Dukart J, Roggenhofer E, Streitbuerger DP, Villringer A, *et al.* Identifying the neural correlates of executive functions in early cerebral microangiopathy: a combined VBM and DTI study. *J Cereb Blood Flow Metab* 2012; **32**: 1869–78.

4 Teipel SJ, Bokde ALW, Meindl T, Amaro E, Soldner J, Reiser MF, *et al.* White matter microstructure underlying default mode network connectivity in the human brain. *Neuroimage* 2010; **49**: 2021–32.

5 Sun Y, Qin L, Zhou Y, Xu Q, Qian L, Tao J, *et al.* Abnormal functional connectivity in patients with vascular cognitive impairment, no dementia: a resting-state functional magnetic resonance imaging study. *Behav Brain Res* 2011; **223**: 388–94.

6 Wu M, Andreescu C, Butters M. Default-mode network connectivity and white matter burden in late-life depression. *Psychiatry Res* 2011; **194**: 39–46.

7 Yi L, Wang J, Jia L, Zhao Z, Lu J, Li K, *et al.* Structural and Functional Changes in Subcortical Vascular Mild Cognitive Impairment: A Combined Voxel-Based Morphometry and Resting-State fMRI Study. *PLoS One* 2012; **7**: e44758.

8 Stoodley C. The Cerebellum and Cognition: Evidence from Functional Imaging Studies. *Cerebellum* 2012; **11**: 352–65.

9 Lohmann G, Margulies DS, Horstmann A, Pleger B, Lepsien J, Goldhahn D, *et al.* Eigenvector Centrality Mapping for Analyzing Connectivity Patterns in fMRI Data of the Human Brain. *PLoS One* 2010; **5**: e10232.

10 Wahlund LO, Barkhof F, Fazekas F, Bronge L, Augustin M, Sjogren M, *et al.* A new rating scale for age-related white matter changes applicable to MRI and CT. *Stroke* 2001; **32**: 1318–22.

11 Cummings JL. Anatomic and Behavioral Aspects of Frontal-Subcortical Circuitsa. *Ann NY Acad Sci* 1995; **769**: 1–14.

12 Schroeter ML, Stein T, Maslowski N, Neumann J. Neural correlates of Alzheimer's disease and mild cognitive impairment: a systematic and quantitative meta-analysis involving 1351 patients. *Neuroimage* 2009; **47**: 1196–206.

13 Venkatraman VK, Aizenstein H, Guralnik J, Newman AB, Glynn NW, Taylor C, *et al.* Executive control function, brain activation and white matter hyperintensities in older adults. *Neuroimage* 2010; **49**: 3436–42.

14 Aizenstein H, Andreescu C. fMRI correlates of white matter hyperintensities in late-life depression. *Am J Psychiatry* 2011; **168**: 1075–82.

15 Mennes M, Kelly C, Zuo X-N, Di Martino A, Biswal BB, Castellanos FX, *et al.* Inter-individual differences in resting-state functional connectivity predict task-induced BOLD activity. *Neuroimage* 2010; **50**: 1690–701.

Supplement

Preprocessing Pipeline

The preprocessing of T1 anatomical and rs-fMRI data were carried out using FMRIB Software Library (FSL)[1], Analysis of Functional NeuroImages (AFNI)[2], Freesurfer[3] and Statistical Parametric Mapping (SPM)[4]. The preprocessing is based on the fcon1000 scripts, which can be downloaded from fcon_1000.projects.nitrc.org. We changed only steps 1), 3) and 4) to improve skull-striping and to add field-map and slice-time correction.

The preprocessing comprised the following steps, where brackets denote the function and software package used: 1) Skull-striping of initial anatomical T1 scan (recon all, Freesurfer). 2) Discarding the first four volumes from each resting-state scan to allow for signal equilibration (3dcalc, AFNI). 3) Slicetime correction (slicetimer, AFNI). 4) Motion and b0 fieldmap correction using realign & unwarp (SPM8). 5) 6 mm Full Width Half Maximum (FWHM) spatial smoothing (fslmaths, FSL). 6) 4D mean-based intensity normalization (fslmaths, FSL). 7) Removing linear and quadratic trends (3dDetrend, AFNI). 8) Segmenting skull striped T1 images into white matter (WM), grey matter (GM) and cerebrospinal fluid (CSF) masks (fast, FSL). 9) Linear registration of WM and CSF masks to native functional space (flirt, FSL). 10) 6 mm Full Width Half Maximum (FWHM) spatial smoothing (fslmaths, FSL). 11) Linear registration of WM and CSF masks to Montreal Neurological Institute (MNI)[5] space (flirt, FSL). 12) Multiplication of WM and CSF masks with MNI CSF and WM prior maps (fslmaths, FSL). 13) Registering WM and CSF maps back to native space (flirt, FSL). 14) Thresholding WM mask at 0.66 and CSF mask at 0.4 (fslmaths, FSL). 15) Regressing out eight nuisance signals (white matter, cerebrospinal fluid and six motion parameters) using film_gls (FSL). 16) Band-pass temporal filtering (0.01-0.1 Hz, 3dFourier, AFNI). The spatial normalization of the functional volume was performed via linear normalization to MNI[5] space and the individual skull-stripped T1 as a prior (flirt, FSL).

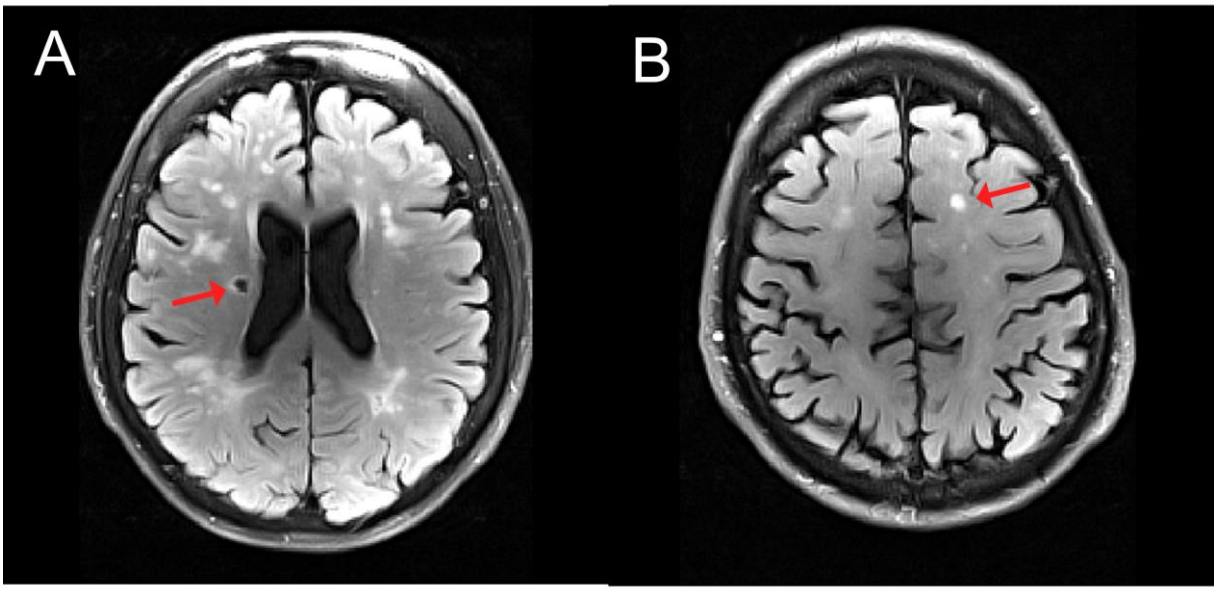

Figure S1 FLAIR image with examples for markers of structural changes in small vessel disease. Characteristic abnormality related to lacune (A) and white matter lession (B).

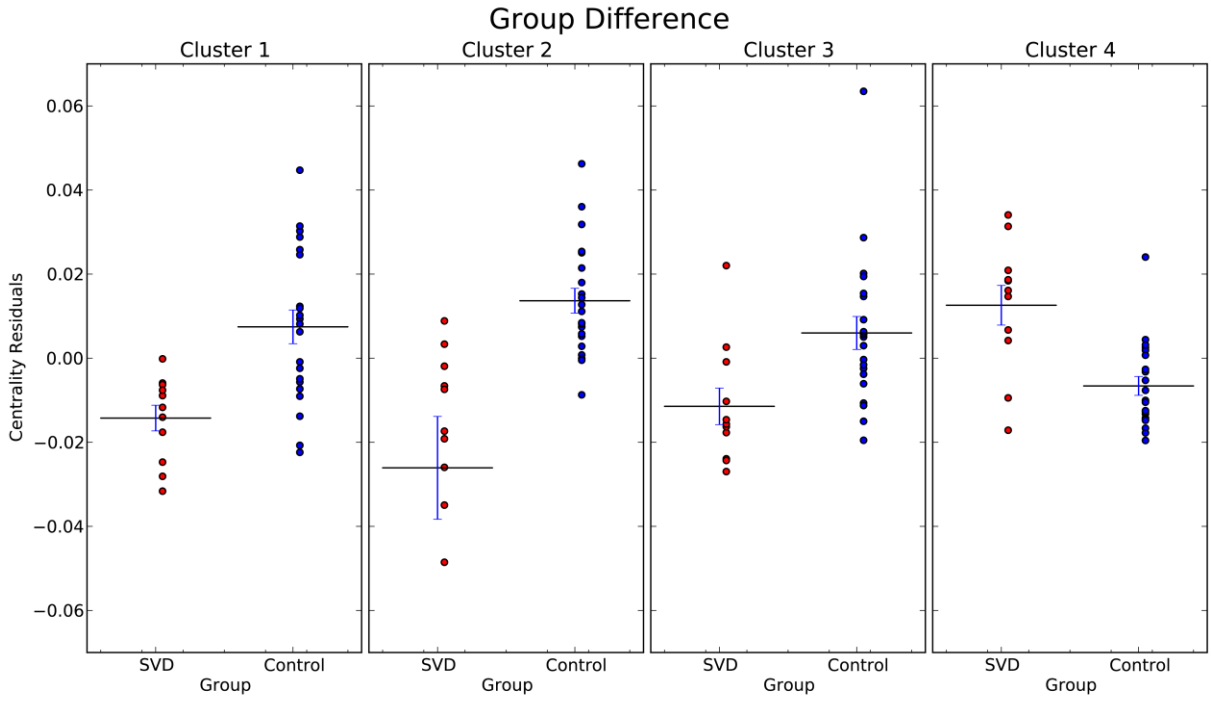

Figure S2 Plot of average centrality for significant clusters in the Group Difference (see Figure 1a and Supplementary Table S3). Red dots mark subjects in the small vessel disease group, blue dots mark healthy controls.

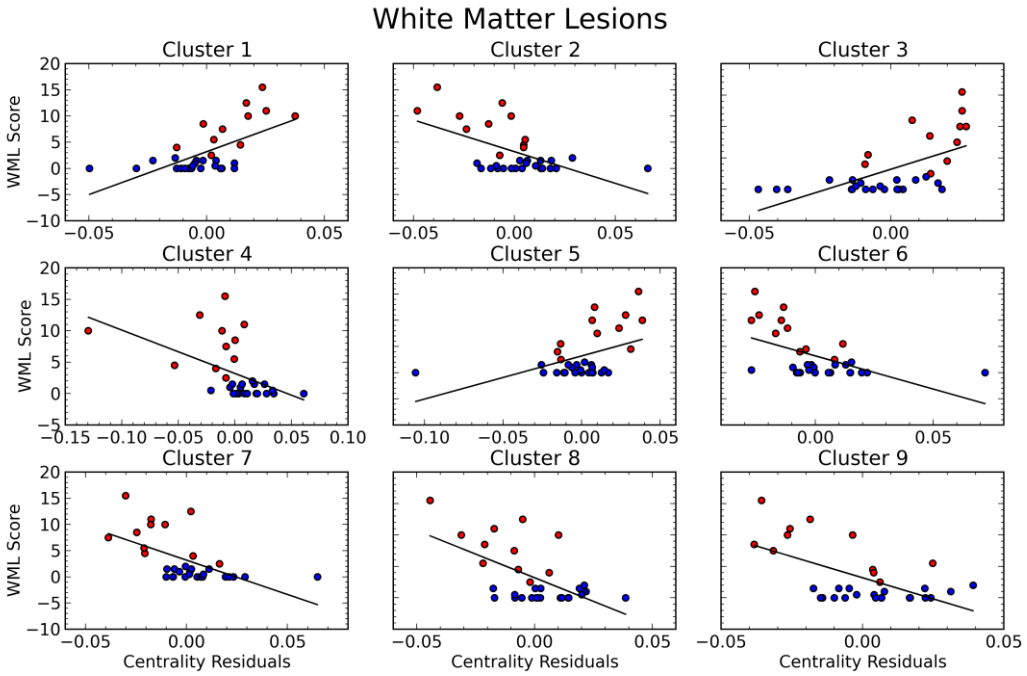

Figure S3 Plot for clusters with significant correlation between centrality and white matter lesion scores (see Figure 1b). For cluster locations see Supplementary Table S4. Red dots mark subjects in the small vessel disease group, blue dots mark healthy controls.

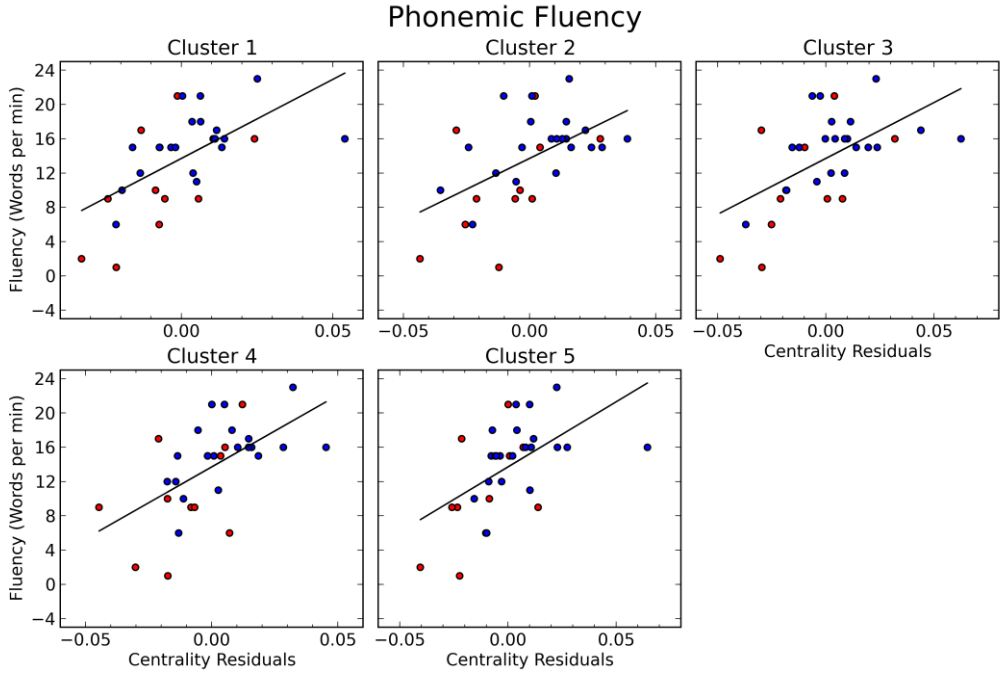

Figure S4 Plot for clusters with significant correlation between centrality and number of words produced per minute in a phonemic fluency task (Figure 2a). For cluster locations see Supplementary Table S5. Red dots mark subjects in the small vessel disease group, blue mark healthy controls.

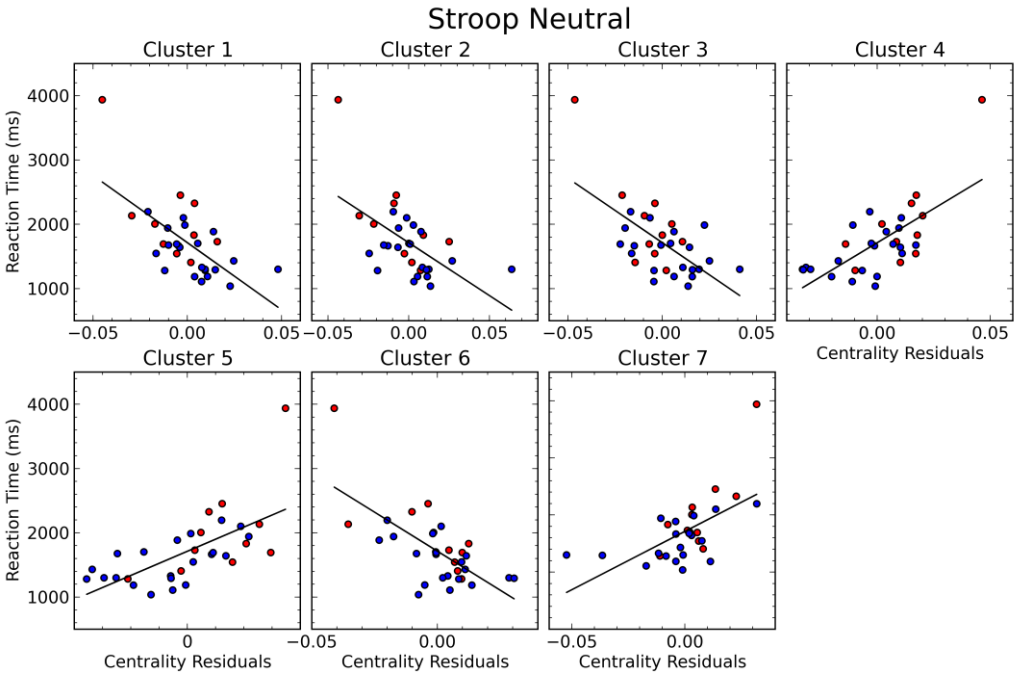

Figure S5 Plot for clusters with significant correlation between centrality and time needed in the neutral condition of the Stroop task (Figure 2b). For cluster locations see Supplementary Table S7. Red dots mark subjects in the small vessel disease group, blue mark healthy controls.

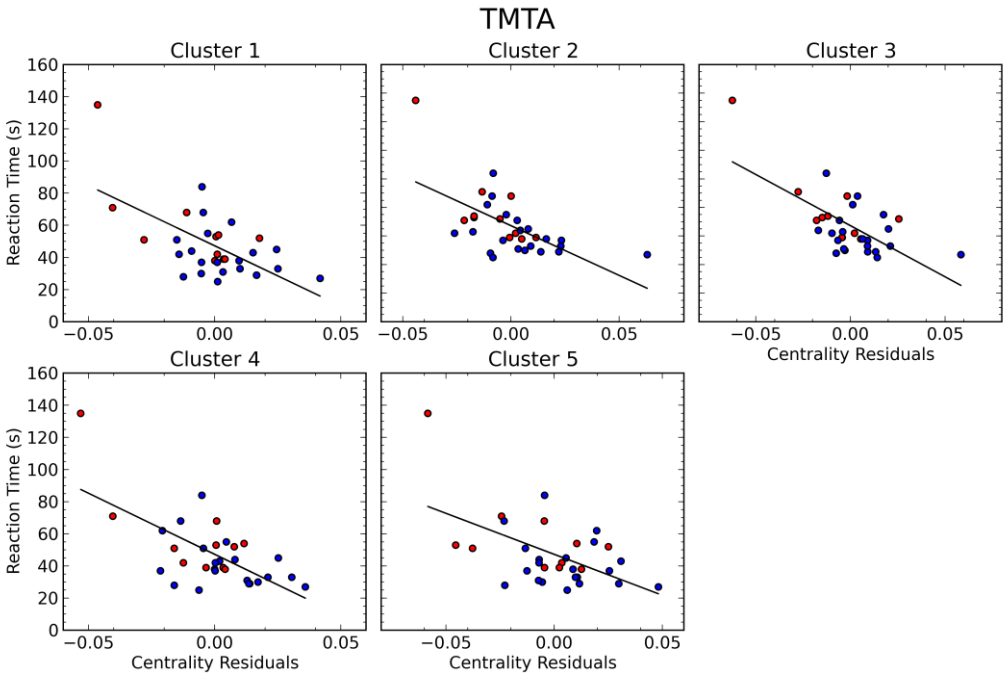

Figure S6 Plot for clusters with significant correlation between centrality and time needed in a visual attention task (Figure 2c). For cluster locations see Supplementary Table S6. Red dots mark subjects in the small vessel disease group, blue mark healthy controls.

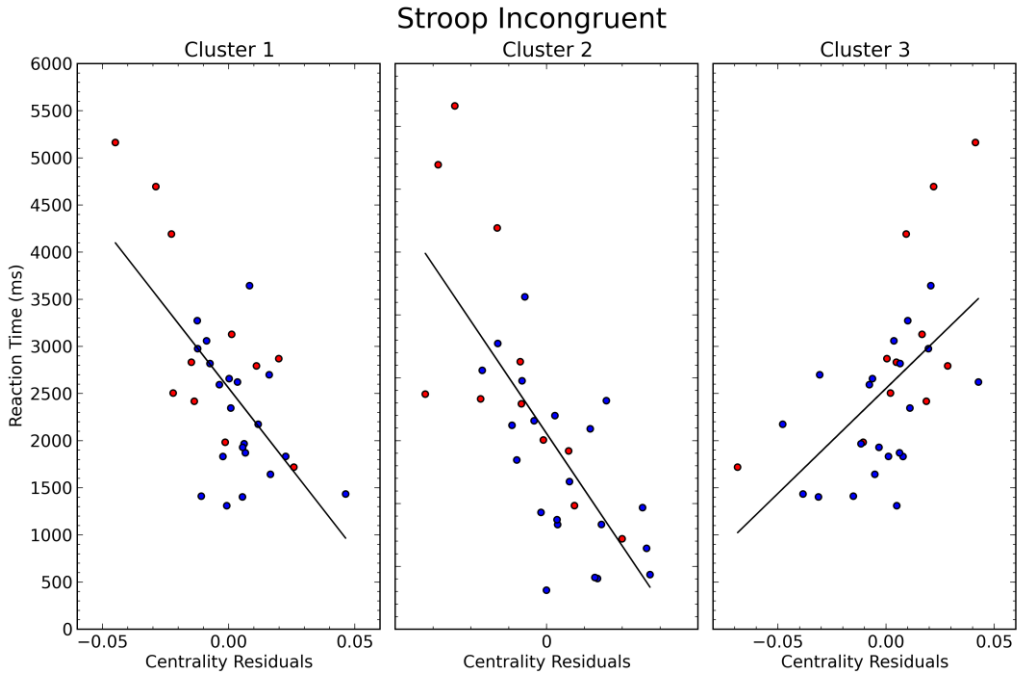

Figure S7 Plot for clusters with significant correlation between centrality and time needed in in the incongruent condition of the Stroop task (Figure 2d). For cluster locations see Supplementary Table S8. Red dots mark subjects in the small vessel disease group, blue mark healthy controls

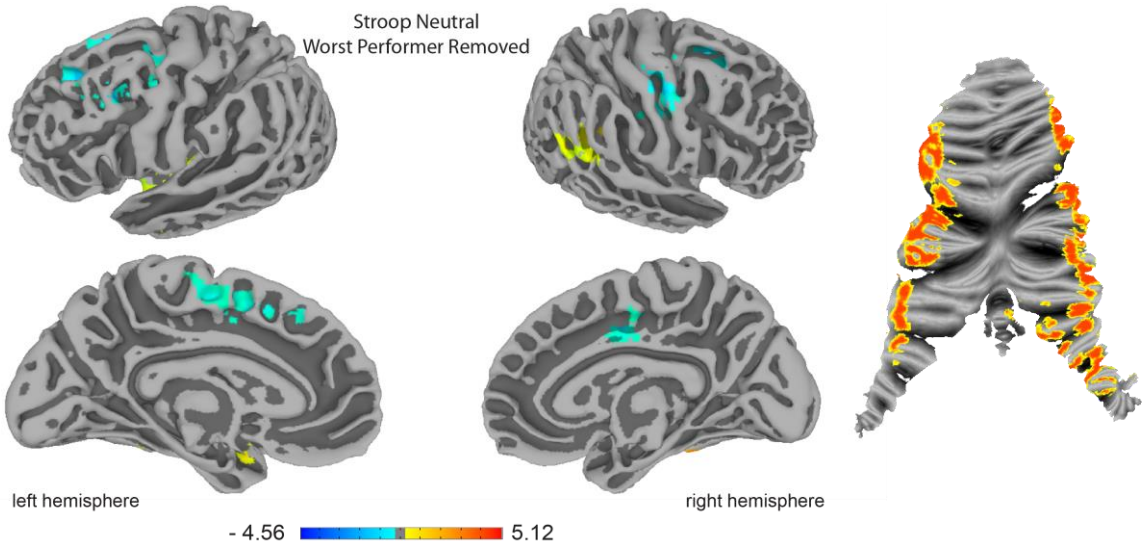

Figure S8 Correlation between centrality and time needed in the neutral condition of the Stroop task (compare to Figure 2b) after removing the slowest subject in this task (Figure S5). Cerebrum surface visualization (left) and cerebellum flat map (right). Blue colors indicate negative correlations and red colors positive correlation with time needed in the Stroop task neutral condition ($p<0.05$, cluster corrected).

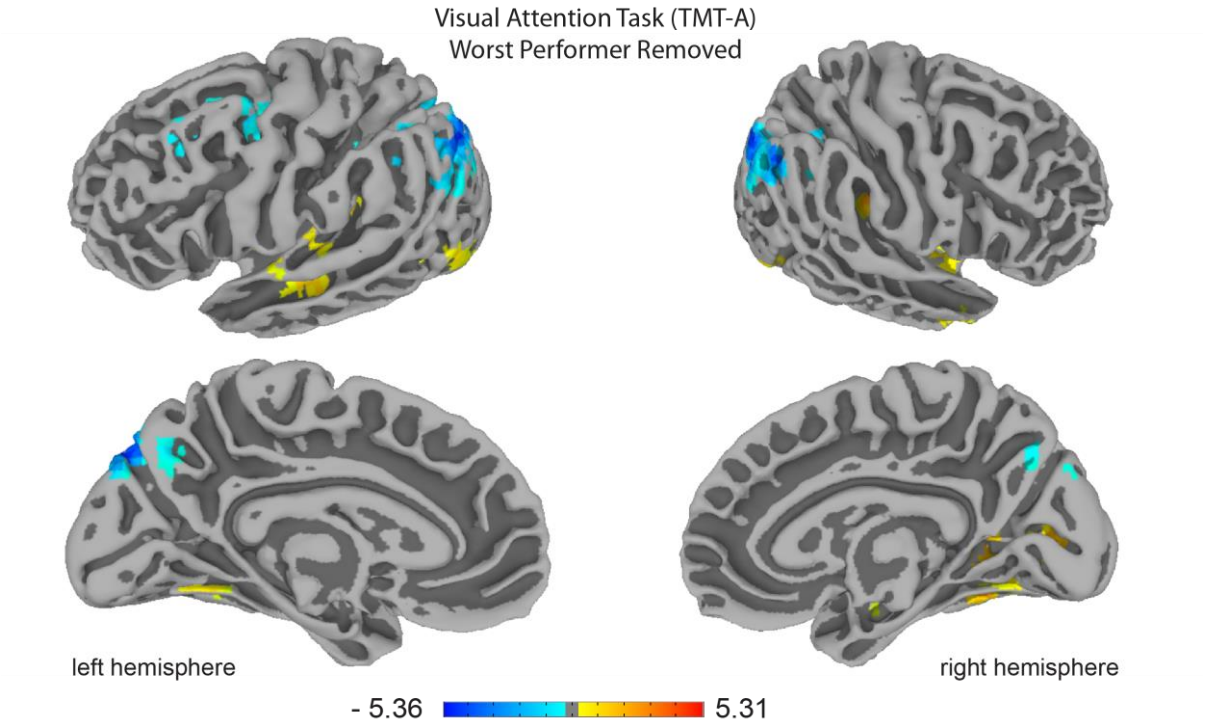

Figure S9 Cerebrum surface visualization of Correlation between centrality and time needed in visual attention task (compare to Figure 2c) after removing the slowest subject in this task (Figure S6). Blue colors indicate negative correlations and red colors positive correlation with time needed in visual attention task ($p<0.05$, cluster corrected).

Table S1 Demographic data of patients with small vessel disease and healthy control subjects (see Quinque et al.[6]).

Characteristics	*Small vessel disease (n=11)*		*Healthy control group (n=21)*		
	Mean	*s.d.*	*Mean*	*s.d.*	P
Age (years)	61.4	6.3	66.0	6.7	0.09
Sex (male/female)	7/4		13/8		0.92
Education (years)	13.8	3.0	14.3	2.4	0.79
Premorbid intelligence (IQ)	105.3	10.1	110.1	8.7	0.17
Mini-Mental State Examination	27.6	1.5	28.6	1.1	0.10
Mean Frame Displacement (mm)	0.30	0.13	0.22	0.81	0.09
White matter lesion total score	8.3	4.0	0.5	0.7	**<0.001**
Frontal subscore	3.2	1.1	0.3	0.5	**<0.001**
Parieto-occipital subscore	3.0	1.5	0.1	0.3	**<0.001**
Temporal subscore	0.8	0.8	0.0	0.0	**<0.01**
Basal ganglia subscore	0.8	1.1	0.1	0.3	**<0.05**
Infratentorial subscore	0.2	0.6	0.0	0.0	0.41
Lacunes total score	1.9	2.4	0.3	0.5	**<0.02**
Frontal subscore	0.1	0.3	0.0	0.0	0.70
Parieto-occipital subscore	0.0	0.2	0.0	0.0	0.70
Temporal subscore	0.2	0.6	0.0	0.0	0.70
Basal ganglia subscore	1.1	1.7	0.3	0,5	0.09
Infratentorial subscore	0.5	0.8	0.0	0.0	0.10

All group comparisons were performed using Mann–Whitney *U*-tests (χ^2-test for sex). Mean values, standard deviations (s.d.), and *P* values are reported. Significant values are displayed in bold.

Table S2 Cognitive performance in patients with small vessel disease and healthy control subjects (see Quinque et al.[6]).

Cognitive function domain and subtest	*Small vessel disease (n=11)*		*Healthy control group (n=21)*		
	Mean	*s.d.*	*Mean*	*s.d.*	P
Executive functions—processing speed					
Trail-Making-Test part A—time	58.4	27.7	41.5	15.2	**<0.03**
Trail-Making-Test part B—time[a]	127.9	59.2	100.4	46.1	0.25
Stroop neutral—time	2.1	0.7	1.5	0.3	**<0.03**
Stroop incongruent—time	3.1	1.1	2.3	0.7	**<0.03**
Semantic fluency	19.8	5.7	25.6	4.7	**<0.01**
Phonemic fluency	10.5	6.3	15.4	3.9	**<0.03**
Executive functions—planning, error monitoring					
Trail-Making-Test part A—errors	0.2	0.4	0.2	0.4	0.73
Trail-Making-Test part B—errors[a]	0.1	0.9	0.7	0.3	0.13
Stroop neutral—errors	1.8	2.9	1.9	4.2	0.76
Stroop incongruent—errors	6.5	7.7	4.7	4.6	0.88
Executive functions—cognitive flexibility/inhibition adjusted for speed					
Trail-Making-Test part B/A—time	2.4	1.4	2.6	1.5	0.64
Stroop incongruent/neutral—time	1.5	0.4	1.5	0.3	0.48
Memory, figure copying, picture naming					
Immediate recall	19.6	5.8	21.6	3.5	0.46
Delayed recall	7.1	1.8	7.8	1.5	0.43
Recognition	19.0	1.7	19.5	0.7	0.76
Figure recall	8.7	4.0	9.8	2.7	0.56
Figure copy	10.0	1.5	10.3	1.2	0.58
Boston naming test	14.6	0.7	14.7	0.6	0.56

[a]Two patients and one healthy control subject failed to complete the task. For these subjects Trail-Making-Test part B time is set to 240 seconds the maximum time allowed for completion; Trail-Making-Test part B errors could not be calculated for these subjects and Trail-Making-Test part B errors were therefore excluded from any further analysis. All group comparisons were performed using Mann-Whitney *U*-tests. Mean values, standard deviations (s.d.), and *P* values are reported. Significant values are displayed in bold.

Table S3 Group difference for centrality between early small vessel disease and control subjects. Peak coordinates in MNI space.

#Coordinate order = RAI (Right Anterior Inferior)

#Volume	RL	AP	IS
#------	-----	-----	-----
53	-12.0	-6.0	36.0

51	0.0	-57.0	-21.0
51	-18.0	66.0	60.0
46	-6.0	57.0	-12.0

Table S4 Correlation between centrality and white matter lesion score. Peak coordinates in MNI space.

#Coordinate order = RAI (Right Anterior Inferior)

#Volume	RL	AP	IS
#------	-----	-----	-----
222	54.0	27.0	-27.0
150	-51.0	45.0	42.0
87	30.0	51.0	-51.0
75	0.0	-54.0	-3.0
53	-51.0	12.0	-39.0
53	30.0	69.0	30.0
49	12.0	0.0	72.0
44	-15.0	24.0	39.0
40	12.0	39.0	42.0

Table S5 Correlation between centrality and phonemic fluency. Peak coordinates in MNI space.

#Coordinate order = RAI (Right Anterior Inferior)

#Volume	RL	AP	IS
#------	-----	-----	-----
154	-18.0	9.0	69.0
103	-30.0	33.0	51.0
65	24.0	54.0	66.0
63	33.0	0.0	57.0
52	9.0	-3.0	60.0

Table S6 Correlation between centrality and Trail Making Test (TMT) A

#Coordinate order = RAI (Right Anterior Inferior)

#Volume	RL	AP	IS
#------	-----	-----	-----
154	-18.0	9.0	69.0
103	-30.0	33.0	51.0
65	24.0	54.0	66.0
63	33.0	0.0	57.0
52	9.0	-3.0	60.0

Table S7 Correlation between centrality and Stroop task performance – Neutral condition. Peak coordinates in MNI space.

#Coordinate order = RAI (Right Anterior Inferior)

#Volume	RL	AP	IS
#------	-----	-----	-----
610	24.0	-18.0	39.0
171	-27.0	-6.0	57.0
91	-12.0	0.0	42.0
69	-36.0	51.0	-48.0
55	12.0	69.0	-45.0
41	57.0	42.0	9.0
40	-57.0	45.0	18.0

Table S8 Correlation between centrality and Stroop task performance – Incongruent condition. Peak coordinates in MNI space.

#Coordinate order = RAI (Right Anterior Inferior)

#Volume	RL	AP	IS
#------	-----	-----	-----
89	36.0	84.0	-18.0
71	33.0	0.0	60.0
56	21.0	75.0	-27.0

Referencess

1 Jenkinson M, Beckmann CF, Behrens TEJ, Woolrich MW, Smith SM. Fsl. *Neuroimage* 2012; **62**: 782–90.

2 Cox RW. AFNI: software for analysis and visualization of functional magnetic resonance neuroimages. *Comput Biomed Res* 1996; **29**: 162–73.

3 Dale AM, Fischl B, Sereno MI. Cortical surface-based analysis: I. Segmentation and surface reconstruction. *Neuroimage* 1999; **9**: 179–94.

4 Friston KJ, Ashburner JT, Kiebel SJ, Nichols TE, Penny WD. *Statistical Parametric Mapping: The Analysis of Functional Brain Images: The Analysis of Functional Brain Images*. Academic Press, 2011.

5 Mazziotta JC, Toga AW, Evans A, Fox P, Lancaster J. A probabilistic atlas of the human brain: theory and rationale for its development the international consortium for brain mapping (ICBM). *Neuroimage* 1995; **2**: 89–101.

6 Quinque EM, Arélin K, Dukart J, Roggenhofer E, Streitbuerger D-P, Villringer A, *et al.* Identifying the neural correlates of executive functions in early cerebral microangiopathy: a combined VBM and DTI study. *J Cereb Blood Flow Metab* 2012; **32**: 1869–78.

2.3 Dynamic modulation of intrinsic functional connectivity by transcranial direct current stimulation

Sehm B.*, **Schäfer A.***, Kipping J., Margulies D., Conde V., Villringer A., and Ragert P., Dynamic modulation of intrinsic functional connectivity by transcranial direct current stimulation, Journal of Neurophysiology, 108(12), 3253–3263, 2012

* equally contributing authors

J Neurophysiol 108: 3253–3263, 2012.
First published September 19, 2012; doi:10.1152/jn.00606.2012.

Dynamic modulation of intrinsic functional connectivity by transcranial direct current stimulation

Bernhard Sehm,[1,2]* Alexander Schäfer,[1]* Judy Kipping,[1] Daniel Margulies,[1] Virginia Conde,[1] Marco Taubert,[1] Arno Villringer,[1,2] and Patrick Ragert[1]

[1]*Department of Neurology, Max Planck Institute for Human Cognitive and Brain Sciences, Leipzig, Germany; and* [2]*Clinic for Cognitive Neurology, University of Leipzig, Leipzig, Germany*

Submitted 16 July 2012; accepted in final form 19 September 2012

Sehm B, Schäfer A, Kipping J, Margulies D, Conde V, Taubert M, Villringer A, Ragert P. Dynamic modulation of intrinsic functional connectivity by transcranial direct current stimulation. *J Neurophysiol* 108: 3253–3263, 2012. First published September 19, 2012; doi:10.1152/jn.00606.2012.—Transcranial direct current stimulation (tDCS) is a noninvasive brain stimulation technique capable of modulating cortical excitability and thereby influencing behavior and learning. Recent evidence suggests that bilateral tDCS over both primary sensorimotor cortices (SM1) yields more prominent effects on motor performance in both healthy subjects and chronic stroke patients than unilateral tDCS over SM1. To better characterize the underlying neural mechanisms of this effect, we aimed to explore changes in resting-state functional connectivity during both stimulation types. In a randomized single-blind crossover design, 12 healthy subjects underwent functional magnetic resonance imaging at rest before, during, and after 20 min of unilateral, bilateral, and sham tDCS stimulation over SM1. Eigenvector centrality mapping (ECM) was used to investigate tDCS-induced changes in functional connectivity patterns across the whole brain. Uni- and bilateral tDCS over SM1 resulted in functional connectivity changes in widespread brain areas compared with sham stimulation both during and after stimulation. Whereas bilateral tDCS predominantly modulated changes in primary and secondary motor as well as prefrontal regions, unilateral tDCS affected prefrontal, parietal, and cerebellar areas. No direct effect was seen under the stimulating electrode in the unilateral condition. The time course of changes in functional connectivity in the respective brain areas was nonlinear and temporally dispersed. These findings provide evidence toward a network-based understanding regarding the underpinnings of specific tDCS interventions.

centrality; graph-based analysis; noninvasive brain stimulation; primary sensorimotor cortex; resting-state fMRI

TRANSCRANIAL DIRECT CURRENT stimulation (tDCS) is a noninvasive brain stimulation technique known to modulate cortical excitability in a polarity-specific manner (Nitsche et al. 2008). For example, anodal tDCS applied over the primary sensorimotor cortex (SM1) increases corticospinal excitability even beyond the stimulation period, whereas cathodal tDCS decreases it (Nitsche and Paulus 2000). Studies using excitability measurements of the living human brain with transcranial magnetic stimulation (TMS) as well as pharmacological interventions suggested that an increase of excitability induced by anodal stimulation and a decrease of excitability induced by cathodal stimulation depend on changes in the neuronal membrane potential (Nitsche et al. 2003a, 2005). More specifically, anodal tDCS has been shown to result in a depolarization while cathodal stimulation leads to a hyperpolarization of the resting membrane potential. Furthermore, at least for anodal stimulation, a study using magnetic resonance spectroscopy provided evidence that anodal tDCS leads to locally reduced GABA while cathodal stimulation causes reduced glutamatergic neuronal activity with a highly correlated reduction in GABA (Stagg et al. 2009).

In light of these findings, the application of tDCS has reemerged in the last decade as a tool to effectively modulate brain function. Until now, behavioral effects of tDCS have been extensively studied in motor control and motor learning (for review, see Reis et al. 2008). For example, anodal tDCS delivered over SM1 has been consistently shown to transiently improve performance and/or learning of various motor tasks in both healthy subjects (Nitsche et al. 2003c; Stagg et al. 2011) and chronic stroke patients (Hummel et al. 2005; Lindenberg et al. 2010). Furthermore, when applied in multiple sessions on 5 consecutive days, long-term improvements in a sequential pinch force task for up to 3 mo were observed (Reis et al. 2009). These results, together with findings in animal studies showing that tDCS acts upon brain-derived neurotrophic factor (BDNF)-dependent synaptic plasticity, further strengthen its potential as an adjuvant tool in neurorehabilitation (Fritsch et al. 2010).

One important yet open question relates to the optimal arrangement of the tDCS electrodes in order to achieve maximum stimulation effects. In the motor domain, a commonly used tDCS setup consists of a unilateral anodal tDCS electrode over SM1 contralateral to the moving/learning extremity (unilateral tDCS), while the other electrode is applied to the contralateral supraorbital region. More recently, a new tDCS electrode arrangement, which uses simultaneous anodal tDCS of one SM1 and cathodal tDCS of the homologous SM1 (bilateral tDCS), yielded more prominent behavioral effects in healthy subjects during a finger sequence task (Vines et al. 2008) and led to an improvement of the motor deficit in chronic stroke patients (Lindenberg et al. 2010). The more powerful effects of bilateral tDCS over SM1 have been assumed to be related to a more pronounced interference with interhemispheric information processing compared with unilateral tDCS over SM1 (Vines et al. 2008). However, the exact underlying neural mechanisms still remain elusive and certainly require further investigation.

The concurrent use of neuroimaging techniques such as functional magnetic resonance imaging (fMRI) and noninvasive brain stimulation has the potential to uncover neural

* B. Sehm and A. Schäfer made equal contributions to this work.

Address for reprint requests and other correspondence: B. Sehm, Max Planck Inst. for Human Cognitive and Brain Sciences, Dept. of Neurology, Stephanstr. 1a, D-04103 Leipzig, Germany (e-mail: sehm@cbs.mpg.de).

mechanisms of both uni- and bilateral SM1 tDCS effects as proposed for concurrent TMS and fMRI (see Bestmann et al. 2008 for review). Likewise, a number of studies have investigated tDCS-induced changes of functional activation with both fMRI and positron emission tomography during performance of a motor task (Antal et al. 2011; Baudewig et al. 2001; Holland et al. 2011; Kwon and Jang 2011; Lang et al. 2005; Venkatakrishnan and Sandrini 2012). Unlike task-evoked fMRI changes, resting-state fMRI (rs-fMRI) measures spontaneous fluctuations of the BOLD signal in the absence of task engagement. These fluctuations are not random but temporally coherent, thus providing a measure of the brain's intrinsic functional architecture (Fox and Raichle 2007). Recently, a longitudinal learning study provided compelling evidence that patterns of rs-fMRI are persistently modulated by a complex motor skill training over several weeks (Taubert et al. 2011). Furthermore, with the use of unilateral tDCS over SM1, it was demonstrated that rs-fMRI measurements (pre-post design) are capable of depicting tDCS-induced aftereffects on functional connectivity (Pena-Gomez et al. 2012; Polania et al. 2011b).

In the present study, we aimed to investigate changes in intrinsic functional connectivity elicited by both unilateral and bilateral tDCS over SM1 during and after stimulation without any task engagement. Only recently, a first proof-of-concept study validated the technical feasibility of concurrent tDCS and rs-fMRI measurements (Alon et al. 2011). Here the authors investigated changes in functional connectivity between both SM1, using a region of interest approach during short blocks of anodal tDCS (7 min) over right SM1. Despite a highly variable response to tDCS, most likely due to the small sample size of five subjects, the aforementioned study revealed a decrease in functional connectivity from the right to the left SM1 during tDCS.

In this study we aimed at extending these findings by various important factors. First, we aimed at tracking changes in functional connectivity during the course of 20 min of tDCS. This stimulation duration has been most commonly used in studies of motor behavior and learning (Reis et al. 2009; Vines et al. 2008). Second, in order to obtain information regarding potential aftereffects of the stimulation, we continued scanning for a further ~15 min. Third, we compared two different stimulation setups (bilateral and unilateral tDCS over SM1) with sham stimulation to better understand the neurophysiological underpinnings. Fourth, we aimed at investigating the effects of both stimulation approaches on large-scale brain networks by using eigenvector centrality mapping (ECM). ECM is a graph-based measure for centrality in functional brain networks that attributes a value to each voxel in the brain such that a voxel receives a large value if it is strongly correlated with many other nodes that are themselves central within the network. Thus it allows for the exploratory tracking of changes in network architecture across the whole brain (Lohmann et al. 2010; Zuo et al. 2012).

Using this experimental setup, we tested the hypothesis that bilateral and unilateral tDCS over SM1 relative to sham stimulation result in differential time-dependent engagements of intrinsic functional connectivity networks in human subjects.

METHODS

Subjects. We enrolled a total of 12 healthy young volunteers in the study (mean ± SD age 25.8 ± 3.2 yr; 4 women, 8 men). All subjects gave written informed consent to participate in the experiment according to the Declaration of Helsinki, and the ethics committee of the University of Leipzig approved the study. Prior to participation, all subjects underwent a comprehensive neurological examination to screen for potential exclusion criteria. They were not taking any medication. Subjects that did not meet the protocol criteria and/or had contraindications for tDCS or MRI measurements were excluded from participation. In each subject, handedness was assessed based on the Edinburgh Handedness Inventory (Oldfield 1971). Patients reported their hand preference (i.e., right, left, or ambidextrous) in response to 10 questions (e.g., Which hand do you use to light a match? Use scissors? Write?). Responses to the 10 questions were converted to a laterality quotient (LQ) with the formula $(R - L)/(R + L) \times 100$. LQ scores thus might range from −100 (corresponding to strong left-handedness) to +100 (corresponding to strong right-handedness). For our study, only moderately to strongly right-handed subjects, e.g., subjects with an LQ of at least +60 (92.08 ± 11.64; mean ± SD) were included (see, e.g., Isaacs et al. 2006).

Experimental design. Each subject participated in a total of three sessions that comprised concurrent tDCS over SM1 and rs-fMRI in a crossover design. The only difference between each session was the type of tDCS: unilateral tDCS (with the anode placed over the right SM1 and the cathode placed over the contralateral orbit), bilateral tDCS (with anodal stimulation of right and cathodal stimulation of left SM1), or sham stimulation (here, the setup of the unilateral or bilateral tDCS condition was randomly chosen). The order of the sessions was randomized between and within subjects. Sessions were separated by at least 1 wk to avoid any carryover effects.

Transcranial direct current stimulation. tDCS was delivered by a battery-driven DC current stimulator (Neuroconn, Ilmenau, Germany) with a pair of electrodes in a 5 × 7-cm saline-soaked sponge. The electrodes were manufactured to be compatible with the MR scanner environment (Neuroconn) and equipped with ~5-kΩ resistors in each wire to avoid sudden temperature increases due to induction currents from radio frequency pulses, as described previously (Antal et al. 2011). The electrode cables ran through the MR room and passed a radio frequency filter in the MR cabin wall in order to reduce potential artifacts during image acquisition. The cables were connected to a MR-compatible DC stimulator that was placed outside the scanner room. Two filter boxes (Neuroconn) were placed between electrodes and stimulator.

Before MRI scanning, the electrodes were attached to the subject's head with elastic bands. We deployed different electrode montages for each session in accordance with a previously published study (Vines et al. 2008). For unilateral right SM1 stimulation, the anode was centered over C4 according to the International 10-20 System while the cathode was attached to the forehead above the contralateral orbit. For bilateral SM1 stimulation, the anode was centered over C4 (corresponding to right SM1) while the cathode was centered over C3 (corresponding to the left SM1; see also Fig. 1*A*).

For all experimental conditions (unilateral and bilateral tDCS over SM1 and sham stimulation), the current was increased in a ramplike fashion over the first 30 s of stimulation to a maximum of 1 mA, eliciting a transient tingling sensation on the scalp. tDCS was delivered for 20 min in the uni- and bilateral tDCS conditions and for up to 30 s in the sham stimulation condition. During stimulation, a continuous monitoring of the impedance revealed no changes throughout the experiment. The current density at the stimulation electrodes at our maximum setting of 1 mA for uni- and bilateral tDCS over SM1 was 0.028 mA/cm^2. Total charge as expressed by current density × total stimulation duration (s) was 0.034 C/cm^2. Thereafter, currents were turned off slowly over a few seconds, precluding sensory differences between conditions (Nitsche et al. 2003b). This strategy has been shown to be efficient in blinding of the procedure (Gandiga et al. 2006; Ragert et al. 2008).

Scanning protocol. fMRI data were acquired under eyes-closed conditions on a Siemens Magnetom Tim Trio 3 Tesla scanner

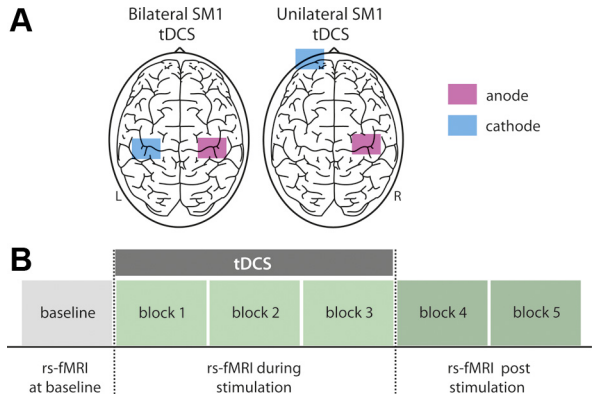

Fig. 1. Experimental setup showing the different electrode montages used (*A*) and the time course of 1 experiment (*B*). *A*: for bilateral transcranial direct current stimulation (tDCS) over primary sensorimotor cortex (SM1), the anode was mounted over the right SM1 while the cathode was mounted over the homologous left SM1. For unilateral SM1 tDCS, the anode was again placed over the right SM1, while the cathode electrode was mounted over the contralateral supraorbital region. *B*: during each experimental session, an initial baseline scan was acquired before tDCS application. Subsequently, the respective tDCS (unilateral, bilateral, or sham SM1 tDCS) was applied for 20 min during the next 3 blocks (total of 600 volumes, duration of ~23 min), followed by 2 additional echo-planar imaging (EPI) blocks (duration of ~15.3 min) that were acquired directly after tDCS. The same procedure applied for the sham stimulation condition except that the tDCS was only applied for ~30 s. For details, see METHODS. rs-fMRI, resting-state fMRI.

equipped with a standard eight-channel head coil. During each session, a total of 6 blocks of echo-planar imaging (EPI) were acquired with 200 whole-brain volumes, each using the following parameters: acquisition matrix = 64 × 64, slice thickness = 3 mm (1-mm gap), voxel dimensions = 3 × 3 × 4 mm, 34 slices, TR = 2,300 ms, TE = 30 ms, flip angle = 90°, bandwidth = 1,825 Hz. The total time for each fMRI session was ~55 min. Before scanning, tDCS electrodes were attached to the scalp of each subject outside of the scanner room (see also tDCS procedures above). Subsequently, subjects were brought into the scanner room, and one EPI sequence (duration ~7.6 min) was acquired before tDCS application (rs-fMRI at baseline). Subsequently, the respective tDCS condition (unilateral, bilateral, or sham tDCS over SM1) was started and applied for 20 min for the *verum* conditions during the next three blocks (total of 600 volumes, duration of ~23 min) followed by two additional EPI blocks (total of 400 volumes, duration of ~15.3 min) that were acquired directly after the stimulation (also see Fig. 1*B*). The same procedure applied for the sham stimulation condition except that the tDCS was only delivered for ~30 s.

Preprocessing and statistical analysis of fMRI data. In brief, as described previously (Lohmann et al. 2010; Taubert et al. 2011), preprocessing of fMRI data was performed with LIPSIA (Lohmann et al. 2001) and included motion correction, band-pass filtering (1/90–1/10 Hz), and spatial smoothing [6-mm full-width half-maximum (FWHM) smoothing]. Preprocessed data sets were registered into standard MNI152 (Montreal Neurological Institute) brain space and resampled to an isotropic voxel grid with a resolution of 3 × 3 × 3 mm. ECM (Lohmann et al. 2010) was used to map changes in network architecture induced by tDCS. ECM is a graph-based method that aims to map the central hubs of functional connectivity networks. ECM specifically weights nodes based on their degree of connection within the network. It does so by counting both the number and the quality of connections so that a node with relatively few connections to some high-ranking other nodes may outrank one with a larger number of mediocre contacts. Google's "PageRank" algorithm is a variant of eigenvector centrality. Compared with other centrality measures, ECM is computationally fast and does not depend on a preselected set of nodes (Zuo et al. 2012). This measure may be applied to all voxels in the brain, thereby avoiding any selection bias. Here we performed voxelwise analyses of rs-fMRI data. This requires in our study a large region of interest of ~63,000 voxels covering the whole brain including the cerebellum, rendering other centrality measures, such as betweenness centrality, computationally intractable (Lohmann et al. 2010). ECM enabled us to obtain whole-brain centrality maps and use them in a manner similar to contrast maps obtained in standard regression analyses. Furthermore, ECM does not depend on a prespecified threshold for correlation values and captures small-world characteristics of the human brain in contrast to other measures such as, e.g., degree centrality (Bonacich 2007; Lohmann et al. 2010). One of the strengths of ECM compared with other related analysis techniques [such as independent component analysis (ICA)] is that ECM captures the centrality of each voxel in a given network while methods such as ICA rather identify subnetworks on a whole-brain level. Thus only voxels changing their network association would be identified with ICA analyses. In light of this knowledge, we decided to use ECM instead of ICA in the present study.

Changes in eigenvector centrality of functional connectivity are described as "eigenvector centrality changes" or "centrality changes in functional connectivity" for the sake of simplicity throughout the text.

After preprocessing, single-subject eigenvector centrality maps were computed for each condition (bilateral, unilateral, and sham SM1 stimulation) and each scanning block (baseline, *blocks 1–5*). Subsequently, ECM maps were used for group-level analysis using general linear regression. z-Maps were thresholded at $z > 3.3$ on a voxel level. Furthermore, corrections for multiple comparisons were implemented at the cluster level with alphasim (cluster significance $P < 0.05$, corrected), which is a cluster size-based Monte Carlo simulation (Forman et al. 1995).

Changes in eigenvector centrality during stimulation were analyzed as follows: z-Maps of the stimulation period (e.g., average of *blocks 1*, *2*, and *3*; refer to Fig. 1*B*) were contrasted against baseline for each condition separately and compared with sham stimulation, in line with a recently published study (Keeser et al. 2011): (bilateral > baseline) > (sham > baseline); (unilateral > baseline) > (sham > baseline).

In a next step, we performed an additional linear regression analysis (see above) comparing differences in eigenvector centrality between bilateral and unilateral tDCS over SM1 during stimulation (*blocks 1–3*): (bilateral > baseline) > (unilateral > baseline); (unilateral > baseline) > (bilateral > baseline).

The aftereffects of the stimulation on eigenvector centrality were analyzed in a similar way by averaging *blocks 4* and *5* contrasted with baseline for both conditions (bi- and unilateral tDCS over SM1) relative to sham stimulation. Subsequently, we performed stepwise comparisons for each block (*blocks 1–5*) against baseline compared with sham stimulation in order to detect potential dynamic changes in eigenvector centrality over time.

As an additional analysis step, differences in eigenvector centrality between stimulation conditions at baseline were analyzed by contrasting the baseline block of each condition (sham, unilateral, bilateral tDCS over SM1) with each other: baseline (sham) vs. baseline unilateral; baseline sham vs. baseline bilateral; baseline unilateral vs. baseline bilateral.

RESULTS

Differences in eigenvector centrality between conditions at baseline. First, we performed baseline comparisons between conditions (bilateral, unilateral, and sham tDCS over SM1). This analysis revealed differences in eigenvector centrality between the three stimulation conditions in several subcortical and cortical areas (Fig. 2).

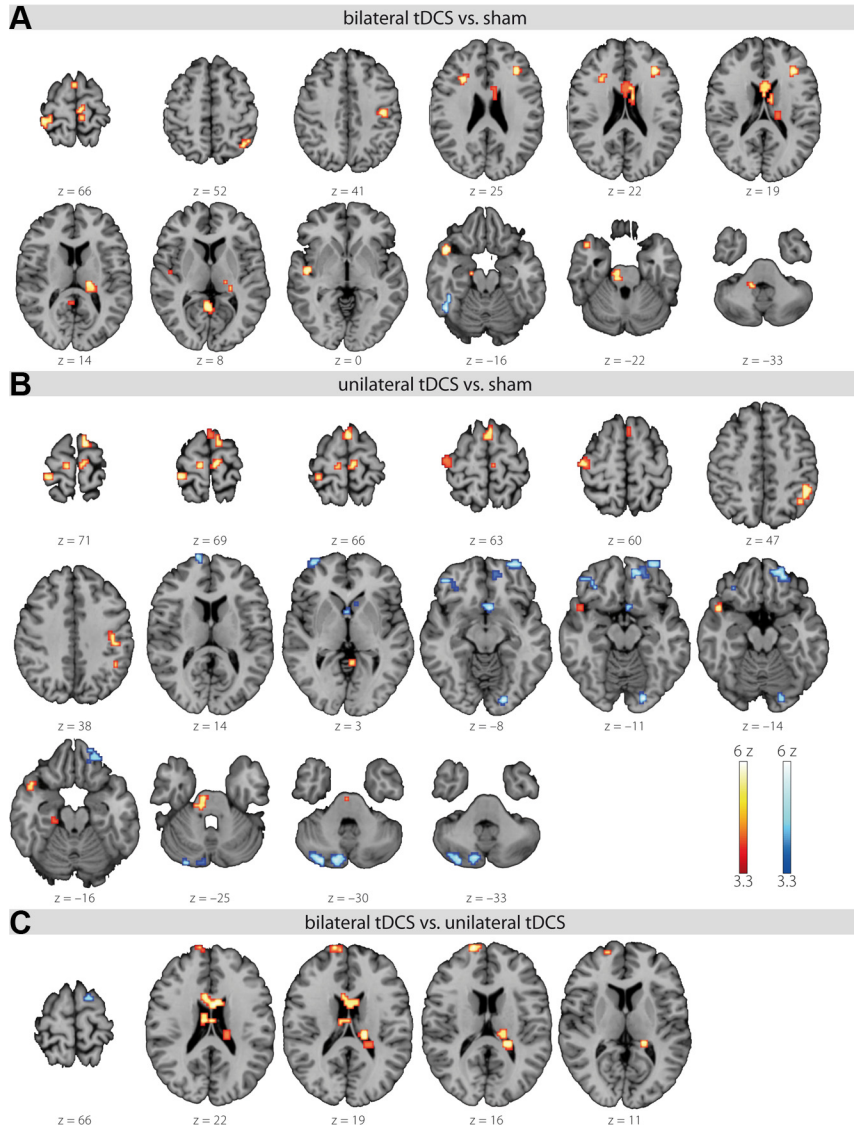

Fig. 2. Baseline comparisons between conditions (bilateral, unilateral, and sham SM1 tDCS). *A*: significant clusters of the comparison bilateral > sham are displayed in red and the inverse contrast (sham > bilateral) in blue. *B*: significant clusters of the comparison unilateral > sham are displayed in red and the inverse contrast (sham > unilateral) in blue. *C*: significant clusters of the comparison bilateral > unilateral are displayed in red and the inverse contrast (unilateral > bilateral) in blue. For the analysis, only the 1st scanning block (baseline, see Fig. 1) of each condition was used. All clusters are presented on axial slices at a threshold of $z > 3.3$ ($P < 0.05$, corrected on cluster level).

Changes in eigenvector centrality during bi- and unilateral SM1 stimulation. Twenty minutes of bilateral tDCS over SM1 (*blocks 1–3*) resulted in increased eigenvector centrality in networks that included motor-related regions such as right primary motor cortex (M1), dorsal premotor cortex (PMd), and bilateral supplementary motor area (SMA) compared with sham stimulation. Furthermore, prefrontal regions were also modulated, such as right superior frontal gyrus (SFG), inferior frontal gyrus (IFG), and left middle frontal gyrus (MFG).

In contrast, during unilateral tDCS only left fronto-temporal and bilateral parietal areas showed a significantly increased centrality in functional connectivity compared with sham stimulation. Furthermore, we found an increase within the right cerebellum (lobule VIIa), ipsilateral to the site of stimulation ($P < 0.001$, corrected; see Fig. 3 and Table 1). Interestingly, no change in eigenvector centrality was found in the cortical area below the stimulating tDCS electrode: the right SM1.

Differential effects on eigenvector centrality during bi- and unilateral SM1 stimulation. A direct comparison between eigenvector centrality changes during 20 min of bi- and unilateral tDCS over SM1 (*blocks 1–3*) revealed differential effects between stimulation types. Bilateral tDCS over SM1 resulted in significantly larger eigenvector centrality changes predominantly in primary and secondary motor areas (including right M1, PMd, and left SMA/pre-SMA), bilateral prefrontal areas (SFG), and subcortical regions compared with unilateral tDCS over SM1. On the other hand, unilateral compared with bilateral tDCS over SM1 resulted in significantly larger increases in right prefrontal (SFG), left parieto-temporal, and subcortical areas including the globus pallidum ($P < 0.001$, corrected, see Fig. 4; for details see Table 2).

Aftereffects of uni- and bilateral stimulation over SM1 on eigenvector centrality. After bilateral tDCS over SM1 (*blocks 4* and *5*), we observed an increase of centrality in functional connectivity in motor-related brain regions such as right M1, PMd, as well as bilateral SMA. Since these regions also showed a significant modulation during stimulation, this result indicates that the increase in eigenvector centrality in these regions persisted for at least 15 min after termination of stimulation. Furthermore, we observed additional alterations in bilateral prefrontal areas that developed after the stimulation period ($P < 0.001$, corrected; see also Table 3 and Fig. 5).

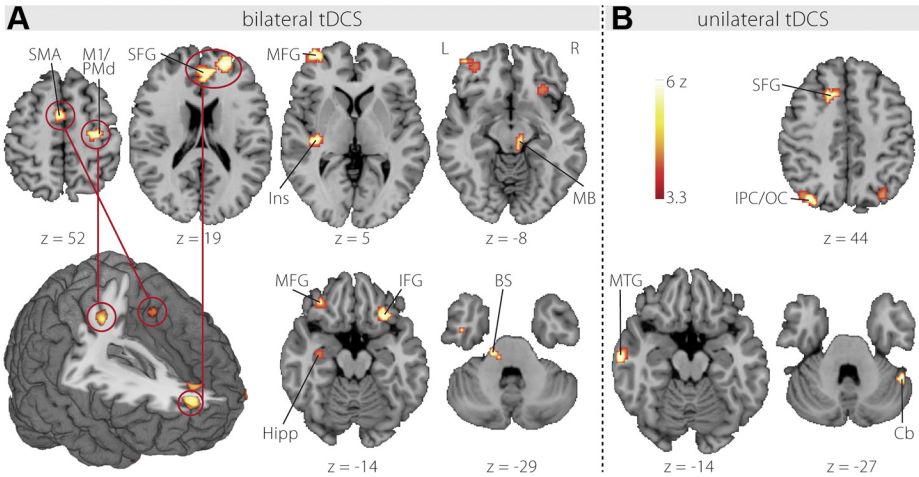

Fig. 3. Brain areas that showed a significant increase in eigenvector centrality during bilateral tDCS over SM1 (*A*) and unilateral tDCS over SM1 (*B*) compared with sham stimulation. Significant clusters are presented on axial slices at a threshold of $z > 3.3$ ($P < 0.05$, corrected on cluster level). Color bars indicate z score in a range of 3.3–6. M1/PMd, primary motor cortex/dorsal premotor cortex; SMA, supplementary motor area; SFG, superior frontal gyrus; MFG, middle frontal gyrus; Ins, posterior insula; MB, midbrain; IFG, inferior frontal gyrus; Hipp, hippocampus; BS, brain stem; IPC/OC, inferior parietal/occipital cortex; MTG, middle temporal gyrus; Cb, cerebellum lobule VIIa hemisphere.

After unilateral tDCS (*blocks 4* and *5*) we observed an increase of eigenvector centrality within the right prefrontal cortex, left middle temporal lobe, right fusiform and middle temporal gyrus, as well as bilateral cerebellum ($P < 0.001$, corrected). See Table 3 for a detailed list of all clusters as well as Fig. 5.

Stepwise comparison of stimulation-induced connectivity changes over time versus baseline. We further assessed changes in eigenvector centrality in each single scanning block (see Fig. 1) compared with baseline, which in turn enabled us to continuously track changes over time, e.g., during (*blocks 1–3*) as well as after (*blocks 4* and *5*) tDCS (for an overview refer to Fig. 6). As described above, bilateral and unilateral tDCS over SM1 resulted in a differential modulation of neuronal networks both during and after stimulation. Moreover, we observed diverse, nonlinear patterns of changes in centrality of functional connectivity within different brain areas over time (see Fig. 6). For example, the bilateral SM1 tDCS condition resulted in a significant change in eigenvector centrality within the cluster of right M1 during the first stimulation block compared with baseline. This effect decreased in *blocks 2* and *3* and subsequently increased again in *blocks 4* and *5* (after stimulation). In contrast, we observed a different pattern over time within right SFG. Here, a steady increase in eigenvector centrality during bilateral SM1 tDCS (*blocks 1–3*) was followed by a decrease after termination of stimulation. Similar diverse patterns are observed in other brain areas for uni- as well as bilateral SM1 tDCS as shown in Fig. 6. In general, these results disclose a temporally and spatially dispersed nonlinear pattern of tDCS-induced centrality changes of whole-brain functional connectivity for both conditions.

Table 1. *Brain regions that show significant increases in eigenvector centrality during bilateral and unilateral tDCS over SM1 compared with sham stimulation*

Brain Area	H	BA	Coordinates (tal)			z Max	Cl
			x	*y*	*z*		
Bilateral tDCS							
M1/PMd	R	4/6	26	−18	49	4.95	837
SMA	L	6	−3	0	52	4.34	486
anterior SFG	R	10	20	51	19	6	3,726
MFG	L	10	−38	57	5	4.99	1,161
		11	−35	48	−11	3.95	621
IFG (p. orbit.)	R	47	26	24	−14	5.54	1,080
Posterior insula	L	13	−38	−24	3	5.72	756
Midbrain	R		9	−24	−8	4.42	459
Hippocampus	L		−32	−12	−19	4.82	648
Brain stem	L		−17	−21	−25	4.41	513
Unilateral tDCS							
SFG	L	8	−17	18	44	4.32	459
IPC/OC	L	19/39	−35	−78	41	5.29	999
IPC/OC	R	19/39	32	−72	38	4.78	783
MTG	L	21	−64	−15	−14	4.92	513
Cb Lob VIIa Hem	R		46	−51	−27	5.02	405

tDCS, transcranial direct current stimulation; SM1, primary sensorimotor cortex; H, hemisphere; BA, Brodmann area; tal, Talairach space; z max, maximum z value; Cl, cluster size; M1, primary motor cortex; PMd, dorsal premotor cortex; SMA, supplementary motor area; SFG, superior frontal gyrus; MFG, middle frontal gyrus; IFG (p. orbit.), inferior frontal gyrus, pars orbitalis; IPC, inferior parietal cortex; OC, occipital cortex; MTG, middle temporal gyrus; Cb, cerebellum.

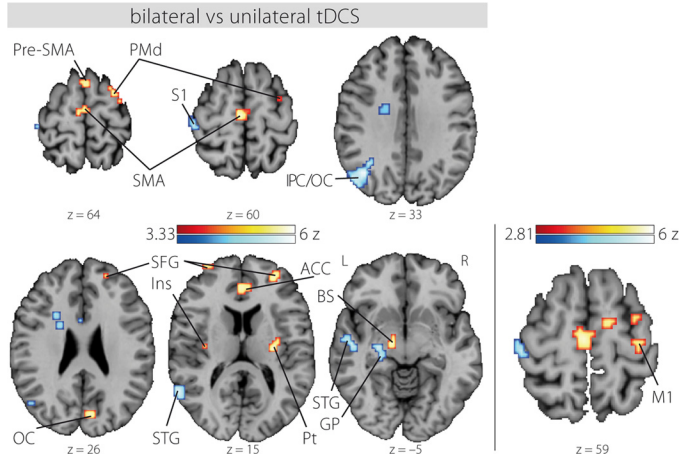

Fig. 4. Differential effects of bilateral vs. unilateral tDCS over SM1 on eigenvector centrality. Bilateral tDCS results in stronger eigenvector centrality increases in primary and secondary motor areas (including right M1, PMd, and left SMA/pre-SMA), bilateral prefrontal areas (SFG), and subcortical regions when directly compared to unilateral SM1 tDCS (bilateral > unilateral tDCS, clusters shown in red). Significant clusters of the inverse contrast (unilateral > bilateral tDCS) are shown in blue. The corrected threshold was set to $z > 3.3$. Color bars indicate z score in a range of 2.8–6 ($P < 0.05$, corrected on cluster level). Pre-SMA, pre-supplementary motor area; Ins, insula; Pt, putamen; S1, primary somatosensory cortex; STG, superior temporal gyrus; GP, globus pallidum.

Table 2. *Differential effects of bilateral and unilateral tDCS over SM1 on eigenvector centrality during stimulation*

Brain Area	H	BA	Coordinates (tal)			z Max	Cl
			x	*y*	*z*		
Bilateral tDCS > unilateral tDCS							
PMd	R	6	26	−12	69	4.29	594
M1	R	4	35	−23	58	3.31	
Pre-SMA	L	6	−3	15	69	4.73	486
SMA	L	6	−3	−18	58	4.87	783
SFG	R	10	29	51	11	4.79	1,458
SFG	L	10	−32	60	16	3.88	945
ACC	L	32	−3	39	14	4.35	783
OFC	R	11	23	30	−16	4.19	432
Insula	L	13	−35	−15	16	4.23	405
OC	R	18	6	−78	25	4.43	486
Putamen	R		29	−15	14	5.13	432
BS	L		−12	−15	−8	5.71	594
Cb Lob VIIb Vermis	L		−3	−72	−25	5.85	837
Unilateral tDCS > bilateral tDCS							
SFG	R	8	17	21	49	4.62	432
S1	L	1	−46	−27	60	4.83	729
IPC/OC	L	39/19	−38	−66	33	5.69	3,267
STG	L	22	−58	−57	14	4.86	1,512
STG	L	22	−52	−12	−3	5.58	1,026
GP	L		−26	−18	−5	4.49	675

ACC, anterior cingulate cortex; OFC, orbitofrontal cortex; BS, brain stem; S1, primary somatosensory cortex; STG, superior temporal gyrus; GP, globus pallidum.

DISCUSSION

Here we provide novel evidence that tDCS over SM1 is capable of modulating functional whole-brain resting-state network connectivity during as well as after stimulation (Zheng et al. 2011). The experimental setup with concurrent tDCS and fMRI allowed us to continuously track tDCS-induced effects on resting-state functional connectivity over time. We showed that bilateral tDCS over SM1 resulted in widespread connectivity changes such as in primary and secondary motor as well as prefrontal cortex. In contrast, unilateral tDCS over SM1 predominantly modulated functional connectivity in prefrontal, parietal, and cerebellar areas. Furthermore, we observed for both stimulation types differential effects not only during but also after tDCS that persisted for at least 15 min. The time course of changes in functional connectivity in the respective brain areas was nonlinear and temporally dispersed.

The combination of noninvasive brain stimulation and modern neuroimaging techniques enables investigation of not only local but also global effects of tDCS on brain networks, e.g., by combining noninvasive brain stimulation and fMRI or EEG measurements (Bestmann et al. 2008; Kirimoto et al. 2011; Neuling et al. 2012). However, until now, only a small number of studies have investigated the effect of noninvasive brain stimulation protocols such as repetitive (r)TMS (e.g., van der Werf et al. 2010) on resting-state networks. Even less is known regarding the effects of tDCS on resting-state functional connectivity. In a first proof of concept on five healthy subjects, the technical feasibility of concurrent tDCS and rs-fMRI measurements could be demonstrated (Alon et al. 2011). Data analysis was restricted to both SM1 (region of interest approach), showing that a decrease in functional connectivity from right to left SM1 was induced by 7 min of anodal tDCS delivered over right SM1. In the present study, we used ECM analysis to identify changes in functional connectivity on a whole-brain level. The use of a centrality measure such as ECM is based on the assumption that important brain regions (hubs) interact with many other regions and facilitate integrative processes (Rubinov and Sporns 2010). The neurobiological interpretation of this measure is that nodes with a high value are interacting functionally with many other nodes in the network. Thus changes in centrality represent reorganizational processes within this functional network architecture.

In contrast to other centrality measures such as betweenness or degree centrality, ECM is parameter free and computationally fast and does not depend on prior assumptions (a priori information) (Lohmann et al. 2010). Previous studies commonly used an anatomical template of 90 regions of interest (Achard et al. 2006; He et al. 2009). However, we aimed to perform voxelwise analysis with our functional data. This required a large region of interest of ~63,000 voxels in our study, which makes measures such as betweenness centrality computationally intractable. The computational speed of ECM enabled us to obtain whole-brain centrality maps and use them in a manner similar to contrast maps obtained in standard regression analyses. Furthermore, in contrast to degree centrality, ECM does not depend on a prespecified threshold for correlation values and captures small-world characteristics of the human brain that degree centrality does not (Bonacich 2007; Lohmann et al. 2010). This method has been used before to detect reorganizational processes in functional connectivity induced by complex motor skill learning (Taubert et al. 2011). In our study, the use of ECM was motivated by findings of concurrent fMRI-TMS experiments showing that noninvasive brain stimulation over SM1 modifies the BOLD signal not only locally within the stimulated or adjacent cortical regions but

Table 3. *Aftereffects of bilateral and unilateral tDCS over SM1 on eigenvector centrality*

Brain Area	H	BA	Coordinates (tal)			z Max	Cl
			x	*y*	*z*		
Bilateral tDCS							
M1/PMd	R	4/6	26	−18	49	5.29	1,809
SMA	R	6	6	−24	66	4.16	621
	L	6	−6	−3	49	4.31	459
	R	6	9	−12	49	4.89	405
Pre-SMA	R	6	3	24	66	4.71	567
MFG	R	9	12	39	33	5.98	7,101
	R	9	43	21	36	4.22	459
OFC	L	11	−23	57	−11	5.1	3,834
IFG (p. orbit.)	R	47	29	24	−19	4.64	459
MTG	R	21	61	−21	−14	5.77	1,134
ITG	L	20	−52	−12	−25	5.24	729
Posterior insula	L		−38	−3	−11	4.18	513
TTG	L	41	−35	−27	8	4.99	594
Cb Lob VIIa Hem	R		38	−75	−27	4.54	702
Unilateral tDCS							
SFG	R	8	20	42	41	5.3	1,971
PHC	L	36	−38	−33	−8	5.43	2,430
FG	R	19	35	−66	−5	4.38	540
MTG	R	21	55	−15	−14	4.3	459
Cb Lob VI Hem	R		9	−66	−16	4.41	729
Cb Lob VIIa Hem	L		−43	−66	−16	3.67	405
Cb Lob VIIa Hem	R		46	−51	−25	5.5	594

ITG, inferior temporal gyrus; TTG, transverse temporal gyrus; PHC, parahippocampal gyrus; FG, fusiform gyrus.

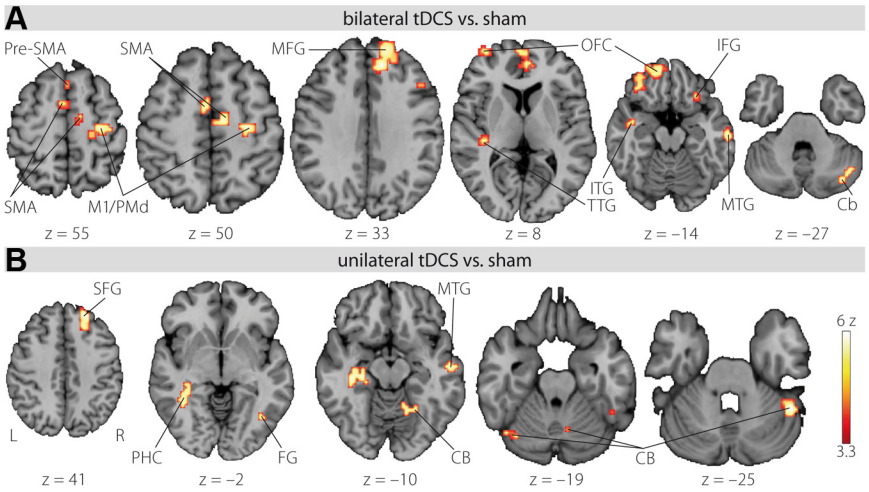

Fig. 5. Brain areas that showed a significant increase in eigenvector centrality after bilateral (*A*) and unilateral (*B*) tDCS over SM1 compared with sham stimulation. Significant clusters are presented on axial slices at a threshold of $z > 3.3$ ($P < 0.05$, corrected on cluster level). See also Table 3 for a detailed cluster list. OFC, orbitofrontal cortex; ITG, inferior temporal gyrus; TTG, transverse temporal gyrus; CB, cerebellum; PHC, parahippocampal cortex; FG, fusiform gyrus.

also in remote interconnected brain areas (Bestmann et al. 2004).

Other graph-theoretical analyses have been previously applied to investigate tDCS-induced neuroplastic changes. With the use of EEG (Polania et al. 2010) as well as fMRI (Polania et al. 2011b), it has been demonstrated that tDCS evokes intra- and interhemispheric connectivity changes after 10 min of stimulation over left M1. These effects were seen not only over the stimulated M1 but also in bilateral frontal, parietal, and premotor cortical regions (Polania et al. 2010). Furthermore, with the help of the higher spatial resolution in fMRI, it was demonstrated that 10 min of anodal tDCS over left SM1 increased short-range connections from M1 to premotor and parietal cortical regions, while concomitantly increasing interconnectedness in prefrontal cortex in resting brain dynamics (Polania et al. 2011b). Compared with our study, there are

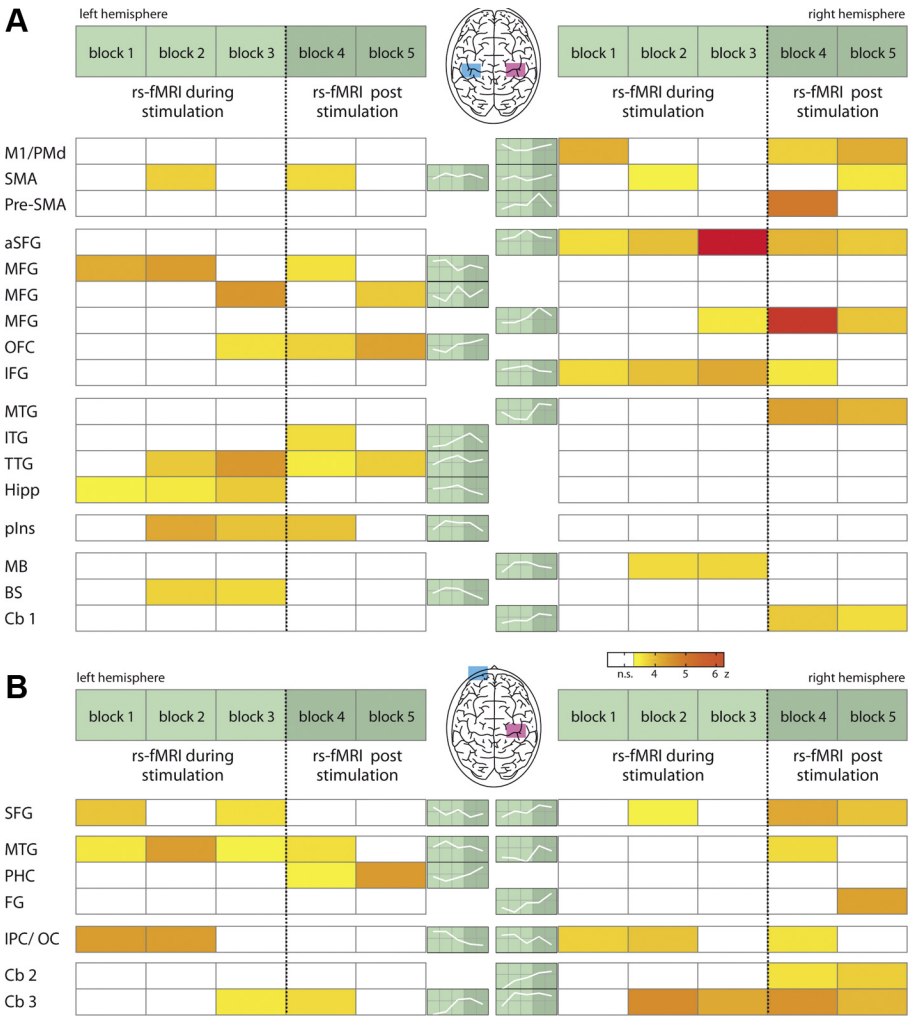

Fig. 6. Dynamic progression of changes in eigenvector centrality during (*blocks 1–3*) and after (*blocks 4* and *5*) bilateral (*A*) and unilateral (*B*) tDCS over SM1 compared with sham stimulation. Color-coded fields represent the z values resulting from the contrasts of a single block (*1–5*) and the baseline at a threshold of $z > 3.3$. During both conditions (*A* and *B*), distributed brain areas are modulated by tDCS. Note that the pattern of changes for both stimulation types seems to be nonlinear and temporally dispersed. The small line plots on green background represent continuous eigenvector centrality mapping (ECM) changes throughout the time course of the experiment and include below-threshold z values. Color bars indicate the z score in a range of 3.3–6.3; n.s., not significant. aSFG, anterior part of superior frontal gyrus; pIns, posterior insula; Cb, cerebellum, lobule VI.

some essential differences regarding the stimulation setup: Polania and colleagues used unilateral anodal tDCS of the left SM1, while in our study anodal tDCS was applied over the right SM1. Furthermore, the stimulation duration differed remarkably between the aforementioned studies (10 min in the study of Polania et al. vs. 20 min in our study). Despite methodological differences in these studies, tDCS in general seems to modulate widespread changes not only in local but also in distant brain areas.

Here we further extend previous work on tDCS-induced brain network changes by investigating two important issues. First, we provide novel evidence regarding dynamic online effects on large-scale networks during 20 min of tDCS. We chose this timescale to be consistent with relevant studies investigating behavioral effects of tDCS (e.g., Reis et al. 2009; Vines et al. 2008). Second, we provide evidence regarding differential tDCS effects induced by uni- and bilateral tDCS over SM1.

Effects of tDCS on functional connectivity during stimulation. During bilateral tDCS over SM1, we detected increases within a cluster covering right M1/PMd, e.g., the cortical area under the anodal electrode. Since a tDCS-related change in right M1/PMd was only elicited by bilateral (right anodal and left cathodal) and not unilateral (only right anodal) SM1 stimulation, it seems likely that not only the local facilitatory effect of the right anodal stimulation but also the additional cathodal (inhibitory) stimulation of the left SM1 contributed to this effect. As shown previously, cathodal tDCS leads to a decrease in corticospinal excitability, most likely through a hyperpolarization of the resting membrane potential, and/or through a modification of synaptic efficacy (Nitsche et al. 2005; Stagg and Nitsche 2011). Thus it is tempting to speculate that downregulation of left SM1 by cathodal tDCS results in a disinhibition of the interhemispheric inhibitory drive from the left to the right M1, which in turn causes the observed increase of eigenvector centrality of the homologous SM1. Alternatively, as shown recently in the somatosensory domain, a modulation of interhemispheric inhibitory interactions between primary somatosensory cortices might as well account for this effect (Ragert et al. 2011).

Since all subjects were right-handed, we cannot rule out that this effect might be due to a modulation of lateralized interhemispheric interactions between both M1 (Baumer et al. 2007). To elucidate this, further studies should investigate the effects of a converse stimulation setup. Nonetheless, our results raise the hypothesis that the previously reported superior effects of bilateral compared with unilateral right SM1 stimulation (Vines et al. 2008) are at least partly mediated by a modulation of functional connectivity in the right primary motor cortex.

Apart from eigenvector centrality changes in right SM1, bilateral tDCS over SM1 resulted in significant changes in secondary motor areas such as the premotor cortex (right PMd) and SMA. Previous animal and human studies showed that both areas are tightly interconnected with the stimulated SM1 (Civardi et al. 2001; Strick et al. 1998). Therefore, bilateral tDCS over SM1 might also result in changes within interconnected brain areas that are reflected by ECM. Similarly, remote effects of noninvasive brain stimulation in SMA have been successfully identified with the use of concurrent TMS over M1 and fMRI measurements (Bestmann et al. 2008).

In contrast to bilateral tDCS over SM1, no online changes in eigenvector centrality were found in SM1 or premotor areas during unilateral tDCS over SM1. The absence of unilateral tDCS effects in these areas was surprising and certainly requires further investigation. One important aspect of our experimental design is the fact that in the unilateral SM1 tDCS condition the right, nondominant motor cortex was the target area of anodal tDCS. This stimulation setup is consistent with the study by Vines and colleagues (Vines et al. 2008) that compared the effects of uni- and bilateral tDCS over the motor cortex on motor performance. With our experimental design we cannot rule out that different effects on functional connectivity would be observed if tDCS were applied over M1 of the dominant (left) hemisphere (Nitsche et al. 2003c), an issue that requires further investigation. In this vein, a recent study suggests that the dominance of the targeted motor cortex does differentially contribute to stimulation-induced aftereffects (Schade et al. 2012). Another important point with respect to this experimental condition pertains to the attachment of the cathodal electrode over the left supraorbital region. With our—well-established—stimulation setup it is not unlikely that a modulation of frontal activity by this electrode also contributes significantly to changes in functional connectivity that we observed on the whole-brain level.

Apart from the divergent results in SM1 and secondary motor areas, we observed changes in centrality in prefrontal areas during both uni- and bilateral tDCS over SM1. Studies in primates suggested that the prefrontal cortex is involved in motor control such as context-dependent movement selection (Matsumoto et al. 2003), supported by anatomical findings in macaques showing multisynaptic connections between prefrontal and premotor/motor cortex (Miyachi et al. 2005). Nevertheless, it still remains elusive whether centrality changes in prefrontal areas are directly related to a modulation of SM1 or rather reflect a general effect of tDCS on the resting-state network per se. Furthermore, as discussed above, in the unilateral SM1 tDCS condition it might be that the "reference" electrode attached to the contralateral supraorbital region also contributed at least partially to centrality changes within prefrontal areas that are in close spatial proximity to the electrode. At least for the bilateral SM1 tDCS condition, it is reasonable to assume that tDCS is capable of modulating the connectivity not only within adjacent, but also remote, brain areas such as the prefrontal cortex.

Interestingly, only unilateral facilitatory stimulation over right SM1, but not bilateral tDCS, with facilitatory right and inhibitory left SM1 stimulation induced an increase of centrality within the ipsilateral right cerebellum. Only recently could it be demonstrated that tDCS applied over the cerebellum modulates the overall inhibitory tone that exerts the cerebellum over the motor cortex (Galea et al. 2009). In our study it is tempting to speculate that the increase in centrality of the cerebellum during ipsilateral facilitation of SM1 might be mediated via facilitatory cerebrocerebellar interactions (Kelly and Strick 2003).

What is the potential meaning of the present study for future applications of tDCS in patient populations such as those with chronic stroke? The present data on healthy individuals certainly do not allow us to speculate as to whether one or the other setup might be more efficient in motor rehabilitation (Hummel et al. 2005; Lindenberg et al. 2010) but might help to

generate hypotheses for future studies. Given that we observed very different patterns of changes depending on the stimulation setup, it might be that patients who differ, e.g., in their lesion location might also differentially benefit from one stimulation setup or the other. Future studies need to address these questions in patient populations in order to identify benchmarks for the establishment of individualized adjuvant tDCS protocols in motor rehabilitation.

It remains noteworthy that a considerable part of the areas modulated by tDCS are not specifically related to motor planning or execution. Furthermore, in the unilateral SM1 stimulation condition we did not detect changes in eigenvector centrality within the stimulated cortex. Our results showing changes in remote regions induced by tDCS are in line with previous studies combining TMS and fMRI or PET. With this methodological approach, changes in activation (BOLD signal) in remote but interconnected regions have consistently been observed, even in the absence of significant changes in activity at the stimulation site (Bestmann et al. 2003, 2004; Bohning et al. 1999; Denslow et al. 2005). However, we applied well-established stimulation parameters (electrode size, stimulation intensity, stimulation duration; e.g., Vines et al. 2008). Thus we are confident that our results are, even though not specific to the motor system, specific to the tDCS conditions that were applied: bilateral and unilateral tDCS over primary sensorimotor cortices.

Dynamics of stimulation-induced centrality changes. Our study design using concurrent tDCS and high-resolution fMRI enabled us to continuously track changes in functional connectivity not only during but also after stimulation in order to unravel the dynamic processes of tDCS-induced neuroplasticity.

Here, covering both online effects and aftereffects of stimulation, we provide novel evidence that the pattern of tDCS-induced engagements of different neural networks is temporally dispersed. Previously, it was suggested that neuroplastic changes after the application of noninvasive brain stimulation protocols do not necessarily appear directly after the stimulation but may arise with a temporal delay. For example, after paired-associative stimulation (PAS), a specific form of noninvasive brain stimulation, functional changes in corticospinal excitability have been reported to appear after an interval of 20–30 min postintervention (Missitzi et al. 2011). The authors speculated that only after a latent interval might the optimal strengthening of the synaptic efficacy be consolidated and become apparent. It is tempting to translate this observation into the dynamic and diverse temporal onsets of functional resting-state changes as seen in our study. Along these lines, recent neuroimaging studies suggested that other plasticity-inducing interventions like motor sequence learning (Steele and Penhune 2010) or complex motor skill learning (Taubert et al. 2011) may result in not only steadily increasing (linear) brain alterations but, at least to some extent, also diverse, nonlinear dynamic changes within different brain areas.

Finally, the present study has some limitations. First, our method (ECM) relies on resting-state measurements of the BOLD signal; thus we do not have a behavioral measure that could prove the relevance of our stimulation protocols. Hence, we cannot directly claim that the effects that we observed are linked to behavioral consequences of tDCS. However, we used an established and frequently tested stimulation setup known to improve motor performance and learning (see e.g., Nitsche et al. 2003c; Vines et al. 2008). Here we aimed to study changes in functional connectivity elicited by these established stimulation protocols. Therefore, our study should be considered in line with previous studies that explored neurophysiological effects of tDCS in the absence of a behavioral task (e.g., Nitsche et al. 2003a; Nitsche and Paulus 2000; Polania et al. 2011b; Zheng et al. 2011). Second, by using rs-fMRI and a data-driven analysis approach (ECM), we certainly cannot claim to provide a complete picture of tDCS-induced connectivity changes. However, the scope of the present study was to obtain a global picture of tDCS-induced functional connectivity changes without hypotheses about special brain regions. To further elucidate the specific involvement of certain brain regions, such as the stimulated M1, more hypothesis-driven approaches should address these issues in future studies. Third, to avoid any potential bias from baseline differences in ECM between conditions (sham, bilateral, and unilateral tDCS over SM1) we normalized the ECM maps during and after tDCS against baseline. This analysis is in line with a recently published study investigating aftereffects of tDCS over the dorsolateral prefrontal cortex. Since we found in an additional analysis that baseline ECM maps were in fact different between conditions, the possibility remains that baseline differences per se might have influenced the tDCS-induced ECM changes. Similar findings have been reported in recent noninvasive brain stimulation studies, a phenomenon known as homeostatic plasticity (Ziemann and Siebner 2008). More specifically, we cannot entirely rule out the possibility that the individual preinterventional state might have had an impact on subsequent tDCS-induced ECM changes. The impact of homeostatic plasticity on ECM changes should therefore be of interest in future investigations.

In the present study, we did not record respiration and heartbeat to model physiological noise. Therefore, we cannot rule out the possibility that these parameters might influence our research findings. However, a previous study investigated the influence of these parameters on rs-fMRI data and highlighted that default-mode network changes cannot be explained by cardiorespiratory processes alone and are likely related to cognitive neuronal processing (van Buuren et al. 2009). Therefore, we are confident that the observed tDCS-induced ECM changes are not contaminated by physiological noise.

In summary, we have demonstrated that tDCS over SM1 induces widespread and dynamic changes in resting-state functional connectivity both during and after stimulation. The pattern of network connectivity changes is temporally and spatially dispersed and critically depends on the stimulation setup (unilateral and bilateral tDCS over SM1).

DISCLOSURES

No conflicts of interest, financial or otherwise, are declared by the author(s).

AUTHOR CONTRIBUTIONS

Author contributions: B.S., D.M., A.V., and P.R. conception and design of research; B.S., M.T., and P.R. performed experiments; B.S., A.S., J.K., D.M., and V.C. analyzed data; B.S., A.S., J.K., D.M., V.C., M.T., A.V., and P.R. interpreted results of experiments; B.S., A.S., and J.K. prepared figures; B.S., V.C., and M.T. drafted manuscript; B.S., A.S., J.K., D.M., V.C., M.T., A.V., and P.R. edited and revised manuscript; B.S., A.S., J.K., D.M., V.C., M.T., A.V., and P.R. approved final version of manuscript.

REFERENCES

Achard S, Salvador R, Whitcher B, Suckling J, Bullmore E. A resilient, low-frequency, small-world human brain functional network with highly connected association cortical hubs. *J Neurosci* 26: 63–72, 2006.

Alon G, Roys SR, Gullapalli RP, Greenspan JD. Non-invasive electrical stimulation of the brain (ESB) modifies the resting-state network connectivity of the primary motor cortex: a proof of concept fMRI study. *Brain Res* 1403: 37–44, 2011.

Antal A, Polania R, Schmidt-Samoa C, Dechent P, Paulus W. Transcranial direct current stimulation over the primary motor cortex during fMRI. *Neuroimage* 55: 590–596, 2011.

Baudewig J, Nitsche MA, Paulus W, Frahm J. Regional modulation of BOLD MRI responses to human sensorimotor activation by transcranial direct current stimulation. *Magn Reson Med* 45: 196–201, 2001.

Baumer T, Dammann E, Bock F, Kloppel S, Siebner HR, Munchau A. Laterality of interhemispheric inhibition depends on handedness. *Exp Brain Res* 180: 195–203, 2007.

Bestmann S, Baudewig J, Siebner HR, Rothwell JC, Frahm J. Subthreshold high-frequency TMS of human primary motor cortex modulates interconnected frontal motor areas as detected by interleaved fMRI-TMS. *Neuroimage* 20: 1685–1696, 2003.

Bestmann S, Baudewig J, Siebner HR, Rothwell JC, Frahm J. Functional MRI of the immediate impact of transcranial magnetic stimulation on cortical and subcortical motor circuits. *Eur J Neurosci* 19: 1950–1962, 2004.

Bestmann S, Ruff CC, Blankenburg F, Weiskopf N, Driver J, Rothwell JC. Mapping causal interregional influences with concurrent TMS-fMRI. *Exp Brain Res* 191: 383–402, 2008.

Bohning DE, Shastri A, McConnell KA, Nahas Z, Lorberbaum JP, Roberts DR, Teneback C, Vincent DJ, George MS. A combined TMS/fMRI study of intensity-dependent TMS over motor cortex. *Biol Psychiatry* 45: 385–394, 1999.

Bonacich P. Some unique properties of eigenvector centrality. *Social Netw* 29: 555–564, 2007.

Civardi C, Cantello R, Asselman P, Rothwell JC. Transcranial magnetic stimulation can be used to test connections to primary motor areas from frontal and medial cortex in humans. *Neuroimage* 14: 1444–1453, 2001.

Denslow S, Lomarev M, George MS, Bohning DE. Cortical and subcortical brain effects of transcranial magnetic stimulation (TMS)-induced movement: an interleaved TMS/functional magnetic resonance imaging study. *Biol Psychiatry* 57: 752–760, 2005.

Forman SD, Cohen JD, Fitzgerald M, Eddy WF, Mintun MA, Noll DC. Improved assessment of significant activation in functional magnetic resonance imaging (fMRI): use of a cluster-size threshold. *Magn Reson Med* 33: 636–647, 1995.

Fox MD, Raichle ME. Spontaneous fluctuations in brain activity observed with functional magnetic resonance imaging. *Nat Rev Neurosci* 8: 700–711, 2007.

Fritsch B, Reis J, Martinowich K, Schramba HM, Ji Y, Cohen LG, Lu B. Direct current stimulation promotes BDNF-dependent synaptic plasticity: potential implications for motor learning. *Neuron* 66: 198–204, 2010.

Galea JM, Jayaram G, Ajagbe L, Celnik P. Modulation of cerebellar excitability by polarity-specific noninvasive direct current stimulation. *J Neurosci* 29: 9115–9122, 2009.

Gandiga PC, Hummel FC, Cohen LG. Transcranial DC stimulation (tDCS): a tool for double-blind sham-controlled clinical studies in brain stimulation. *Clin Neurophysiol* 117: 845–850, 2006.

He Y, Wang J, Wang L, Chen ZJ, Yan C, Yang H, Tang H, Zhu C, Gong Q, Zang Y, Evans AC. Uncovering intrinsic modular organization of spontaneous brain activity in humans. *PLoS One* 4: e5226, 2009.

Holland R, Leff AP, Josephs O, Galea JN, Desikan M, Price CJ, Rothwell JC, Crinion J. Speech facilitation by left inferior frontal cortex stimulation. *Curr Biol* 21: 1403–1407, 2011.

Hummel F, Celnik P, Giraux P, Floel A, Wu WH, Gerloff C, Cohen LG. Effects of non-invasive cortical stimulation on skilled motor function in chronic stroke. *Brain* 128: 490–499, 2005.

Isaacs KL, Barr WB, Nelson PK, Devinsky O. Degree of handedness and cerebral dominance. *Neurology* 66: 1855–1858, 2006.

Keeser D, Meindl T, Bor J, Palm U, Pogarell O, Mulert C, Brunelin J, Möller HJ, Reiser M, Padberg E. Prefrontal transcranial direct current stimulation changes connectivity of resting-state networks during fMRI. *J Neurosci* 31: 15284–15293, 2011.

Kelly RM, Strick PL. Cerebellar loops with motor cortex and prefrontal cortex of a nonhuman primate. *J Neurosci* 23: 8432–8444, 2003.

Kirimoto H, Ogata K, Onishi H, Oyama M, Goto Y, Tobimatsu S. Transcranial direct current stimulation over the motor association cortex induces plastic changes in ipsilateral primary motor and somatosensory cortices. *Clin Neurophysiol* 122: 777–783, 2011.

Kwon YH, Jang SH. The enhanced cortical activation induced by transcranial direct current stimulation during hand movements. *Neurosci Lett* 492: 105–108, 2011.

Lang N, Siebner HR, Ward NS, Lee L, Nitsche MA, Paulus W, Rothwell JC, Lemon RN, Frackowiak RS. How does transcranial DC stimulation of the primary motor cortex alter regional neuronal activity in the human brain? *Eur J Neurosci* 22: 495–504, 2005.

Lindenberg R, Renga V, Zhu LL, Nair D, Schlaug G. Bihemispheric brain stimulation facilitates motor recovery in chronic stroke patients. *Neurology* 75: 2176–2184, 2010.

Lohmann G, Margulies DS, Horstmann A, Pleger B, Lepsien J, Goldhahn D, Schloegl H, Stumvoll M, Villringer A, Turner R. Eigenvector centrality mapping for analyzing connectivity patterns in FMRI data of the human brain. *PLoS One* 5: e10232, 2010.

Lohmann G, Muller K, Bosch V, Mentzel H, Hessler S, Chen L, Zysset S, von Cramon DY. LIPSIA—a new software system for the evaluation of functional magnetic resonance images of the human brain. *Comput Med Imaging Graph* 25: 449–457, 2001.

Matsumoto K, Suzuki W, Tanaka K. Neuronal correlates of goal-based motor selection in the prefrontal cortex. *Science* 301: 229–232, 2003.

Missitzi J, Gentner R, Geladas N, Karandreas N, Classen J, Klissouras V. Plasticity in human motor cortex is in part genetically determined. *J Physiol* 589: 297–306, 2011.

Miyachi S, Lu X, Inoue S, Iwasaki T, Koike S, Nambu A, Takada M. Organization of multisynaptic inputs from prefrontal cortex to primary motor cortex as revealed by retrograde transneuronal transport of rabies virus. *J Neurosci* 25: 2547–2556, 2005.

Neuling T, Rach S, Wagner S, Wolters CH, Herrmann CS. Good vibrations: oscillatory phase shapes perception. *Neuroimage* 63: 771–778, 2012.

Nitsche MA, Cohen LG, Wassermann EM, Priori A, Lang N, Antal A, Paulus W, Hummel F, Boggio PS, Fregni F, Pascual-Leone A. Transcranial direct current stimulation: state of the art 2008. *Brain Stimul* 1: 206–223, 2008.

Nitsche MA, Fricke K, Henschke U, Schitterlau A, Liebetanz D, Lang N, Henning S, Tergau F, Paulus W. Pharmacological modulation of cortical excitability shifts induced by transcranial direct current stimulation in humans. *J Physiol* 553: 293–301, 2003a.

Nitsche MA, Liebetanz D, Lang N, Antal A, Tergau F, Paulus W. Safety criteria for transcranial direct current stimulation (tDCS) in humans. *Clin Neurophysiol* 114: 2220–2222, 2003b.

Nitsche MA, Paulus W. Excitability changes induced in the human motor cortex by weak transcranial direct current stimulation. *J Physiol* 527: 633–639, 2000.

Nitsche MA, Schauenburg A, Lang N, Liebetanz D, Exner C, Paulus W, Tergau F. Facilitation of implicit motor learning by weak transcranial direct current stimulation of the primary motor cortex in the human. *J Cogn Neurosci* 15: 619–626, 2003c.

Nitsche MA, Seeber A, Frommann K, Klein CC, Rochford C, Nitsche MS, Fricke K, Liebetanz D, Lang N, Antal A, Paulus W, Tergau F. Modulating parameters of excitability during and after transcranial direct current stimulation of the human motor cortex. *J Physiol* 568: 291–303, 2005.

Oldfield RC. The assessment and analysis of handedness: the Edinburgh inventory. *Neuropsychologia* 9: 97–113, 1971.

Pena-Gomez C, Sala-Lonch R, Junque C, Clemente IC, Vidal D, Bargallo N, Falcon C, Valls-Sole J, Pascual-Leone A, Bartres-Faz D. Modulation of large-scale brain networks by transcranial direct current stimulation evidenced by resting-state functional MRI. *Brain Stimul* 5: 252–263, 2012.

Polania R, Nitsche MA, Paulus W. Modulating functional connectivity patterns and topological functional organization of the human brain with transcranial direct current stimulation. *Hum Brain Mapp* 32: 1236–1249, 2011a.

Polania R, Paulus W, Antal A, Nitsche MA. Introducing graph theory to track for neuroplastic alterations in the resting human brain: a transcranial direct current stimulation study. *Neuroimage* 54: 2287–2296, 2011b.

Ragert P, Nierhaus T, Cohen LG, Villringer A. Interhemispheric interactions between the human primary somatosensory cortices. *PLoS One* 6: e16150, 2011.

Ragert P, Vandermeeren Y, Camus M, Cohen LG. Improvement of spatial tactile acuity by transcranial direct current stimulation. *Clin Neurophysiol* 119: 805–811, 2008.

Reis J, Robertson EM, Krakauer JW, Rothwell J, Marshall L, Gerloff C, Wassermann E, Pascual-Leone A, Hummel F, Celnik PA, Classen J, Floel A, Ziemann U, Paulus W, Siebner HR, Born J, Cohen LG. Consensus: can transcranial direct current stimulation and transcranial magnetic stimulation enhance motor learning and memory formation? *Brain Stimul* 1: 363–369, 2008.

Reis J, Schambra HM, Cohen LG, Buch ER, Fritsch B, Zarahn E, Celnik PA, Krakauer JW. Noninvasive cortical stimulation enhances motor skill acquisition over multiple days through an effect on consolidation. *Proc Natl Acad Sci USA* 106: 1590–1595, 2009.

Rubinov M, Sporns O. Complex network measures of brain connectivity: uses and interpretations. *Neuroimage* 52: 1059–1069, 2010.

Schade S, Moliadze V, Paulus W, Antal A. Modulating neuronal excitability in the motor cortex with tDCS shows moderate hemispheric asymmetry due to subjects' handedness: a pilot study. *Restor Neurol Neurosci* 30: 191–198, 2012.

Stagg CJ, Best JG, Stephenson MC, O'Shea J, Wylezinska M, Kincses ZT, Morris PG, Matthews PM, Johansen-Berg H. Polarity-sensitive modulation of cortical neurotransmitters by transcranial stimulation. *J Neurosci* 29: 5202–5206, 2009.

Stagg CJ, Jayaram G, Pastor D, Kincses ZT, Matthews PM, Johansen-Berg H. Polarity and timing-dependent effects of transcranial direct current stimulation in explicit motor learning. *Neuropsychologia* 49: 800–804, 2011.

Stagg CJ, Nitsche MA. Physiological basis of transcranial direct current stimulation. *Neuroscientist* 17: 37–53, 2011.

Steele CJ, Penhune VB. Specific increases within global decreases: a functional magnetic resonance imaging investigation of five days of motor sequence learning. *J Neurosci* 30: 8332–8341, 2010.

Strick PL, Dum RP, Picard N. Motor areas on the medial wall of the hemisphere. *Novartis Found Symp* 218: 64–75, 1998.

Taubert M, Lohmann G, Margulies DS, Villringer A, Ragert P. Long-term effects of motor training on resting-state networks and underlying brain structure. *Neuroimage* 57: 1492–1498, 2011.

van Buuren M, Gladwin TE, Zandbelt BB. Cardiorespiratory effects on default-mode network activity as measured with fMRI. *Hum Brain Mapp* 30: 3031–3042, 2009.

van der Werf YD, Sanz-Arigita EJ, Menning S, van den Heuvel OA. Modulating spontaneous brain activity using repetitive transcranial magnetic stimulation. *BMC Neurosci* 11: 145, 2010.

Venkatakrishnan A, Sandrini M. Combining transcranial direct current stimulation and neuroimaging: novel insights in understanding neuroplasticity. *J Neurophysiol* 107: 1–4, 2012.

Vines BW, Cerruti C, Schlaug G. Dual-hemisphere tDCS facilitates greater improvements for healthy subjects' non-dominant hand compared to uni-hemisphere stimulation. *BMC Neurosci* 9: 103, 2008.

Zheng X, Alsop DC, Schlaug G. Effects of transcranial direct current stimulation (tDCS) on human regional cerebral blood flow. *Neuroimage* 58: 26–33, 2011.

Ziemann U, Siebner HR. Modifying motor learning through gating and homeostatic metaplasticity. *Brain Stimul* 1: 60–66, 2008.

Zuo XN, Ehmke R, Mennes M, Imperati D, Castellanos FX, Sporns O, Milham MP. Network centrality in the human functional connectome. *Cereb Cortex* 22: 1862–1875, 2012.

2.4 Three-dimensional mean-shift edge bundling for the visualization of functional connectivity in the brain

Böttger J., Schäfer A., Lohmann G., Villringer A., and Margulies D., Three-dimensional mean-shift edge bundling for the visualization of functional connectivity in the brain, IEEE Transactions of Visualization and Computer Graphics, 20 (3), 471–480, 2014

Three-Dimensional Mean-Shift Edge Bundling for the Visualization of Functional Connectivity in the Brain

Joachim Böttger, Alexander Schäfer, Gabriele Lohmann, Arno Villringer, and Daniel S. Margulies

Abstract—Functional connectivity, a flourishing new area of research in human neuroscience, carries a substantial challenge for visualization: while the end points of connectivity are known, the precise path is not. Although a large body of work already exists on the visualization of anatomical connectivity, the functional counterpart lacks similar methods. To optimize the clarity of whole-brain and complex connectivity patterns in 3D brain space, we develop mean-shift edge bundling, which reveals the multitude of connections as derived from correlations in brain activity of cortical regions.

Index Terms—Visualization applications, information visualization, visualization techniques and methodologies

1 Introduction

A core challenge in understanding brain organization is the visualization of its connectivity. Sophisticated visualizations of anatomical tracts based in diffusion weighted imaging (DWI) have proven essential to elevating the methodology. However, *functional connectivity*, an emerging approach based in the correlations of spontaneous brain activity, lacks effective visualization methods to clarify the inherent complexity of the connectivity graph.

Visualization of connectivity has almost exclusively focused on depicting spatially constrained anatomical tracts. However, *functional connectivity* [1] presents a novel problem for visualization. Functional connectivity is based on the statistically determined similarity between time-courses of activity in different brain areas. Since the first description of this method using data acquired "at rest" in 1995 [2], it has grown into a flourishing field of research (for a review, see [3]). Although it represents connections between brain regions, the precise anatomical path is unknown. This poses an exciting opportunity for visualization, as the representation of connections is constrained only by the optimization of visual clarity, and not the requirement to represent anatomical paths.

We describe our development of an *edge bundling* method to obtain a clearer picture of functional brain connectivity. To our knowledge, this is the first application of a visualization method to show high-resolution functional connectivity data across functional networks in its native anatomical space. Our method does not require selection of seed regions of interest, subdivision of the data into supposedly independent components, or other reduction steps such as spatial downsampling. Although the edge-bundling algorithm we use is an adaption of previous work, it contributes a stable and straightforward implementation for brain connectivity data. In this paper, we first introduce the data, and then describe our method to visualize full graphs of functional brain connectivity in anatomical 3D brain space.

• *The authors are with the Max-Planck Institute for Human Cognitive and Brain Sciences, 04103 Leipzig, Germany.*
E-mail: {boettgerj, aschaefer, lohmann, villringer, margulies}@cbs.mpg.de.

Manuscript received 6 Sept. 2012; revised 3 Apr. 2013; accepted 4 Aug. 2013; published online 13 Aug. 2013.
Recommended for acceptance by R. Machiraju.
For information on obtaining reprints of this article, please send e-mail to: tvcg@computer.org, and reference IEEECS Log Number TVCG-2012-09-0187.
Digital Object Identifier no. 10.1109/TVCG.2013.114.

2 Background

2.1 Connectomics

The defining feature of the nervous system has long been recognized as its interconnectedness, but the tools to actually map such connections noninvasively have only become feasible in the past decade. Notably, Francis Crick, codiscoverer of the molecular structure of DNA, lamented the dearth of knowledge on the connectivity of the human brain, and outlined an agenda for pursuing this line of research [4]. Twenty years later, this research agenda is at the forefront of the neuroscience communities current concerns, and several major initiatives have brought further support to this research (e.g., Human Connectome Project[1] and International Neuroimaging Data-Sharing Initiative[2]).

2.2 Types of Connectivity

Anatomical and functional connectivity are related, but also capture distinct aspects of brain organization [5]. Brain function relies on networks consisting of spatially distributed areas. Although the anatomical connections are the primary feature defining white matter, the computational units are neurons, lying in the gray matter. The latter are the basis of functional connectivity.

2.2.1 Anatomical Connectivity

The anatomical structure of white-matter tracts can be noninvasively mapped using DWI. This method takes

1. http://www.humanconnectomeproject.org.
2. http://fcon_1000.projects.nitrc.org.

advantage of the nonisotropic movement of water molecules, which is impeded to various extents by the organization and trajectory of white-matter tracts.

The success of this method is partly attributable to advanced visualization methods, which are widely accepted and applied in research as well as in clinical settings (for a review, see [6]). The most basic methods to visualize diffusion data are voxel-based coloring schemes for local measures such as fractional anisotropy, maximum diffusion, or the direction of the largest eigenvector (for example, [7]). Higher-dimensional measurements are visualized with glyph-based approaches (for example, [8]).

Diffusion data can also be used to trace the likely paths of underlying connections between gray matter areas, resulting in *deterministic* [9], [10], [11] reconstructions of white-matter tracts. The visualization of these tracts can then be clarified, for example, by using similarities between tracts to schematize and colorize bundles [12], or using nonphotorealistic rendering techniques [13]. Instead of deterministic paths, the likelihood of the existence of anatomical connections can be calculated using *probabilistic* tractography, though visualization of the probability maps is more challenging [14], [15], [16], [17].

2.2.2 Functional Connectivity

Functional MRI (fMRI) is traditionally used to measure task-evoked activity in gray matter. In addition to the activation of areas in response to a task stimulus, fMRI data contain spontaneous fluctuations. Although this task-unrelated activity was long assumed to be noise, evidence now indicates that this activity is functionally meaningful for describing large-scale networks. Most easily acquired in the absence of task demands, "resting-state functional connectivity" uses correlations between the activity fluctuations across the brain to calculate connection strengths. Brain activity is sampled in regions of 3D space with sizes ranging upwards from single raw voxels (several cubic millimeters) to averaging signal over whole lobes (several cubic centimeters). The strength of functional connectivity is then calculated by correlating the different time-courses of activity.

The visualization of the resulting data is much less well developed than for anatomical connectivity. So far, the focus in the field lay on the development of a multitude of analytic methods. Local measures of functional connectivity exist, and are visualized with standardized color schemes. The standard "seed"-based method calculates the connectivity of a single selected region, which can then be visualized using standardized color scales. Interactive and explorative software using this approach exist, and allow for movement of the seed with simultaneous observation of the changing connectivity patterns [18], [19], [20], [21], but they can show only a fraction of the whole connectivity data in a single image. Showing all the available information at once is impossible due to overlapping connectivity from different seed points. There are many other sophisticated methods for the analysis of functional connectivity (for a review of analysis methods, see [22]), most of which would profit from the development of equally sophisticated visualization methods of the results in the anatomical space. One such family of analysis methods is the attempt to decompose resting-state data into distinct components, using methods like independent component analysis or principal component analysis (ICA/PCA). These components are postulated to represent distributed functional networks, but partially overlap spatially. Worsley et al. [23] visualized PCA components in conjunction with thresholded connections between voxels in anatomical space. As Worsley et al. [23] note, the overlap makes ICA/PCA components ill-suited for simultaneous display of multiple components. Color coding has been proposed to visualize the three most prominent PCA components in a data set [24]. Graph-theory-based analysis has been the basis for sophisticated visualizations of whole-brain functional connectivity (for examples, [25], [26]), where the distances between nodes reflect functional connectivity strengths. However, these graph representations sacrifice anatomical information. For the purpose of representing both connectivity graphs and underlying anatomical space, manually illustrated abstract schematics have been used (for examples, see [27, Fig. 4], or [28, Fig. 6]). Nevertheless, similar clarity has not yet been achieved for the rendering of real connectivity data.

Our interest lies in visualization of functional connectivity on a level that parallels its anatomical counterpart in showing the multitude of connections in a single image. We believe such visualization methods can aid in the clarification and unification of the different modalities used in brain research: the anatomical and the more abstract functional knowledge. First steps to combine these two complementary aspects have recently been undertaken: both functional and anatomical connectivity have unique advantages. For instance, functional connectivity is more accurate for describing the precise termination areas of long distance connectivity, while anatomical connectivity can describe the paths between those areas [5], [29], [30]. Calamante et al. [31] take advantage of the strengths of each method to visualize the functional connectivity-informed anatomical paths by combining whole-brain probabilistic tractograms with the information from single seed-based or ICA derived functional connectivity networks. After summing the FC-values along the tracts, they create renderings that show specifically the anatomical tracts connecting the functional areas.

What sets functional connectivity apart from anatomical connectivity is that white-matter tracts have not only a defined beginning and end position, but also a well-defined shape of the connections between them, while functional connectivity lacks this connection with a well-defined shape. The termination points of functional connectivity have anatomical positions, but only the strength of the connection can be assessed from the data, as there is no knowledge of the path shape. The connectivity can be expressed through a square matrix with connectivity values for each pair of termination points, and their associated anatomical positions. This data should be visualized, ideally in connection with additional spatial information to indicate anatomical location.

2.3 Edge Bundling

The problem of visualizing functional connectivity is, at its foundation, the issue of visualizing a complex graph. With

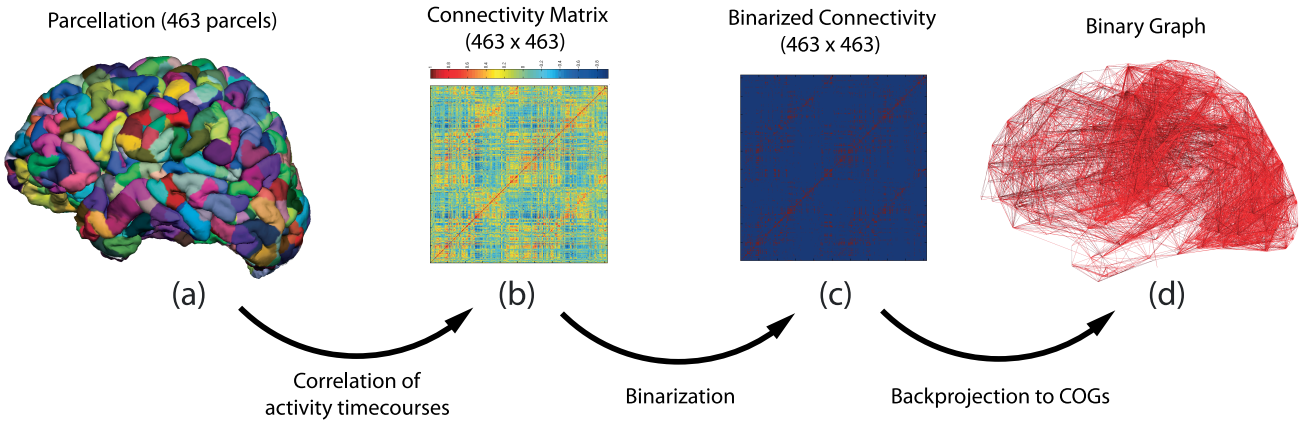

Fig. 1. Whole-brain functional connectivity data. The data that we visualize are derived from fMRI time-courses in cortical areas (a), and calculation of a correlation matrix between every pair of these regions (b). The matrix is, then, thresholded (c), and transformed into a binary graph. Shown is our whole-brain group-level connectivity data set; this example of connectivity between 463 cortical nodes is derived from 122 individual resting-state fMRI scans over 10 minutes each, which are then registered to a common standard coordinate system. In the unbundled graphs using straight lines, (d) almost no structure is visible. We apply edge bundling to alleviate this problem.

high-resolution information, graphs of connectivity can easily contain many thousands of edges. The approach of drawing straight edges for all connections suffers from heavy clutter, and yields visualizations that resemble a ball of wool, and are not able to clearly convey the structure of the connections between different parts of the brain (Fig. 1d).

Similar visualization problems for data such as airline traffic or migration patterns have been successfully improved using *edge bundling* approaches [32], [33], [34], [35], [36], [37], [38], [39], [40]. Pioneered by Holten [32], these methods strive to change the shape of the connections visually so that related edges are grouped together, while leaving the terminal points of the connections unchanged.

The original approach, which requires a preexisting hierarchical partition of the anatomy, has recently been used for the visualization of functional connectivity [21], [33], [34]. Mapping the different parts of the brain to an abstract two-dimensional circular layout before application of the bundling algorithm has yielded beautiful visualizations of whole-brain functional connectivity. One problem with this approach, however, is that the brain is not clearly subdivided into an anatomically distributed hierarchical structure. Also, understanding the anatomical placement of the regions in the abstract layout requires the viewer to learn a new standardized layout.

Both abstract and anatomically faithful layouts have advantages and disadvantages depending on the context. For our main interest, the high-resolution voxel-level mapping of anatomical areas on the cortex, visualization of functional connectivity in the native brain space would be advantageous. Using the anatomical space is also an advantage in the clinical setting, where pathologies may alter brain structure and make the use of standardized parcellations impossible.

In contrast to methods requiring a hierarchical partition [32], [35], newer methods do not [36], [37], [38], [39], [40], [41], [42]. Holton and Wijk [36] have improved upon his original method, and presented a nonhierarchical edge bundling method for general graphs, *force-directed edge bundling (FDEB)*. This elegant method is applicable to the visualization of connectivity in the anatomical space without previous calculation of a hierarchical subdivision. However, as Hurter et al. [37] have noted, the method has several heuristically determined parameters, and relies on an unstable equilibrium between forces. Other works have addressed improvements on scalability [38], and the application to three-dimensional space [39]. However, all of these methods either require relatively complicated implementation for the required control structures [40], or possess an algorithmic element, such as sampling to image space, which makes application to three-dimensional data difficult or impossible [41], [42]. One of the latter methods is *kernel density estimation edge-bundling (KDEEB)* [37], which calculates the gradient of the density of the edges in that space by summation of kernels based at the subdivision points or around the edges, and then iteratively moves subdivision points into regions with higher density.

Our approach, which is described in the next section, combines FDEBs straightforward applicability in 3D space and its concept of compatibility with the numerical stability and ease of use of KDEEB.

3 Mean-Shift Edge Bundling for the Visualization of Functional Connectivity

Our approach to advance the visualization of functional connectivity is to apply edge bundling to improve the clarity of the data in the 3D anatomical brain space. Our method is strongly inspired by FDEB and KDEEB, and we present here its first application to functional connectivity.

3.1 Data

We visualize resting-state connectivity from two data sets. First, a *whole-brain data set* derived from a group of participants for an overview of large-scale connectivity. Second, a *detail data set* of the left hemisphere derived from a single participant, to show the feasibility of our approach even for single cases, and to be able to show the details present in such data, which potentially get lost in group level analysis.

Both data sets consist of binary graphs with the nodes consisting of subdivisions of the brain (voxels or small parcels of cortex), and edges between strongly connected

nodes. For the whole-brain group data, 122 data sets from healthy participants between the ages of 18 and 60 were downloaded from fcon_1000.projects.nitrc.org, and preprocessed as previously described [43]. All data sets were collected by the Nathan Kline Institute and made available by the International Data Sharing Initiative [44]. Part of the preprocessing was the parcellation of the data sets into 463 cortical and subcortical parcels [45]. For each data set, a connectivity matrix was then calculated using Pearson correlation between the average time series of these parcels.

After Fisher's r-to-z transformation, the correlation values were averaged across subjects and the connections further thresholded to only leave the top 7.5 percent ($z > 0.432$). We use a binary graph because inclusion of all weighted connections would not be feasible due to current memory and computational limitations. Thresholding also has the neuroscientific advantage of excluding nonsignificant and negative correlations, whose anatomical significance is ambiguous [46], [47]. We selected our threshold for visual clarity of known anatomical structures in the result. The influence of the binarization threshold on the resulting bundlings is shown in Fig. 6. After binarization, short edges (<20 mm) were removed, resulting in 6,630 connections (Fig. 1).

To clarify how sensitive the method is to the application to different data sets, we also picked 20 randomly picked single cases and 20 groups of 20 subjects each (Figs. S1-S4, which can be found on the Computer Society Digital Library at http://doi.ieeecomputersociety.org 10.1109/TVCG.2013.114 available online). To further show the transferability of the method, we derived and spatially aligned an independent connectivity graph from a DWI example data set (Fig. 5 and S6, available in the online supplemental material).

Our detail data set from a healthy participant was acquired and preprocessed as previously described [48]. To show the detail inherent in connectivity, two ROIs were defined in the left frontal and temporal lobe after extracting the surface of the cortex. Then, only connections between these ROIs were thresholded ($z > 0.35$), and short edges (<20 mm) were removed to create a second binary graph consisting of 7,799 edges (Fig. 2).

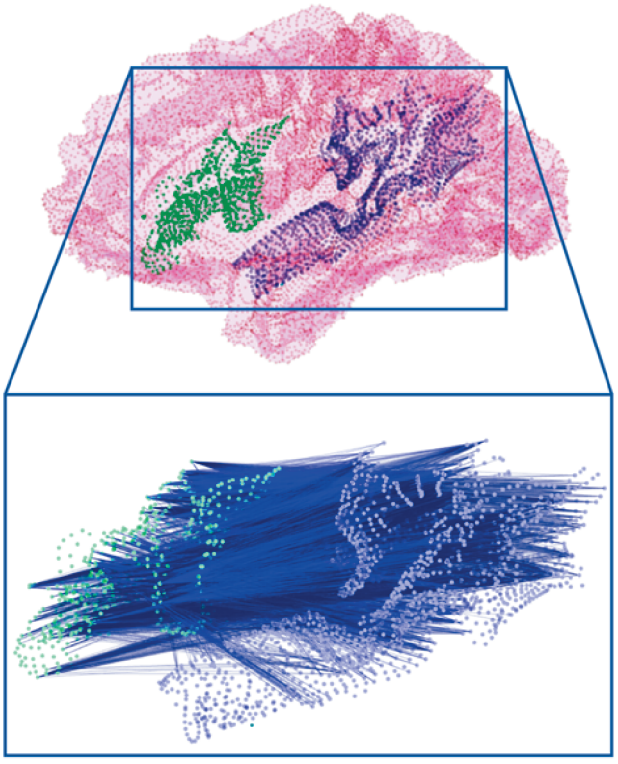

Fig. 2. Detail data of connectivity between 1,000 nodes in two ROIs (in green and blue) in left-lateral prefrontal and temporal areas in a single brain, which are, among others, involved in language processing and production. As in Fig. 1, in the unbundled graph the structure is not apparent before our application of edge bundling.

3.2 Algorithm

Our bundling algorithm combines steps from FDEB [36] and KDEEB [37]. We first calculate a measure of similarity between edges, which guarantees that only *compatible* edges are bundled together. We iteratively subdivide the edges, and move subdivision points to areas with higher density.

3.2.1 Compatibility

We use the definition of pairwise similarity between edges from FDEB. *Compatibility* is defined as a product of four geometrical criteria: similarities of angle and length, distance between midpoints, and the visibility. These criteria are mapped to ranges between 1 for identical edges, and 0 with growing dissimilarity. We refer to the original paper for the details [36].

3.2.2 Iteration and Subdivision Scheme

We iteratively subdivide the edges. Similar to FDEB, we use a scheme of k cycles consisting of i iterations. Between cycles, we subdivide the edges by insertion of subdivision points p_1 to p_n at regular intervals along the edges. FDEB doubles the number of line segments with each cycle. We chose to use a noninteger factor for the increase of subdivision points per cycle, such as in the implementation of FDEB available in JFlowMap.[3] We set the number of segments to 1.3^c, with c being the number of the current cycle. Compared with doubling, this results in a slower growth of the number of subdivision points. In addition, the connections are smoothed between cycles, since new subdivision points are created between the subdivision points from the old cycle. We found that a linear reduction of iterations over cycles leads to good results. Our iteration scheme consists of 10 cycles, starting with 10 iterations, and ending with one.

3.2.3 Mean-Shift of Subdivision Points

To calculate the new position for each subdivision point in each iteration, we use a method similar to mean-shift clustering [49], a nonparametric method that does not require the explicit number of clusters as input. We move each point to a weighted mean of all *compatible* surrounding control points. Like in FDEB, we consider subdivision points compatible, if they occupy the same position along the edges, and the compatibility between the edges is above a user-defined threshold c_{thr}.

The weights for the calculation of the new position are determined using a Gaussian kernel $K(d) = e^{-d^2 / 2\sigma^2}$ on the

3. http://code.google.com/p/jflowmap.

distance d between subdivision points. The width of the Gaussian kernel σ, and the aforementioned compatibility threshold c_{thr} influence the results globally: c_{thr} influences how many distinct bundles emerge. Similarly, σ influences whether the bundling is coarser or more fine grained. To determine optimal parameters, we calculated solutions for different compatibility thresholds and Gaussian kernel widths (see Fig. S5, available in the online supplemental material). We picked a solution that was not underbundled or overbundled by visual inspection of all results; although the decision of optimal parameters remains subjective, we based it on clarity of the known connectomic structures. The result of changing the parameters is well predictable; changing the compatibility threshold influences the number of distinct bundles, while changing the kernel width influences the curvature of the resulting bundles. Although both parameters also influence each other, this makes it possible to iteratively refine a result until the desired granularity and appearance are reached. We heuristically determined the following parameters for our visualizations: $c_{thr} = 0.8$ for the detail data set, and 0.7 for the whole-brain data set, and $\sigma = 5$ mm for both data sets.

3.2.4 Bundle Clustering

The mean-shift method is used for clustering, and in our case moves compatible groups of subdivision points toward their common center of gravity. Since the points in the middle of the connections are moved through more iterations compared with the ones closer to the termination points, these parts of the connections are pulled together especially close, which makes the connections bundle into distinct bundles. It seems, therefore, natural to use the distance of the connections after the bundling process to find such a subdivision algorithmically to be able to colorize the individual bundles differently.

We, therefore, detect such bundles after the bundle process as follows: We iterate through the connections, and assign them to a new bundle if they are not closer than a small radius $r = 0.5$ mm to a connection that is already assigned to a bundle. If connections inside that radius are already assigned to a bundle, we assign the connection to the bundle of the closest connection inside the radius r.

3.2.5 Implementation and Efficiency

We implemented the algorithm in C++, and make our source code available on GitHub.[4] The calculation of the two examples takes 16 and 8 s, for the whole-brain and the detail data set, respectively. Note that the more complex data set takes less time to compute, since the higher c_{thr} reduces the number of required interactions between edges. The computations were performed on an 8-core CPU with 3.4 GHz.

3.2.6 Rendering

For the visualization of the resulting connectivity bundles in connection with anatomical surface features, we believe transparent rendering, high-quality lighting, shadow, and depth cues play an important role. For our renderings of the results of the bundling process in connection with the anatomy of the brain, we exported cortical surfaces derived with Freesurfer, a software that is able to perform extraction of this surface from MRI data [50], and the edge bundles to Cinema 4D, a cinematic rendering software package (MAXON Computer GmbH).

4. https://github.com/NeuroanatomyAndConnectivity/brainbundler.

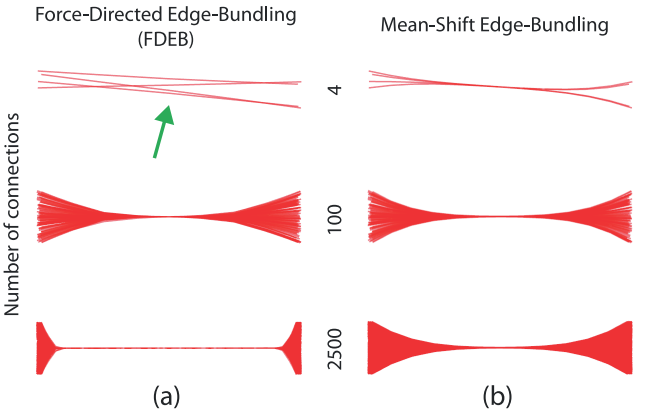

Fig. 3. This artificial example shows the difference of force-directed edge bundling and our method in the application to bundles with different densities. FDEB (a) bundles denser bundles faster than bundles containing only few connections. This leaves the latter underbundled in comparison with the denser bundles (green arrow). Our algorithm bundles all bundles evenly (b).

3.3 Results

The result of our method are spline-like bundles of similar connections, which avoid clutter by sharing screen-space in their middle section, and this way taking up less overall space than the straight lines. In the context of visualizing brain connectivity, our method has the advantage that the shape of the resulting bundles is independent from the density of connections in different parts of the space (Fig. 3).

Functional connectivity data consist of heterogeneous groups of connections between brain areas with different sizes. Therefore, some of the resulting bundles consist only of a few edges, while others consist of hundreds or thousands. We found that with the original simulation of electrostatic forces the large bundles tend to get bundled too quickly, while smaller bundles are still unbundled. The result of application of FDEB for an artificial example of two bundles with extremely different density is shown in Fig. 3a. The problem is compounded by the extreme differences in bundle size in brain data, and the fact that the bundles also influence each other.

The effect of our method is that bundles with different density converge evenly, and without the numerical issues that arise with the simulation of physical forces in FDEB. The result of the application of our adapted method is shown in Fig. 3b. KDEEB has a similar independence from the bundle density, but the calculation of a global density field for all subdivision points prohibits the incorporation of a pairwise compatibility measure, which we found necessary to avoid unsatisfactory bundlings in three dimensions.

In the group data (Fig. 4), our method shows networks of long-range connectivity that are well established in the neuroimaging literature (for example, [51]). These include the default-mode network, as well as visual, sensorimotor, and the dorsal fronto-parietal networks. The most obvious feature in the visualizations is the wide-scale lateral

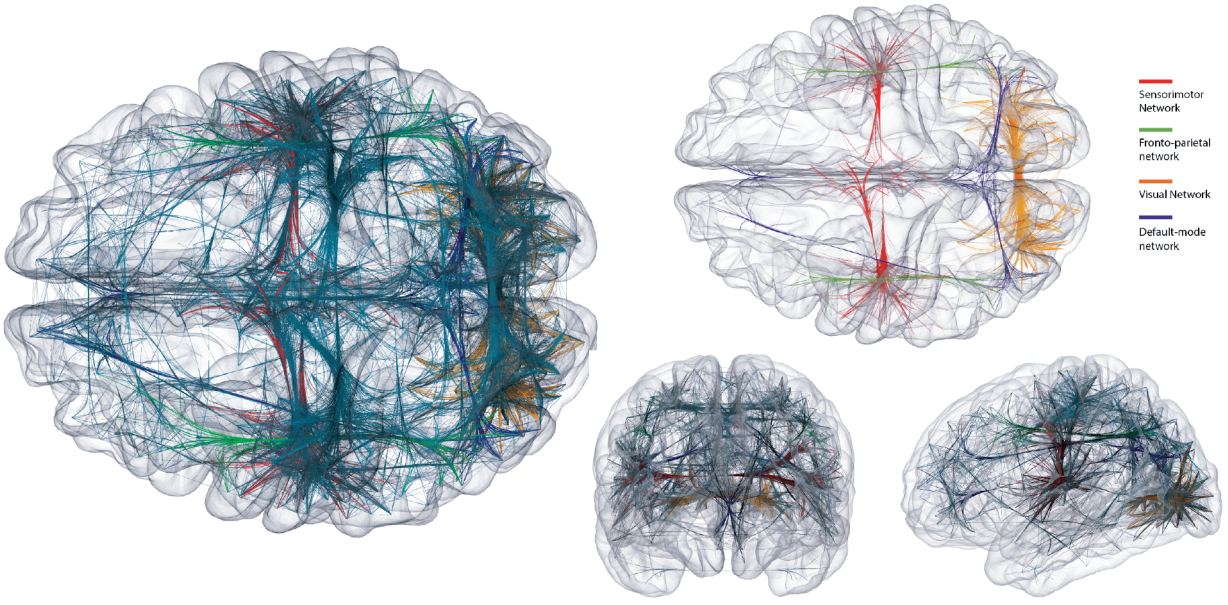

Fig. 4. Whole-brain group-level connectivity: While in the unbundled graph (see Fig. 1d), nearly no structure is visible, our visualization exhibits several well-known functional networks, wide-scale lateral symmetry of brain organization, as well as fine details in functional organization. The four labeled networks (top right) were manually selected and colored for clarification of their embedding in the overall visualization.

symmetry in the connections between the two hemispheres, especially in the sensorimotor system.

That our bundling method is stable with regard to the application to different data sets is shown by the high similarity between the bundlings of the group data and the randomly selected individual data sets and subgroups (Figs. S1-S4, available in the online supplemental material). Even for an independent data set with connectivity derived from DWI data, bundling with identical parameters yields a satisfying bundling (Fig. 5 and S6, available in the online supplemental material).

There is substantial precedence in the literature on structural and functional connectivity to account for the differences observed between the two sets of bundling results. One reason for the lack of a one-on-one correspondence between structural and functional connectivity lies in indirect functional connections between areas, thus demonstrating functional connectivity in the absence of a direct structural connection [5]. In addition, the dynamics of functional connectivity indicate that they may be guided by anatomical connections, but not determined by them [52].

Robustness with regard to the binarization threshold and the associated change in number of edges can be seen in Fig. 6. These results support the possibility of using our method for a wide range of brain data without requiring drastic changes to the parameters.

In the detail data set (Fig. 7), the visualization is able to clearly show that the chosen frontal and temporal areas consist of several interconnected centers. These areas on the left hemisphere are among others associated with language processing and production, as reported in the literature [28]. For the latter example, the data were subdivided into

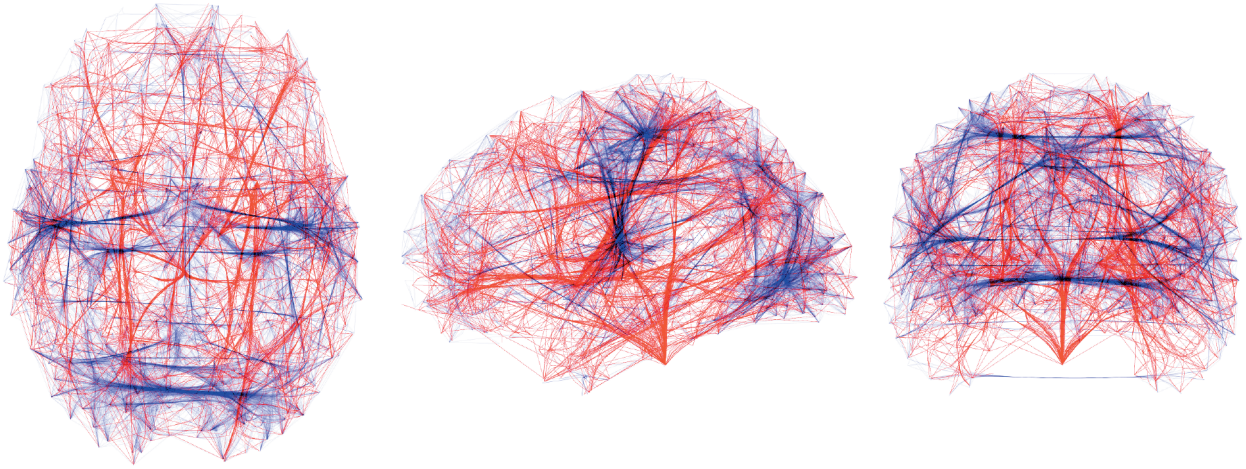

Fig. 5. Comparison between functional (blue) and anatomical (red) connectivity. The anatomical connectivity data are a binary graph derived from DWI data, using probabilistic fiber tracking. We bundled both data sets with the same parameters ($c_{thr} = 0.7$, $\sigma = 5$ mm). Both bundlings do not necessarily follow anatomical fiber tracts, but are abstract visualizations of connectivity in anatomical space.

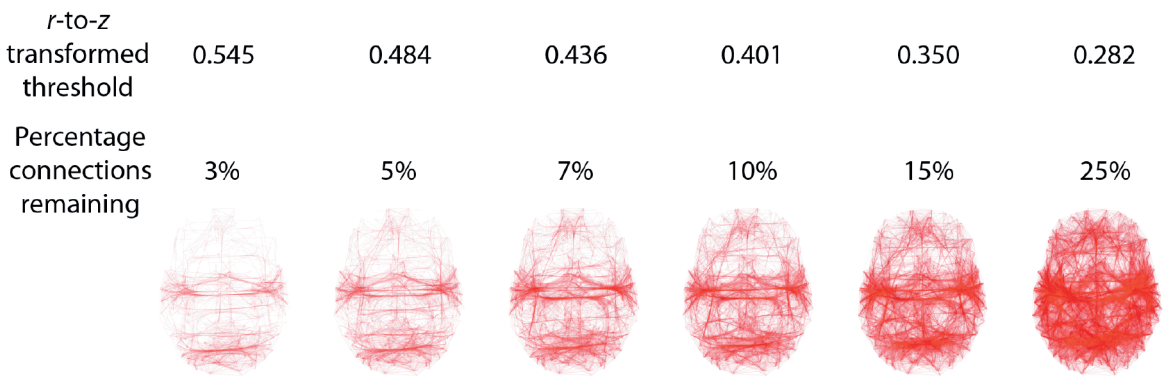

Fig. 6. Influence of binarization threshold on the bundling results, using the functional connectivity whole-brain group average data. Identical values for compatibility threshold and Gaussian kernel width ($c_{thr} = 0.7$, $\sigma = 5$ mm). The structure of the bundlings remains similar.

17 distinct bundles by the procedure described in Section 3.2. We colored the bundles with arbitrarily chosen distinct colors, which help to determine the connections between the different centers by facilitating the visual differentiation of independent clusters of connections (Fig. 7).

4 Conclusion

We have presented here the first application of an edge bundling technique to functional connectivity graphs in native 3D brain space. The result of our technique, which is based on FDEB and KDEEB, is visualizations that are able to show full graphs of functional connectivity as well as fine details in high-resolution single-brain data.

Although for an overview of global connectivity patterns and their changes, more abstract layouts might be more appropriate, the anatomical faithfulness of our method makes it a valuable tool in the exploration of the human connectome, for example, for illustrating results from statistical comparisons of connectivity differences between groups. Due to the same property, the application to clinical contexts especially neurosurgery is also promising, offering a quick overview over distorted connectivity patterns. From a practical standpoint, rs-fMRI has numerous advantages over task-based approaches for clinical application [20], [53], [54], mainly due to its short acquisition time and post hoc versatility. The method could be especially helpful for presurgical planning prior to tumor resections. Information about the localization of functional areas in relation to a lesion can potentially influence the decision to intervene, the surgical approach, and the degree of resection; resolution, neighborhood, and distance relations are essential for such applications.

Edge bundling may also provide a valuable modeling tool for the development of white-matter tracts in conjunction with morphometric constraints. A comparison of the results from edge bundling and the anatomical shape of the white-matter tracts are promising. In the future, inclusion of

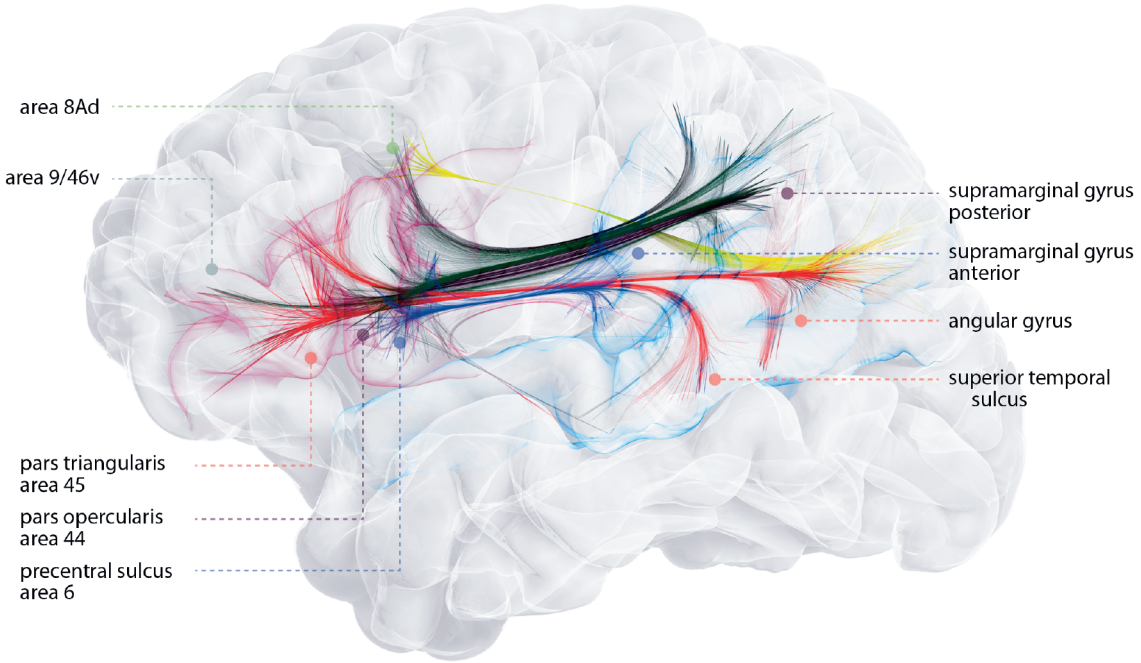

Fig. 7. Single-case connectivity detail: While the unbundled graph (see Fig. 2) makes it hard to discern any structure, after bundling, our visualization shows several functionally connected areas. The colorization of the distinct bundles is the result of our bundle clustering technique described in Section 3.2.

anatomical constraints (interhemispheric fibers have to pass through the corpus callosum, etc.) may bring us closer to a simulation of white-matter fiber behavior and, therefore, inform us about their organization. It is important to keep in mind that we visualize abstract connectivity information, which is related to, but does not necessarily coincide with the underlying anatomical connections. For the aforementioned applications, however, the correspondence with the anatomical space is crucial. Calamante et al. [31] (see Section 2.2.2) have proven that combining the two connectivity modalities can yield informative and aesthetically impressive renderings of functionally informed anatomy. A similar combination of edge bundling with structural data could also lead to highly informative visualizations. However, our method currently facilitates the visualization of functional connectivity independently from diffusion data. We believe the differences between functional and anatomical connectivity patterns presented in Fig. 5 further underline the caution that should be taken in attempting to superficially drive the results of one form of connectivity using the other.

Exploratory connectivity visualization may benefit from following even more radically different paths than nature. Mapping anatomy and connections to topology-preserving partially or fully inflated brains, or flatmaps [55], as well as forcing connections to run outside of the cortical surface in the manner of annotations, may facilitate visual comprehension, while also informing about underlying anatomy (for example, see [56, Fig. 5]).

As Dixhoorn et al. [21] have pointed out, the problem of the visualization of functional connectivity is located at the nexus of scientific and information visualization. They consequentially adapted techniques from visual analytics, such as multiple coupled anatomical and abstract views to aid the iterative explorative selection of interesting parts from the entire data set. Similar methods are frequently used in the analysis of DWI data, and we plan to incorporate them in future development of interactive software.

Visual analytics strives to incorporate a back and forth between visualization and analytic techniques. We believe the distinction between methods to computationally extract information, and the methods to visualize it, is often arbitrary, and an integrated solution is necessary to make exploration of the data successful. Edge bundling offers a method from the visualization community to help clarify the combined complexity of integrating graph information with three-dimensional space—a problem at the heart of understanding the brain. Future elaboration of these approaches will no doubt facilitate research into the intricate organization of neural connections.

Acknowledgments

The authors would like to thank Tobias S. Hoffmann for expert assistance with the rendering of the visualizations, Krzysztof J. Gorgolewski for his helpful comments on the manuscript, and the members of the Neuro Bureau for continued creative input. This work was made possible through support from the Max-Planck Society.

References

[1] K.J. Friston, C.D. Frith, P.F. Liddle, and R.S. Frackowiak, "Functional Connectivity: The Principal-Component Analysis of Large (Pet) Data Sets," *J. Cerebral Blood Flow and Metabolism,* vol. 13, no. 1, pp. 5-14, 1993.

[2] B. Biswal, F.Z. Yetkin, V.M. Haughton, and J.S. Hyde, "Functional Connectivity in the Motor Cortex of Resting Human Brain Using Echo-Planar MRI," *Magnetic Resonance Medicine,* vol. 34, no. 4, pp. 537-541, 1995.

[3] M.D. Fox and M.E. Raichle, "Spontaneous Fluctuations in Brain Activity Observed with Functional Magnetic Resonance Imaging," *Nature Rev. Neuroscience,* vol. 8, no. 9, pp. 700-711, 2007.

[4] F. Crick and E. Jones, "Backwardness of Human Neuroanatomy," *Nature,* vol. 361, no. 6408, pp. 109-110, 1993.

[5] M.P. van den Heuvel, R.C.W. Mandl, R.S. Kahn, and H.E. Hulshoff Pol, "Functionally Linked Resting-State Networks Reflect the Underlying Structural Connectivity Architecture of the Human Brain," *Human Brain Mapping,* vol. 30, no. 10, pp. 3127-3141, 2009.

[6] Y. Masutani, S. Aoki, O. Abe, N. Hayashi, and K. Otomo, "MR Diffusion Tensor Imaging: Recent Advance and New Techniques for Diffusion Tensor Visualization," *European J. Radiology,* vol. 46, no. 1, pp. 53-66, 2003.

[7] S. Pajevic and C. Pierpaoli, "Color Schemes to Represent the Orientation of Anisotropic Tissues from Diffusion Tensor Data: Application to White Matter Fiber Tract Mapping in the Human Brain," *Magnetic Resonance Medicine,* vol. 42, no. 3, pp. 526-540, 1999.

[8] T. Schultz and G.L. Kindlmann, "Superquadric Glyphs for Symmetric Second-Order Tensors," *IEEE Trans. Visualization and Computer Graphics,* vol. 16, no. 6, pp. 1595-1604, Nov./Dec. 2010.

[9] T.E. Conturo, N.F. Lori, T.S. Cull, E. Akbudak, A.Z. Snyder, J.S. Shimony, R.C. McKinstry, H. Burton, and M.E. Raichle, "Tracking Neuronal Fiber Pathways in the Living Human Brain," *Proc. Nat'l Academy of Sciences of USA,* vol. 96, no. 18, pp. 10422-10427, 1999.

[10] S. Mori, B.J. Crain, V.P. Chacko, and P.C. van Zijl, "Three-Dimensional Tracking of Axonal Projections in the Brain by Magnetic Resonance Imaging," *Ann. Neurology,* vol. 45, no. 2, pp. 265-269, 1999.

[11] V. Wedeen, "Diffusion Aniostropy and White Matter Tracts," *Proc. Second Int'l Conf. Functional Mapping of the Human Brain,* 1996.

[12] R. Jianu, C. Demiralp, and D.H. Laidlaw, "Exploring Brain Connectivity with Two-Dimensional Neural Maps," *IEEE Trans. Visualization & Computer Graphics,* vol. 18, no. 6, pp. 978-987, June 2012.

[13] M.H. Everts, H. Bekker, J.B.T.M. Roerdink, and T. Isenberg, "Depth-Dependent Halos: Illustrative Rendering of Dense Line Data," *IEEE Trans. Visualization & Computer Graphics,* vol. 15, no. 6, pp. 1299-1306, Nov./Dec. 2009.

[14] T. Schultz, H. Theisel, and H.-P. Seidel, "Topological Visualization of Brain Diffusion MRI Data," *IEEE Trans. Visualization & Computer Graphics,* vol. 13, no. 6, pp. 1496-1503, Nov./Dec. 2007.

[15] A. Berres, M. Goldau, M. Tittgemeyer, G. Scheuermann, and H. Hagen, "Tractography in Context: Multimodal Visualization of Probabilistic Tractograms in Anatomical Context," *Proc. Eurographics Workshop Visual Computing for Biology and Medicine,* pp. 9-16, 2012.

[16] A. von Kapri, T. Rick, S. Caspers, S.B. Eickhoff, K. Zilles, and T. Kuhlen, "Evaluating a Visualization of Uncertainty in Probabilistic Tractography," *Proc. SPIE,* vol. 7625, 2010.

[17] D.S. Margulies, J. Bottger, A. Watanabe, and K.J. Gorgolewski, "Visualizing the Human Connectome," *NeuroImage,* vol. 80, pp. 445-461, 2013.

[18] Z.S. Saad and R.C. Reynolds, "Suma," *NeuroImage,* vol. 62, no. 2, pp. 768-773, 2012.

[19] R.W. Cox, "AFNI: Software for Analysis and Visualization of Functional Magnetic Resonance Neuroimages," *Computers and Biomedical Research,* vol. 29, no. 3, pp. 162-173, 1996.

[20] J. Böttger, D.S. Margulies, P. Horn, U.W. Thomale, I. Podlipsky, I. Shapira-Lichter, S.J. Chaudhry, C. Szkudlarek, K. Mueller, G. Lohmann, T. Hendler, G. Bohner, J.B. Fiebach, A. Villringer, P. Vajkoczy, and A. Abbushi, "A Software Tool for Interactive Exploration of Intrinsic Functional Connectivity Opens New Perspectives for Brain Surgery," *Acta Neurochirurgica (Wien),* vol. 153, no. 8, pp. 1561-1572, 2011.

[21] A. van Dixhoorn, B. Vissers, L. Ferrarini, J. Milles, and C.P. Botha, "Visual Analysis of Integrated Resting State Functional Brain Connectivity and Anatomy," *Proc. Eurographics Workshop Visual Computing for Biology and Medicine,* pp. 57-64, 2010.

[22] D.S. Margulies, J. Bottger, X. Long, Y. Lv, C. Kelly, A. Schafer, D. Goldhahn, A. Abbushi, M.P. Milham, G. Lohmann, and A. Villringer, "Resting Developments: A Review of fMRI Post-Processing Methodologies for Spontaneous Brain Activity," *MAGMA,* vol. 23, nos. 5/6, pp. 289-307, 2010.

[23] K.J. Worsley, J.-I. Chen, J. Lerch, and A.C. Evans, "Comparing Functional Connectivity via Thresholding Correlations and Singular Value Decomposition," *Philosophical Trans. Royal Soc. London Series B, Biological Sciences,* vol. 360, no. 1457, pp. 913-920, 2005.

[24] S. Mikula and E. Niebur, "A Novel Method for Visualizing Functional Connectivity Using Principal Component Analysis," *Int'l J. Neuroscience,* vol. 116, no. 4, pp. 419-429, 2006.

[25] R. Salvador, J. Suckling, M.R. Coleman, J.D. Pickard, D. Menon, and E. Bullmore, "Neurophysiological Architecture of Functional Magnetic Resonance Images of Human Brain," *Cerebral Cortex,* vol. 15, no. 9, pp. 1332-1342, 2005.

[26] S. Achard, R. Salvador, B. Whitcher, J. Suckling, and E. Bullmore, "A Resilient, Low-Frequency, Small-World Human Brain Functional Network with Highly Connected Association Cortical Hubs," *J. Neuroscience,* vol. 26, no. 1, pp. 63-72, 2006.

[27] D.S. Margulies, J.L. Vincent, C. Kelly, G. Lohmann, L.Q. Uddin, B.B. Biswal, A. Villringer, F.X. Castellanos, M.P. Milham, and M. Petrides, "Precuneus Shares Intrinsic Functional Architecture in Humans and Monkeys," *Proc. Nat'l Academy of Sciences of USA,* vol. 106, no. 47, pp. 20069-20074, 2009.

[28] C. Kelly, L.Q. Uddin, Z. Shehzad, D.S. Margulies, F.X. Castellanos, M.P. Milham, and M. Petrides, "Broca's Region: Linking Human Brain Functional Connectivity Data and Non-Human Primate Tracing Anatomy Studies," *European J. Neuroscience,* vol. 32, no. 3, pp. 383-398, 2010.

[29] M.D. Greicius, K. Supekar, V. Menon, and R.F. Dougherty, "Resting-State Functional Connectivity Reflects Structural Connectivity in the Default Mode Network," *Cerebral Cortex,* vol. 19, no. 1, pp. 72-78, 2009.

[30] T.E. Behrens and O. Sporns, "Human Connectomics," *Current Opinion in Neurobiology,* vol. 22, no. 1, pp. 144-153, 2012.

[31] F. Calamante, R.A.J. Masterton, J.-D. Tournier, R.E. Smith, L. Willats, D. Raffelt, and A. Connelly, "Track-Weighted Functional Connectivity (TW-FC): A Tool for Characterizing the Structural-Functional Connections in the Brain," *NeuroImage,* vol. 70, pp. 199-210, 2013.

[32] D. Holten, "Hierarchical Edge Bundles: Visualization of Adjacency Relations in Hierarchical Data," *IEEE Trans. Visualization & Computer Graphics,* vol. 12, no. 5, pp. 741-748, Sep./Oct. 2006.

[33] J. McGonigle, A.L. Malizia, and M. Mirmehdi, "Visualizing Functional Connectivity in fMRI Using Hierarchical Edge Bundles," *Proc. Abstract and Poster Presented at the 17th Ann. Meeting of the Organization for Human Brain Mapping,* 2011.

[34] A. Irimia, M.C. Chambers, C.M. Torgerson, and J.D.V. Horn, "Circular Representation of Human Cortical Networks for Subject and Population-Level Connectomic Visualization," *NeuroImage,* vol. 60, no. 2, pp. 1340-1351, 2012.

[35] M. Balzer and O. Deussen, "Level-of-Detail Visualization of Clustered Graph Layouts," *Proc. Sixth Int'l Asia-Pacific Symp. Visualisation (APVIS '07),* 2007.

[36] D. Holten and J.J. van Wijk, "Force-Directed Edge Bundling for Graph Visualization," *Computer Graphics Forum,* vol. 28, no. 3, pp. 983-990, 2009.

[37] C. Hurter, O. Ersoy, and A. Telea, "Graph Bundling by Kernel Density Estimation," *Computer Graphics Forum,* vol. 31, no. 3, pp. 865-874, 2012.

[38] E.R. Gansner, H. Yifan, S. North, and C. Scheidegger, "Multilevel Agglomerative Edge Bundling for Visualizing Large Graphs," *Proc. IEEE Pacific Visualization Symp. (PacificVis),* pp. 187-194. 2011.

[39] A. Lambert, R. Bourqui, and D. Auber, "3D Edge Bundling for Geographical Data Visualization," *Proc. 14th Int'l Conf. Information Visualisation (IV),* pp. 329-335, 2010.

[40] W. Cui, H. Zhou, H. Qu, P.C. Wong, and X. Li, "Geometry-Based Edge Clustering for Graph Visualization," *IEEE Trans. Visualization & Computer Graphics,* vol. 14, no. 6, pp. 1277-1284, Nov./Dec. 2008.

[41] O. Ersoy, C. Hurter, F.V. Paulovich, G. Cantareira, and A. Telea, "Skeleton-Based Edge Bundling for Graph Visualization," *IEEE Trans. Visualization & Computer Graphics,* vol. 17, no. 12, pp. 2364-2373, Dec. 2011.

[42] A. Telea and O. Ersoy, "Image-Based Edge Bundles: Simplified Visualization of Large Graphs," *Computer Graphics Forum,* vol. 29, no. 3, pp. 843-852, 2010.

[43] B.B. Biswal, M. Mennes, X.-N. Zuo, S. Gohel, C. Kelly, S.M. Smith, C.F. Beckmann, J.S. Adelstein, R.L. Buckner, S. Colcombe, A.-M. Dogonowski, M. Ernst, D. Fair, M. Hampson, M.J. Hoptman, J.S. Hyde, V.J. Kiviniemi, R. Kötter, S.-J. Li, C.-P. Lin, M.J. Lowe, C. Mackay, D.J. Madden, K.H. Madsen, D.S. Margulies, H.S. Mayberg, K. McMahon, C.S. Monk, S.H. Mostofsky, B.J. Nagel, J.J. Pekar, S.J. Peltier, S.E. Petersen, V. Riedl, S.A.R.B. Rombouts, B. Rypma, B.L. Schlaggar, S. Schmidt, R.D. Seidler, G.J. Siegle, C. Sorg, G.-J. Teng, J. Veijola, A. Villringer, M. Walter, L. Wang, X.-C. Weng, S. Whitfield-Gabrieli, P. Williamson, C. Windischberger, Y.-F. Zang, H.-Y. Zhang, F.X. Castellanos, and M.P. Milham, "Toward Discovery Science of Human Brain Function," *Proc. Nat'l Academy of Sciences of USA,* vol. 107, no. 10, pp. 4734-4739, 2010.

[44] M.P. Milham, "Open Neuroscience Solutions for the Connectome-Wide Association Era," *Neuron,* vol. 73, no. 2, pp. 214-218, 2012.

[45] L. Cammoun, X. Gigandet, D. Meskaldji, J.P. Thiran, O. Sporns, K.Q. Do, P. Maeder, R. Meuli, and P. Hagmann, "Mapping the Human Connectome at Multiple Scales with Diffusion Spectrum MRI," *J. Neuroscience Methods,* vol. 203, no. 2, pp. 386-397, 2012.

[46] M.D. Fox, D. Zhang, A.Z. Snyder, and M.E. Raichle, "The Global Signal and Observed Anticorrelated Resting State Brain Networks," *J. Neurophysiology,* vol. 101, no. 6, pp. 3270-3283, 2009.

[47] K. Murphy, R.M. Birn, D.A. Handwerker, T.B. Jones, and P.A. Bandettini, "The Impact of Global Signal Regression on Resting State Correlations: Are Anti-Correlated Networks Introduced?" *NeuroImage,* vol. 44, no. 3, pp. 893-905, 2009.

[48] M. Taubert, G. Lohmann, D.S. Margulies, A. Villringer, and P. Ragert, "Long-Term Effects of Motor Training on Resting-State Networks and Underlying Brain Structure," *NeuroImage,* vol. 57, no. 4, pp. 1492-1498, 2011.

[49] K. Fukunaga and L.D. Hostetler, "Estimation of Gradient of a Density-Function, with Applications in Pattern-Recognition," *IEEE Trans. Information Theory,* vol. IT-21, no. 1, pp. 32-40, Jan. 1975.

[50] A.M. Dale, B. Fischl, and M.I. Sereno, "Cortical Surface-Based Analysis. I. Segmentation and Surface Reconstruction," *NeuroImage,* vol. 9, no. 2, pp. 179-194, 1999.

[51] S.M. Smith, P.T. Fox, K.L. Miller, D.C. Glahn, P.M. Fox, C.E. Mackay, N. Filippini, K.E. Watkins, R. Toro, A.R. Laird, and C.F. Beckmann, "Correspondence of the Brain's Functional Architecture during Activation and Rest," *Proc. Nat'l Academy of Sciences of USA,* vol. 106, no. 31, pp. 13040-13045, 2009.

[52] R.L. Buckner, F.M. Krienen, and B.T.T. Yeo, "Opportunities and Limitations of Intrinsic Functional Connectivity MRI," *Nature Neuroscience,* vol. 16, no. 7, pp. 832-837, June 2013.

[53] J.S. Shimony, D. Zhang, J.M. Johnston, M.D. Fox, A. Roy, and E.C. Leuthardt, "Resting-State Spontaneous Fluctuations in Brain Activity: A New Paradigm for Presurgical Planning Using fMRI," *Academic Radiology,* vol. 16, no. 5, pp. 578-583, 2009.

[54] D. Zhang, J.M. Johnston, M.D. Fox, E.C. Leuthardt, R.L. Grubb, M.R. Chicoine, M.D. Smyth, A.Z. Snyder, M.E. Raichle, and J.S. Shimony, "Preoperative Sensorimotor Mapping in Brain Tumor Patients Using Spontaneous Fluctuations in Neuronal Activity Imaged with Functional Magnetic Resonance Imaging: Initial Experience," *Neurosurgery,* vol. 65, suppl. no. 6, pp. 226-236, 2009.

[55] B. Fischl, M.I. Sereno, and A.M. Dale, "Cortical Surface-Based Analysis. II: Inflation, Flattening, and a Surface-Based Coordinate System," *NeuroImage,* vol. 9, no. 2, pp. 195-207, 1999.

[56] J.R. Foucher, P. Vidailhet, S. Chanraud, D. Gounot, D. Grucker, D. Pins, C. Damsa, and J.-M. Danion, "Functional Integration in Schizophrenia: Too Little or Too Much? Preliminary Results on fMRI Data," *NeuroImage,* vol. 26, no. 2, pp. 374-388, 2005.

Joachim Böttger received the diploma in computational visualistics from Magdeburg University, in 2003, and the doctorate in computer science from the University of Konstanz, in 2009. He was a research scientist in the Department for Neurosurgery of Charité - University Medicine Berlin, and is currently a researcher at the Max-Planck Institute for Human Brain and Cognitive Sciences in Leipzig; he has authored or coauthored 11 scientific papers. His current research interests include the visualization of functional connectivity and its clinical application.

Alexander Schäfer received the diploma in computer science in 2009, and is currently working toward the graduate degree at the Max-Planck Institute for Human Brain and Cognitive Sciences in Leipzig. His research interests include the application of graph-theory to neuroscience.

Gabriele Lohmann received the diploma in mathematics in 1984, and the doctorate in computer science in 1991; she is currently a senior researcher at the Max-Planck Institute for Human Brain and Cognitive Sciences in Leipzig. She develops new analysis methods for imaging data.

Arno Villringer received the MD degree from Freiburg University in 1984, and trained in neurology at the University of Munich (1986-1992). He is currently the director of the Max-Planck Institute for Human Brain and Cognitive Sciences in Leipzig, the director of the clinic for cognitive neurology at the University Hospital, Leipzig, a coordinator of the German competence net stroke, and a speaker of the Berlin School of Mind and Brain. His research interest focuses on stroke.

Daniel S. Margulies received the doctorate for his research on applications of resting-state functional connectivity to the study of neuroanatomy, for which he received the Otto Hahn Medal in 2010. He is currently the group leader of the Max Planck Research Group: Neuroanatomy & Connectivity in Leipzig.

2.5 Dynamic network participation of functional connectivity hubs assessed by resting-state fMRI

Schaefer A., Margulies D., Lohmann G., Gorgolewski K., Smallwood J., Kiebel S., and Villringer A., Dynamic network participation of functional connectivity hubs assessed by resting-state fMRI, Frontiers in Human Neuroscience, 8(195), 2014

Dynamic network participation of functional connectivity hubs assessed by resting-state fMRI

Short Title: Connectivity clusters and dynamic hubs

Authors: Alexander Schaefer[1*], Daniel S. Margulies[2], Gabriele Lohmann[3], Krzysztof J. Gorgolewski[2], Jonathan Smallwood[4], Stefan J. Kiebel[1,5], Arno Villringer[1,6,7,8]

[1] Max Planck Institute for Human Cognitive and Brain Sciences, Department of Neurology, Leipzig, Germany
[2] Max Planck Institute for Human Cognitive and Brain Sciences, Research Group Neuroanatomy and Connectivity, Leipzig, Germany
[3] Max Planck Institute for Biological Cybernetics, Department of High-field Magnetic Resonance, Tübingen, Germany
[4] Department of Psychology, The University of York, Hesslington, United Kingdom
[5] Biomagnetic Center, Department of Neurology, University Clinics Jena, Jena, Germany
[6] Mind and Brain Institute, Berlin School of Mind and Brain, Berlin, Germany
[7] Department of Cognitive Neurology, University Hospital Leipzig, Leipzig, Germany
[8] Center for Stroke Research, Charité - Universitätsmedizin, Berlin, Germany

* Corresponding author:
Alexander Schäfer
MPI for Human Cognitive and Brain Sciences
Stephanstrasse 1a
04103 Leipzig
Germany
Phone: +49 341 9940-2433
aschaefer@cbs.mpg.de

The authors declare no conflicting or financial interests.

Abstract

Network studies of large-scale brain connectivity have demonstrated that highly connected areas, or 'hubs', are a key feature of human functional and structural brain organization. We use resting-state functional MRI data and connectivity clustering to identify multi-network hubs and show that while hubs can belong to multiple networks their degree of integration into these different networks varies dynamically over time. The extent of the network variation was related to the connectedness of the hub. In addition, we found that these network dynamics were inversely related to positive self-generated thoughts reported by individuals and were further decreased with older age. Moreover, the left caudate varied its degree of participation between a default mode subnetwork and a limbic network. This variation was predictive of individual differences in the reports of past-related thoughts. These results support an association between ongoing thought processes and network dynamics and offer a new approach to investigate the brain dynamics underlying mental experience.

1. Introduction

One of the computational principles underlying behavior is that neuronal networks interact in a highly dynamic fashion (Dickinson, 1995; Marder and Bucher, 2001, 2007). While single neurons have been found to participate in multiple networks by means of the modulation of their synaptic connectivity (Hooper and Moulins, 1989; Weimann and Marder, 1994), it is an open question whether these dynamic events have an equivalent at the macroscopic, interregional level. Recent neuroimaging research in humans supports this hypothesis by demonstrating correspondence between large-scale brain networks and EEG microstates (Britz et al., 2010; Musso et al., 2010), which are transient, quasi-stable patterns in the EEG signal (Musso et al., 2010); as well as varying correlations between regions in the default-mode and task-positive networks (Chang and Glover, 2010). The existence of different large-scale brain states (Smith et al., 2012; Allen et al., 2012) suggests a spatially overlapping organization of specific areas. It is therefore conceivable that the dynamics of these regions allow brain areas to be members of multiple networks by varying their degree of membership over time.

One question facing cognitive neuroscience is how the full repertoire of cognitive capacities can be managed in a flexible manner. The finding of dynamic connectivity raises the possibility that temporal changes in brain connectivity may influence both mental states and behavior (Hutchison et al., 2013b; Allen et al., 2012). For example, the observation of a relationship between connectivity dynamics and heart rate variability provides support for a association to the current mental state (Chang et al., 2013). Other work has demonstrated that dynamic physiological measures such as pupillometry (Smallwood et al., 2012), the electroencephalogram (Barron et al., 2011), and changes in fMRI (Christoff et al., 2009; Smallwood et al., 2013) have all been linked to variations in mental state. A recent study found that alterations in current task performance are predicted by the extent of anti-correlation between the average signal of networks shortly preceding the task (Thompson et al., 2013). Furthermore, the flexibility of functional network configuration during a learning task has been shown to be predictive of later learning performance (Bassett et al., 2011). Given these findings, the hypothesis is that the dynamic interplay of different brain networks modulates ongoing thoughts or the current mental state. Ongoing thoughts during the resting-state can be assessed by a subsequent introspective self-report. Here, we want to examine if there is a relation between ongoing dynamics of functional connectivity and later self reported thoughts.

Highly connected brain areas or hubs, which can be detected using structural (Hagmann et al., 2008; Gong et al., 2009) and functional (Buckner et al., 2009; Lohmann et al., 2010; Zuo et al., 2012) neuroimaging, have been shown to play a central role in whole brain communication (Sporns et al., 2007; van den Heuvel and Sporns, 2013). Here, we hypothesized that multi-network-hubs at the intersection of different networks may serve as dynamic relay stations to support communication between these networks as indicated by animal studies (Dickinson, 1995; Marder and Bucher, 2001, 2007). To examine this dynamic hypothesis, we tested if multi-network hubs keep their participation in each network at a constant level over time or rather dynamically change their degree of membership. We applied an edge clustering approach (Ahn et al., 2010) to cluster connectivity itself, thereby allowing regions to participate in multiple networks. The advantage of using this connectivity clustering algorithm is that we can directly assess the dynamically changing degree of participation of multi-network hubs in their networks. To address the relationship between changes in network dynamics and ongoing cognition, we tested whether the dynamics of hub participation varied across individuals with respect to the contents of thought that they reported at the end of the resting-state experiment.

In the context of resting state connectivity dynamics, recent reports about the importance of BOLD signal variability (Garrett et al., 2011, 2013) are of relevance. As Garrett et al. could show the signal variability is not only reduced in poorer performing (Garrett et al., 2013), but

is also further diminished in older subjects (Garrett et al., 2011, 2013). Here, we also tested for a link between aging and a reduction of network dynamics.

2. Materials and methods

2.1 Data and subjects: Data was acquired using a Siemens 3 Tesla Trio scanner and included resting state functional magnetic resonance imaging (rs-fMRI) and a T1 anatomical scan. The rs-fMRI data were acquired over 900 volumes with 40 slices, a TR of 0.645 seconds and a resolution of 3 mm isotropic. Further, the sequence (Xu et al., 2012) comprised the following parameters TE= 30ms, flip angle of 60 degrees and a multiband factor of 4. Subjects were instructed to keep their eyes open and fixate a crosshair. T1 anatomical scans were obtained using a MPRAGE sequence with a resolution of 1mm isotropic.
From the initial 231 subjects we excluded 7 due to imaging artifacts and 44 for having maximum motion of more than 3 mm. To reduce potential micro motion artifacts we further removed 72 subjects with summed micro movements (Van Dijk et al., 2012) above the group mean (0.1152 mm/volume). In addition, in the further analysis we still accounted for micro movements as a covariate.

The resulting 108 subjects had a mean age of 37.71 (std. 18.4) including 47 male and 61 female subjects. All data sets used in this study are part of the NKI Enhanced dataset (Nooner et al., 2012) and are publicly available by the international neuroimaging data sharing initiative (Biswal et al., 2010). Institutional Review Board Approval was obtained at the Nathan Kline Institute and Montclair State University. Written informed consent was obtained for all study participants.

2.2 Preprocessing: The preprocessing of resting state fMRI data was carried out using FSL (Jenkinson et al., 2012), AFNI (Cox, 1996) and FreeSurfer (Dale et al., 1999). The steps comprised: 1) discarding the first four EPI volumes from each resting-state scan to allow for signal equilibration, 2) 3D motion correction, 3) slice time correction 4) 4D mean-based intensity normalization, 5) removing linear trends, 6) regressing out eleven nuisance signals (six motion parameters and five top components from a principal components analysis of high variance signals (CompCor (Behzadi et al., 2007; Chai et al., 2012)) and 7) band-pass temporal filtering (0.01-0.1 Hz). The output of these preprocessing steps is one 4D residual functional volume for each participant. In order to reduce partial volume effects no spatial smoothing was performed. We did not use global signal regression as the global signal is tightly coupled to the underlying neuronal signal (Schölvinck et al., 2010).
A nonlinear transformation from T1 to a 3 mm isotropic MNI template (created from 152 subjects, provided with FSL) was calculated for individual T1 images using ANTs (Avants et al., 2011). This transformation was combined with the EPI to T1 transformation (bbregister (Greve and Fischl, 2009)) to warp the EPI volumes to standard MNI space.
The preprocessing pipelines used for this manuscript can be downloaded from https://github.com/alexschaefer83/DynamicHubs and used together with BIPS (https://github.com/INCF/BrainImagingPipelines) which is based on nipype (Gorgolewski et al., 2011).

2.3 Graph construction: A graph is an abstract representation of a network. A graph G consists of a set of vertices V and a set of edges E. An edge indicates the presence of a relationship between two vertices, which in case of this study is functional connectivity. We will also refer to edges as *connections*. To account for different strength of functional connectivity we use an edge weighted graph.
For the graph construction we parcellated the functional images into 200 cortical and subcortical regions. The parcellation is based on spatially constrained spectral clustering

(Craddock et al., 2012) which aims to create spatially coherent regions of functional homogenous connectivity. The parcellation is publicly available (www.nitrc.org/projects/cluster_roi). In the proposed analysis we used the version derived from the best performing clustering in the publication by Craddock et al. (2012) (two-level clustering with the rt similarity metric). Each parcel is one unique vertex in our graph. To estimate the relationships between the vertices, the average signal within each parcel was extracted and its pairwise correlation with the signals (spatial averages over all voxels of a parcel) of all other parcels computed. The resulting correlation values were Fisher z-transformed in order to allow for an unbiased analysis in the further steps. We then averaged the z-values over all subjects. For the graph we assigned an edge (or connection) between two vertices (or parcels) if their respective correlation value belonged to the highest 10% (2000 edges) in the group average. Furthermore we weighted the edge by the corresponding z value. This technique shows good reliability (Schwarz and McGonigle, 2011) as it incorporates only strong connections with relatively high reliability (Patriat et al., 2013). Visualization of brain graphs was performed using braingl (Böttger et al., 2014) and conview (http://conview.googlecode.com).

2.4 Connectivity clustering: An efficient way to cluster connections has been proposed by Ahn et al. (2010). We used an implementation of this idea by Kalinka and Tomancak (2011).

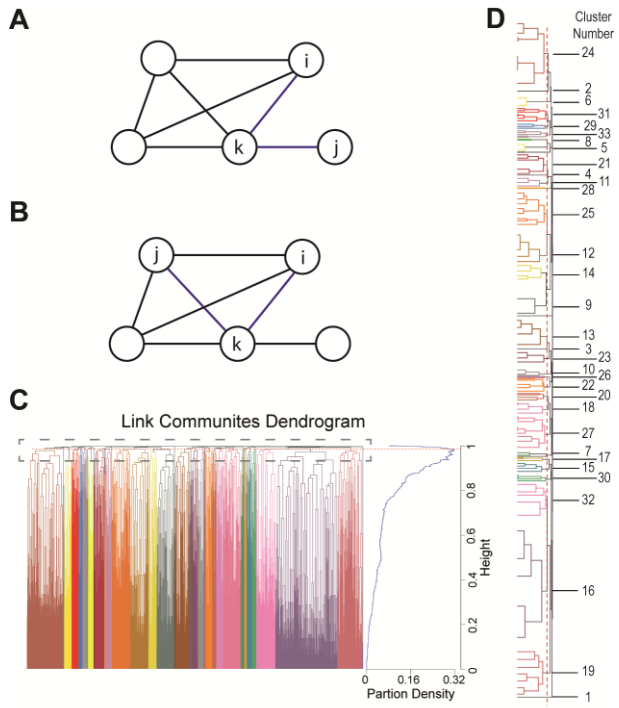

Fig. 1 Connectivity clustering approach. (A) Example for two connections with low similarity. The common neighborhood of vertices i and j is only k therefore the similarity is S=1/3. **(B)** An example for two connections with high similarity. As vertices i and j have the same neighborhood the similarity is 1. **(C)** Dendrogram (left) based on calculated similarities together with a plot of estimated partition densities (right). Red dotted line indicates the cutoff of the dendrogram estimated by maximizing partion density. **(D)** Zoomed view of the top of the dendrogram from Fig. 1C together with network numbers from Fig. 3.

In order to cluster connections one requires a measurement of their similarity. Ahn et al. (2010) proposed the Jaccard coefficient to estimate the similarity between connections e_{ik} and e_{ik} that share a vertex k:

$$S(e_{ik}, e_{jk}) = \frac{|n(i) \cap n(j)|}{|n(i) \cup n(j)|}$$

where *n(i)* and *n(j)* is the first order neighborhood of vertex *i* and *j* respectively. An example for two connections with low similarity is illustrated in Fig. 1A. The similarity is S=1/3 as the common neighborhood of vertices i and j is only vertex k. An example for two connections with high simarity (S=1) is illustrated in Fig. 1B as i and j have the same neighborhood. To better account for the different strength of connections we use a weighted version called Tanimoto coefficient:

$$S(e_{ik}, e_{jk}) = \frac{w_i w_j}{|w_i|^2 + |w_j|^2 - w_i w_j}$$

where $\mathbf{w_i}$ is a vector describing the weights of the connections between vertex *i* and the vertices in the first order neighborhood of *i* and *j*. After calculating the pairwise Tanimoto coefficients between all links in the network, a hierarchical clustering is performed using McQuitty`s similarity method (McQuitty, 1966). The optimal cut off for the resulting dendrogram (tree diagram, Fig. 1C) is determined by maximizing the partition density (Ahn et al., 2010). This is the density within the

clusters, normalized for the maximum and minimum number of possible connections within each network. More explicitly, for a network with M connections, $\{P_1, \dots, P_C\}$ is a partition of the connections into C subsets. A subset P_c has m_c=$|P_c|$ connections and n_c= $\left|\cup_{e_{ij} \in P_c}(i,j)\right|$ vertices. Then Ahn et al. define the partition density of a subset C:

$$D_c = \frac{m_c - (n_c - 1)}{\frac{n_c(n_c-1)}{2} - (n_c - 1)}$$

This is m_c normalized by the minimum and maximum numbers of connections possible between n_c vertices. The partition density, D, is the average of D_c, weighted by the fraction of present connections:

$$D = \frac{2}{M}\sum_c m_c \frac{m_c - (n_c - 1)}{(n_c - 2)(n_c - 1)}$$

The maximum partition density gives the optimal cutoff for the dendrogram which determines the number of connectivity clusters in our solution (Fig. 1C).

2.5 Reliability of clustering: To evaluate the reliability of the new clustering method we use a split half test. In order to not compare clustering over different elements (connections) we used the same connections as in the full group for both clusterings (see 2.3 Graph Construction). To evaluate reliability of the cluster results we divided our subjects into two groups, one of subjects with odd index and one of subjects with even index, and performed the clustering for both of them separately. As distance between the two found clustering solutions (even and odd index) we computed the so-called cophenetic correlation coefficient (Sokal and Rohlf, 1962). To compute confidence intervals for the results we performed a mantel statistic using 999 permutations (Mantel, 1967) which creates a permutation baseline. The two found clustering solutions correlated with r=0.8954 (p<0.001, 95% CI=0.001185). The similarity of the results across subgroups implies a certain generalizability of our cluster results across a larger population.

2.6 Windowing of temporal dynamics: To investigate the underlying dynamics of the resulting connectivity clusters instead of correlating signals over the whole scan session, a shifting time window is used:

$$r_t = corr\left(x\left(t \cdot w : (t+1) \cdot w - 1\right), y\left(t \cdot w : (t+1) \cdot w - 1\right)\right)$$

where *t* is the timepoint with *t=1:11*, *w* is the window with *w*=77 (or 49,7 sec) and *x*, *y* are the time series of two (out of 200) parcels. All estimated *r* values are Fisher's *z* transformed, resulting in eleven *z* values per connection and subject. Each of these eleven values is adjusted to a within subject baseline by subtracting from the estimated *z* value for the complete scan time. These normalized values reflect, for each subject, the temporal change of the connection strength over the eleven time intervals.

2.7 Analysis of temporal dynamics: To investigate if the connections within a connectivity cluster change, over time, more similarly than over connectivity clusters we measured the variance of connectivity change within (var1, var2 in Fig. 2B) and without clusters (var3 in Fig. 2B). Timepoints were not averaged over subjects as subjects are likely in a different state of dynamic functional connectivity and therefore not comparable. We tested whether the within cluster variance was significantly smaller to the variance over clusters using a Wilcoxon test.

To analyze if regions in multiple networks show a dynamically varying degree of membership between its belonging networks we used the following strategy. To test if a region changes the degree of membership between its networks, we estimated the average strength of connections assigned to one network and compared it to the average strength of connections belonging to another network using a dynamic windowing (50 sec) approach. These "variation" events are illustrated as State B and State D scenario in Fig. 2C and can be well captured by the mean squared error (MSE) between the average correlation strengths. To

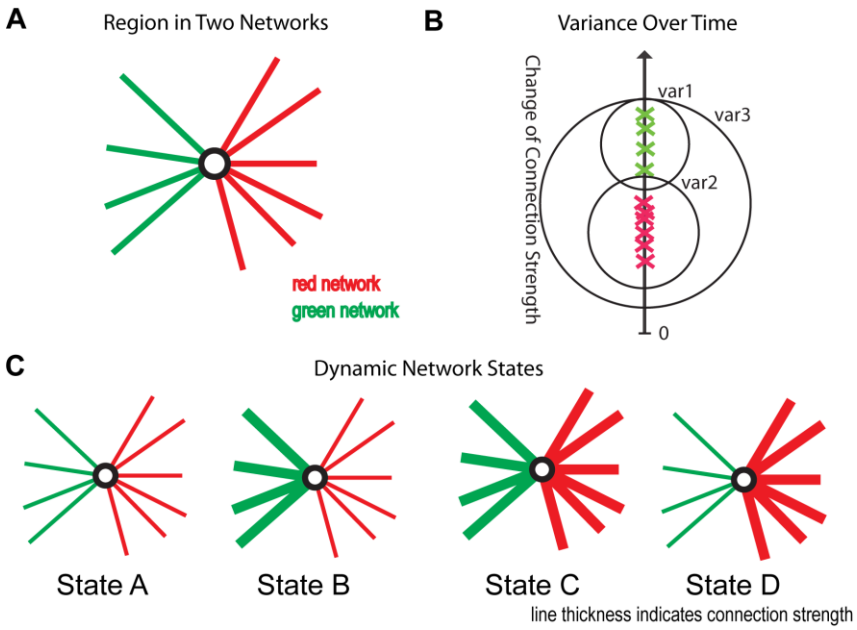

Fig. 2 Illustration of research ideas. **(A)** One region as part of two connectivity clusters (red and green). **(B)** Green crosses mark connectivity change of connections within the green cluster, the red crosses of connections within the red cluster. The y-axis gives the amount of change of the respective connections. Var1, var2 are the variances within the red and green cluster, while var3 gives the variance over all connections. **(C)** Four possible scenarios of changing connectivity: State A: reduction of both clusters, State B: reduction of red cluster and increase of green cluster, State C: increase of both clusters and State D: reduction of green cluster and increase of red cluster.

test the significance of our results we used permutation testing based on random clustering. In this clustering we chose randomly connections from the same hub regions without caring about assigned cluster values. The number of connections was equal to the original clusters. We created 10,000 times two corresponding random clusters and computed the MSE between them. The results are plotted in Fig. 5C.

For the whole brain analysis we aimed at ensuring that networks tested included enough connections for a stable signal. Therefore we chose only regions where the second largest network included at least two connections (151 of 200 regions, Fig. 4C). The MSE was then averaged over all of pairs of networks which shared participation of the particular hub.

2.8 Experiment: self-generated thoughts

To assess thoughts and feelings during the scan the subjects were interviewed directly after MRI session using the New York Cognition Questionnaire (NYC-Q). The beginning of the interview was approximately 45 minutes after the resting state scan that we analyzed. The NYC-Q is a self-report tool consisting of two sections, the first containing questions about the content of thought (23 questions), the second containing questions about the form that these thoughts take (8 questions). In each question subjects were asked to indicate how well a statement described their thoughts on a scale from 1 (“Completely did not describe my thoughts”) to 9 (“Completely did describe my thoughts”). Therefore a high score on a component relates to the subjective experience of mind-wandering which also implies that one strong thought yield a similar score as multiple seemingly insignificant thoughts. We used the data and code available online (https://github.com/NeuroanatomyAndConnectivity/NYC-Q) provided and described in greater detail by (Gorgolewski et al.). The 23 answers about the content of thought collected from 166 subjects were factorized into five categories. The factorization was performed using principal axis factor analysis together with an oblimin rotation (Revelle, 2011) to increase interpretability. The number of factors was estimated using Parallel Analysis (Horn, 1965).

Individual-level scores were computed applying the method by Ten Berge et al. (1999). We used the names and interpretation of these categories as described in the original study, namely thoughts about the past (Past), the future (Future), positive thoughts (Positive), negative thoughts (Negative) or thoughts about relationships (Social Cognition). The eight questions about the form of thought were factorized into three factors as described above. The factors were named as in the original study: in form of words (Words), in form of images (Images) and specificity of words (Vague). As the factorization employed does not enforce orthogonality of the components, we performed for each component a partial correlation analysis with the respective other seven components as covariates. A more detailed description about NYC-Q and the factorization employed can be found in the study by (Gorgolewski et al.).

Fig. 3 Connectivity networks. All thirty-three connectivity networks found in the hierarchical cluster analysis of time and group averaged connectivity. Networks can also be inspected interactively and in three dimensions online (http://openscience.cbs.mpg.de/schaefer).

Network	Vertices (Regions)	Edges (Connections)
1	5	8
2	6	6
3	6	8
4	5	4
5	16	33
6	18	46
7	8	18
8	6	8
9	19	105
10	16	36
11	14	35
12	24	109
13	31	92
14	34	49
15	21	30
16	33	369
17	16	16
18	32	41
19	59	147
20	19	20
21	20	64
22	21	42
23	28	41
24	26	217
25	38	111
26	7	7
27	34	106
28	4	3
29	14	23
30	19	26
31	25	41
32	31	114
33	20	25
Average	20.5	60.6

Table 1 Descriptive information of connectivity networks (Fig. 3). Connectivity networks together with their respective number of vertices (regions) and number of edges (connections).

3. Results

3.1 Hub regions belong to multiple networks. Using the edge clustering approach described above (Ahn et al., 2010) we found 33 networks (Fig. 3), several of which are well-characterized networks typically observed in fMRI resting-state experiments. The clusters can be downloaded from https://github.com/alexschaefer83/DynamicHubs and interactively viewed online http://openscience.cbs.mpg.de/schaefer. The number of connections and regions in each network can be found in Table 1. We found that the majority of regions (174 of 200) participated in more than one network. An overview of the amount of multi-network participation is given in Fig. 4 B. In contrast Fig. 4A gives the degree of connectivity of these regions. The relation of the two measures connectivity and multi-network participation is given in Fig. 4D.

3.2 Hub regions vary degree of membership between networks. As an example Fig. 5 presents the results for the analysis on the anterior cingulate cortex (ACC). While an overview for whole brain results is given in Fig. 4C, we chose the ACC as a representative area to illustrate the typical results for a single area. We found the ACC to participate in two spatially separated networks: a temporal network and a frontal-parietal network (Fig. 5A).

To test if connectivity changes occur more within clusters than between clusters we estimated the variance of connectivity change across timepoints and subjects. We found the variance of change within the red cluster ($p=0.0181$) and within the blue cluster ($p=1.156*10^{-23}$) to be smaller than the variance of connectivity change over both clusters.

To test if a region changes the degree of membership between its networks, we estimated the average strength of ACC connections assigned to one network and compared it to the average strength of ACC connections belonging to another network. As shown in Fig. 5B, we found changes in the degree of membership, which we quantified by the mean squared difference in participation. We used permutation tests to show that these changes between networks were statistically significant, see Fig. 5C. We found there were significantly stronger changes in the degree of participation between specific clusters than would be expected between randomly selected clusters (Fig. 5C).

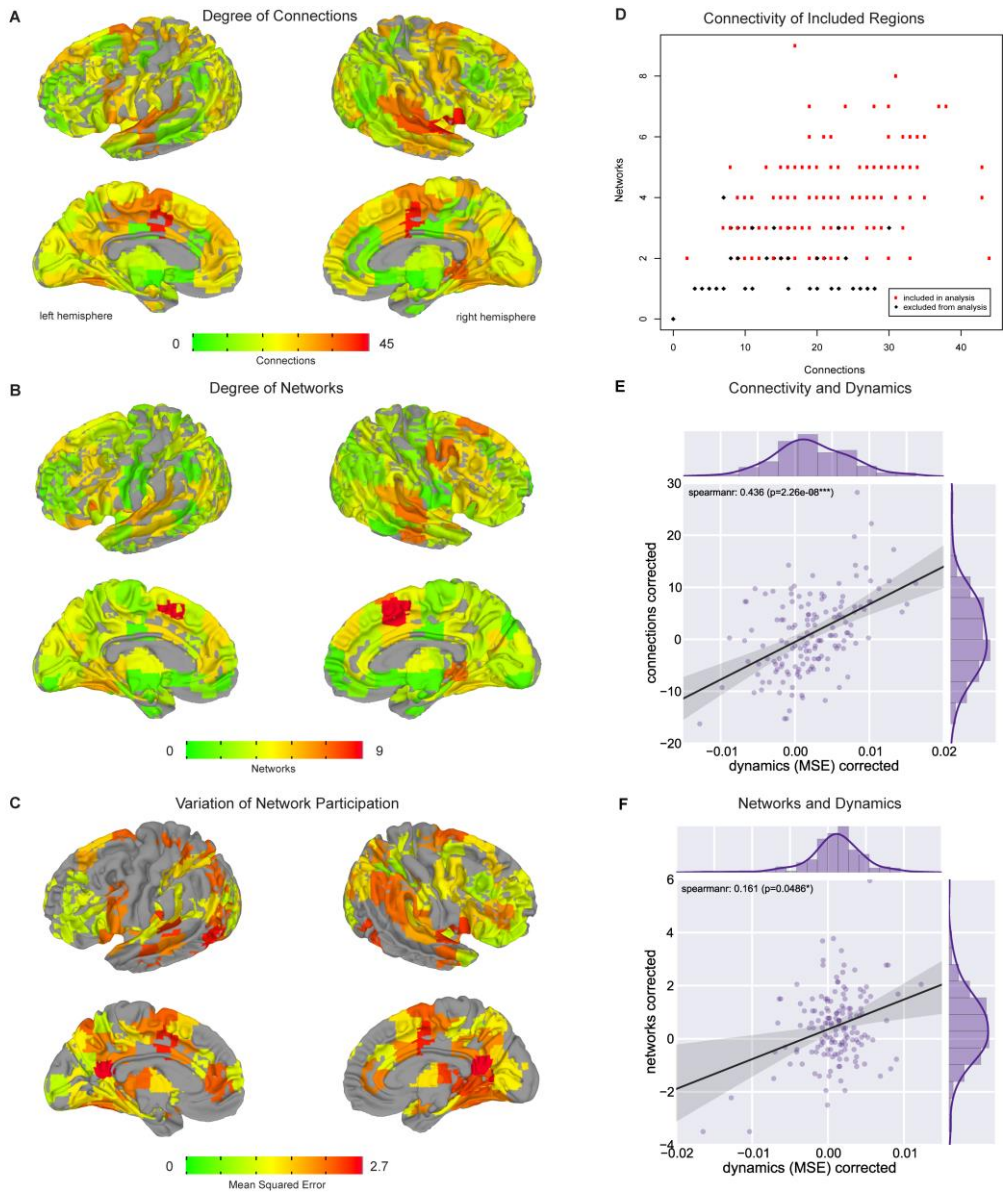

Fig. 4 Whole brain regional overview. (A) Brain areas colored by their degree of connectivity. Areas with more connections are displayed in red, whereas regions with fewer connections are in green. **(B)** Brain areas colored by the number of networks they are part of. Regions participating in a higher number of networks are displayed in red. Regions which are part of fewer networks are depicted in green. **(C)** Brain areas colored by their variation of network participation. Areas with higher variation are colored in red, whereas regions with lower variation are shown in yellow and green. **(D)** Relation between number of connections and number of networks each brain region is part of. In the further analysis we only included regions which are part of at least two networks and for which the second largest belonging network consisted of at least two connections. These regions are colored in red. **(E)** Relation between number of connections (Fig. 4A) and variation of network participation (Fig. 4C) measured across brain areas included in analysis. (**F**) Relation between number of networks (Fig. 4B) and variation of network participation (Fig. 4C) measured across brain areas included in analysis.

A whole-brain overview of the amount of variation in network participation can be seen in Fig. 4C. We also investigated if there is a relation between dynamic (Fig. 4C) and connectivity-hubness (Fig. 4A) or network-hubness (Fig. 4B). We found a positive correlation (Spearman r=0.44, p=2*10^-8, n=151) between variation of network participation and the degree of connectivity (Fig. 4E) while we accounted for the number of networks. Further, we also found a weaker correlation (Spearman r=0.16, p=0.049, n=151) between the dynamics of a region

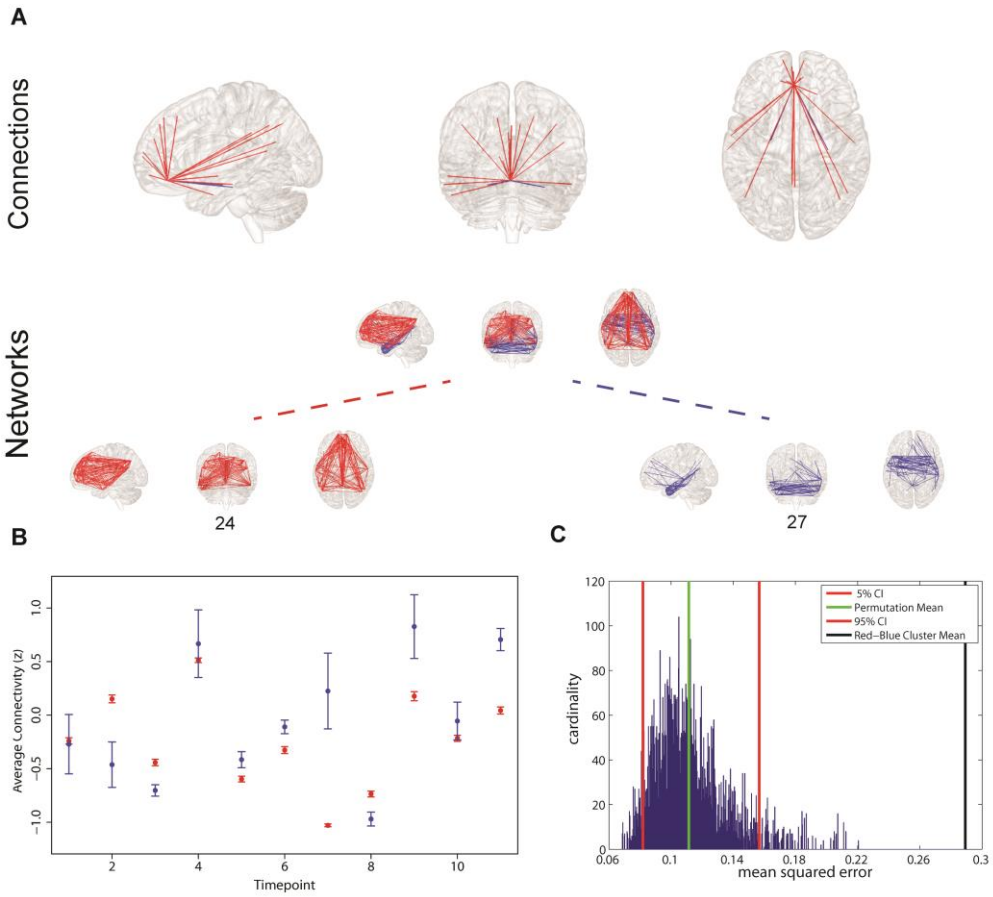

Fig. 5 Representative region for variation of network participation. (A) Anterior cingulate cortex (ACC) participating in two networks (networks 24 and 27). **(B)** Example plot of ACC participation in the two networks in a 50 second interval. Timepoint 2 and 7 are good examples of a variation in network participation (State B or State D, Figure1 C). **(C)** Permutation test shows that variation behavior measured by mean squared error is more pronounced in the found clustering than in a random clustering.

and the amount of networks the region participates in (Fig. 4F) while accounting for the number of connections.

3.3 Association between variation of network participation and self-generated thoughts.

We found a reduction of whole brain averaged variation of network participation in subjects which reported to have more positive thoughts during the scan (Fig. 6C, Spearman r=-0.47, p=0.0001 (corrected for 8 comparisons), n=78). An overview of whole brain participation variation is also given in Fig 4D. We further investigated if the variation of network participation of a specific region correlates with a domain of self-generated thoughts. We found an increased variation of network participation of the left caudate in subjects which reported to have more thoughts about the past during the scan (Fig. 7, Spearman r=0.47, p=0.02 (corrected for 1600 comparisons (8 categories * 200 regions)), n=78).

3.4 Decrease of dynamics in age. As the variability of the fMRI signal has been found to decrease in ageing (Garrett et al., 2011, 2013), we tested whether similar effects can be found for the dynamic of network participation of brain regions between networks. Critically, we found a significant age effect on connectivity changes across the whole brain (spearman r=-0.24, p=0.011, n=106, Fig. 6A). While we used micro-movements as a covariate we also tested for a relationship between network dynamics and micro-movements. However, we did not find a relation between whole brain dynamics and micro-movements (r=0.03, p=0.747, n=106, Fig. 6B). We found no significant correlation between age and positive self-generated

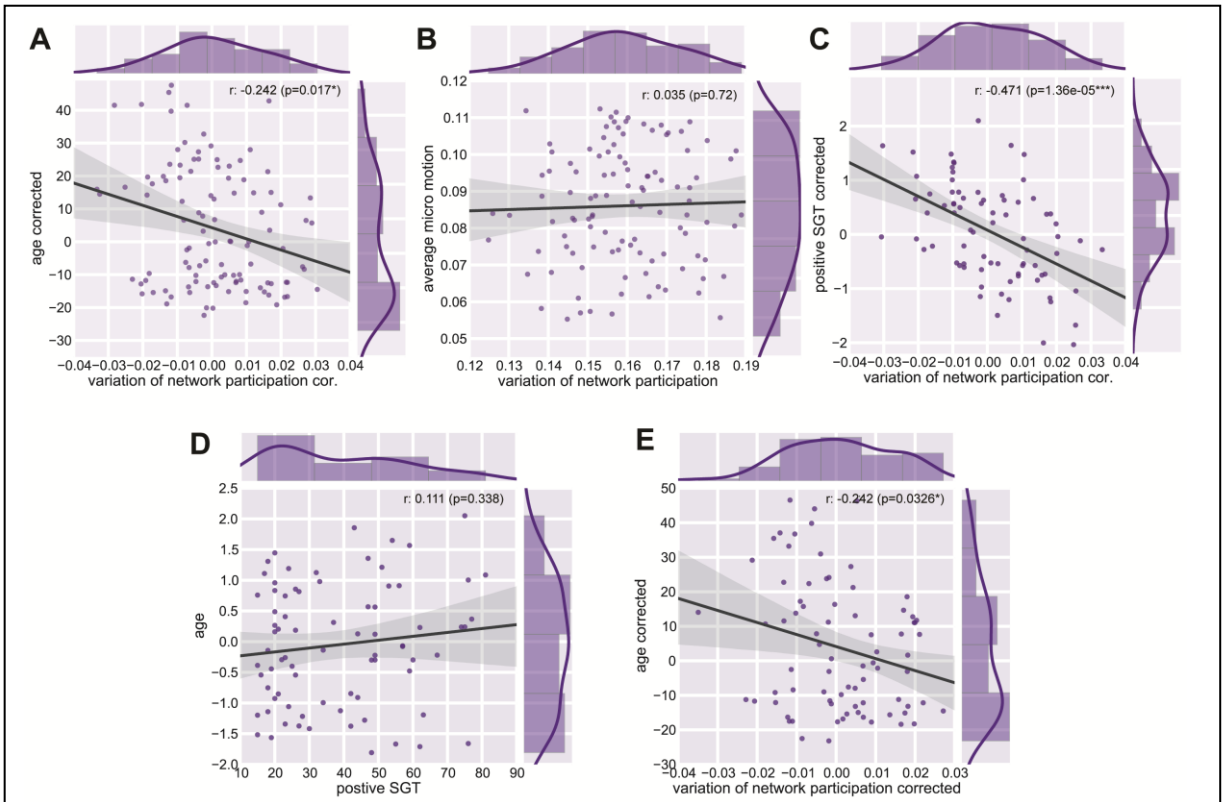

Fig. 6 Whole Brain Variation of Participation. **(A)** Partial correlation between average variation of participation and age corrected for micro-movements. **(B)** Correlation between average variation and average micro-motion. **(C)** Partial correlation between average variation of participation and positive self-generated thoughts (SGT) corrected for micro-movements, age, gender and the respective other four factors of SGT. **(D)** Correlation between age and positive self-generated thoughts (SGT), micro-movements. **(E)** Partial correlation between average variation of participation and age corrected for positive self-generated thoughts (SGT), micro-movements.

thoughts (SGT) corrected for micromovements (r=0.111, p=0.338, n=78, Fig. 6D). However, when we added positive SGT as a covariate the negative correlation between age and participation remained similar (spearman r=-0.24, p=0.033, n=78, Fig. 6E).
The impact of different initial graph thresholds onto the three main results of this paper are shown in Table 2. In this manuscript we used a threshold of 10% or 2000 connections. All results remained significant for thresholds from 7.5% (1500 connections) to 15% (3000 connections). For a threshold of 17.5% (3500 connections) the caudate finding became insignificant. The clustering of connectivity for sparsity thresholds of 20% and higher resulted in a single network, whereas for sparsity threshold of 5% and lower the left Caudate was part of a single network. In this context no effect sizes were calculated.

4. Discussion

We have shown that multi-network hubs vary their degree of participation into different networks over time. In addition, we found that these network dynamics were inversely related to age and to positive self-generated thoughts reported by subjects. These results demonstrate a novel analytic approach which enables a testable framework for quantifying dynamic network interaction across regions on an individual-level.

To facilitate this analysis we used an algorithm to cluster connectivity itself rather than brain regions based on their connectivity profiles (Power et al., 2011). This approach offers the advantage to maintain whole brain information in connectivity space rather than reducing it to the regional space. This is important as we are interested in functional brain networks which includes connections and regions rather than only regions (Damoiseaux et al., 2006; Power et al., 2011). This domain shift also includes the conceptual advantage that brain regions can participate in multiple networks. While the later advantage is shared by other network

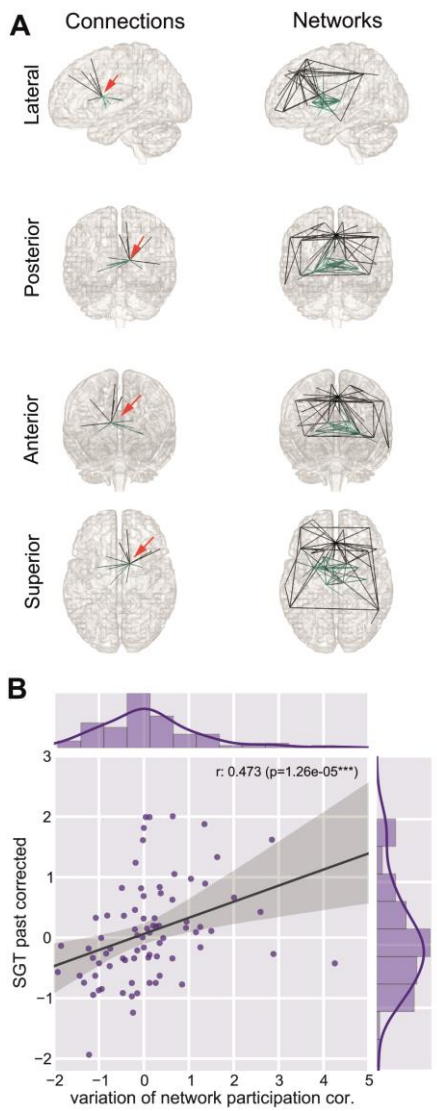

Fig. 7 Left Caudate region and self-generated thoughts about past events. (A) Left Caudate region is part of two connectivity networks, a sub cortical network (network 10) and a subnetwork of the default mode network (network 31). Red arrow indicates the position of the Left Caudate region. **(B)** Increased correlation between variation of network participation of the Left Caudate region and self-generated thoughts about past events.

decomposition methods which allow networks to overlap like independent component analysis (ICA, (Calhoun et al., 2001; Beckmann et al., 2005)), non-negative matrix factorization (NMF, (Lee et al., 2011)) and Latent Dirichlet Allocation (LDA, (Yeo et al., 2014)) it is still conceptually different as these networks exist in the spatial location but not in the connectivity space.

One of the limitations of connectivity clustering is that an initial arbitrary threshold onto the connectivity has to be applied. While we found that the effect sizes of our main results are comparable at a range of thresholds 7.5% to 15% (Table 2) we also found that for a threshold of the 17.5% the relation between caudate switching and past self generated thoughts got insignificant. One reason for this might be the higher connectedness of the left Caudate at this threshold which makes the left Caudate a part of ten networks, in contrast to two networks at 10% sparsity. For even higher thresholds the network clustering resulted in a single network. In this context a threshold between 7.5% and 15% seems recommendable for similar future analyses.

While brain regions in our framework are allowed to participate in multiple networks we tested the hypothesis that this participation is not necessarily static over time. To illustrate this using the example of the ACC, Fig. 5 shows a region in the ACC which takes part in two networks (networks 24 and 27). The [blue] network is spatially similar to the medial temporal lobe subsystem of the default mode networks (DMN), as described by (Andrews-Hanna et al., 2010) and the [red] network is spatially similar to the dorsal medial prefrontal cortex subnetwork of the DMN (Andrews-Hanna et al., 2010). However, we found that the participation of the ACC region in these two subnetworks is not static over time (Figure 5B). This offers further interpretation of how these two subnetworks may interact in the DMN: the affiliation of this portion of ACC varies between them over time. Additionally, the variation network participation in single brain regions may in part account for the diversity of functions often associated with hub regions (Cole et al., 2013) like the ACC (Devinsky et al., 1995).

While a recent primate study has shown dynamic of functional connectivity even in the absence of consciousness (Hutchison et al., 2013b), more recent human studies show relations of dynamic functional connectivity and physiology (Chang et al., 2013) as well as task performance (Thompson et al., 2013). Here we expand this picture by showing a relationship between dynamic functional connectivity and ongoing thought processes.

Threshold	whole brain VNP / positive SGT (r)	whole brain VNP / age (r)	Caudate VNP / past SGT (r)
17.5 % (3500 edges)	-0.46	-0.21	0.14
15% (3000 edges)	-0.43	-0.26	0.41
12.5% (2500 edges)	-0.49	-0.20	0.38
10% (2000 edges)	-0.47	-0.24	0.47
7.5 % (1500 edges)	-0.46	-0.21	0.40

Table 2 Impact of different initial graph thresholds for the main results of the manuscript. The threshold of 10% (2000 edges) was used in this study. Main results are partial correlation between whole brain averaged Variation of Network Participation (VNP) and positive Self Generated Thoughts (SGT), whole brain averaged VNP and age, VNP of left Caudate and SGT about the past.

We found that variation in network participation was correlated with self-generated thought content across individuals; specifically it was related to thoughts about the past and those with a positive tone. Neurobiological studies suggest that there exist at least two different memory systems, one more cognitive system which relies upon medial temporal lobe and hippocampus areas and a stimulus-response system which banks in the basal ganglia (Poldrack and Packard, 2003). The default-mode network is a cortical network that connects middle temporal with the posterior cingulate and prefrontal areas, the subcortical network associated with the left caudate connects subcortical regions such as thalamus, putamen and caudate. Here we found that the left caudate is a hub involved in varying its degree of participation between these two networks and its specific behavior was correlated with self-generated thoughts about past events.

Self-generated thoughts about the past are known correlates of unhappiness (Smallwood and O'Connor, 2011) and may mark the temporal precursor of negative mood (Ruby et al., 2013). Self-generated thoughts of the past are also accompanied by greater disengagement, or decoupling, from external processes, as indexed by worse task performance (Smallwood et al., 2009, 2007). Altogether these studies illustrate that retrospective self-generated experiences may at times be both intrusive and unpleasant. The heightened variation in network participation of the caudate nucleus with increasing retrospective focus could therefore reflect the greater competition that accompanies especially repetitive or intrusive self-generated thoughts. Broadly consistent with this account we found that positive thoughts were associated with less variation in network participation at a whole brain level. In contrast to retrospective thoughts, pleasant experiences were associated with more consistent network dynamics, possibly reflecting the relatively calm form that positive experiences may take.

Variability of the fMRI signal, an univariate measure of brain dynamics, has been found to play an important role in behavioral performance (Garrett et al., 2013; McIntosh et al., 2010). One crucial observation is its reduction in older individuals or those who performing poorly in a variation of cognitive tasks (Garrett et al., 2013). While the biological reason for the loss of variability might arise from a dysregulation of dopamine and glutamate (Hong and Rebec, 2012), the behavioral implications might be explained by computational models (Deco *et al.*, 2011). These models suggest that variability of brain signal is important for exploring the repertoire of possible brain states (Deco *et al.*, 2011), while lower variability will raise the potential for remaining in a single state—resulting in inflexible behavior. Here we have shown a decline of variation in network participation during aging. Aging is therefore not only associated with decreased signal variability but also reduced interplay between networks, suggesting that dynamic network participation may underlie behavioral flexibility. However, the interaction of dynamics and age was not linear, indicating a more complex relation between dynamics and age which might be investigated in future studies.

Interactions of networks have been studied to date with respect to their average signal. The anticorrelation between the average signal of the DMN and the average signal of the task

positive network has been found to be predictive of individual behavior during task and rest (Kelly et al., 2008). Recently it has been shown that this relationship changes during the task based on the current performance (Thompson et al., 2013). A relationship between this anticorrelation and variation in network participation is possible, but not straightforward. As anti-correlation is based on the average signals of all vertices in respective networks the variation in network participation describes the varying integration of single regions into the networks.

In the analysis of dynamic network participation we only included regions which belonged to two or more networks and where the second largest consisted of at least two connections (Fig. 4D). While this property is fulfilled by all highly connected regions (Fig. 4D) there were also few sparsely connected areas included into the analysis. In this context we focused stronger on multi-network hubs then their pure connectedness, while we also found a correspondence between these two properties (Fig. 4D).

While we hypothesized that dynamic network interaction takes place in highly connected areas we also found that the extent of these dynamics is related to the extent of the hubness (Fig. 4E). This evidence further supports our hypothesis that hub areas might serve as relay stations which enable information integration. However, the effect of multi-network hubness was much weaker (Fig. 4F) and more connections could just improve the detectability of the underlying dynamic process.

The description of dynamic organization in resting state connectivity (Chang and Glover, 2010; Britz et al., 2010; Majeed et al., 2009; Musso et al., 2010; Smith et al., 2012; Handwerker et al., 2012) raised concerns about the potential artifactual origin of these BOLD synchrony fluctuations. Studies using EEG-fMRI data, however, have established a neuronal origin of dynamic resting state connectivity (Tagliazucchi et al., 2012; Britz et al., 2010; Musso et al., 2010). Another recent functional connectivity study in anesthetized macaques demonstrated dynamic functional connectivity in the absence of any motion (Hutchison et al., 2013b). In order to avoid potential confounds in our study, we selected datasets with minimal motion and tested for remaining influences. We did not find that subject motion accounted for the increased variation in network participation (Fig. 6B).

A limitation of the current study is the fixed window length of 50s which we chose based on the size of our bandpass filter (10sec to 100sec). This length might not always coincide with the dynamic of ongoing cognitive processes. To give evidence for the robustness of our findings we reanalyzed the data with window lengths of 65s (100 volumes). All our main results remained significant. However, a data-driven approach to detect temporal change points as described recently by Cribben et al. (2012) gives an adaptive window length which could further enhance sensitivity to dynamic processes. A potentially confounding influence is the variation of node sizes which could affect the extracted time series differently by noise. While the parcellation used in this study aimed to reduce the variation of node sizes (Craddock et al., 2012, Table1) a potential influence cannot be ruled out. A limitation in the current study design is the correlational approach to relate behavior and resting-state dynamics. We cannot rule out that an unknown third variable may have caused the observed effects. To what extent a manipulation of the content of self-generated thoughts could affect the dynamics of functional connectivity requires further research.

Understanding the dynamics of brain (Smith et al., 2012; Allen et al., 2012; Hutchison et al., 2013a) and mental states (Smallwood, 2013) is thought to be important as it may explain the flexible way that cognition unfolds over time. We identified dynamics in network participation for brain regions that occurred at multi-second time-scales which are correlated with alterations in self-reported experience. Although traditional functional connectivity approaches have until recently often ignored fluctuations over time, our findings suggest that understanding the dynamics of cognition may depend upon methods that interrogate the complexity and flexibility of brain dynamics. Our demonstration of a relation between the

dynamic variation in network participation of brain regions and psychological measures of experience, therefore, indicates that understanding the temporal brain dynamics could illuminate the processes through which different characteristics of self-generated experience arise.

Acknowledgements

We like to thank Joachim Böttger and Katja Heuer for their help in visualizing connectivity graphs.

References

Ahn, Y. Y., Bagrow, J. P., and Lehmann, S. (2010). Link communities reveal multiscale complexity in networks. *Nature* 466, 761–764.

Allen, E. A., Damaraju, E., Plis, S. M., Erhardt, E. B., Eichele, T., and Calhoun, V. D. (2012). Tracking Whole-Brain Connectivity Dynamics in the Resting State. *Cereb Cortex* in press.

Andrews-Hanna, J. R., Reidler, J. S., Sepulcre, J., Poulin, R., and Buckner, R. L. (2010). Functional-anatomic fractionation of the brain's default network. *Neuron* 65, 550–62.

Avants, B. B., Tustison, N. J., Song, G., Cook, P., Klein, A., and Gee, J. C. (2011). A reproducible evaluation of ANTs similarity metric performance in brain image registration. *Neuroimage* 54, 2033–44.

Barron, E., Riby, L. M., Greer, J., and Smallwood, J. (2011). Absorbed in Thought The Effect of Mind Wandering on the Processing of Relevant and Irrelevant Events. *Psychol. Sci.* 22, 596–601.

Bassett, D. S., Wymbs, N. F., Porter, M. A., Mucha, P. J., Carlson, J. M., and Grafton, S. T. (2011). Dynamic reconfiguration of human brain networks during learning. *Proc. Natl. Acad. Sci.* 108, 7641–7646.

Beckmann, C. F., DeLuca, M., Devlin, J. T., and Smith, S. M. (2005). Investigations into resting-state connectivity using independent component analysis. *Philos. Trans. R. Soc. B Biol. Sci.* 360, 1001–1013.

Behzadi, Y., Restom, K., Liau, J., and Liu, T. T. (2007). A component based noise correction method (CompCor) for BOLD and perfusion based fMRI. *Neuroimage* 37, 90–101.

Ten Berge, J. M. F., Krijnen, W. P., Wansbeek, T., and Shapiro, A. (1999). Some new results on correlation-preserving factor scores prediction methods. *Linear Algebra Appl.* 289, 311–318.

Biswal, B. B., Mennes, M., Zuo, X.-N., Gohel, S., Kelly, C., Smith, S. M., Beckmann, C. F., Adelstein, J. S., Buckner, R. L., Colcombe, S., et al. (2010). Toward discovery science of human brain function. *Proc. Natl. Acad. Sci. U. S. A.* 107, 4734–4739.

Böttger, J., Schurade, R., Jakobsen, E., Schaefer, A., and Margulies, D. S. (2014). Connexel Visualization: A software implementation of glyphs and edge-bundling for dense connectivity data using brainGL. *Front. Neurosci.* 8.

Britz, J., Van De Ville, D., and Michel, C. M. (2010). BOLD correlates of EEG topography reveal rapid resting-state network dynamics. *Neuroimage* 52, 1162–1170.

Buckner, R. L., Sepulcre, J., Talukdar, T., Krienen, F. M., Liu, H., Hedden, T., Andrews-Hanna, J. R., Sperling, R. a, and Johnson, K. a (2009). Cortical hubs revealed by intrinsic functional connectivity: mapping, assessment of stability, and relation to Alzheimer's disease. *J. Neurosci.* 29, 1860–73.

Calhoun, V. D., Adali, T., Pearlson, G. D., and Pekar, J. J. (2001). A method for making group inferences from functional MRI data using independent component analysis. *Hum. Brain Mapp.* 14, 140–151.

Chai, X. J., Castañón, A. N., Öngür, D., and Whitfield-Gabrieli, S. (2012). Anticorrelations in resting state networks without global signal regression. *Neuroimage* 59, 1420–1428.

Chang, C., and Glover, G. H. (2010). Time-frequency dynamics of resting-state brain connectivity measured with fMRI. *Neuroimage* 50, 81–98.

Chang, C., Metzger, C. D., Glover, G. H., Duyn, J. H., Heinze, H.-J., and Walter, M. (2013). Association between heart rate variability and fluctuations in resting-state functional connectivity. *Neuroimage* 68, 93–104.

Christoff, K., Gordon, A. M., Smallwood, J., Smith, R., and Schooler, J. W. (2009). Experience sampling during fMRI reveals default network and executive system contributions to mind wandering. *Proc. Natl. Acad. Sci. U. S. A.* 106, 8719–24.

Cole, M. W., Reynolds, J. R., Power, J. D., Repovs, G., Anticevic, A., and Braver, T. S. (2013). Multi-task connectivity reveals flexible hubs for adaptive task control. *Nat. Neurosci.* 16, 1348–1355.

Cox, R. W. (1996). AFNI: software for analysis and visualization of functional magnetic resonance neuroimages. *Comput. Biomed. Res.* 29, 162–173.

Craddock, R. C., James, G. A., Holtzheimer, P. E., Hu, X. P., and Mayberg, H. S. (2012). A whole brain fMRI atlas generated via spatially constrained spectral clustering. *Hum. Brain Mapp.* 33, 1914–1928.

Cribben, I., Haraldsdottir, R., Atlas, L. Y., Wager, T. D., and Lindquist, M. A. (2012). Dynamic connectivity regression: Determining state-related changes in brain connectivity. *Neuroimage* 61, 907–920.

Dale, A. M., Fischl, B., and Sereno, M. I. (1999). Cortical surface-based analysis: I. Segmentation and surface reconstruction. *Neuroimage* 9, 179–194.

Damoiseaux, J. S., Rombouts, S. A. R. B., Barkhof, F., Scheltens, P., Stam, C. J., Smith, S. M., and Beckmann, C. F. (2006). Consistent resting-state networks across healthy subjects. *Proc. Natl. Acad. Sci. U. S. A.* 103, 13848–13853.

Deco, G., Jirsa, V. K., and McIntosh, A. R. (2011). Emerging concepts for the dynamical organization of resting-state activity in the brain. *Nat. Rev. Neurosci.* 12, 43–56.

Devinsky, O., Morrell, M. J., and Vogt, B. A. (1995). Contributions of anterior cingulate cortex to behaviour. *Brain* 118, 279–306.

Dickinson, P. S. (1995). Interactions among neural networks for behavior. *Curr. Opin. Neurobiol.* 5, 792–798.

Van Dijk, K. R. A., Sabuncu, M. R., and Buckner, R. L. (2012). The influence of head motion on intrinsic functional connectivity MRI. *Neuroimage* 59, 431–438.

Garrett, D. D., Kovacevic, N., McIntosh, A. R., and Grady, C. L. (2011). The Importance of Being Variable. *J. Neurosci.* 31, 4496–4503.

Garrett, D. D., Kovacevic, N., McIntosh, A. R., and Grady, C. L. (2013). The Modulation of BOLD Variability between Cognitive States Varies by Age and Processing Speed. *Cereb. Cortex* 23, 684–693.

Gong, G., He, Y., Concha, L., Lebel, C., Gross, D. W., Evans, A. C., and Beaulieu, C. (2009). Mapping anatomical connectivity patterns of human cerebral cortex using in vivo diffusion tensor imaging tractography. *Cereb. cortex* 19, 524–536.

Gorgolewski, K., Burns, C. D., Madison, C., Clark, D., Halchenko, Y. O., Waskom, M. L., and Ghosh, S. S. (2011). Nipype: a flexible, lightweight and extensible neuroimaging data processing framework in python. *Front. Neuroinform.* 5.

Gorgolewski, K. J., Lurie, D., Urchs, S., Kipping, J. A., Craddock, R. C., Milham, M. P., Margulies, D. S., and Smallwood, J. A correspondence between the brain's intrinsic functional architecture and the content and form of self-generated thoughts. under revi.

Greve, D. N., and Fischl, B. (2009). Accurate and robust brain image alignment using boundary-based registration. *Neuroimage* 48, 63–72.

Hagmann, P., Cammoun, L., Gigandet, X., Meuli, R., Honey, C. J., Wedeen, V. J., and Sporns, O. (2008). Mapping the structural core of human cerebral cortex. *PLoS Biol.* 6, e159.

Handwerker, D. a, Roopchansingh, V., Gonzalez-Castillo, J., and Bandettini, P. a (2012). Periodic changes in fMRI connectivity. *Neuroimage* 63, 1712–9.

Van den Heuvel, M. P., and Sporns, O. (2013). An anatomical substrate for integration among functional networks in human cortex. *J. Neurosci.* 33, 14489–14500.

Hong, S. L., and Rebec, G. V (2012). Biological Sources of Inflexibility in Brain and Behavior with Aging and Neurodegenerative Diseases. *Front. Syst. Neurosci.* 6.

Hooper, S. L., and Moulins, M. (1989). Switching of a neuron from one network to another by sensory-induced changes in membrane properties. *Science (80-.).* 244, 1587–1589.

Horn, J. L. (1965). A rationale and test for the number of factors in factor analysis. *Psychometrika* 30, 179–185.

Hutchison, R. M., Womelsdorf, T., Allen, E. a, Bandettini, P. a, Calhoun, V. D., Corbetta, M., Della Penna, S., Duyn, J. H., Glover, G. H., Gonzalez-Castillo, J., et al. (2013a). Dynamic functional connectivity: promise, issues, and interpretations. *Neuroimage* 80, 360–378.

Hutchison, R. M., Womelsdorf, T., Gati, J. S., Everling, S., and Menon, R. S. (2013b). Resting-state networks show dynamic functional connectivity in awake humans and anesthetized macaques. *Hum. Brain Mapp.* 34, 2154–2177.

Jenkinson, M., Beckmann, C. F., Behrens, T. E. J., Woolrich, M. W., and Smith, S. M. (2012). Fsl. *Neuroimage* 62, 782–790.

Kalinka, A. T., and Tomancak, P. (2011). linkcomm: an R package for the generation, visualization, and analysis of link communities in networks of arbitrary size and type. *Bioinformatics* 27, 2011–2012.

Kelly, A. M. C., Uddin, L. Q., Biswal, B. B., Castellanos, F. X., and Milham, M. P. (2008). Competition between functional brain networks mediates behavioral variability. *Neuroimage* 39, 527–537.

Lee, J.-H., Hashimoto, R., Wible, C. G., and Yoo, S.-S. (2011). Investigation of spectrally coherent resting-state networks using non-negative matrix factorization for functional MRI data. *Int. J. Imaging Syst. Technol.* 21, 211–222.

Lohmann, G., Margulies, D. S., Horstmann, A., Pleger, B., Lepsien, J., Goldhahn, D., Schloegl, H., Stumvoll, M., Villringer, A., and Turner, R. (2010). Eigenvector Centrality Mapping for Analyzing Connectivity Patterns in fMRI Data of the Human Brain. *PLoS One* 5, e10232.

Majeed, W., Magnuson, M., and Keilholz, S. D. (2009). Spatiotemporal dynamics of low frequency fluctuations in BOLD fMRI of the rat. *J. Magn. Reson. imaging* 30, 384–393.

Mantel, N. (1967). The detection of disease clustering and a generalized regression approach. *Cancer Res.* 27, 209–220.

Marder, E., and Bucher, D. (2001). Central pattern generators and the control of rhythmic movements. *Curr. Biol.* 11, 986–996.

Marder, E., and Bucher, D. (2007). Understanding circuit dynamics using the stomatogastric nervous system of lobsters and crabs. *Annu. Rev. Physiol.* 69, 291–316.

McIntosh, a R., Kovacevic, N., Lippe, S., Garrett, D., Grady, C., and Jirsa, V. (2010). The development of a noisy brain. *Arch. Ital. Biol.* 148, 323–337.

McQuitty, L. L. (1966). Similarity analysis by reciprocal pairs for discrete and continuous data. *Educ. Psychol. Meas.* 26, 825–831.

Musso, F., Brinkmeyer, J., Mobascher, A., Warbrick, T., and Winterer, G. (2010). Spontaneous brain activity and EEG microstates. A novel EEG/fMRI analysis approach to explore resting-state networks. *Neuroimage* 52, 1149–1161.

Nooner, K. B., Colcombe, S. J., Tobe, R. H., Mennes, M., Benedict, M. M., Moreno, A. L., Panek, L. J., Brown, S., Zavitz, S. T., Li, Q., et al. (2012). The NKI-Rockland Sample: A Model for Accelerating the Pace of Discovery Science in Psychiatry. *Front Neurosci* 6, 152.

Patriat, R., Molloy, E. K., Meier, T. B., Kirk, G. R., Nair, V. A., Meyerand, M. E., Prabhakaran, V., and Birn, R. M. (2013). The effect of resting condition on resting-state fMRI reliability

and consistency: A comparison between resting with eyes open, closed, and fixated. *Neuroimage* 78, 463–473.

Poldrack, R. a, and Packard, M. G. (2003). Competition among multiple memory systems: converging evidence from animal and human brain studies. *Neuropsychologia* 41, 245–51.

Power, J. D., Cohen, A. L., Nelson, S. M., Wig, G. S., Barnes, K. A., Church, J. A., Vogel, A. C., Laumann, T. O., Miezin, F. M., Schlaggar, B. L., et al. (2011). Functional network organization of the human brain. *Neuron* 72, 665–678.

Revelle, W. (2011). Psych: Procedures for psychological, psychometric, and personality research. *R Packag. version* 1019.

Ruby, F. J. M., Smallwood, J., Engen, H., and Singer, T. (2013). How Self-Generated Thought Shapes Mood—The Relation between Mind-Wandering and Mood Depends on the Socio-Temporal Content of Thoughts. *PLoS One* 8, e77554.

Schölvinck, M. L., Maier, A., Ye, F. Q., Duyn, J. H., and Leopold, D. A. (2010). Neural basis of global resting-state fMRI activity. *Proc Natl Acad Sci U S A* 107, 10238–10243.

Schwarz, A. J., and McGonigle, J. (2011). Negative edges and soft thresholding in complex network analysis of resting state functional connectivity data. *Neuroimage* 55, 1132–1146.

Smallwood, J. (2013). Distinguishing how from why the mind wanders: A process--occurrence framework for self-generated mental activity. *Psychol. Bull.* 139, 519.

Smallwood, J., Brown, K. S., Baird, B., Mrazek, M. D., Franklin, M. S., and Schooler, J. W. (2012). Insulation for daydreams: a role for tonic norepinephrine in the facilitation of internally guided thought. *PLoS One* 7, e33706.

Smallwood, J., Fitzgerald, A., Miles, L. K., and Phillips, L. H. (2009). Shifting moods, wandering minds: negative moods lead the mind to wander. *Emotion* 9, 271.

Smallwood, J., and O'Connor, R. C. (2011). Imprisoned by the past: unhappy moods lead to a retrospective bias to mind wandering. *Cogn. Emot.* 25, 1481–1490.

Smallwood, J., O'Connor, R. C., Sudbery, M. V, and Obonsawin, M. (2007). Mind-wandering and dysphoria. *Cogn. Emot.* 21, 816–842.

Smallwood, J., Tipper, C., Brown, K., Baird, B., Engen, H., Michaels, J. R., Grafton, S., and Schooler, J. W. (2013). Escaping the here and now: Evidence for a role of the default mode network in perceptually decoupled thought. *Neuroimage* 69, 120–125.

Smith, S. M., Miller, K. L., Moeller, S., Xu, J., Auerbach, E. J., Woolrich, M. W., Beckmann, C. F., Jenkinson, M., Andersson, J., Glasser, M. F., et al. (2012). Temporally-independent functional modes of spontaneous brain activity. *Proc. Natl. Acad. Sci. U. S. A.* 109, 3131–3136.

Sokal, R. R., and Rohlf, F. J. (1962). The Comparison of Dendrograms by Objective Methods. *Taxon* 11, 33–40.

Sporns, O., Honey, C. J., and Kötter, R. (2007). Identification and classification of hubs in brain networks. *PLoS One* 2, e1049.

Tagliazucchi, E., Von Wegner, F., Morzelewski, A., Brodbeck, V., and Laufs, H. (2012). Dynamic BOLD functional connectivity in humans and its electrophysiological correlates. *Front Hum Neurosci* 6.

Thompson, G. J., Magnuson, M. E., Merritt, M. D., Schwarb, H., Pan, W.-J., McKinley, A., Tripp, L. D., Schumacher, E. H., and Keilholz, S. D. (2013). Short-time windows of correlation between large-scale functional brain networks predict vigilance intraindividually and interindividually. *Hum. Brain Mapp.* 34, 3280–3298.

Weimann, J. M., and Marder, E. (1994). Switching neurons are integral members of multiple oscillatory networks. *Curr. Biol.* 4, 896–902.

Xu, J., Moeller, S., Strupp, J., Auerbach, E. J., Chen, L., Feinberg, D. A., Ugurbil, K., and Yacoub, E. (2012). Highly accelerated whole brain imaging using aligned-blipped-controlled-aliasing multiband EPI. in *Proceedings of the 20th Annual Meeting of ISMRM, Melbourne, Australia*, 2306.

Yeo, B. T. T., Krienen, F. M., Chee, M. W. L., and Buckner, R. L. (2014). Estimates of segregation and overlap of functional connectivity networks in the human cerebral cortex. *Neuroimage* 88, 212–227.

Zuo, X. N., Ehmke, R., Mennes, M., Imperati, D., Castellanos, F. X., Sporns, O., and Milham, M. P. (2012). Network Centrality in the Human Functional Connectome. *Cereb Cortex* 22, 1862–1875.

3 Summary

Dissertation zur Erlangung des akademischen Grades
Dr. rer. med.
Identifying Changes of Functional Brain Networks using Graph Theory
eingereicht von: Alexander Schäfer
angefertigt am Max-Planck-Institut für Kognitions- und Neurowissenschaften
betreut von Prof. Dr. Arno Villringer und Dr. Daniel S. Margulies
April 2014

Brain disorders are described as one of the core health challenges for the 21st century (Wittchen et al., 2011) as their prevalence in developed countries surpasses those of cardiovascular diseases and cancer (Collins et al., 2011). While functional Magnetic Resonance Imaging (fMRI) was expected to be a key method for the diagnosis and prognosis of brain disorders (Thulborn et al., 1996), it has seen very little success in translations to the clinical realm (Matthews et al., 2006; Bullmore, 2012). For a long time fMRI experiments focused on specific brain areas which were expected to show atypical activation in experiments with specific task designs. This task-based fMRI stands in stark contrast to the more successful structural neuroimaging methods (e.g. CT, MRI), which provide whole brain images without the need for patient compliance. However, functional neuroimaging is crucial to detect pathologic changes at an early stage. In this thesis, I have described the possible usage of resting-state fMRI (rs-fMRI) and network theory to investigate clinically relevant functional changes in the human brain without regional constraints or the need for a specific task.

The present thesis reviewed graph theoretic approaches to analyze brain network properties using rs-fMRI data (Study 1). I applied a centrality measure to investigate the relation of widespread white matter lesions and associated behavioral impairments to changes in whole-brain functional networks (Study 2). However, changes in functional brain networks can not only occur in pathology but can also be externally induced for therapeutic reasons. We investigated the impact of an electrical stimulation on functional whole-brain networks

during and after tDCS stimulation using a centrality measure (Study 3). Centrality approaches reduce the information of networks. One of the reasons for this reduction is a lack of good visualization methods. We addressed this limitation by bundling connections that connect similar areas in the brain (Study 4). This method enhances the information gained for a human viewer and may prove relevant in a neurosurgical context. While the previous studies implicitly assumed functional brain networks to be static within an fMRI scan, in Study 5 we also investigated the ongoing dynamic changes within an fMRI scan. We could show a relationship to ongoing cognitive processes which is evidence for the non-artifactual origin of these changes. These ongoing changes open up a new window for rs-fMRI to further elucidate brain function and pathology.

In Publication 1 we capitalized on resting-state fMRI which is based on the effect that intrinsic spontaneous low frequency fluctuations in the fMRI BOLD signal show correlated signal in functionally coupled networks (Biswal, 1995). These networks persist across various states and resemble task-based co-activation maps (Smith et al., 2009). rs-fMRI is well-suited for clinical applications as it offers several advantages compared to task-based fMRI: it requires minimal patient compliance, can be performed under anesthesia, is easy to standardize (Fox and Greicius, 2010), provides a good signal to noise ratio and enables the study of multiple brain networks simultaneously. In the current work, we investigated functional brain networks in the well-defined framework of graph theory. We showed the usability and applicability of this framework to the clinical realm at the example of concrete and clinically relevant cases, such as network centrality to detect changes in functional networks of patients with small vessel disease. As there is a large and further increasing number of tools and methods to analyze rs-fMRI data we reviewed this important topic in Publication 1 (Margulies et al., 2010). The review provides an introduction and general overview of tools to analyze rs-fMRI data, including seed-based functional connectivity, independent component analysis, clustering, pattern classification, local methods and the main topic of this thesis: graph theory.

The aim of this thesis is to demonstrate the applicability of measures from graph theory described in Publication 1 to investigate changes in functional brain networks captured by rs-fMRI. These changes can occur due to brain pathology such as vascular lesions which can disrupt or alter the structural connections of the brain. One prominent disease that can lead to vascular lesions is small vessel disease. To investigate the impact of early small vessel disease on gray matter functional connectivity we performed Study 2 (Schaefer et al., 2014b). Early cerebral small vessel disease is mainly characterized by small white matter lesions. While white matter lesions are also common in otherwise asymptomatic individuals, the presence and severity of white matter lesions doubles the risk of a later dementia (Vermeer et al., 2003). Furthermore, white matter lesions can lead to cognitive impairment which worsens with increased lesioning (Longstreth et al., 2005). To measure changes in whole brain connectivity due to vascular lesions we applied graph theoretical eigenvector centrality, a voxel-based network centrality analysis. We found reduced connectivity in cerebral gray matter networks and at a concurrent increase of cerebellar connectivity in patients with early small vessel disease. Furthermore, we found a very similar picture when we related the severity of the disease with whole-brain eigenvector centrality maps. Small vessel disease often leads to a behavioral psychomotor slowing. In our patient cohort we also found an increase in reaction times across various cognitive tests. Specifically, we found

reduced connectivity of premotor areas and increased cerebellar connectivity in slower performing subjects.

The reduction of cerebral gray matter connectivity in the context of white matter lesions might not be surprising but it offers a mechanistic link between the two modalities. In the future, this link could be further examined using a prediction model that predicts the connectivity reduction based on the location and size of the individual lesion. However, to evaluate and validate such a model, a larger sample size is required with lesions in similar locations. Such a single-subject model can then be directly translated into a clinical application.

Another clinically relevant application, especially in the context of therapeutic rehabilitation, is electrical stimulation of specific brain areas. In Study 3 (Sehm et al., 2012) we actively manipulated gray matter connectivity using electrical brain stimulation. More precisely, we analyzed the impact of anodal and bilateral tDCS over the motor cortex during and after the stimulation while participants underwent fMRI. Here, we again used the method of eigenvector centrality to investigate connectivity alterations. We found that a bilateral tDCS leads to an increase of functional connectivity in primary and secondary motor as well as frontal areas in comparison to the sham stimulation. These effects were present during bilateral tDCS and persisted after the stimulation. As suggested by researchers using other modalities (Bestmann et al., 2004; Denslow et al., 2005), the effects were widespread and not limited to the motor cortex. We can thus conclude that electrical brain stimulation not only alters the connectivity within the stimulated sub-network (motor network) but also to other interconnected sub-networks.

tDCS and other electrical brain stimulation methods show a large inter-individual variability in their ability and efficacy to enhance behavioral performance (Datta et al., 2012). Therefore, a growing interest exists to test protocols in order to optimize the stimulation performance (Sehm et al., 2013). Estimating the change in functional brain networks during electrical stimulation not only improves our understanding of the stimulation process, as we have shown here, but may also provide a basis to control efficacy of a particular stimulation setting on the single-subject level.

While we could observe whole brain alterations of connectivity using eigenvector centrality, the investigation also revealed one limitation of centrality analysis. By measuring and representing the amount of connectivity of each region (voxel) to the rest of the brain, we lose the spatial information of the connections. By this the connectivity information gets reduced to the sheer amount of connections without any spatial information. In other words, the connectivity is mapped from the network space to the region space. To address the specific spatial connectivity information to the stimulation side, we conducted a study (Sehm et al., 2013) using a seed-based analysis targeting specifically the motor cortex and its changes in connectivity to the rest of the brain. While this approach preserves the spatial connectivity information of the specific area, it hides the connectivity changes of all other areas.

An ideal approach might not perform any reduction at all. Other than some statistical considerations (Zalesky et al., 2010) one of the main problems is visualizing so many connections (Margulies et al., 2013). Many current neuroimaging visualization tools, especially in the context of fMRI, are designed to map out areas and not connections. In contrast to structural connections functional connectivity is not a determined track but rather a connection between two points. The visualization of high-resolution connectivity as straight

lines in anatomical space can clutter heavily. To overcome this limitation we proposed a method to bundle connections with similar start and end points (Study 4: (Böttger et al., 2014a)). Our method is especially valuable in any setting where the anatomical context of the functional connectivity is important, for example neurosurgical planning or a refined psychiatric diagnostics. The method has also recently been implemented into an open-source brain visualization software (Böttger et al., 2014b) to make it usable to a wider public.

Both the shift from the regional to the connectivity space as aimed in Study 4 (Böttger et al., 2014a) as well as the dynamical aspect of brain networks (Study 3) were incorporated in Study 5 (Schaefer et al., 2014a).

In the connectivity space we did not aim to bundle similar connections for visualization purposes but grouped edges that connect similar areas into networks. This is in contrast to other methods which aim to cluster regions based on their connectivity profile (Bellec et al., 2010; Power et al., 2011; Yeo et al., 2011) and thereby reduce networks to the regional space. In the framework of connectivity networks regions can belong to multiple networks. Further, the method performs no reduction from the connectivity space to the regional space.

In the context of recent studies on functional connectivity dynamics (Allen et al., 2014; Smith et al., 2012) we also addressed the question of how stable the network constellations are during the period of a single scan. To investigate whether such ongoing dynamics are artifactual or indeed meaningful they need to be related to ongoing physiological or behavioral measurements (Hutchison et al., 2013a). To this end, we investigated the dynamics of functional networks during an rs-fMRI scan and its relation to ongoing self-generated thought processes. In contrast to Study 2 and 3 (Schaefer et al., 2014b; Sehm et al., 2012) we assessed the changes of functional networks related to internal processes without external manipulation. We found a relation between ongoing dynamics and the content of ongoing self-generated thoughts (SGT). Subjects who reported more positive SGT showed a reduction in overall dynamics. Furthermore, we found that the variation of connectivity of the left caudate between a subcortical and a default mode subnetwork was increased when individuals reported to have thought about the past. This observation is especially interesting in the context of earlier findings of competing cortical and subcortical memory systems with a heavy involvement of the caudate area (Poldrack and Packard, 2003). We found that the dynamics on a whole-brain level was further reduced in older subjects. These results shed new light onto earlier findings of reduced fMRI signal variability in older subjects (Garrett et al., 2011). In general our findings give further evidence for a non-artifactual origin of dynamic resting state functional connectivity. This is important, as dynamic functional connectivity methods might become a very valuable tool for clinical purposes (Hutchison et al., 2013a). In this context, these methods might enable to increase the reliability and or sensitivity of future diagnostic tools. This additional benefit will come without additional costs, as the same dataset can be analyzed with both, static and dynamic functional connectivity methods. Thus, the investigation of differences in the dynamics of pathologically changed brains might substantially enhance our understanding of brain diseases but also of healthy brain function.

This thesis gives an overview on how to estimate changes in functional brain networks using graph theoretical measures. It explains the assessment and definition of functional brain networks derived from fMRI data. More explicitly, this thesis provides examples and newly developed methods on the measurement and visualization of changes due to pathology, external electrical stimulation or ongoing internal thought processes. These changes can

occur on long as well as on short time scales and might be a key to understanding brain pathologies and their development. Furthermore, this thesis describes new methods to investigate and visualize these changes on both time scales and provides a more complete picture of the brain as a dynamic and constantly changing network.

4 Bibliography

Aizenstein, H., and Andreescu, C. (2011). fMRI correlates of white matter hyperintensities in late-life depression. *Am J Psychiatry* 168, 1075–1082.

Allen, E. A., Damaraju, E., Plis, S. M., Erhardt, E. B., Eichele, T., and Calhoun, V. D. (2014). Tracking whole-brain connectivity dynamics in the resting state. *Cereb. Cortex* 24, 663–76.

Bellec, P., Rosa-Neto, P., Lyttelton, O. C., Benali, H., and Evans, A. C. (2010). Multi-level bootstrap analysis of stable clusters in resting-state fMRI. *Neuroimage* 51, 1126–1139.

Bestmann, S., Baudewig, J., Siebner, H. R., Rothwell, J. C., and Frahm, J. (2004). Functional MRI of the immediate impact of transcranial magnetic stimulation on cortical and subcortical motor circuits. *Eur. J. Neurosci.* 19, 1950–1962.

Biswal, B. (1995). Functional connectivity in the motor cortex of resting human brain using echo-planar mri. *Magn. Reson. Med.* 34, 537–541.

Bolognini, N., Vallar, G., Casati, C., Latif, L. A., El-Nazer, R., Williams, J., Banco, E., Macea, D. D., Tesio, L., Chessa, C., et al. (2011). Neurophysiological and behavioral effects of tDCS combined with constraint-induced movement therapy in poststroke patients. *Neurorehabil. Neural Repair* 25, 819–829.

Böttger, J., Schäfer, A., Lohmann, G., Villringer, A., and Margulies, D. S. (2014a). Three-Dimensional Mean-Shift Edge Bundling for the Visualization of Functional Connectivity in the Brain. *IEEE Trans. Vis. Comput. Graph.* 20, 471–480.

Böttger, J., Schurade, R., Jakobsen, E., Schaefer, A., and Margulies, D. S. (2014b). Connexel visualization: a software implementation of glyphs and edge-bundling for dense connectivity data using brainGL. *Front. Neurosci.* 8, 15.

Britz, J., Van De Ville, D., and Michel, C. M. (2010). BOLD correlates of EEG topography reveal rapid resting-state network dynamics. *Neuroimage* 52, 1162–1170.

Bullmore, E. (2012). The future of functional MRI in clinical medicine. *Neuroimage* 62, 1267–1271.

Cammoun, L., Gigandet, X., Meskaldji, D., Thiran, J. P., Sporns, O., Do, K. Q., Maeder, P., Meuli, R., and Hagmann, P. (2012). Mapping the human connectome at multiple scales with diffusion spectrum MRI. *J Neurosci Methods* 203, 386–397.

Chang, C., and Glover, G. H. (2010). Time-frequency dynamics of resting-state brain connectivity measured with fMRI. *Neuroimage* 50, 81–98.

Chang, C., Metzger, C. D., Glover, G. H., Duyn, J. H., Heinze, H.-J., and Walter, M. (2013). Association between heart rate variability and fluctuations in resting-state functional connectivity. *Neuroimage* 68, 93–104.

Collins, P. Y., Patel, V., Joestl, S. S., March, D., Insel, T. R., Daar, A. S., Bordin, I. A., Costello, E. J., Durkin, M., Fairburn, C., et al. (2011). Grand challenges in global mental health. *Nature* 475, 27–30.

Craddock, R. C., James, G. A., Holtzheimer, P. E., Hu, X. P., and Mayberg, H. S. (2012). A whole brain fMRI atlas generated via spatially constrained spectral clustering. *Hum. Brain Mapp.* 33, 1914–1928.

Creutzfeldt, O. D., Fromm, G. H., and Kapp, H. (1962). Influence of transcortical dc currents on cortical neuronal activity. *Exp. Neurol.* 5, 436–452.

Datta, A., Truong, D., Minhas, P., Parra, L. C., and Bikson, M. (2012). Inter-individual variation during transcranial direct current stimulation and normalization of dose using MRI-derived computational models. *Front. Psychiatry* 3.

Deco, G., Jirsa, V. K., and McIntosh, A. R. (2011). Emerging concepts for the dynamical organization of resting-state activity in the brain. *Nat. Rev. Neurosci.* 12, 43–56.

Denslow, S., Lomarev, M., George, M. S., and Bohning, D. E. (2005). Cortical and subcortical brain effects of transcranial magnetic stimulation (TMS)-induced movement: an interleaved TMS/functional magnetic resonance imaging study. *Biol. Psychiatry* 57, 752–760.

Diestel, R. (2005). Graph theory. 2005. *Grad. Texts Math*.

Dosenbach, N. U. F., Nardos, B., Cohen, A. L., Fair, D. a, Power, J. D., Church, J. a, Nelson, S. M., Wig, G. S., Vogel, A. C., Lessov-Schlaggar, C. N., et al. (2010). Prediction of individual brain maturity using fMRI. *Science* 329, 1358–61.

Van Essen, D. C., Ugurbil, K., Auerbach, E., Barch, D., Behrens, T. E. J., Bucholz, R., Chang, A., Chen, L., Corbetta, M., Curtiss, S. W., et al. (2012). The human connectome project: a data acquisition perspective. *Neuroimage* 62, 2222–2231.

Fornito, A., Zalesky, A., and Breakspear, M. (2013). Graph analysis of the human connectome: Promise, progress, and pitfalls. *Neuroimage* in press.

Fox, M. D., and Greicius, M. (2010). Clinical applications of resting state functional connectivity. *Front Syst Neurosci* 4, 19.

Fox, M. D., and Raichle, M. E. (2007). Spontaneous fluctuations in brain activity observed with functional magnetic resonance imaging. *Nat. Rev. Neurosci.* 8, 700–11.

Friedman, J., Hastie, T., and Tibshirani, R. (2008). Sparse inverse covariance estimation with the graphical lasso. *Biostatistics* 9, 432–41.

Garrett, D. D., Kovacevic, N., McIntosh, A. R., and Grady, C. L. (2011). The Importance of Being Variable. *J. Neurosci.* 31, 4496–4503.

Hutchison, R. M., Womelsdorf, T., Allen, E. a, Bandettini, P. a, Calhoun, V. D., Corbetta, M., Della Penna, S., Duyn, J. H., Glover, G. H., Gonzalez-Castillo, J., et al. (2013a). Dynamic functional connectivity: promise, issues, and interpretations. *Neuroimage* 80, 360–378.

Hutchison, R. M., Womelsdorf, T., Gati, J. S., Everling, S., and Menon, R. S. (2013b). Resting-state networks show dynamic functional connectivity in awake humans and anesthetized macaques. *Hum. Brain Mapp.* 34, 2154–2177.

Keeser, D., Meindl, T., Bor, J., Palm, U., Pogarell, O., Mulert, C., Brunelin, J., Möller, H.-J., Reiser, M., and Padberg, F. (2011). Prefrontal transcranial direct current stimulation changes connectivity of resting-state networks during fMRI. *J. Neurosci.* 31, 15284–15293.

Koch, M. A., Norris, D. G., and Hund-Georgiadis, M. (2002). An investigation of functional and anatomical connectivity using magnetic resonance imaging. *Neuroimage* 16, 241–250.

Lindenberg, R., Renga, V., Zhu, L. L., Nair, D., and Schlaug, G. (2010). Bihemispheric brain stimulation facilitates motor recovery in chronic stroke patients. *Neurology* 75, 2176–2184.

Logothetis, N. K. (2002). The neural basis of the blood-oxygen-level-dependent functional magnetic resonance imaging signal. *Philos. Trans. R. Soc. Lond. B. Biol. Sci.* 357, 1003–37.

Logothetis, N. K., Pauls, J., Augath, M., Trinath, T., and Oeltermann, A. (2001). Neurophysiological investigation of the basis of the fMRI signal. *Nature* 412, 150–157.

Lohmann, G., Margulies, D. S., Horstmann, A., Pleger, B., Lepsien, J., Goldhahn, D., Schloegl, H., Stumvoll, M., Villringer, A., and Turner, R. (2010). Eigenvector Centrality Mapping for Analyzing Connectivity Patterns in fMRI Data of the Human Brain. *PLoS One* 5, e10232.

Longstreth, W. T., Arnold, A. M., Beauchamp, N. J., Manolio, T. A., Lefkowitz, D., Jungreis, C., Hirsch, C. H., O'Leary, D. H., and Furberg, C. D. (2005). Incidence, Manifestations, and Predictors of Worsening White Matter on Serial Cranial Magnetic Resonance Imaging in the Elderly The Cardiovascular Health Study. *Stroke* 36, 56–61.

Lv, Y., Margulies, D. S., Cameron Craddock, R., Long, X., Winter, B., Gierhake, D., Endres, M., Villringer, K., Fiebach, J., and Villringer, A. (2013). Identifying the perfusion deficit in acute stroke with resting-state functional magnetic resonance imaging. *Ann Neurol* 73, 136–140.

Margulies, D. S., Böttger, J., Long, X., Lv, Y., Kelly, C., Schäfer, A., Goldhahn, D., Abbushi, A., Milham, M. P., Lohmann, G., et al. (2010). Resting developments: a review of fMRI post-processing methodologies for spontaneous brain activity. *MAGMA* 23, 289–307.

Margulies, D. S., Böttger, J., Watanabe, A., and Gorgolewski, K. J. (2013). Visualizing the human connectome. *Neuroimage* 80, 445–461.

Matthews, P. M., Honey, G. D., and Bullmore, E. T. (2006). Applications of fMRI in translational medicine and clinical practice. *Nat. Rev. Neurosci.* 7, 732–44.

Mukamel, R., Gelbard, H., Arieli, A., Hasson, U., Fried, I., and Malach, R. (2005). Coupling between neuronal firing, field potentials, and FMRI in human auditory cortex. *Science (80-.).* 309, 951–954.

Musso, F., Brinkmeyer, J., Mobascher, A., Warbrick, T., and Winterer, G. (2010). Spontaneous brain activity and EEG microstates. A novel EEG/fMRI analysis approach to explore resting-state networks. *Neuroimage* 52, 1149–1161.

Nitsche, M. A., Fricke, K., Henschke, U., Schlitterlau, A., Liebetanz, D., Lang, N., Henning, S., Tergau, F., and Paulus, W. (2003a). Pharmacological modulation of cortical excitability shifts induced by transcranial direct current stimulation in humans. *J. Physiol.* 553, 293–301.

Nitsche, M. A., Schauenburg, A., Lang, N., Liebetanz, D., Exner, C., Paulus, W., and Tergau, F. (2003b). Facilitation of implicit motor learning by weak transcranial direct current stimulation of the primary motor cortex in the human. *J. Cogn. Neurosci.* 15, 619–626.

Nooner, K. B., Colcombe, S. J., Tobe, R. H., Mennes, M., Benedict, M. M., Moreno, A. L., Panek, L. J., Brown, S., Zavitz, S. T., Li, Q., et al. (2012). The NKI-Rockland Sample: A Model for Accelerating the Pace of Discovery Science in Psychiatry. *Front Neurosci* 6, 152.

Ogawa, S., Lee, T. M., Stepnoski, R., Chen, W., Zhu, X. H., and Ugurbil, K. (2000). An approach to probe some neural systems interaction by functional MRI at neural time scale down to milliseconds. *Proc. Natl. Acad. Sci. U. S. A.* 97, 11026–31.

Patriat, R., Molloy, E. K., Meier, T. B., Kirk, G. R., Nair, V. A., Meyerand, M. E., Prabhakaran, V., and Birn, R. M. (2013). The effect of resting condition on resting-state fMRI reliability and consistency: A comparison between resting with eyes open, closed, and fixated. *Neuroimage* 78, 463–473.

Poldrack, R. a, and Packard, M. G. (2003). Competition among multiple memory systems: converging evidence from animal and human brain studies. *Neuropsychologia* 41, 245–51.

Power, J. D., Cohen, A. L., Nelson, S. M., Wig, G. S., Barnes, K. A., Church, J. A., Vogel, A. C., Laumann, T. O., Miezin, F. M., Schlaggar, B. L., et al. (2011). Functional network organization of the human brain. *Neuron* 72, 665–678.

Reijneveld, J. C., Ponten, S. C., Berendse, H. W., and Stam, C. J. (2007). The application of graph theoretical analysis to complex networks in the brain. *Clin. Neurophysiol.* 118, 2317–31.

Schaefer, A., Margulies, D. S., Lohmann, G., Gorgolewski, K. J., Smallwood, J., Kiebel, S. J., and Villringer, A. (2014a). Dynamic network participation of functional connectivity hubs assessed by resting-state fMRI. *Front. Hum. Neurosci.* 8, 195.

Schaefer, A., Quinque, E. M., Kipping, J. a, Arélin, K., Roggenhofer, E., Frisch, S., Villringer, A., Mueller, K., and Schroeter, M. L. (2014b). Early small vessel disease affects frontoparietal and cerebellar hubs in close correlation with clinical symptoms--a resting-state fMRI study. *J. Cereb. Blood Flow Metab.* 34, 1091–5.

Schölvinck, M. L., Maier, A., Ye, F. Q., Duyn, J. H., and Leopold, D. A. (2010). Neural basis of global resting-state fMRI activity. *Proc Natl Acad Sci U S A* 107, 10238–10243.

Schwarz, A. J., and McGonigle, J. (2011). Negative edges and soft thresholding in complex network analysis of resting state functional connectivity data. *Neuroimage* 55, 1132–1146.

Sehm, B., Kipping, J., Schäfer, A., Villringer, A., and Ragert, P. (2013). A Comparison between Uni- and Bilateral tDCS Effects on Functional Connectivity of the Human Motor Cortex. *Front. Hum. Neurosci.* 7, 183.

Sehm, B., Schaefer, a., Kipping, J., Margulies, D., Conde, V., Taubert, M., Villringer, a., and Ragert, P. (2012). Dynamic modulation of intrinsic functional connectivity by transcranial direct current stimulation. *J. Neurophysiol.* 108, 3253–63.

Selnes, O. A., and Vinters, H. V (2006). Vascular cognitive impairment. *Nat Clin Pr. Neuro* 2, 538–547.

Shehzad, Z., Kelly, A. M. C., Reiss, P. T., Gee, D. G., Gotimer, K., Uddin, L. Q., Lee, S. H., Margulies, D. S., Roy, A. K., Biswal, B. B., et al. (2009). The resting brain: unconstrained yet reliable. *Cereb. cortex* 19, 2209–2229.

Shmuel, A., Augath, M., Oeltermann, A., and Logothetis, N. K. (2006). Negative functional MRI response correlates with decreases in neuronal activity in monkey visual area V1. *Nat. Neurosci.* 9, 569–577.

Smith, S. M., Fox, P. T., Miller, K. L., Glahn, D. C., Fox, P. M., Mackay, C. E., Filippini, N., Watkins, K. E., Toro, R., Laird, A. R., et al. (2009). Correspondence of the brain's functional architecture during activation and rest. *Proc. Natl. Acad. Sci.* 106, 13040–13045.

Smith, S. M., Miller, K. L., Moeller, S., Xu, J., Auerbach, E. J., Woolrich, M. W., Beckmann, C. F., Jenkinson, M., Andersson, J., Glasser, M. F., et al. (2012). Temporally-independent functional modes of spontaneous brain activity. *Proc. Natl. Acad. Sci. U. S. A.* 109, 3131–3136.

Smith, S. M., Miller, K. L., Salimi-Khorshidi, G., Webster, M., Beckmann, C. F., Nichols, T. E., Ramsey, J. D., and Woolrich, M. W. (2011). Network modelling methods for FMRI. *Neuroimage* 54, 875–91.

Tagliazucchi, E., Von Wegner, F., Morzelewski, A., Brodbeck, V., and Laufs, H. (2012). Dynamic BOLD functional connectivity in humans and its electrophysiological correlates. *Front Hum Neurosci* 6.

Thompson, G. J., Magnuson, M. E., Merritt, M. D., Schwarb, H., Pan, W.-J., McKinley, A., Tripp, L. D., Schumacher, E. H., and Keilholz, S. D. (2013). Short-time windows of correlation between large-scale functional brain networks predict vigilance intraindividually and interindividually. *Hum. Brain Mapp.* 34, 3280–3298.

Thulborn, K. R., Davis, D., Erb, P., Strojwas, M., and Sweeney, J. A. (1996). Clinical fMRI: implementation and experience. *Neuroimage* 4, 101–107.

Tzourio-Mazoyer, N., Landeau, B., Papathanassiou, D., Crivello, F., Etard, O., Delcroix, N., Mazoyer, B., and Joliot, M. (2002). Automated anatomical labeling of activations in SPM using a macroscopic anatomical parcellation of the MNI MRI single-subject brain. *Neuroimage* 15, 273–289.

Varoquaux, G., and Craddock, R. (2013). Learning and comparing functional connectomes across subjects. *Neuroimage* 80, 405–415.

Varoquaux, G., Gramfort, A., Pedregosa, F., Michel, V., and Thirion, B. (2011). Multi-subject dictionary learning to segment an atlas of brain spontaneous activity. in *Information processing in medical imaging*, 562–573.

Venkatraman, V. K., Aizenstein, H., Guralnik, J., Newman, A. B., Glynn, N. W., Taylor, C., Studenski, S., Launer, L., Pahor, M., Williamson, J., et al. (2010). Executive control function, brain activation and white matter hyperintensities in older adults. *Neuroimage* 49, 3436–42.

Vermeer, S. E., Prins, N. D., den Heijer, T., Hofman, A., Koudstaal, P. J., and Breteler, M. M. B. (2003). Silent brain infarcts and the risk of dementia and cognitive decline. *N. Engl. J. Med.* 348, 1215–22.

Vines, B., Cerruti, C., and Schlaug, G. (2008). Dual-hemisphere tDCS facilitates greater improvements for healthy subjects' non-dominant hand compared to uni-hemisphere stimulation. *BMC Neurosci.* 9, 103.

Wittchen, H. U., Jacobi, F., Rehm, J., Gustavsson, a, Svensson, M., Jönsson, B., Olesen, J., Allgulander, C., Alonso, J., Faravelli, C., et al. (2011). The size and burden of mental disorders and other disorders of the brain in Europe 2010. *Eur. Neuropsychopharmacol.* 21, 655–79.

Yeo, B. T. T., Krienen, F. M., Sepulcre, J., Sabuncu, M. R., Lashkari, D., Hollinshead, M., Roffman, J. L., Smoller, J. W., Zöllei, L., Polimeni, J. R., et al. (2011). The organization of the human cerebral cortex estimated by intrinsic functional connectivity. *J. Neurophysiol.* 106, 1125–1165.

Zalesky, A., Fornito, A., and Bullmore, E. T. (2010). Network-based statistic: Identifying differences in brain networks. *Neuroimage* 53, 1197–1207.

Zuo, X. N., Ehmke, R., Mennes, M., Imperati, D., Castellanos, F. X., Sporns, O., and Milham, M. P. (2012). Network Centrality in the Human Functional Connectome. *Cereb Cortex* 22, 1862–1875.

5. Appendix

5.1 Erklärung über die eigenständige Abfassung der Arbeit

Hiermit erkläre ich, dass ich die vorliegende Arbeit selbständig und ohne unzulässige Hilfe oder Benutzung anderer als der angegebenen Hilfsmittel angefertigt habe. Ich versichere, dass Dritte von mir weder unmittelbar noch mittelbar geldwerte Leistungen für Arbeiten erhalten haben, die im Zusammenhang mit dem Inhalt der vorgelegten Dissertation stehen, und dass die vorgelegte Arbeit weder im Inland noch im Ausland in gleicher oder ähnlicher Form einer anderen Prüfungsbehörde zum Zweck einer Promotion oder eines anderen Prüfungsverfahrens vorgelegt wurde. Alles aus anderen Quellen und von anderen Personen übernommene Material, das in der Arbeit verwendet wurde oder auf das direkt Bezug genommen wird, wurde als solches kenntlich gemacht. Insbesondere wurden alle Personen genannt, die direkt an der Entstehung der vorliegenden Arbeit beteiligt waren.

....

Datum Unterschrift

5.2 Curriculum vitae

5.2.1 Education

2010 – now	Ph.D. stipend in Neuroscience, Department of Neurology, Max Planck Institute for Human Cognitive and Brain Sciences, Leipzig. Advisor: Dr. Daniel Margulies and Prof. Dr. Arno Villringer
2003 – 2009	Diploma in Computer Science, Department of Math and Computer Science, University Jena.

5.2.2 Research Experience

2009	Chair for Computational Complexity, University Jena Diploma thesis: The Parameterized Complexity of the s-Club Problem Advisor: Dipl. Bioinf. Christian Komusiewicz, Dipl. Inf. Hannes Moser and Prof. Dr. Rolf Niedermeier
2008-2010	Clinic for Psychiatry and Psychotherapy, University Clinic Jena Research Assistant: Multivariate Methods for Analyzing the Relationship of Genetic and Imaging Data Advisor: Prof. Dr. Ralf Schloesser
2007-2008	Chair for Computer Vision, University Jena Study thesis: Offline-Methods for 3D-Reconstruction of Planar Scenes Advisor: Dipl. Inf. Olaf Kähler and Prof. Dr. Joachim Denzler

5.2.3 Talks

2012	Schäfer, A. (2012). Connectivity clusters in human brain graphs. Talk presented at 2nd Einstein Fellowship Symposium on "Decision-making". Berlin, Germany. 2012-05-24–2012-05-25
	Schäfer, A. (2012). Dynamics underlying the mismatch between structure and function. Talk presented at Donders Discussions 2012. Nijmegen, the Netherlands. 2012-10-25–2012-10–26

5.2.4 Teaching

2013	Neumann J., Müller K., Bernhardt B., **Schäfer A.**, Hellrung L., Trampel R., Anwander A., Knösche T., and Grigutsch M. Analysis of structural and functional imaging data and brain connectivity. Lecture Series, Summer Term 2013

5.2.5 Summer School

2012 European Campus of Excellence / MPS-UCL Symposium and Advanced Course on Computational Psychiatry and Ageing, Ringberg Castle, Bavaria, Germany, September 16–22, 2012

5.2.6 Conference Posters and Abstracts

2013 Can serotonin put your mind at rest?, **Schäfer A.**, Burmann I., Ralf R., Arélin K., Pampel A., Villringer A., Margulies D., and Sacher J., Poster presented at 51st Annual Meeting of the American College of Neuropsychopharmacology, Hollywood, FL, USA

OpenCL Accelerated Connectome Analysis in Python, **Schäfer A.,** and Hellrung L., Poster Presented at Neuroinformatics 2013, Stockholm, Sweden

Obesity and ageing related changes in brain structure and function, Kharabian S., Horstmann A., Arelin K., Müller K., **Schäfer A.**, Neumann J., Schroeter M., Riedel-Heller S., Sturmvoll M., and Villringer A., Abstract at 29th Anual Meeting of the German Adipositas Society, Hannover, Germany

A probabilistic atlas of cerebello-cerebral functional connectivity, Kipping J., **Schäfer A.**, Villringer A., and Margulies D., Abstract at 43rd annual meeting of the Society for Neuroscience, San Diego, USA

The Neural Basis of Emotion Regulation: Plastic Effects Following Training of Executive Control, Cohen N., Margulies D., Taubert M., **Schäfer A.**, Ashkenazi S., Henik A., Villringer A., and Okon-Singer H., Poster presented at 3rd IMPRS summer school, Leipzig, Germany

Early small vessel disease affects fronto-parietal and cerebellar hubs in close correlation with clinical symptoms – A resting state MRI study, **Schäfer A.**, Quinque E., Kipping J., Arélin K., Roggenhofer E., Frisch S., Villringer A., Mueller K., and Schroeter M., Poster presented at 19th Annual Meeting of the Organization for Human Brain Mapping, Seattle, USA

A single dose of escitalopram decreases resting-state functional-connectivity, Burmann I., **Schäfer A.**, Regenthal R., Arélin K., Villringer A., Margulies D., and Sacher J., Poster presented at 19th Annual Meeting of the Organization for Human Brain Mapping, Seattle, WA, USA

2012 Communities of Connectivity Change in rs-fMRI, **Schäfer A.**,

Margulies D., Böttger J., Kipping J., Kiebel S., Lohman G., and Villringer A., Poster presented at 3rd Biennial Conference on Resting State Brain Connectivity, Magdeburg, Germany

Functional dissociation of cerebello-frontal and cerebello-parietal networks – individual and group-level data of intrinsic functional connectivity, Kipping J., **Schäfer A.**, Villringer A., and Margulies D., Poster presented at 3rd Biennial Conference on Resting State Brain Connectivity, Magdeburg, Germany

Connectivity Clusters show dynamic participation of brain regions in multiple networks, **Schäfer A.**, Margulies D., Lohman G., and Villringer A., Poster presented at 18th Annual Meeting of the Organization for Human Brain Mapping, Beijing, China

A cerebellocentric approach to brain parcellation, Kipping J., **Schäfer A.**, Villringer A., and Margulies D., Poster presented at 18th Annual Meeting of the Organization for Human Brain Mapping, Beijing, China

Connectivity concordance for characterizing consistent subregions of the prefrontal cortex, Margulies D., **Schäfer A.,** and Petrides M., Poster presented at 18th Annual Meeting of the Organization for Human Brain Mapping, Beijing, China

Force-directed edge-bundling for the visualization of functional connectivity, Böttger J., **Schäfer A.**, Lohman G., Villringer A., and Margulies D., Poster presented at 18th Annual Meeting of the Organization for Human Brain Mapping, Beijing, China 2011

2011 Classification of ADHD in children using graph theoretic features derived from resting state fMRI, **Schäfer A.**, Margulies D., Villringer A., Craddock C., and Lohmann G., Poster presented at Annual Scientific Meeting of the European Society for Magnetic Resonance in Medicine and Biology (ESMRMB), Leipzig, Germany.

s-Club: Consistent density patterns in functional brain networks, **Schäfer A.**, Margulies D., Lohman G., and Villringer A., Poster presented at 17th Annual Meeting of the Organization for Human Brain Mapping (HBM), Quebec City, QC, Canada

5.3 Publications

2014

Early small vessel disease affects fronto-parietal and cerebellar hubs in close correlation with clinical symptoms – A resting state MRI study, **Schaefer A.**, Quinque E., Kipping J., Arélin K., Roggenhofer E., Frisch S., Villringer A., Mueller K., and Schroeter M., Journal of Cerebral Blood Flow and Metabolism, 34(7), 1091-1095 2014, Feature Article

Dynamic network participation of functional connectivity hubs assessed by resting-state fMRI, **Schaefer A.**, Margulies D., Lohmann G., Gorgolewski K., Smallwood J., Kiebel S., and Villringer A., Frontiers in Human Neuroscience, 8(15), 2014

Connexel Visualization: A software implementation of glyphs and edge-bundling for dense connectivity data using brainGL, Böttger J., Schurade R., Jakobsen E., **Schaefer A.,** and Margulies D., Frontiers in Human Neuroscience, 8(15), 2014

Three-dimensional mean-shift edge bundling for the visualization of functional connectivity in the brain, Böttger J., **Schäfer A.**, Lohmann G., Villringer A., and Margulies D., IEEE Transactions on Visualization and Computer Graphics, 20(3), 471-480, 2014

2013

A comparison between uni- and bilateral tDCS effects on functional connectivity of the human motor cortex, Sehm B.∗, Kipping J.∗, **Schäfer A.**, Villringer A., and Ragert P., Frontiers in Human Neuroscience, 7(183), 2013

2012

Dynamic modulation of intrinsic functional connectivity by transcranial direct current stimulation, Sehm B., **Schäfer A.**, Kipping J., Margulies D., Conde V., Villringer A., and Ragert P., Journal of Neurophysiology, 108(12), 3253–3263, 2012

Parameterized computational complexity of finding small-diameter subgraphs, **Schäfer A.**, Komusiewicz C., Moser H., and Niedermeier R., Optimization Letters, 6(5), 883–891, 2012

2010

Resting developments: a review of fMRI post-processing methodologies for spontaneous brain activity, Margulies D., Böttger J., Long X., Lv Y., Kelly C., **Schäfer A.**, Goldhahn D., Abbushi A., Milham M., Lohmann G., and Villringer A., Magnetic Resonance Materials in Physics, Biology and Medicine, 23(5–6), 289–307, 2010

under review

Serotonergic modulation of intrinsic functional connectivity, **Schaefer A.**, Burmann I., Regenthal R., Arélin K., Barth C., Margulies D., and Sacher J., under review

Mapping Functional Connectivity Transitions in the Individual Brain, Margulies D., Gorgolewski K., Haueis P., **Schaefer A.**, Bernhardt B., Bazin P., Petrides M., Lohmann G., and Böttger J., under review

5.4 Acknowledgements

I want to thank my advisors Dr. Daniel Margulies and Prof. Arno Villringer for their time, their supervision and general help throughout all my PhD. Further help and inspiration I received from my fellow colleagues in the Neuroanatomy and Connectivity group as well as from Prof. Stefan Kiebel, Prof. Matthias Schroeter, Dr. Bernhard Sehm and Eva Quinque. Special thanks go to Cornelia Ketscher and Birgit Mittag for their continuous support of all PhD students and the entire department.

I am very grateful to my mother Regina, sister Anja, my cousin Anika and my grandparents for their support during my doctoral thesis and my life. I also like to thank my former university Professors Joachim Denzler and Rolf Niedermeier for their teaching and encouragements during my academic education.

I would like to thank Anja Schäfer, Judy Kipping, Daniel Margulies, Katja Heuer, Julia Huntenburg, Sven Preusser, Sabine Oligschläger, Veronica Witte, Shahrzad Kharabian, Smadar Ovadio-Caro, Sebastian Urchs and Arno Villringer for their intensive proof reading and suggestions. Their help substantially enhanced the readability of this thesis.

I like to thank Judy for all the inspiration and motivation she gave me to write this thesis. But also for all her patience whenever my mind was somewhere else.